https://ntrs.nasa.gov/search.jsp?R=19810018539 2020-03-21T12:11:53+00:00Z

NASA CR-159,060

NASA Contractor Report 159060

NASA-CR-159060
19810018539

Manufacturing Development of DC-10 Advanced Rudder

by A. Cominsky, et al.

MCDONNELL DOUGLAS CORPORATION
DOUGLAS AIRCRAFT COMPANY
LONG BEACH, CALIFORNIA 90846

CONTRACT NAS1-14724
AUGUST 1979

FOR EARLY DOMESTIC DISSEMINATION

Because of its significant early commercial potential, this information which has been developed under a U.S. Government program is being disseminated within the United States in advance of general publication. This information may be duplicated and used by the recipient with the express limitation that it not be published. Release of this information to other domestic parties by the recipient shall be made subject to these limitations. Foreign release may be made only with prior NASA approval and appropriate licenses. This legend shall be marked on any reproduction of this information in whole or in part.

DATE OF GENERAL RELEASE MAY 1981.

LIBRARY COPY

1979

LANGLEY RESEARCH CENTER
LIBRARY, NASA
HAMPTON, VIRGINIA

National Aeronautics and Space Administration

Langley Research Center
Hampton, Virginia 23665
AC 804 827-3966

Technical Report Documentation Page

1. Report No.	2. Government Accession No.	3. Recipient's Catalog No.
CR 159060		

4. Title and Subtitle	5. Report Date
Manufacturing Development of DC-10 Advanced Rudder	September 1979
	6. Performing Organization Code
	8. Performing Organization Report No.
7. Author(s) A. Cominsky	
9. Performing Organization Name and Address McDonnell Douglas Corporation Douglas Aircraft Company Long Beach, Calif. 90846	10. Work Unit No. (TRAIS)
	11. Contract or Grant No.
	13. Type of Report and Period Covered Final Report Dec 6, 1976 - Sept 1, 1979
12. Sponsoring Agency Name and Address National Aeronautics and Space Administration Langley Research Center Hampton, Virginia 23665	14. Sponsoring Agency Code

15. Supplementary Notes

16. Abstract

This is the final technical report covering design, manufacture and ground test activities during development of production methods for an advanced composite rudder for the DC-10 transport aircraft.

17. Key Words	18. Distribution Statement
broadgoods, cost analysis, microcomputer process control, gel temp., silicone rubber bulk modulus and linear thermal coefficient.	

19. Security Classif. (of this report)	20. Security Classif. (of this page)	21. No. of Pages	22. Price
Unclassified	Unclassified	230	

Form DOT F 1700.7 (8-72) Reproduction of completed page authorized

N79-79895 #

MANUFACTURING DEVELOPMENT OF DC-10 ADVANCED RUDDER

by A. Cominsky, et al.

Prepared Under Contract No. NAS1-14724

McDonnell Douglas Corporation
Douglas Aircraft Company
Long Beach, California 90846

for

NASA
National
Aeronautics and
Space
Administration

PREFACE

This report was prepared by the Douglas Aircraft Company, McDonnell Douglas Corporation, Long Beach, California, under Contract NAS1-14724. It is the final technical report covering design, manufacture and ground test activities during development of production methods for an advanced composite rudder for the DC-10 transport aircraft. This work follows on the heels of the effort initiated under Contract NAS1-12954 (Flight Service Program for Advanced Composite Rudders on Transport Aircraft) and its purpose is to provide production and flight service data on primary composite structure for commercial transport aircraft. This work was conducted between December 6, 1976 and October 15, 1978.

The following Douglas personnel were the principal contributors to the program:

A. Cominsky	Project Manager
M. Ashizana	Structural Design
F. Braun	Stress Analysis
R. Palmer	Material and Producibility Engineering
R. Gariss, P. Marra, J. Sullivan	Manufacturing Development
R. Stringham, G. Stuart, G. Hinote	Vibration Testing
D. Hagemaier, V. Cusimano	Non-Destructive Inspection
M. Platte	Cost Analysis

The project was sponsored by the National Aeronautics and Space Administration (NASA), Langley Research Center. Mr. Marvin B. Dow was the Project Engineer for NASA.

NOTICE

Use of commercial products or names of manufacturers in this report does not constitute official endorsement of such products or manufacturers, either expressed or implied, by the National Aeronautics and Space Administration

CONTENTS

CONTENTS (Continued)

ILLUSTRATIONS

ILLUSTRATIONS (Continued)

TABLES

SECTION 1
SUMMARY AND CONCLUSIONS

This final report describes production manufacturing processes and materials for the graphite/epoxy composite upper aft rudder. The fabrication methods are basically the same as those developed under Contract NAS1-12954 and described in Reference 2.

The mold curing of the first test rudder was unsuccessful and a development subprogram was undertaken to improve the rudder box fabrication process. Attention centered on the rubber mandrel properties and size. When this work was successfully accomplished, the production of rudders was resumed and continued to the completion of a test rudder and 10 production rudders suitable for airline flight service.

Throughout the rudder fabrication phase of the program, considerable attention was focused on the recurring labor costs to help establish the extent of economies anticipated from this fabrication process.

This program developed and demonstrated production procedures through the sequential fabrication of 10 composite rudders. The estimated values for recurring labor were not entirely achieved due to unforeseen difficulties with the quality of the woven broadgoods and with the production performance of the machine shop and fiberglass shop. The performance of the latter two departments should have very little bearing on the cost of graphite/epoxy fabrication by means of the trapped rubber process. Very useful recurring labor costs were accumulated. The use of an automated cure cycle control system was implemented and was successfully demonstrated as consistent quality parts were produced. A front spar locator introduced into the fabrication process was instrumental in accurately locating the front spar and reducing the time required to attach the hinge fittings.

The program carried out to establish thermal expansion and bulk modulus properties for Dapco 38-3 silicone rubber was very successful. This permitted the verification of the rubber mandrel size and an estimate for the maximum internal rubber pressure to be achieved during a cure cycle. The consequences of tool spring-back during depressurization could then be properly assessed.

Gel temperature data for Narmco 5208 resin was identified for two heating rates (0.56 and 0.83^{o}K/min.) and rubber mandrel properties were shown to endure for at least 43 cure cycles.

The advanced composite upper aft rudder is satisfactory for production and airline service and a cost saving in a full production manufacturing mode is anticipated.

SECTION 2

INTRODUCTION

The objectives of this program were to develop and demonstrate production manufacturing processes for the graphite/epoxy composite rudder to show that it is cost-competitive with the metal rudder it replaces. The composite rudders were fabricated by the thermal expansion molding (trapped rubber) process. The details of this process as applied to the rudder component were developed under NASA Contract NAS1-12954 from January 1974 through April 1976. The rudder system and dimensions are shown in Figure 1.

This thermal-expansion molding technique consolidated laminated composite elements into a monolithic assembly in a single cure cycle, reducing the need for precision control of detailed parts and secondary bonding operations. The thermal-expansion molding technique exploits the thermal-expansion character-

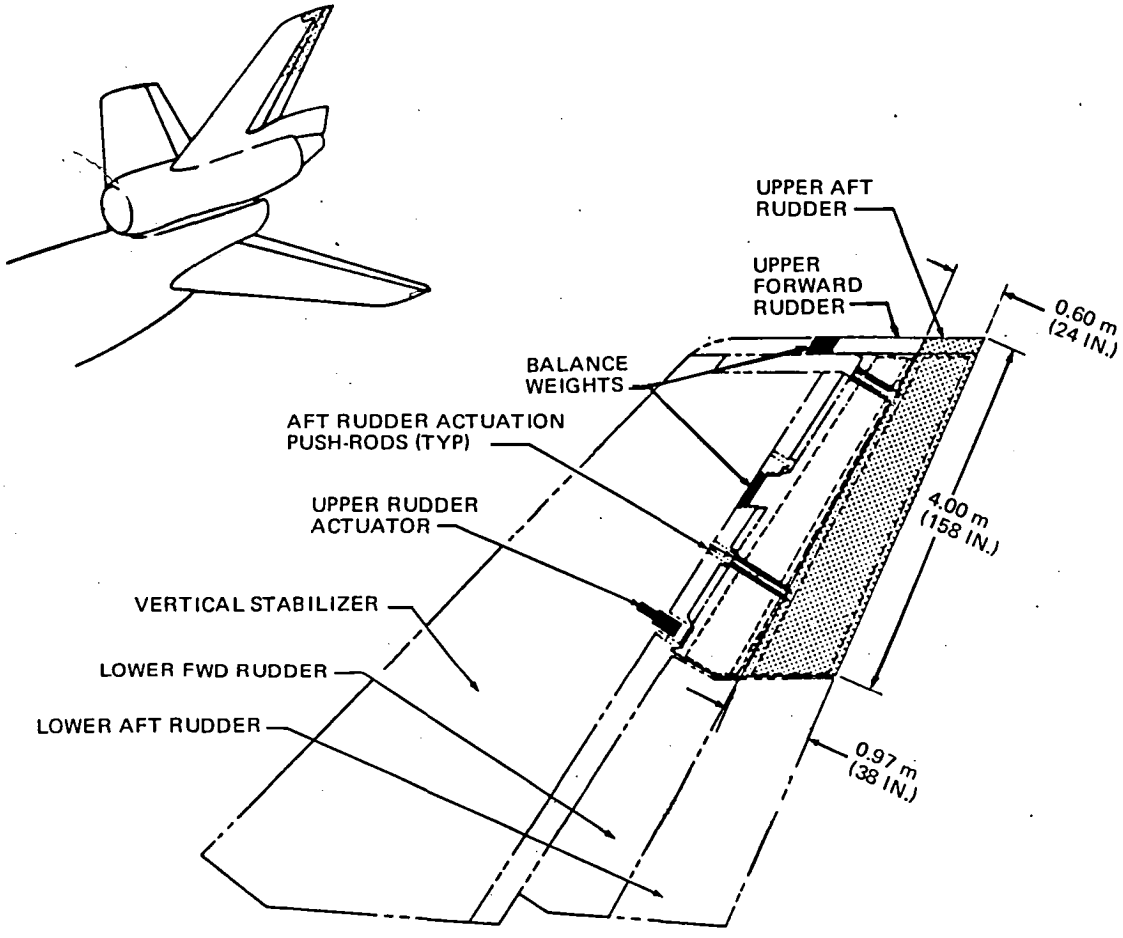

FIGURE 1. GENERAL ARRANGEMENT OF RUDDER SYSTEM

istics of silicone rubber tools to supply curing and bonding pressures. The individual parts of the molding assembly are laid up using uncured laminates, densified, and trimmed to size on simple ancillary tools. The individual parts are then assembled in a curing tool consisting of various metal and silicone rubber elements. The assembled tool is heated so that the thermal expansion of the rubber furnishes the pressure required to consolidate the individual parts into a cured laminate assembly. The heating cycle is controlled to provide the temperature and pressure phasing required to cure and bond the laminates.

The first phase of the program was spent in devising process modifications that would contribute to fabrication economies and then arranging a 10-rudder manufacturing plan incorporating the process improvements. This effort was followed by a quantitative analysis of the anticipated cost savings and the resulting cost of fabricating the 10 production rudders.

At this junction, the Tentative Production Commitment Criteria given in Table 1 were developed. These criteria contain six items which, if satisfied by subsequent events, would tend to show that the use of composite rudders for full production would be economic, serviceable, certifiable, and acceptable.

TABLE 1
PRODUCTION COMMITMENT CRITERIA

1. TARGET MANUFACTURING MAN-HOURS FOR THE GRAPHITE/EPOXY MOLD ASSEMBLIES FOR UNITS 8, 9 AND 10 ARE 1110 HOURS.
2. PROJECTED COMPOSITE RUDDER PRODUCTION CROSSOVER TARGET IS WITHIN 100 UNITS.
3. NO SIGNIFICANT DEFICIENCIES IDENTIFIED IN THE SERVICE EVALUATION PROGRAM OF CONTRACT NAS1-12954.
4. PRODUCTION UNITS WILL HAVE FAA CERTIFICATION (BEING MADE DURING SUBJECT CONTRACT).
5. NO DIFFICULTIES ANTICIPATED FOR PRODUCTION ACCEPTANCE BY AIRLINES.
6. FIRM AND ANTICIPATED DELIVERIES OF DC-10 AIRCRAFT OF AT LEAST 100 AIRCRAFT AFTER THE COMPOSITE RUDDER HAS BEEN INCORPORATED INTO PRODUCTION.

Although the graphite fiber (T300) and resin system (N5208) are the same as were used for the original rudder program, uniwoven and biwoven 1.067-m broadgoods was the form of the material chosen for this contract. Specimen testing was limited to fatigue and bolt-bearing tests since considerable data from the DAC IRAD woven goods specimen test program were available.

Following completion of manufacture of the graphite/epoxy test unit rudder, a vibration shake test was successfully carried out. This test demonstrated that vibration equivalent to twice the level experienced in service will not affect the structural integrity of the composite rudder. The modal survey test was also completed; it led to the conclusion that the rigidity and flutter safety of the upper forward metal rudder fitted with a composite aft rudder are satisfactory.

The test rudder box was loaded into the molding tool (PLM) and cured on October 18, 1977. On removal from the PLM after the cure was completed, it was observed that the front spar had failed in compression and that many ribs were damaged and misshaped. An investigation to determine the causes of the problem revealed that the mandrel rubber had been oversize and had produced the warped rib webs during the PLM loading operation. The oversize mandrel rubber had also produced excessive pressures during the cure cycle, which resulted in excessive tool spring-back loads that crushed the front spar web during tool cooldown.

The situation called for the development of engineering methods for designing and inspecting the rubber mandrels in order to provide confidence in the trapped rubber process. Thus, a manufacturing process development subprogram was added to the contract. This consisted of:

1. The measurement of the linear coefficient of thermal expansion for Dapcocast 38-3 silicone rubber.

2. The determination of values for the bulk modulus of Dapcocast 38-3 silicone rubber.

3. The establishment of a method for designing the rubber size to produce the desired pressure.

4. The establishment of a method for avoiding front spar and rib crushing.

5. The casting of new rubber mandrels.

6. The inspection measurement of the new rubber mandrels to verify their size.

7. The curing of a replacement test rudder.

8. The determination of rubber mandrel pressure during a rudder cure cycle and the durability of these mandrels through subsequent cures.

The manufacturing process development subprogram was carried out successfully. The molding of the second test rudder was considered satisfactory inasmuch as the spars, skins, and ribs were intact. However, a little more than half of the ribs were weak and splintery. This required a search for the cause and a solution to this problem. It was found that this trouble was related to moisture contamination of the uncured rib laminates during the long (6 to 7 months) storage period and that this moisture could be removed by subjecting these parts to a repeat predensification oven cycle.

The majority of the good ribs were located in the upper portion of the rudder box. This circumstance was very fortunate since the test plan required the use of the upper 1.2 m of this rudder box for the vibration shake test specimen.

A production schedule was drawn up that called for the production of one rudder box per week and required another 5 to 6 weeks through final assembly of the full rudder unit. After the curing of the first rudder box, it was determined that the thermocouple information used for the automatic control of the cure cycle process was unreliable. Because thermocouple data were vital to the satisfactory function of the microprocessor, rudder box production was halted for a 3-week period while the wiring of the thermocouples and heaters was renovated. After completion of the rewiring program, rudder production was resumed and continued to completion within the production schedule.

With the completion of the 10th rudder unit, the principal effort was directed toward analyzing the recurring labor cost data. Comparisons were made with estimates arrived at during the cost reduction phase to evaluate the degree of success in meeting the cost-saving goals and in determining the advisability of committing the Douglas Aircraft Company to the production of graphite/epoxy composite upper aft rudders for the remainder of the DC-10 production output.

SECTION 3
PROCESS MODIFICATIONS AND COST ANALYSIS

Process Modifications

The trapped rubber process was the basic manufacturing technique (Figure 2). Process modifications are described in this section which were designed to accomplish substantial cost savings during the fabrication of 10 upper aft composite rudders in a production mode.

The basic material was Thornel 300 graphite with NARMCO resin 5208, the same as was used for the original 10 graphite composite rudders. This prepreg material was purchased in the form of 95-percent unidirectional weave (21 warp count) and bidirectional weave fabric 23 by 24 count, 8 harness satin weave. It was expected that this would help reduce layup man-hours. Both weaves were ordered in 1.067-m (42-inch) widths and design data were available from current IRAD program results (Table 2).

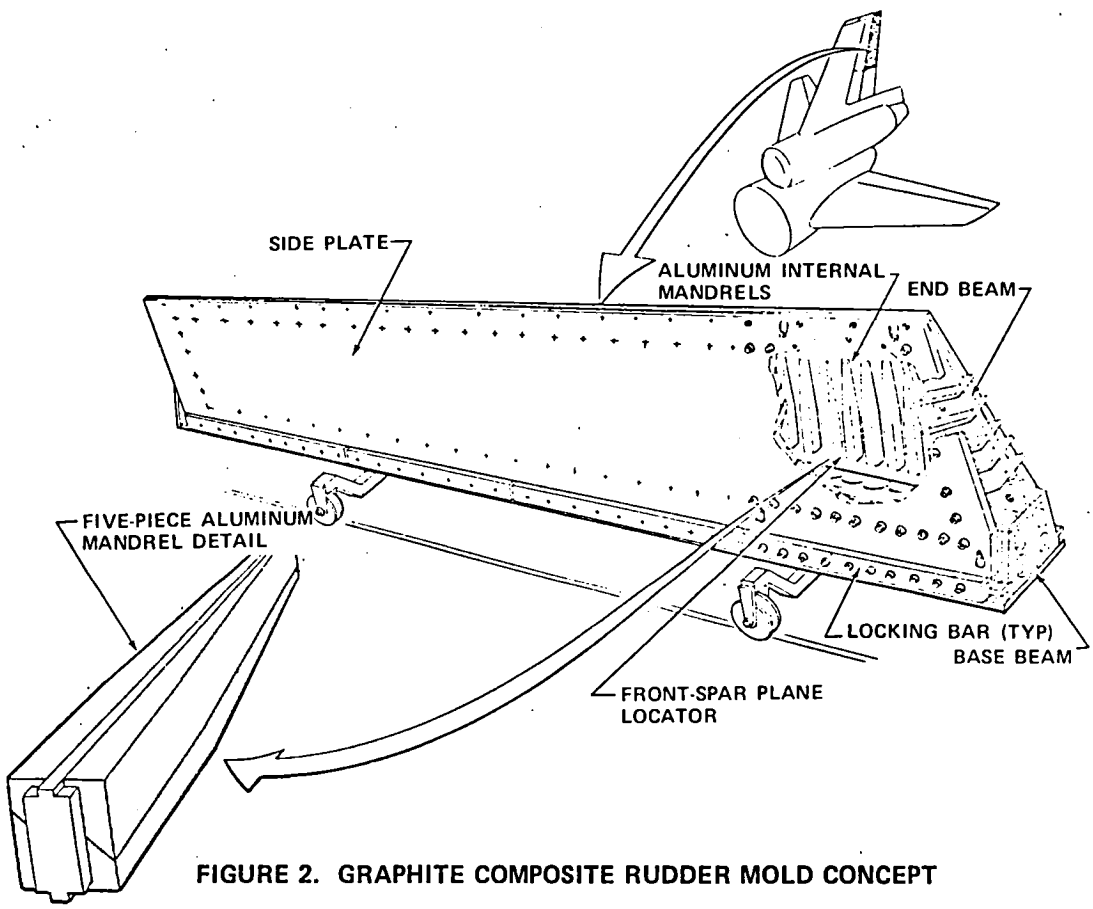

FIGURE 2. GRAPHITE COMPOSITE RUDDER MOLD CONCEPT

TABLE 2

COMPARISON-COMPOSITE MATERIAL
MECHANICAL PROPERTIES – T300/N5208

	3-IN. TAPE (7.62 cm)	95-PERCENT UNI-WEAVE	BI-WEAVE
F_L^t (MPa)	1539	1329	669
F_L^c (MPa)	1393	1160	611
E_L^t (GPa)	147	137	78.6
E_L^c (GPa)	131	132	64.9
P (kg/m^3)	1520	1520	1520
t (mm/ply)	0.14	0.15	0.33

The basic skin panels were made from unidirectional weave fabric with a $(0^o/45^o/-45^o)_s$ layup.

The front spar, rear spar, typical ribs, and the skin doublers were combinations of unidirectional and bidirectional weave fabric, whereas the hinge ribs were entirely bidirectional weave fabric. The thickness of these structural components was expected to increase moderately over those for the original 10 graphite rudders; the estimate of the resulting weight increase is shown in Appendix G.

The strength and stiffness values of these fabric materials are somewhat less than those used for the tape materials. However, the thickness increase of the fabric materials over the tape materials more than compensates for the reduced strength and stiffness (Table 3).

TABLE 3

COMPARISON-RUDDER STIFFNESS
PROPERTIES – WOVEN VERSUS TAPE

RUDDER BOX STIFFNESS PROPERTY	PERCENT INCREASE
AE	3.55
EI_{xx}	4.79
EI_{yy}	3.54
GJ	0

A comparison of the nominal thickness per ply of the tape and the woven forms of the graphite/epoxy material is as follows:

Tape	t	=	0.14 mm	(0.0055 in.)
95-Percent Unidirectional Weave	t	=	0.15 mm	(0.006 in.)
Bidirectional Weave	t	=	0.33 mm	(0.013 in.)

The use of 95-percent unidirectional and bidirectional weave graphite/epoxy cloth in 1.067-m widths was expected to speed the layup process. A 35-percent man-hour savings was anticipated (Table 4).

TABLE 4

PROCESS AND TOOLING MODIFICATIONS

DESCRIPTION	BENEFITS	SAVINGS PER CURE CYCLE
USE UNI-WEAVE AND BI-WEAVE THORNEL 300/NARMCO 5208 RESIN. BUILD OVERHEAD CLOTH DISPENSING TOOL	SPEED LAY-UP	35%
AUTOMATED HEATER CONTROLS	FACILITATE CURE CYCLE	14 MH
REWORK FRONT/SPAR WEB LOCATOR FOR INCREASED ACCURACY	SPEED UP HINGE ASSEMBLY DUE TO REDUCED SHIMMING. REDUCED MOLD, MANDREL AND PERSONNEL DAMAGE.	15%
MAKE SECOND ASSEMBLY JIG	REMOVE ASSEMBLY BOTTLENECK	10% TO 35%
REVISED LAY-UP FOR FIBERGLASS L/E	SPEED LAY-UP	21%

Form Block. — Changing from 7.62 cm graphite tape to woven cloth altered lamination thickness and ply dimensions in the buildup areas. These changes required revising the rib, closing rib and spar form blocks, and associated layout templates. The revised ply dimensions in the skin doubler area required a remake of the two skin master layouts.

Heater Control. — The manual temperature monitoring and control system, used on the ten rudders molded under Contract NAS1-12954 was modified into a computer-controlled cure process system, making this a totally "hands-off" operation. This was expected to result in a savings of 14 man-hours per rudder cure cycle (Table 4). The previous cure process required a minimum of two highly skilled people full time. Portions of the existing system, such as the Triac heater modulator, were utilized in the new system. An ASR 33 teletype terminal was used for producing a permanent record of the cure process (Figure 3).

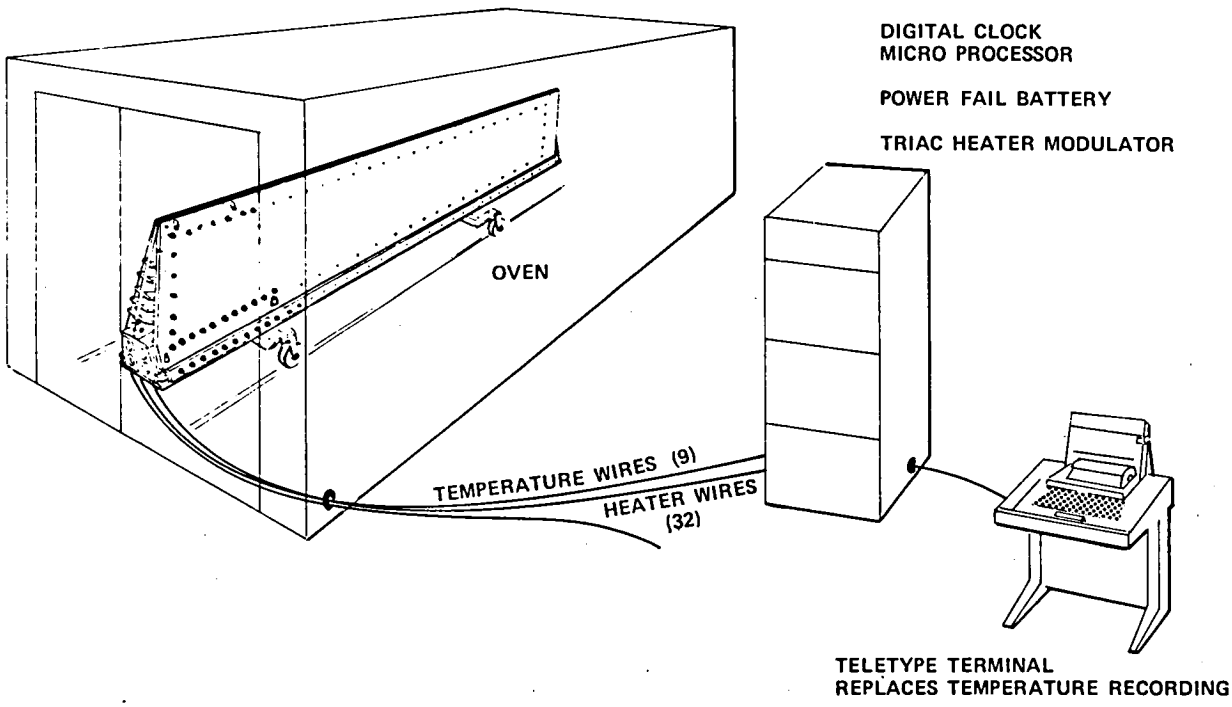

FIGURE 3. TEMPERATURE CONTROL SYSTEM

This modification was considered a must to permit the use of this process by semiskilled labor.

Replacing the individual pedestals on the PLM (Figure 4) with one continuous member allowed the thermocouple conduit to be a straight tube that could greatly reduce tool cleanup time. A means of quickly replacing a faulty heater element was also incorporated into the tool. The old design requires a tool downtime of about 2 days to replace a heater.

Plastic Laminating Mold (PLM). — The rudder box mold tool (PLM) underwent major modification. The front spar web locator was reworked so that the front spar was positioned more accurately. This simplified the assembly of the hinges and the control rod fittings to the rudder box by reducing or eliminating the need for shimming.

The front spar web locator was redesigned to increase its rigidity and to be a net fit on the rib-bay spikes. The individual spike pedestals were eliminated and replaced by one full-length member. The front spar locator and the base beam were reworked so that the front spar locator lifts the cured rudder box assembly from the tool. The increased rigidity could eliminate (1) hand-fitted shims beneath the rudder hinges and (2) a different tool setup

operation (adjusting the jack screw tubes using a depth micrometer, then bolting the spar locator to them). The close fit on the rib-bay spikes should prevent front spar damage if any metal mandrels inadvertently stick to a spike (Figure 4). The rework of the front spar locator was estimated to effect a 15-percent man-hour savings (Table 4).

The front spar access holes were to be molded with removable aluminum rings that index on the spikes. This should eliminate personal injuries and damage to the rubber mandrels as they are removed from the rib-bays.

There was not enough volume for rubber aft of the rear spar web locator to produce the pressure required for rear spar curing. The rear spar web locator was redesigned to correct this condition.

The redesign of the two spar locators necessitated the fabrication of a dummy part and recasting the rubber in these areas. The original dummy part was damaged beyond repair when the existing rubber was cast. The existing rubber mandrels in the area between the two spars had been accidentally burned by overheated heaters in a number of places and the mandrels in the center portion of the rudder were undersized resulting in some low-pressure areas. In view of this, the rubber in the entire tool was recast. To counteract the low-pressure effect of the undersize rubber, the thickness of the shrouds, excluding the closing rib shroud, was increased to 0.762 mm (0.030 in.) per side. The closing rib shroud had shims spot-welded to the two sides. This caused excessive mark-off on the lower edge of the rudders. These shrouds were remade.

Existing Assembly Jig. — The modifications to the existing assembly jig were minimal. Bolted-on locators no longer used due to a change in manufacturing concept were removed.

Second Assembly Jig. — A second assembly jig was required to provide a means of locating and assembling the leading edge details, the trailing edge details, the tip, and the fairing assemblies to the rudder box. These functions were formerly accomplished in the existing assembly jig. Performing these operations in the existing assembly jig caused the tool to become a bottleneck. Splitting these operations off enabled a more efficient use of assembly personnel and was an aid in maintaining the schedule (Figure 5). The man-hour savings is estimated to be between 10 percent and 35 percent (Table 4).

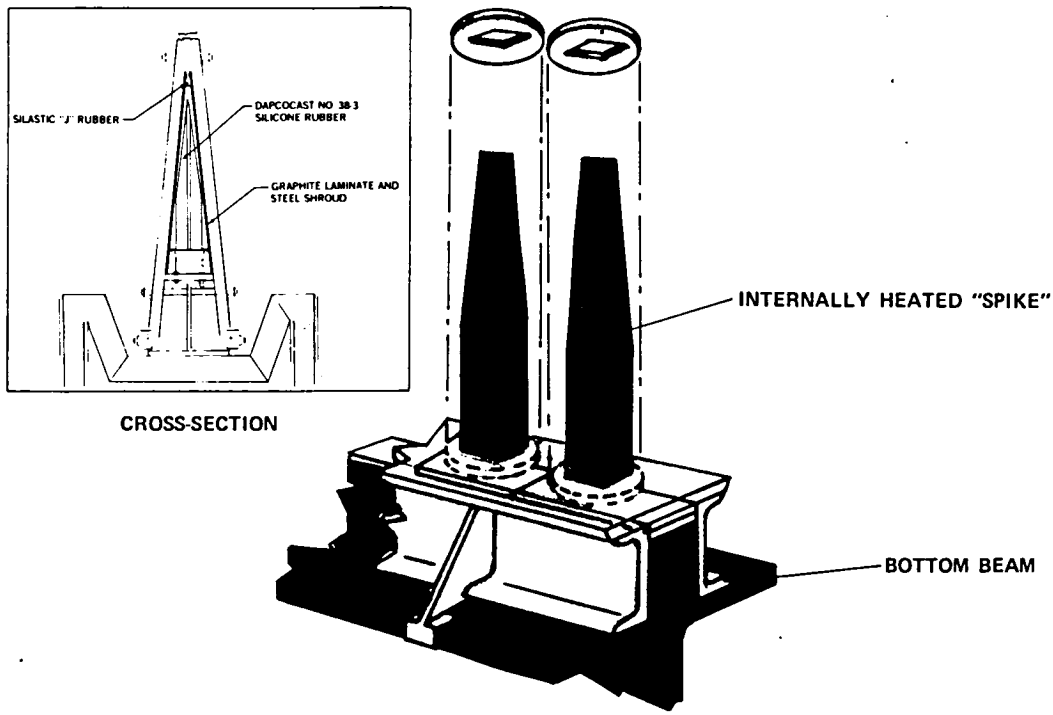

FIGURE 4. PLM SPAR PLANE LOCATOR MODIFICATION

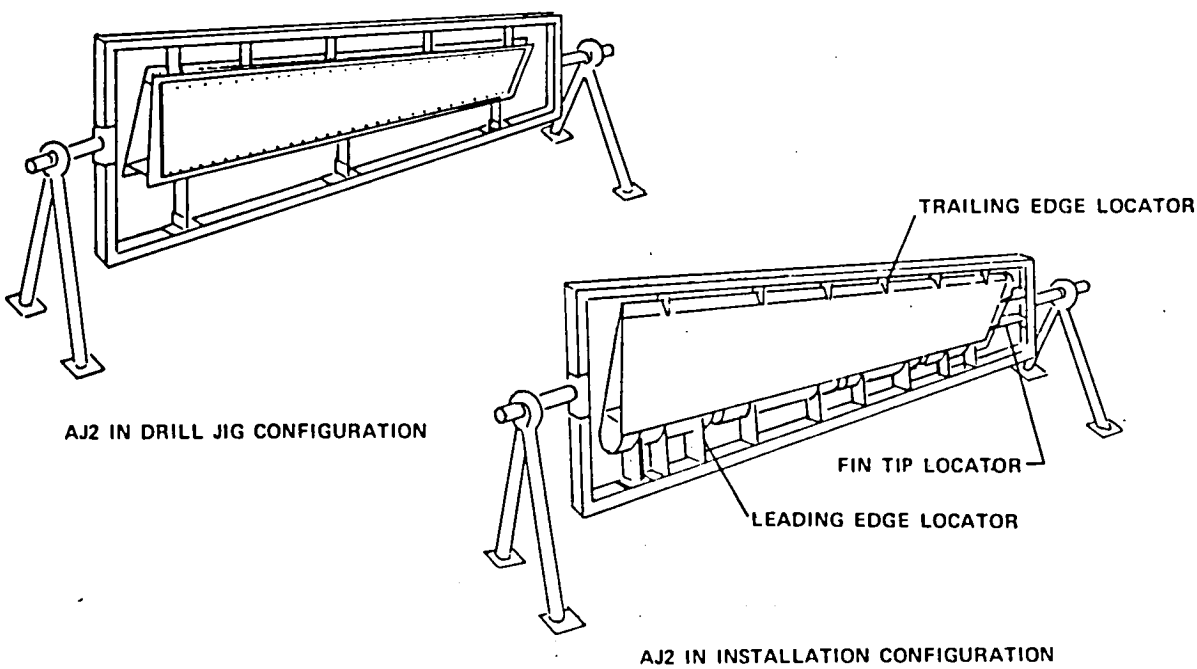

FIGURE 5. DRILL AND LOCATOR ASSEMBLY TOOL

Rudder Box Trim. — The manner in which the existing trim tool is attached to the rudder box was modified to improve the setup time.

Broadgoods Handling System. — A new overhead woven cloth dispenser tool was proposed to ease the handling of large bolts of graphite/epoxy cloth and permit proper fiber orientation with minimal effort. It is very difficult to lay up laminate that is bubble-free and wrinkle-free with tacky wide cloth without some means of supporting the roll of cloth. This condition is not serious with glass cloth because the fiber angular orientation tolerance is not as critical as with graphite.

Fiberglass Leading Edge. — Several small local doublers have been joined into a single doubler and two outer 0.127-mm layers were removed and replaced by one 0.254-mm layer. Several revisions of this nature reduced the handling and layup time substantially. A man-hour savings of 21 percent in layup time was expected to result from this process modification (Table 4).

As a result of the proposed tooling modifications and process refinements, the following man-hour improvements were anticipated per operation (Figure 6).

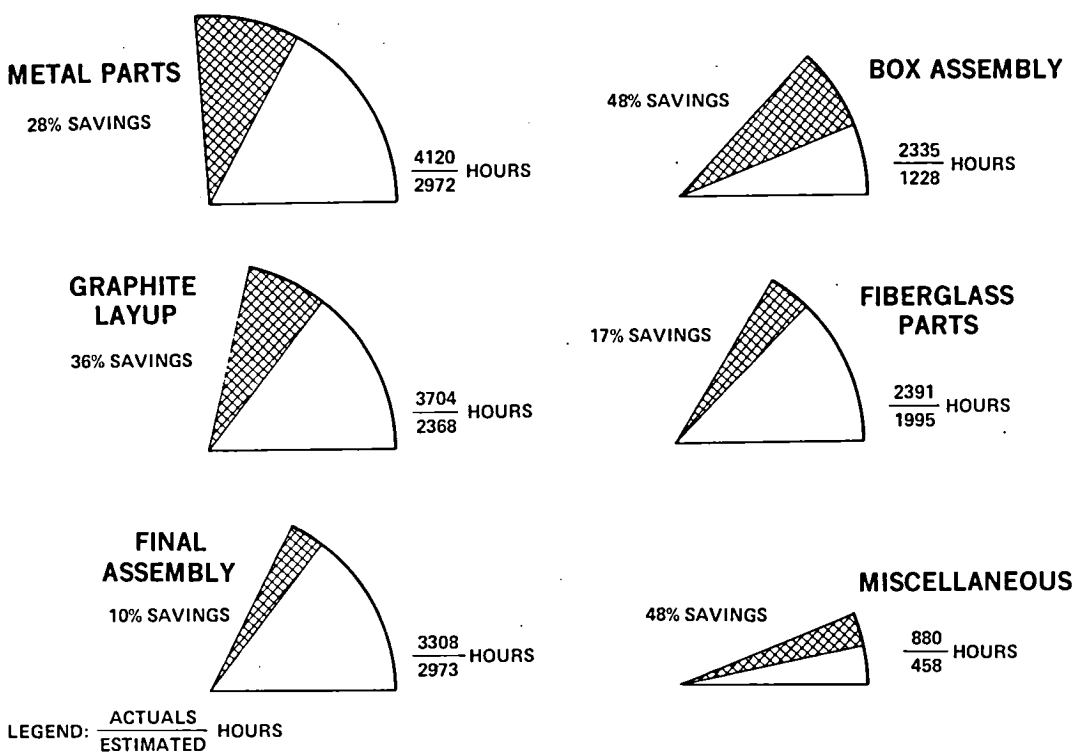

FIGURE 6. EXPECTED MAN-HOUR IMPROVEMENTS

- Metal Parts — 28-percent saving due to single machine setups for 10 shipsets
- Graphite Layup — 36-percent saving due to broadgoods utilization
- Final Assembly — 10-percent saving due to second assembly jig (AJ) implementation
- Box Assembly — 48-percent saving due to automated heat control and elimination of difficult handling operations.
- Fiberglass Parts — 17-percent saving due to redesign of details
- Miscellaneous — 48-percent saving due to process refinements.

These improvements are depicted in Figures 6 and 7 and Tables 5 and 6 and compared with actual labor hours derived from fabrication of the first ten rudders (Ref. 2, p. 95). The source of the estimated values is the result of the bottoms-up estimates.

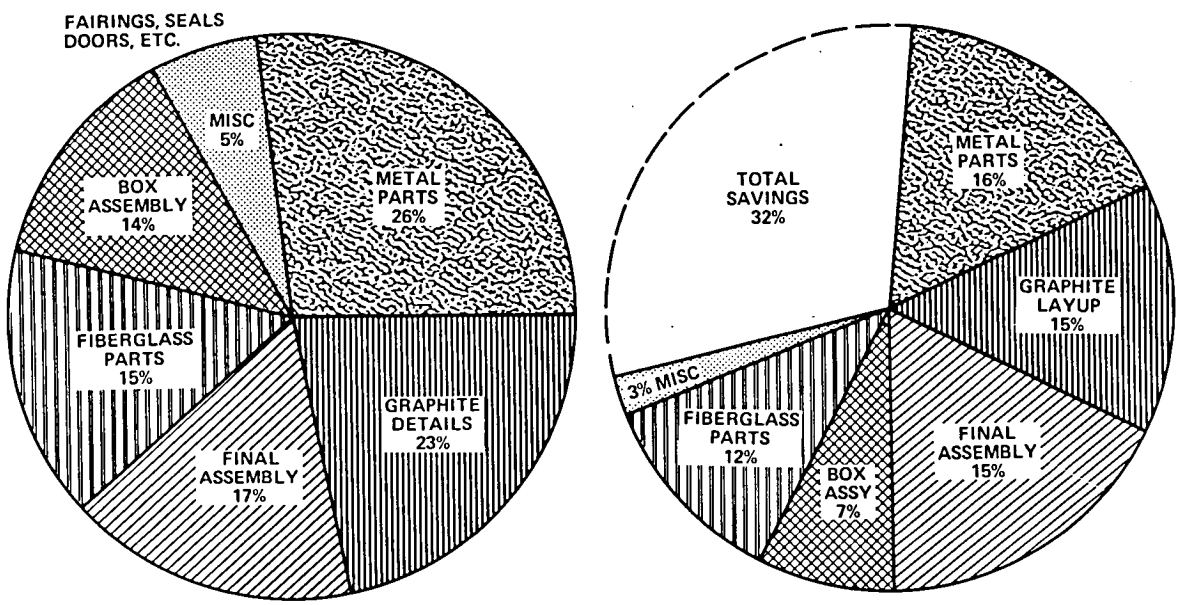

FORMER RUDDER PROGRAM (ACTUAL MAN-HOURS)

CURRENT RUDDER PROGRAM (ESTIMATED MAN-HOURS)

FIGURE 7. RECURRING MANUFACTURING COSTS DC-10 UPPER AFT COMPOSITE RUDDER

TABLE 5

ACTUALS FOR ALL TYPES OF RECURRING LABOR DC-10 COMPOSITE RUDDER

UNITS 1 THROUGH 10 (FIRST RUDDER CONTRACT)

CATEGORY	RECURRING DIRECT LABOR (MANHOURS) FOR GIVEN UNIT NUMBER										
	1	2	3	4	5	6	7	8	9	10	TOTAL
GRAPHITE	941	666	553	640	516	571	604	569	495	484	6,039
FIBERGLASS	356	235	200	278	231	241	191	214	201	244	2,391
METAL FAB.	155	155	155	155	155	116.2	116.2	116.2	116.2	116.2	1,356
MISC. FAB.	88	88	88	88	88	88	88	88	88	88	880
ENGINEERING*	83	83	83	83	83	83	83	83	83	83	830
TOOLING*	110	110	110	110	110	110	110	110	110	110	1,100
PLANNING*	33.5	33.5	33.5	33.5	33.5	33.5	33.5	33.5	33.5	33.5	335
INSP. & NDT	279	236	212	237	210	205	198	187	176	180	2,120
FINAL ASSY.	408	429	359	468	341	272	218	299	257	257	3,308
TOTAL	2453.5	2035.5	1793.5	2092.5	1767.5	1719.7	1641.7	1699.7	1559.7	1595.7	18,359

SOURCE: Reference 2

TABLE 6

ESTIMATES FOR ALL TYPES OF RECURRING LABOR

DC-10 COMPOSITE RUDDER (CURRENT CONTRACT)

CATEGORY	ESTIMATED RECURRING LABOR (MANHOURS) FOR GIVEN UNIT NUMBER										
	11	12	13	14	15	16	17	18	19	20	TOTAL
GRAPHITE LAYUP & MOLD ASSY.	442	405	382	365	354	344	336	328	323	317	3,596
FIBERGLASS FABRICATION	243	224	212	203	197	191	187	183	179	176	1,995
SHEET METAL AND MACHINED PARTS FABRICATION	165.1	160.7	156.9	153.1	150.0	147.0	144.2	141.6	139.3	137.1	1,495
MISCELLANEOUS FABRICATION	49	48	47	47	46	45	45	44	44	43	458
ENGINEERING (SUSTAINING)	71	71	70	70	69	69	67	66	65	54	672
TOOLING (SUSTAINING)	106	90	85	80	74	69	69	64	58	58	753
PLANNING	42	39	38	36	35	35	34	34	33	33	359
INSPECTION AND NDT	165	155	149	144	141	138	136	133	131	129	1,421
FINAL ASSEMBLY	370	308	300	294	294	287	284	281	279	276	2,973
TOTAL	1653.1	1500.7	1439.9	1392.1	1360	1325	1302.2	1274.6	1251.3	1223.1	13,722

The metal parts costs shown in Figures 6 and 7 are for the forward and aft rudder fittings, whereas the metal parts shown in Tables 5 and 6 are for aft rudder fittings only. The pie charts in Figure 7 are a comparison of the recurring costs for the initial rudder program (Units 1 through 10) and the current program (Units 11 through 20). A total saving of 32 percent is anticipated. The savings indicated on these pie charts are a percentage of the total recurring costs.

Cost Analysis

Introduction. — This section contains the results of the cost analysis and the approach taken to arrive at the data that were used to project from the development phase to a production mode. These data include the test rudders from the initial program (NAS 1-12954) and the current program (NAS 1-14724). The 10 rudders from the initial program (NAS 1-12954) have been identified as units 1 through 10, and the 10 rudders in the current program (NAS 1-14724) have been identified as units 11 through 20. The primary objective was to utilize both the estimated data and the actual labor data to project to a production mode and determine the crossover point when cost parity is achieved with conventionally produced rudders.

The Production Commitment Criteria given in Table 1 contain six items of which Items 1 and 2 are concerned with the cost of composite rudder fabrication. Item 1 stipulates that the number of man-hours required to fabricate the graphite/epoxy mold assemblies for Units 18, 19 and 20 is 1110 or less. The actual man-hours expended for these units were 1165 (391 + 385 + 389) or approximately 5 percent over the target value. Item 2 stipulates that the composite rudder crossover occurs within 100 units. This target has been achieved and is shown in Figure 8.

Understanding the composition of the labor data was an important element of the cost analysis effort, particularly when applying these data for the derivation of the crossover point. Since this is a development program, a variety of charges appeared against the labor accounts which were directly attributable to the resolution of development problems. Therefore, it was necessary to adjust the reported man-hours to some degree so that only the man-hours that contributed to the fabrication of the composite rudder units were considered.

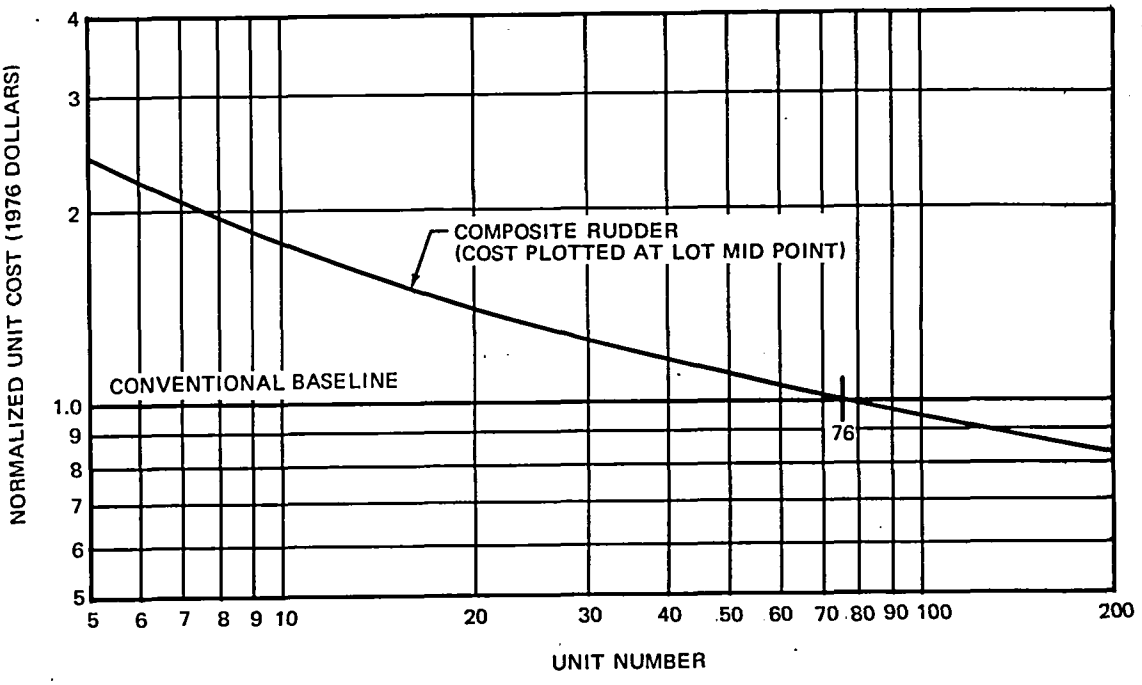

FIGURE 8. DC-10 UPPER AFT RUDDER CROSSOVER

Basic Man-Hour Data. — The basic man-hour data that were generated during the study phase and those data that were also used as the basis for developing crossover points are summarized in the following tables:

Table 5. Actual Recurring Labor, Units 1-10
Table 6. Estimated Recurring Labor, Units 11-20
Table 7. Actual Recurring Labor, Units 11-20

Accumulating and analyzing the basic data for the production of the composite rudders was a prime concern of the rudder fabrication contracts in order to establish an adequate and proper data base from which to estimate the cost benefits resulting from the use of composite rudders.

A description of all aspects of the program under which rudder units 1 through 10 were fabricated is given in Reference 2. Graphical representations of the recurring labor hours in total and also for the graphite portion only for units 1 through 20 are shown in Figures 9 and 10, respectively. While the recurring labor in Figure 9 does not show a continuous reduction in labor with each succeeding unit, it does, however, exhibit a downward trend. The data are also typical of those results that can be expected in a development program. However, the labor hours in this first group of 10 units cover a variety

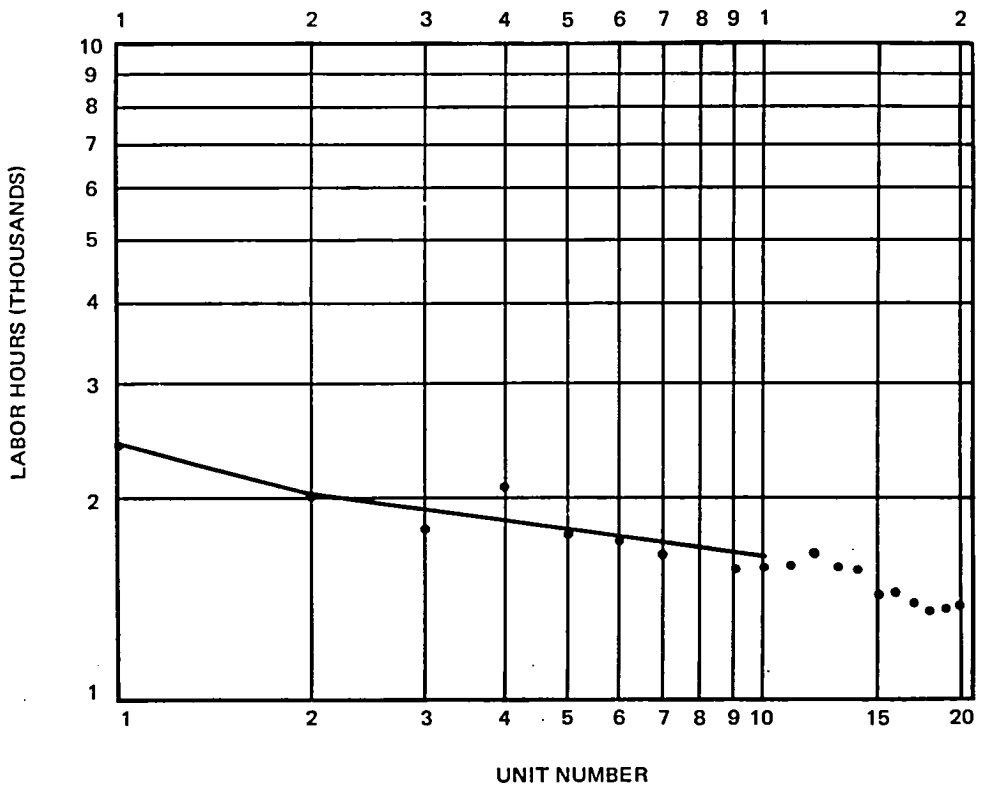

FIGURE 9. TOTAL ACTUAL RECURRING LABOR – UNITS 1 THROUGH 20

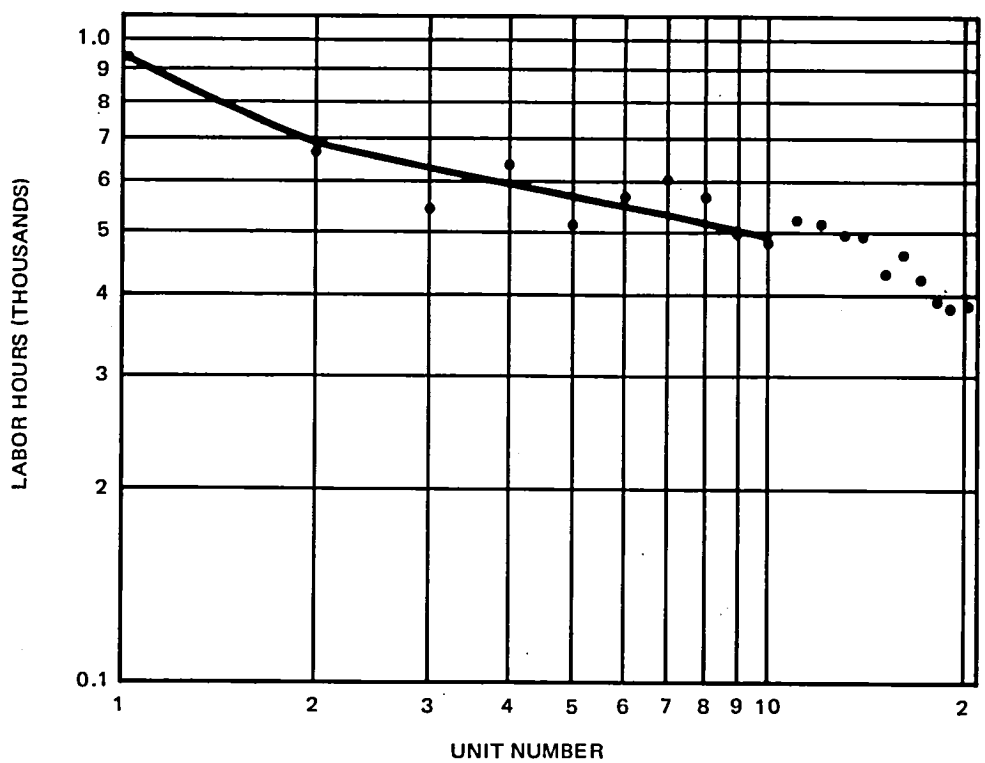

FIGURE 10. COMPOSITE MOLD RECURRING LABOR – UNITS 1 THROUGH 20

TABLE 7
SUMMARY OF ACTUAL RECURRING LABOR – UNITS 11 THROUGH 20

CATEGORY	RECURRING LABOR (MAN-HOURS) PER UNIT NUMBER										
	11	12	13	14	15	16	17	18	19	20	TOTAL
GRAPHITE LAYUP AND MOLD ASSEMBLY	524	516	496	482	435	467	426	391	385	389	4,511
FIBERGLASS FABRICATION	235	235	235	235	235	235	235	235	235	235	2,350
MACHINED PARTS	277	277	277	277	277	277	277	277	277	277	2,770
MISCELLANEOUS FABRICATION	47	47	47	47	47	47	47	47	47	47	470
ENGINEERING (SUSTAINING)	111	111	111	111	111	111	111	111	111	111	1,110
TOOLING (SUSTAINING)	47	47	47	47	47	47	47	47	47	47	470
PLANNING	30	16	16	20	40	16	16	24	36	27	241
INSPECTION AND NDT	147	183	116	137	39	65	89	85	82	111	1,054
FINAL ASSEMBLY	151	199	219	167	175	147	134	113	119	120	1,549
TOTAL	1569	1631	1564	1523	1406	1412	1382	1335	1339	1364	14,525

of problem-solving efforts as well as rework labor, all of which are typical of development. In Figure 10 a similar plot is presented in which only the labor hours for the graphite/epoxy mold are exhibited.

A comparison of estimated and actual recurring costs for units 11 through 20 is shown in Table 8. There are a number of reasons for the variances contained in Table 11. For example, in the case of the graphite layup and mold assembly, the variance of +25 percent (or 915 hours) is felt to be within the estimating tolerances associated with a development program. However, a large portion of the variance is due to the use of broadgoods on the second 10 units (11-20). Initially, it was believed that broadgoods would reduce fabrication labor hours with this particular component. In actuality, the reverse occurred and additional hours were incurred in areas requiring a selective buildup of material. In addition, the broadgoods had a greater waste factor than was experienced with the tape material. Another factor that increased man-hours from the estimated level was the need to rework units 13 and 16 because of

TABLE 8

COMPARISON OF ESTIMATED LABOR HOURS AND ACTUALS

UNITS 11 THROUGH 20

	RECURRING LABOR HOURS		
CATEGORY	ESTIMATES	ACTUALS	PERCENT CHANGE
GRAPHITE LAYUP AND MOLD ASSEMBLY	3,596	4,511	+25
FIBERGLASS FABRICATION	1,995	2,350	+18
MACHINED PARTS	1,495	2,770	+85
MISCELLANEOUS FABRICATION	458	470	+3
ENGINEERING, SUSTAINING	672	1,110	+65
TOOLING, SUSTAINING	753	470	−38
PLANNING	359	241	−33
INSPECTION/NDT	1,421	1,054	−26
FINAL ASSEMBLY	2,973	1,549	−48
TOTAL	13,722	14,525	+6

damage incurred in the process. On balance, the manufacturing development center did reduce the labor hours 25 percent over the first 10 units for the graphite mold assembly, and additional reductions are a reality in the aforementioned areas. Fiberglass details exhibited an 18-percent increase over the estimated level and only 1.7-percent decrease from the first 10 units. Problems with the tooling coupled with physical damage to the parts required new tooling and additional labor hours for fabricating new fiberglass details. One of the largest variances occurred with machined metal parts fabrication; this was attributed to a number of individual setups; utilizing machined details instead of forgings; redesign of a main drive hinge fitting to eliminate an interference problem; and the impact on the labor hours for fabricating new parts. Sustaining engineering* exhibited a sizable increase, which resulted from providing solutions to on-going development/manufacturing problems. With the resolution of these problems, it is anticipated that:

*Some costs originally listed under Tool Sustaining are included in Engineering Sustaining for rudders 11-20.

1. The graphite layup and mold assembly can meet the target** value and provide the estimated reduction.

2. The fiberglass can not only achieve the target** but also achieve an additional reduction of 9.8 percent.

3. The target** hours for machined fittings are not only achievable, but a new target can be established 33 percent lower than the estimated value if forgings are utilized.

4. Sustaining engineering can easily be reduced 40 percent below the target** value.

Projection and Crossover. — The data provided in the previous section clearly establish that there are anomalies in the data base. These anomalies, while not unexpected in a development program, tend to distort subsequent projections to a production mode and mask the potential cost benefits achievable with composites in this particular application. Adjusting the data base provides acceptable crossover points to the extent that the composite concept is competitive with the conventional metal construction. For purposes of this study, it was deemed advisable to maintain a conservative approach and utilize as much of the actuals as was rationally possible in developing a projection to a production mode. In doing this, data were extracted from the actuals of the second 10 units and applied to the first 10 production units. These data are shown in Table 9, the total of which is almost equal to the results obtained for rudders 11-20.

The computational process for deriving the crossover and accomplishing the cost projection is based on the following guidelines:

1. The graphite layup and mold assembly follow a progress improvement curve of 80 percent from units 1 to 100 and 84 percent from units 100 to 220.

2. The cumulative total for the first 10 units and the individual functional totals for these units are the values given in Table 9.

3. Sheet metal and machined parts and miscellaneous fabrication follow a 90-percent progress improvement curve from unit 1.

**Reference Table 8.

4. Final assembly follows an 80-percent progress improvement curve from unit 1.

5. Sustaining engineering and sustaining tooling follow 55.37-percent and 53.7-percent progress improvement slopes, respectively.

6. Planning and inspection are computed as functions of manufacturing hours and the support factors are 4 percent and 13.6 percent, respectively.

7. Graphite material costs are based on data obtained from industry projections as shown in Figure 11.

8. Cost data are plotted at lot midpoints based on the following quantity assumption.

    10 units
    10 units following 10
    20 units following 20
    20 units following 40
    20 units following 60
    20 units following 80
    20 units following 100
    50 units following 120
    50 units following 170

The results of the crossover analysis are plotted as a unit curve in Figure 8. Parity with the conventional rudder is reached at unit 76. Since some uncertainty exists in the pricing of the graphite raw materials, calculations were made to determine the sensitivity of cross-over point with changes in material price. When the price level was increased 50 percent, the cross-over point moved from 76 to 84. At a 100 percent increase in price, a cross-over of 98 was achieved.

TABLE 9

RECURRING LABOR HOURS FOR 10 PRODUCTION UNITS

FUNCTION	LABOR HOURS
LAYUP AND MOLD ASSEMBLY	4,330
FIBERGLASS FABRICATION	2,340
SHEET METAL AND MACHINED PARTS	2,660
MISCELLANEOUS FABRICATION	460
ENGINEERING, SUSTAINING	1,110
TOOLING, SUSTAINING	185
PLANNING	454
INSPECTION/NDT	1,542
FINAL ASSEMBLY	1,549
TOTAL	14,630

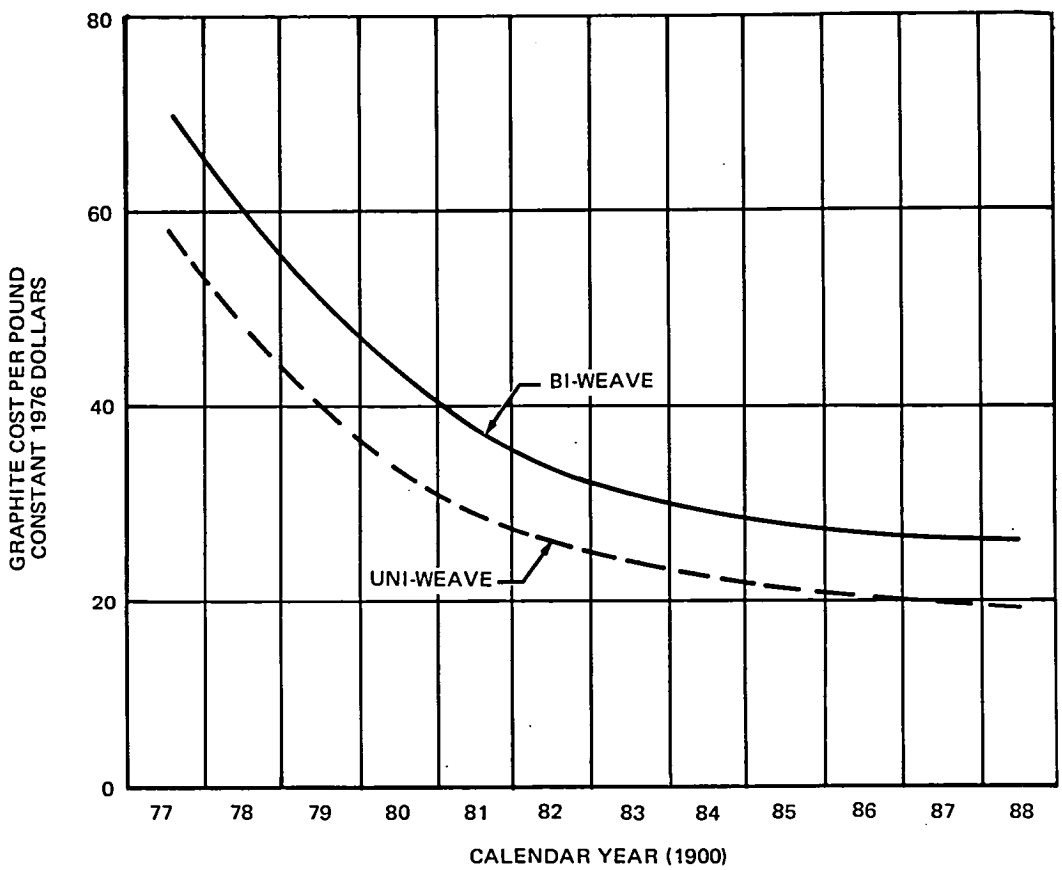

FIGURE 11. GRAPHITE EPOXY MATERIAL COST TREND

SECTION 4
TESTS

A comprehensive program had been carried out within Douglas under an IR&D program to define the strength allowables for the uniwoven and biwoven composite material used in the current program. As a result, only the following specimen and subcomponent tests were considered necessary to verify the static, acoustic, and flutter strength adequacy of the rudders made of woven broadgoods:

1. A fatigue test for biwoven material was performed on a sandwich beam specimen, P/N Z3943311, shown in Figure 12. This provided a means of comparing biwoven material fatigue properties for an isotropic layup with 7.62 cm tape graphite/epoxy material, where both were fabricated from prepreg T300/N5208 graphite/epoxy.

2. A bolt bearing test for a composite of biwoven and uniwoven material was conducted on the bearing specimen, shown in Figure 14. This test verified the bearing strength of the front spar flange layup which was typical of the combined front spar and skin to which the upper drive hinge is attached. The test setup is shown in Figure 13.

3. A subcomponent vibration shake test was conducted to verify the acoustic and vibration structural strength of the woven broadgoods rudder.

4. A modal survey test was conducted on a complete rudder to verify the flutter safety of the upper metal rudder fitted with a composite aft rudder.

Test Results

Test 1 – Fatigue Test. — The results of the fatigue tests of the bidirectional broadgoods specimens (P/N Z3943311) were as follows:

Static Test (one specimen)

Failure Load = 5694 N (1280 lb)

Failure Stress = 344.6 MPa (49,980 psi)

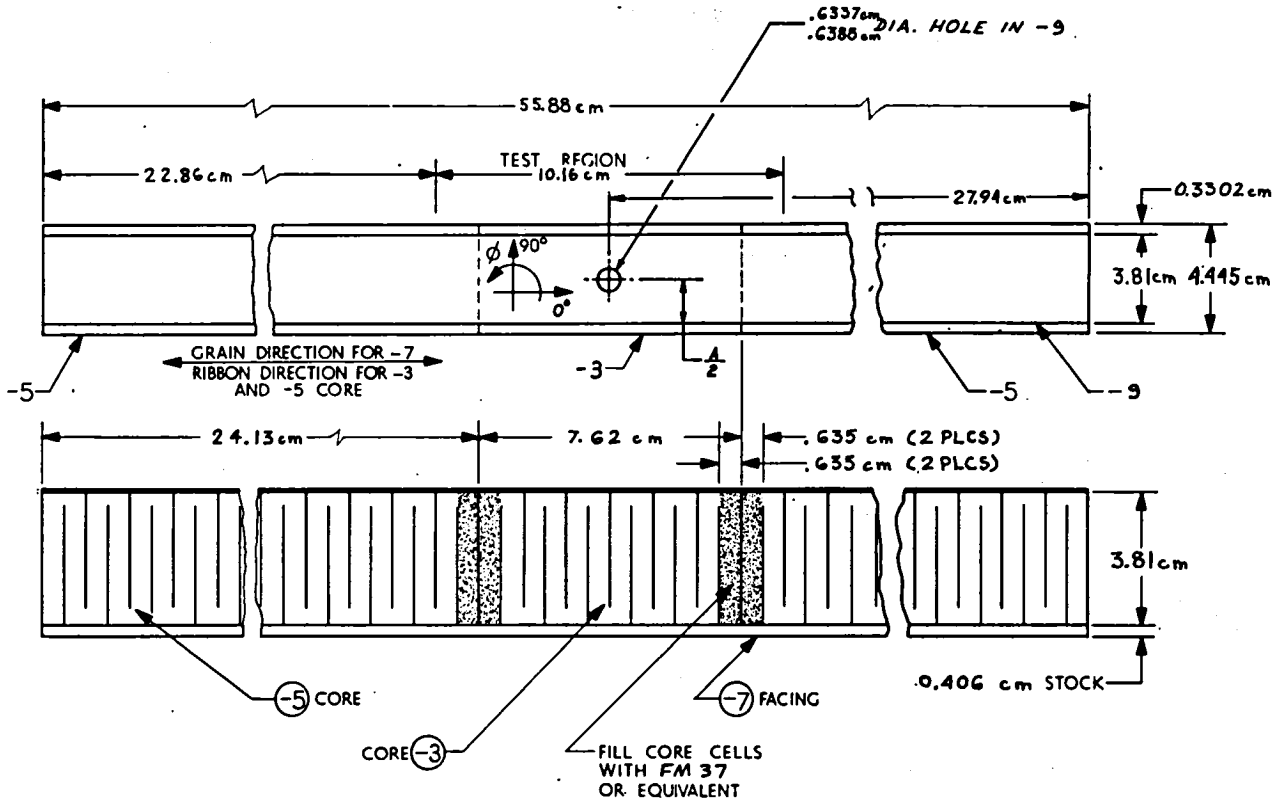

					AR	FM 37 OR EQUIVALENT	FOAMING ADHESIVE						
					1	- 9	FACING		4 LAYERS X (BI-DIRECT) 3.8 X 55.9	7300/NS208 TYPE 2; CL 1 GRAPHITE/EPOXY	DMS 2163		
					1	- 7	FACING		0.406 X 3.8 X 55.9 GR LOWISE	STEEL SHEET 4130	MIL-S-18729 COND N		
					2	- 5	CORE		3.8 X 4.45 X 22.9	ALUMINUM HONEYCOMB 1/8-5052-.006	PURCHASE FROM HEXCEL		
					1	- 3	CORE		3.8 X 4.45 X 10.2	ALUMINUM HONEYCOMB 1/8-2024-.002	PURCHASE FROM HEXCEL		
					AR	HYSOL EA 951	ADHESIVE				DMS 2103		
					ITEM	PART OR IDENTIFYING NO.	NOMENCLATURE OR DESCRIPTION	CODE IDENT. NO.	STOCK SIZE	MATERIAL DESCRIPTION	MATERIAL SPECIFICATION	FIND NO.	ZONE

	LAYER DIRECTION Ø					
	- 9	-	-	-	-	-
1	(0-90)†					
2	(±45)†					
3	(∓45)†					
4	(90-0)†					
5						
6						
7						
8						

PARTS LIST

McDONNELL DOUGLAS CORPORATION PROPRIETARY RIGHTS ARE INCLUDED IN THE INFORMATION DISCLOSED HEREIN. RECIPIENT BY ACCEPTING THIS DOCUMENT AGREES THAT NEITHER THIS DOCUMENT NOR THE INFORMATION DISCLOSED HEREIN NOR ANY PART THEREOF SHALL BE REPRODUCED OR TRANSFERRED TO OTHER DOCUMENTS OR USED OR DISCLOSED TO OTHERS FOR MANUFACTURING OR FOR ANY OTHER PURPOSE EXCEPT AS SPECIFICALLY AUTHORIZED IN WRITING BY McDONNELL DOUGLAS CORPORATION.

DOUGLAS AIRCRAFT COMPANY
McDONNELL DOUGLAS LONG BEACH, CALIFORNIA

SPECIMEN ASSY— COMPOSITE FACING HONEYCOMB SANDWICH BEAM TEST

SIZE	CODE IDENT NO.	
D	88277	Z3943311
SCALE 1/1		SHEET 1 OF 1

FIGURE 12. SPECIMEN ASSEMBLY – COMPOSITE FACING HONEYCOMB SANDWICH BEAM TEST

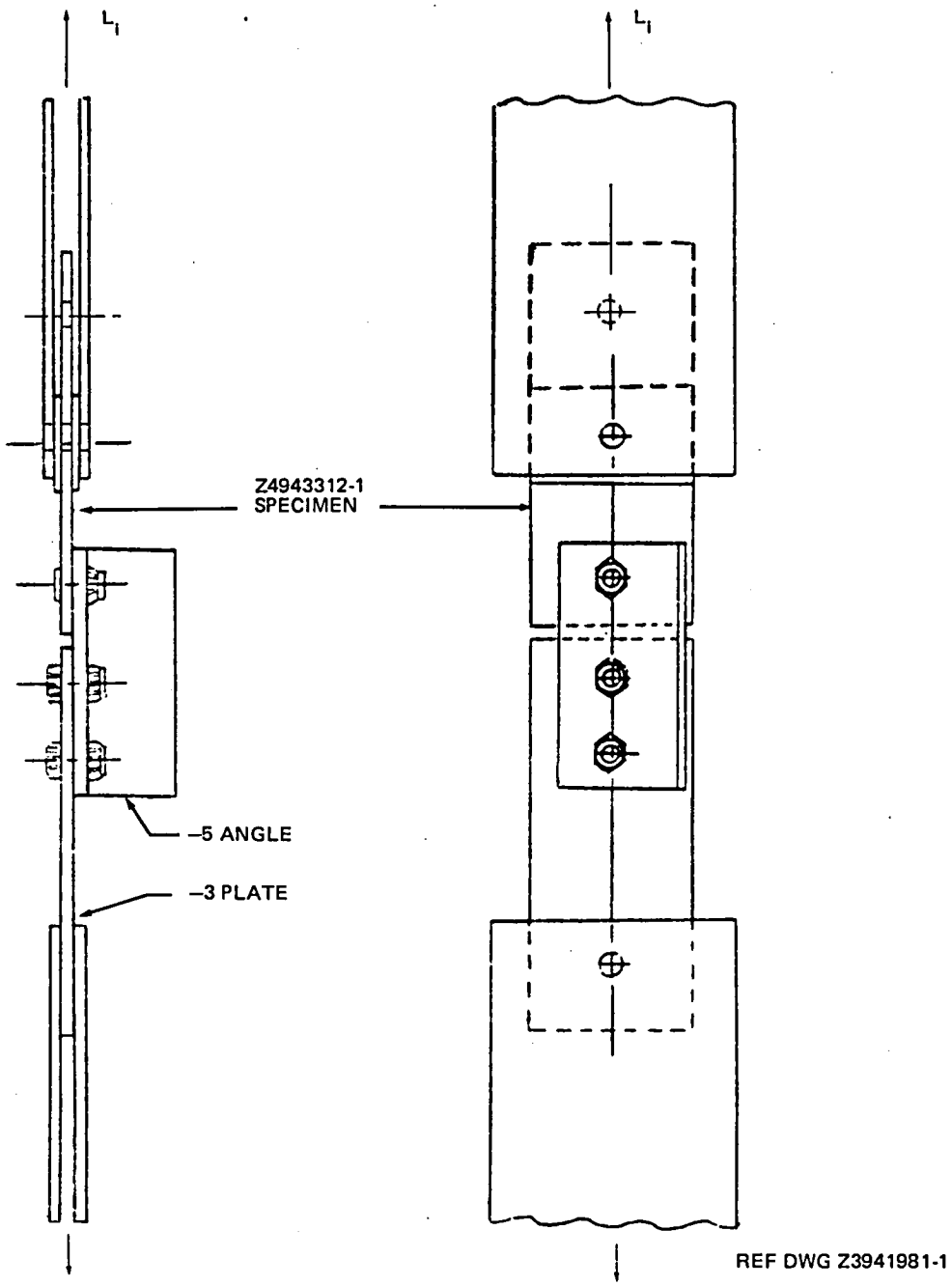

NOTE: THIS SPECIMEN IS DESIGNED TO REPRESENT THE SINGLE SHEAR MODE OF ATTACHMENT OF THE HINGE FITTING TO THE SPAR FLANGE/SKIN COMBINATION. AFTER THE FAILURE AT ONE END, THE SPECIMEN CAN BE LOADED THROUGH THE OTHER END FOR A SECOND TEST.

FIGURE 13. TEST SETUP FOR BOLT BEARING TEST

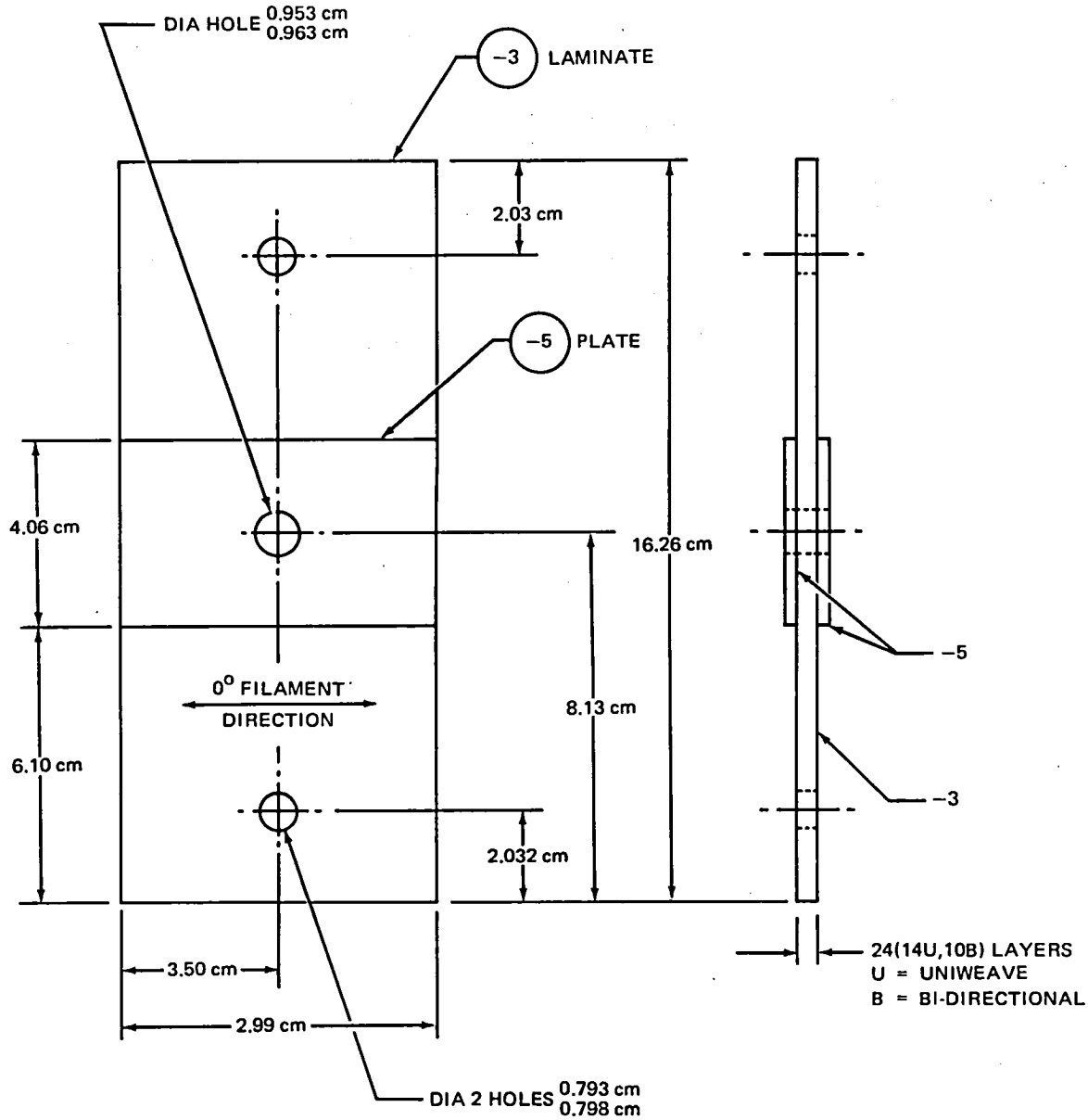

[0, 45, 90, −45, −45, (90-0)*, (±45)*, (90-0)*, (±45)*, (∓45)*, (0-90)*, (∓45)*, (0-90)*, 45, −45, 90, 45, 0 (0-90)*, 45, −45, −45, 45, (90-0)*]$_T$

( )* = BI-DIRECTIONAL

DRAWING NO. Z4943312

2	−5	PLATE	0.254 BY 5.1 BY 7.6	STL SHEET 4130
1	−3	LAMINATE	24[14U, 10B] LAYERS BY 7.6 BY 17.8	T300/N5208 BROADGOODS GRAPHITE/EPOXY
	IDENTIFYING NO.	NOMENCLATURE OR DESCRIPTION	STOCK SIZE cm	MATERIAL DESCRIPTION

FIGURE 14. SPECIMEN ASSEMBLY – BEARING STRESS TEST GR/EP BROADGOODS

Fatigue Test (three specimens)

Loading = ±3003 N (±675 lb)

1. Cycles to Failure = 464,000
2. Cycles to Failure = 605,000
3. Cycles to Failure = 361,000

These tests were conducted at room temperature and normal humidity conditions. Environmental degradation factors should be no worse than for other T300/N5208 graphite/epoxy structures. The results of the tests on the two types of specimens (i.e., the bidirectional broadgoods versus the 7.62-cm tape specimens) are shown in Table 10.

TABLE 10
FATIGUE TEST RESULTS

RUDDER PROGRAM	SPECIMEN P/N LAY UP	NOMINAL t	STATIC TEST		FATIGUE TEST	
			LOAD	F_t	LOADING	AVG CYCLES
ORIGINAL (3-IN. TAPE)	Z3941117-501 $[0^o/\pm45^o/90^o]_s$	1.12 MM (0.044 IN.)	4982 N (1120 LB)	397.2 MPa (56,600 PSI)	±3003 N (±675 LB)	465,000
NEW (BROAD-GOODS)	Z3943311 $[(0\text{-}90)^*(\pm45)^*]_s$	1.37 MM (0.054 IN.)	5649 N (1280 LB)	344.6 MPa (49,980 psi)	±3003 N (±675 LB)	477,000

*BIDIRECTIONAL BROADGOODS

Test 2 — Bolt Bearing Tests. — The purpose of this test was to compare the bearing strength properties of woven broadgoods (current rudder program) with the properties for 7.62-cm tape (original rudder program), where both material forms contained only T300/N5208 graphite/epoxy prepreg. The layup of the bearing specimens was pseudoisotropic and representative of the combined skin and spar flange at the drive hinge attach points.

The test specimen used for the current program is described in Figure 14 and has a layup equivalent to the tape specimens used for the bolt bearing tests of the original rudder program. This specimen was designed so that two tests could be conducted on each specimen. Six specimens were fabricated and a total of 12 tests were conducted using the test setup shown in Figure 13.

The test results are given in Table 11 along with the computation for the standard deviation. The comparison of the bearing strengths shown in Table 12

TABLE 11

BOLT-BEARING TEST RESULTS (RT AND DRY HUMIDITY)

SPECIMEN NO. (i)	Li FAILURE LD (kN)	$Li\text{-}L_{AVG}$ (kN)	FAILURE DESCRIPTION
1	27.69	−1.51	BOLT TENSION
2	31.47	2.27	COMPOSITE BEARING
3	27.25	−1.96	BOLT TENSION
4	28.02	−1.18	BOLT TENSION
5	29.87	−0.67	COMPOSITE BEARING
6	29.02	−0.18	COMPOSITE BEARING
7	27.36	−1.85	BOLT TENSION
8	29.47	0.27	BOLT TENSION
9	27.85	−1.36	BOLT TENSION
10	32.32	3.11	COMPOSITE BEARING
11	30.58	1.38	BOLT TENSION
12	29.51	0.31	BOLT TENSION
AVG	29.20		

$$\text{STANDARD DEVIATION} = \left[\frac{1}{n-1}\Sigma(Li\text{-}L_{AVG})^2\right]^{1/2} = \frac{[29.95]^{1/2}}{11}$$

$$= 1.65 \text{ kN}$$

TABLE 12

COMPARISON OF BEARING STRENGTH

	NEW RUDDER PROGRAM	ORIGINAL RUDDER PROGRAM
AVERAGE LOAD (kN)	29.20	27.17
STANDARD DEVIATION (kN)	1.65	1.94

indicates that the bearing strength for the rudder of the current program is greater than for the original rudder program and the scatter is less. Thus, it will be conservative to use the "A" value and "B" value bearing strength allowables from the data gathered under contract NAS1-12954 for stress analysis purposes.

Test 3 — Subcomponent Vibration Shake Test. — Vibration tests were conducted on a box component (Figure 15) representing the upper end of the composite rudder. The component consisted of the upper eight rib-bays of the rudder, the upper hinge and actuator fitting installations, and appropriate sections of the leading edge, trailing edge, and tip installations. The

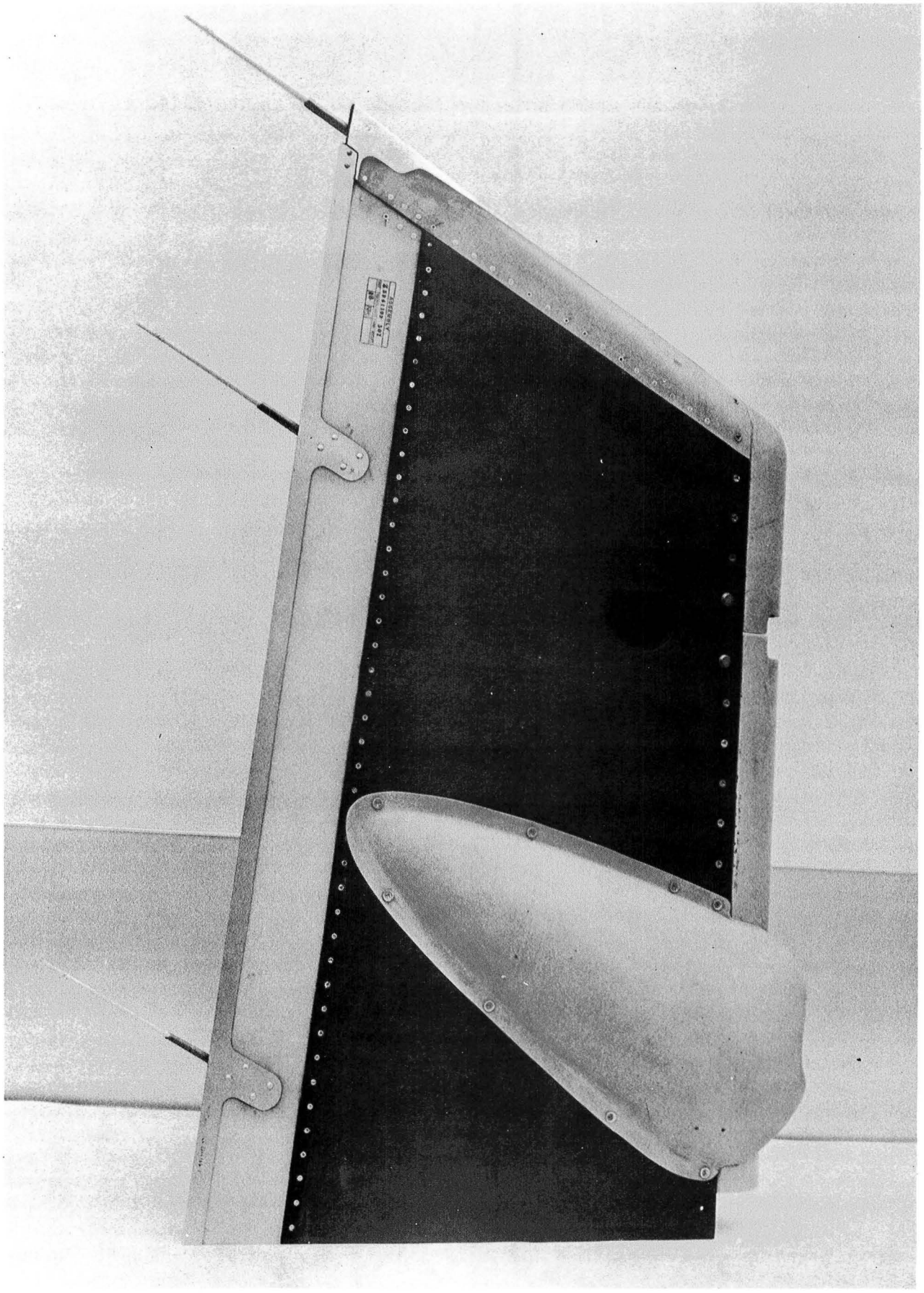

FIGURE 15. BOX COMPONENT – VIBRATION TEST

aerodynamic fairing for the upper actuator fitting was also installed as shown in Figure 15. The component was mounted on a vibration test machine using production pushrods and attaching hardware as shown in Figure 16. The aerodynamic fairing was removed in Figure 16 for clarity.

Prior to the vibration test, the rudder component was inspected by ultrasonic scan and some areas of suspected debonding were detected and marked on the rudder to compare with a posttest scan to establish whether any growth of the debonded areas occurred due to vibration.

A modal survey was conducted first and six channels of strain gages were installed to monitor stresses in the component at selected locations on the skin panels. A random vibration environment, based on measured service conditions at the DC-10 fin tip and on acoustic levels at the upper rudder, was then applied to the specimen. The random vibration input, over a frequency bandwidth from 350 to 1800 Hz, was equivalent to 8.6-g root-mean-square lateral acceleration of the rudder.

The random vibration test was conducted for 46.5 hours, the time required to accumulate 100 million stress cycles in the critical skin panel. This input exceeded the maximum vibration levels encountered in service due to impinging noise and random vibration. At the conclusion of 46.5 hours of testing, a check was made to determine if there had been any change in the previously determined rudder rotation frequency.

The frequencies of the rotation mode and two other modes were measured following the random test. Comparisons of pretest and posttest frequencies are listed below.

Modal Frequencies

Pretest (Hz)	Posttest (Hz)
53 (rotation)	53
111	108.9
174	Not read
197	195.2

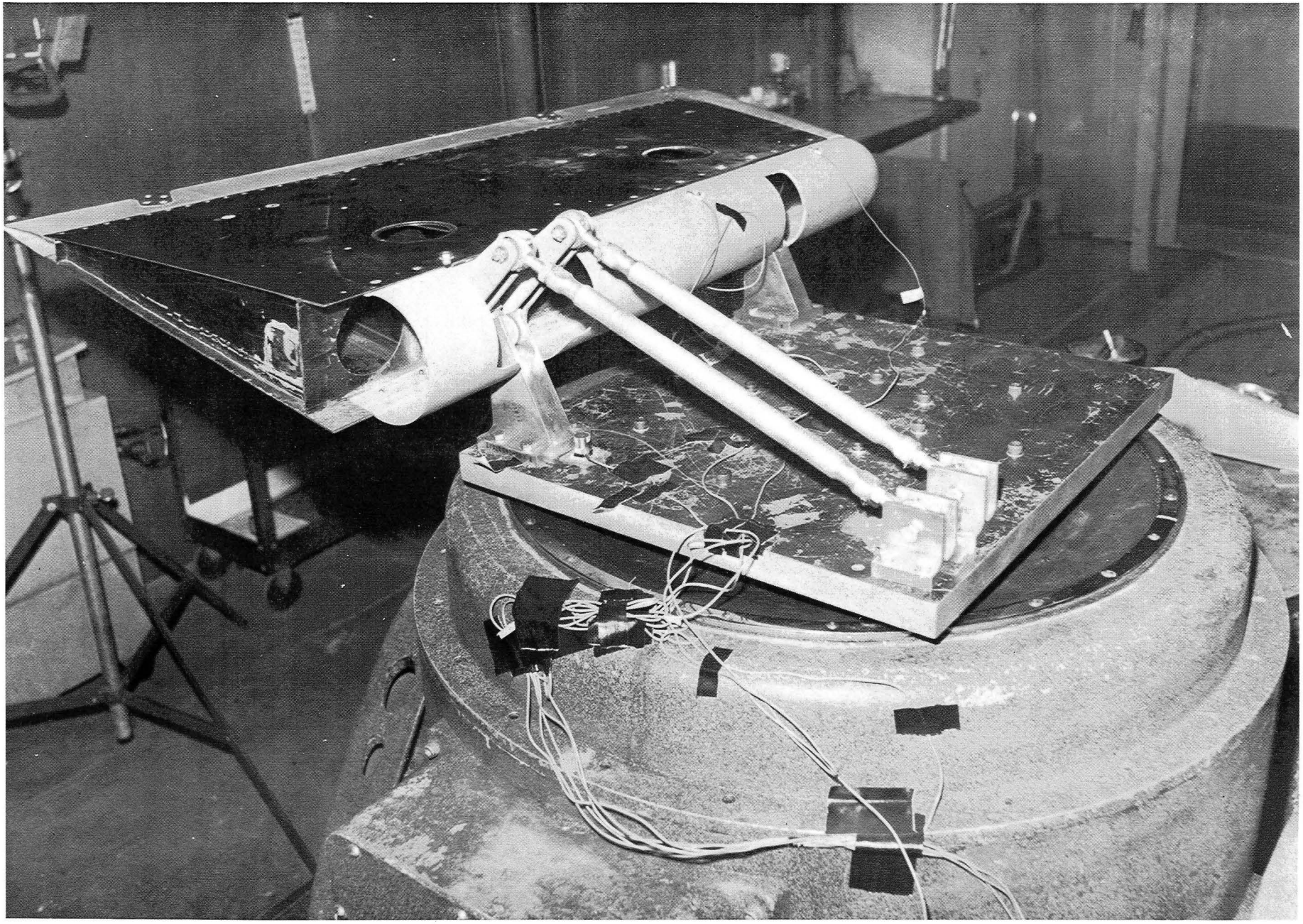

FIGURE 16. BOX – VIBRATION TEST SETUP

Following the vibration test, the rudder section was inspected using the ultrasonic scan and there were no new debonded areas, nor any changes in the pretest debonded areas.

In a separate test with a dwell at the rotation frequency of 53 Hz, the frequency held constant at 53 Hz for 1 hour, then changed from 53 Hz to 51.8 Hz for 466 minutes (7.8 hours). The test was terminated at this point since it appeared that the rotation frequency had stabilized.

It was concluded that the vibration equivalent to twice the level experienced in service will not affect the structural integrity of the composite rudder and that Drawing WMC 7028, Rudder Assembly – Graphite Composite Upper Rudder, complies with the acoustic and vibration structural requirements of the FAA.

Test 4 – Modal Survey Vibration Test and Flutter Analysis. — In order to evaluate the flutter and dynamic characteristics of the woven broadgoods rudder, sinusoidal resonance tests were performed on a complete rudder to obtain the first three resonant frequencies and modes of vibration (Figure 17). Then, the identical modal survey was performed on a tape composite rudder manufactured under Contract NAS1-12954. These tests were conducted as follows:

The upper aft rudders were each suspended on strings, measurement stations were marked, and a 155.7-N peak force shaker attached as shown in Figure 17. The rudder was excited with constant peak force sinusoidal inputs while the frequency was varied from 5 to 200 Hz. Acceleration-versus-frequency response plots were made for each rudder configuration. The first three resonant vibration mode shapes were recorded by measuring and plotting accelerations at many locations along the surface while vibrating at the resonant frequencies. Node lines were plotted as points of zero acceleration in each of the vibration modes.

These laboratory vibration tests of the new composite upper aft rudder were performed to assess whether the change in construction significantly affected the rigidity of the rudder. Table 13 is a summary comparison of test frequencies of the tape layer and woven broadgoods designs. As can be seen, the woven broadgoods design exhibited slightly higher frequencies than did the tape layer design. The mode shapes did not change significantly between the

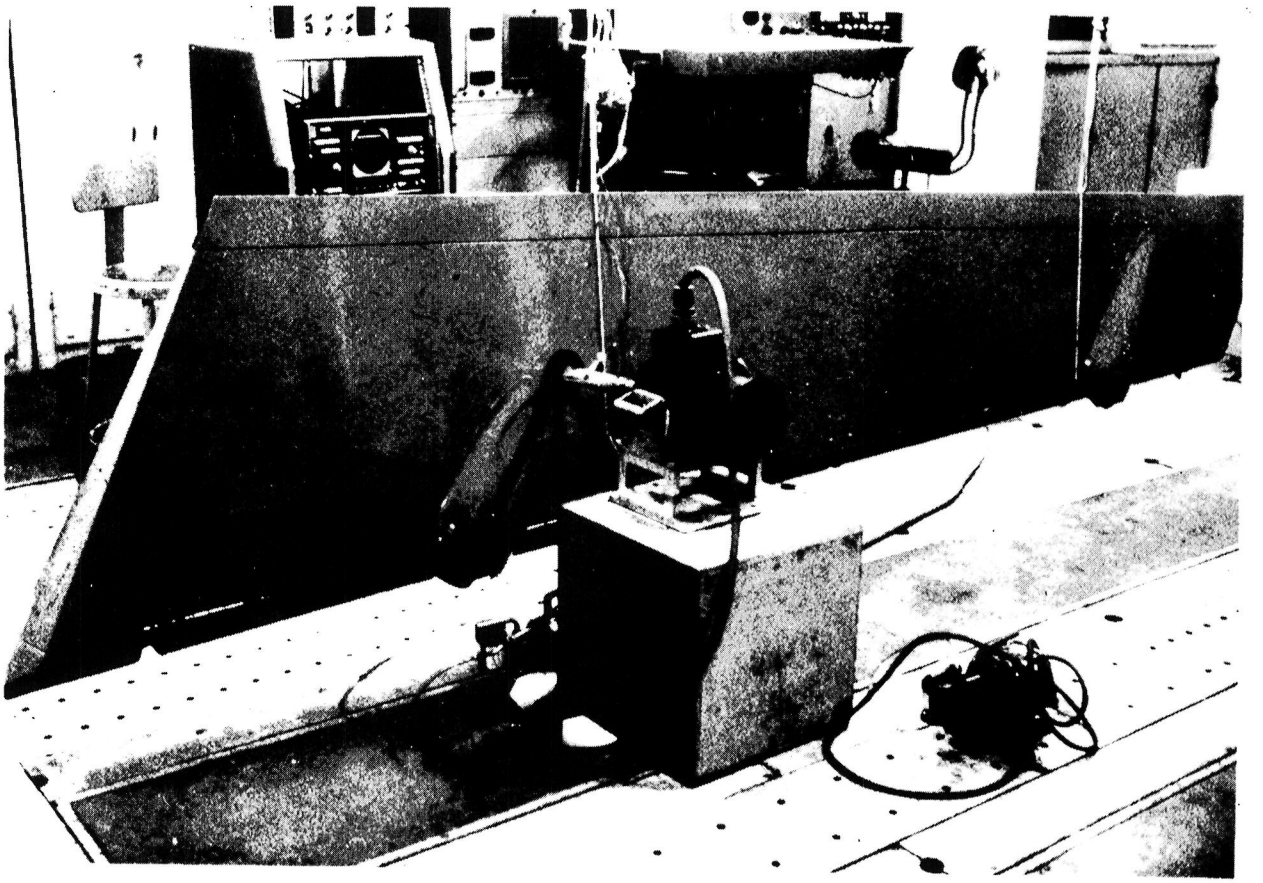

FIGURE 17. SIMPLE LINE SUSPENSION FOR FREE-FREE RUDDER MODAL SURVEY

TABLE 13

DC-10 COMPOSITE UPPER AFT RUDDER FREQUENCIES

MODE	–501 RUDDER* Hz	–503 RUDDER** Hz
1	34.9	38.3
2	73.1	80.8
3	93.3	96.7

*—501 RUDDER IS "TAPE LAYER" CONSTRUCTION
**—503 RUDDER IS "WOVEN BROADCLOTH" CONSTRUCTION

rudders. The data show that the woven broadgood construction increases the first spanwise bending frequency by 9.7 percent, torsion by 10.5 percent, and second spanwise bending by 3.6 percent.

It has been shown that higher aft rudder frequencies are beneficial to flutter speed. Therefore, it is concluded that the flutter speed with the woven broadgoods design will be equal to, or greater than, that of the tape layer design.

SECTION 5
CURE OF THE TEST RUDDER BOX AND RESULTS

One ship-set of graphite/epoxy rudder parts consisting of ribs, front and rear spar, and skins was predensified at 394°K (250°F) for 1 hour at vacuum pressure and stored in a freezer at 255°K (0°F). When all was in readiness, the graphite/epoxy parts were removed from storage, warmed to room temperature, removed from sealed wrappers, and loaded into the rudder molding tool along with the internal metal and rubber mandrels. The steel side plates were bolted into place and the molding tool was rolled into the oven. The thermocouple and heater wire harness terminals were connected to the microprocessor and the rudder box curing procedure was started. The oven was set at a constant 505°K (450°F) during the heat-up period of 4-1/2 hours, at which time all functioning thermocouples indicated 450°K (approximately 350°F). This was considered the start of the cure, and the oven temperature was reduced to 450°K (350°F). This situation continued relatively constant, and the end of cure occurred 2-1/4 hours later, at which time the oven was opened. The molding tool was rolled out of the oven and allowed to cool down overnight.

During the cure, 99 thermocouples in contact with the rudder and the molding tool were monitored. The rudder locations of these thermocouples, as well as typical teletype printouts of temperature readings, are given in Appendix C. Appendix C also contains a survey and plot of skin temperatures through the heat-up and cure periods.

To open the molding tool (PLM), the steel side plates and the closing bars were first removed, thereby permitting the rudder box to be removed by lifting upward. Considerable difficulty was encountered in lifting the rudder box. This was later thought to be caused by the shift of the internal metal mandrels, which in turn was attributed to the use of 6.35-mm (0.25-inch) Teflon insulation plates at the base of each metal mandrel heater spike (see Figure 18).

The external surfaces of the side skins and rear spar were well formed and appeared to have very satisfactory resin content. However, when the rudder was lifted off the PLM, it became apparent that the front spar and ribs were damaged extensively. Due to the difficulty of viewing the damage inside the rudder, the rudder was dissected by a cut made parallel to the front spar and

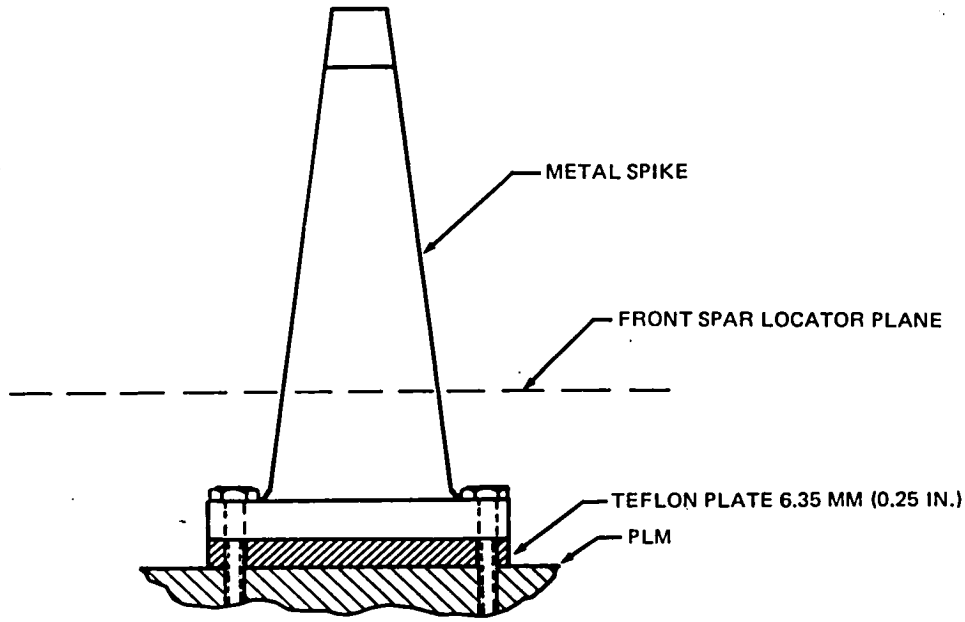

FIGURE 18. DIAGRAM OF 6.35 MILLIMETER (0.25 INCH) TEFLON PLATE AT BASE OF THE PLM METAL SPIKE

5.08 cm (2 inches) aft of the front spar to produce a forward and aft portion of the rudder. Subsequent cuts of the forward portion perpendicular to the front spar provided excellent views of the front spar web cracks. Front spar and rib damage are shown in Figures 19 to 26. A list of the problems encountered with the test rudder box cure is given in Table 14, together with probable causes and the proposed remedies.

The rib indentations (Problem 1 of Table 14) run in the lengthwise direction of most of the rudder ribs. These indentations line up with the edges of the central section of the rubber mandrel between the rib web and the metal mandrel. Location measurements of the rib webs indicate that the central portions of each rib web adjacent to the rib flanges are displaced from their correct locations. From these observations, it was concluded that the rib indentations resulted from loading the molding tool, starting from one end, with rubber mandrels and densified graphite/epoxy details that were too large for the available space in the PLM. These oversize rubber mandrels and graphite/epoxy details, as they were being loaded into the PLM, tended to cause the outer edges of the ribs to be displaced from the central portions of the rib (see Figures 19, 25 and 26).

TABLE 14
TEST RUDDER CURE – LIST OF PROBLEMS

PROBLEM	PROBABLE CAUSE	PROPOSED SOLUTION
1. RIB INDENTATIONS (SEE FIGURES 11 AND 12)	RIB WEBS WERE DEFORMED DURING TOOL LOADING: TOO THICK GR/EP RIB ITEMS TOO MUCH RUBBER	USE MORE ADVANCED DENSIFICATION: 121.1°C (250°F), 3690 PA (100 PSI), 1 HOUR RIBS, FRONT SPAR, SKINS, BLEEDER CLOTH REDUCE RUBBER BY GRINDING OR SANDING
2. RIB FAILURES (SEE FIGURES 9 AND 12)	RIB INDENTATIONS AT TOOL LOADING SQUEEZE OF SKINS AT TOOL LOADING TOOL SPRING BACK AT COOL-DOWN POOR CORNER RADII	MORE ADVANCED DENSIFICATION MORE ADVANCED DENSIFICATION DRILL HOLES IN RUBBER TO REDUCE PRESSURE BOLT UNTORQUING AT OPTIMUM TEMPERATURE STIFFEN TOOL SIDE PLATES RADIUS RUBBER MODERATELY
3. FRONT SPAR CRACKS (SEE FIGURES 7 AND 8)	SQUEEZE OF SKINS AT TOOL LOADING POOR CORNER RADII EXCESSIVE TOOL SPRING-BACK THERMAL STRAIN DUE TO F/S LOCATOR	EXTRA SKIN DENSIFICATION RADIUS RUBBER MODERATELY SAME AS FOR PROBLEM 2 RELAX FIT OF ACCESS HOLE METAL DISCS TO METAL MANDRELS
4. THERMOCOUPLE DENTS IN FRONT SPAR WEB (SEE FIGURE 10)	RELATIVE MOVEMENT OF FRONT SPAR LOCATOR WITH RESPECT TO THE THERMOCOUPLE SUPPORT PINS	THREAD THE SUPPORT PINS AND ADD JAMB NUT UNDER FRONT SPAR LOCATOR
5. LOOSE METAL MANDRELS AFTER CURE CYCLE	DEFORMATION OF 1/4-INCH TEFLON PLATE AT BASE OF EACH METAL MANDREL	REMOVE THE TEFLON PLATE AND REPLACE BY ONE OF ALUMINUM
6. DIFFICULT REMOVAL OF RUDDER AND F/S LOCATOR FROM MOLDING TOOL	PROBLEM 5	SAME AS FOR PROBLEM 5

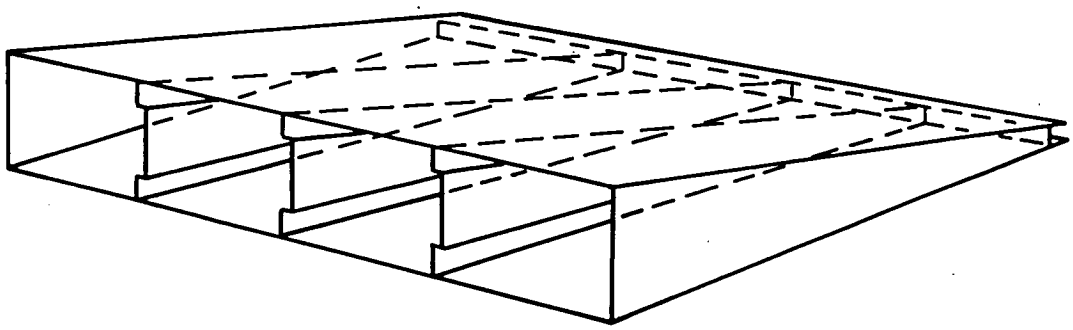

FIGURE 19. RIB INDENTATIONS

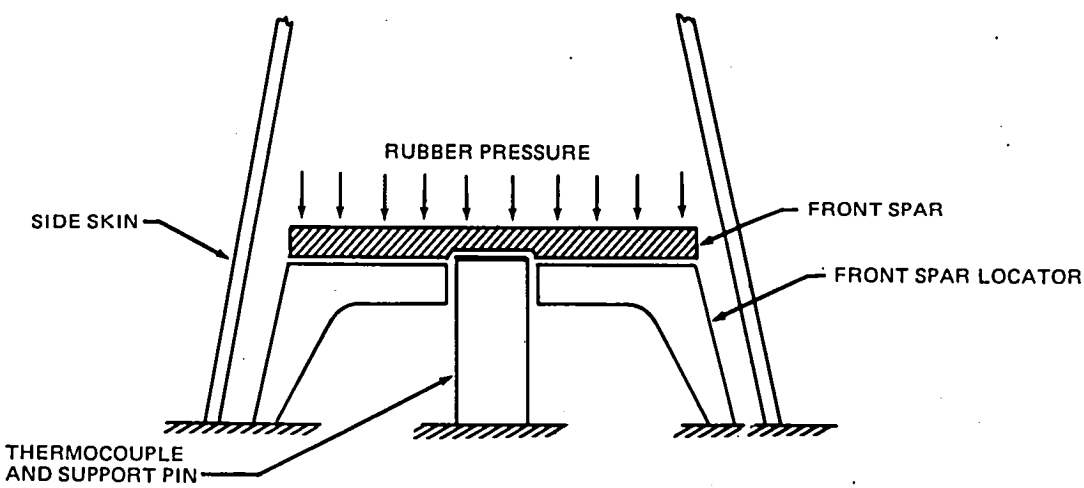

FIGURE 20. THERMOCOUPLE INDENTATIONS

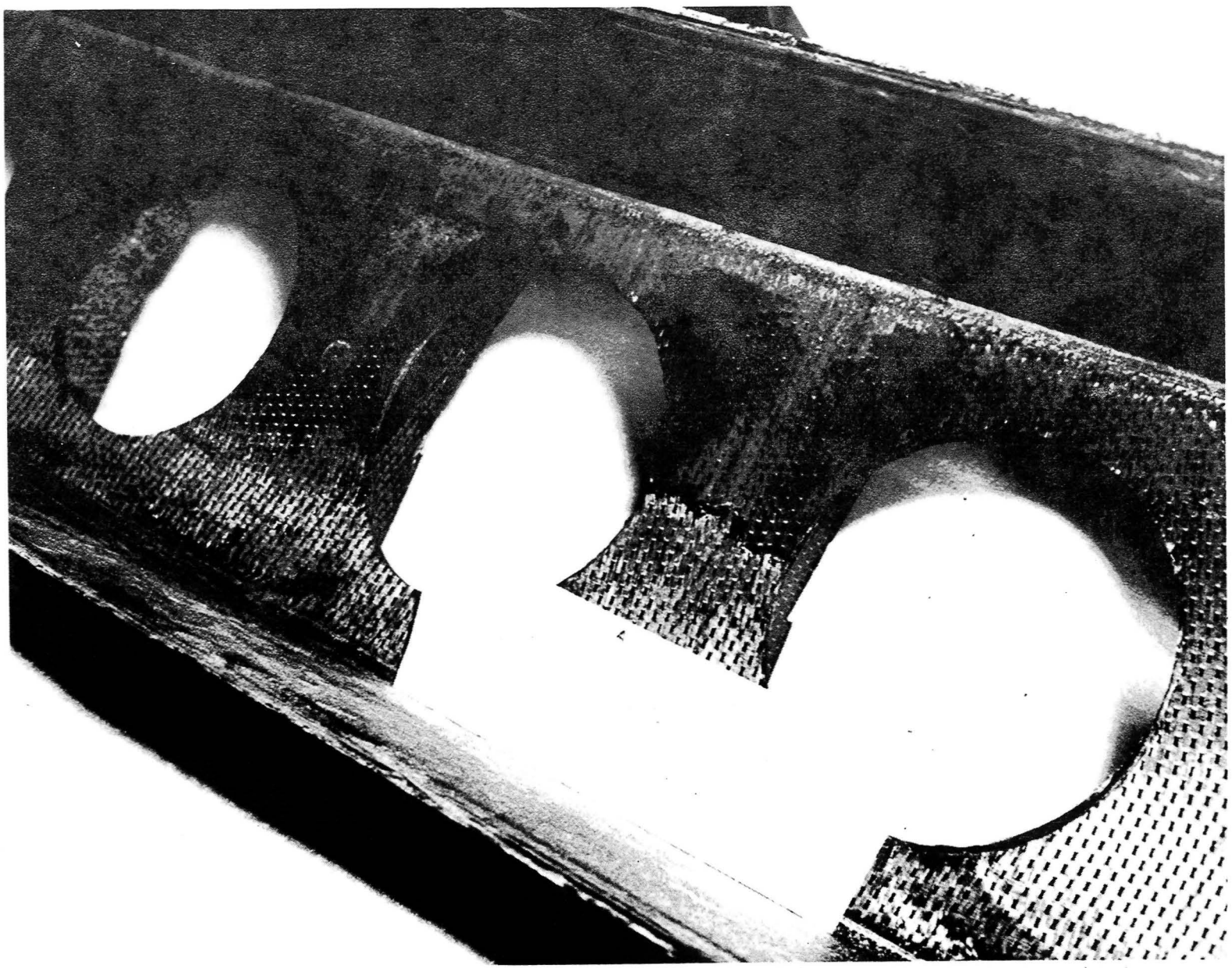

FIGURE 21. FRONT SPAR WEB DAMAGE – STA Z_{AR} = 482.10

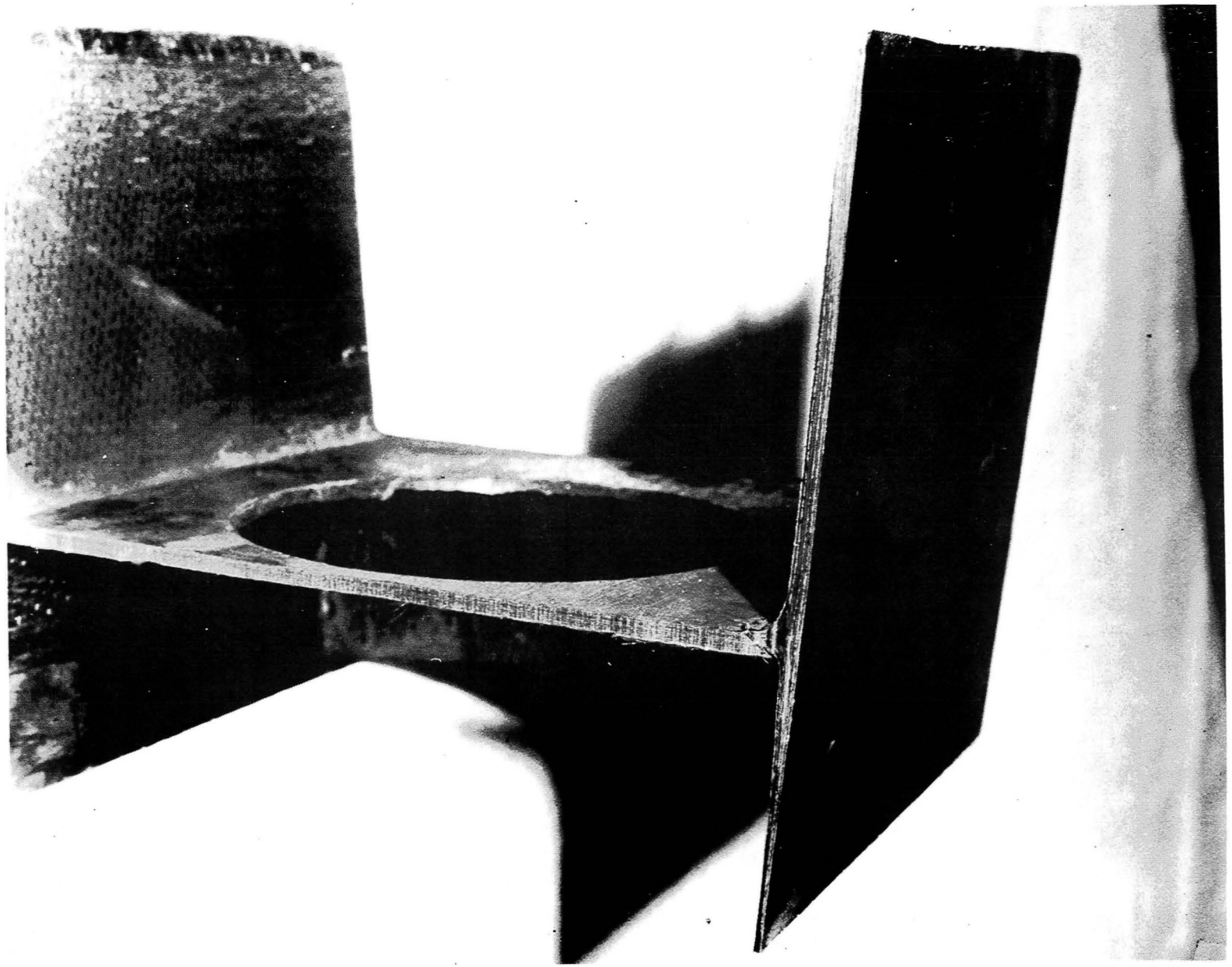

FIGURE 22. FRONT SPAR WEB TO FLANGE DAMAGE

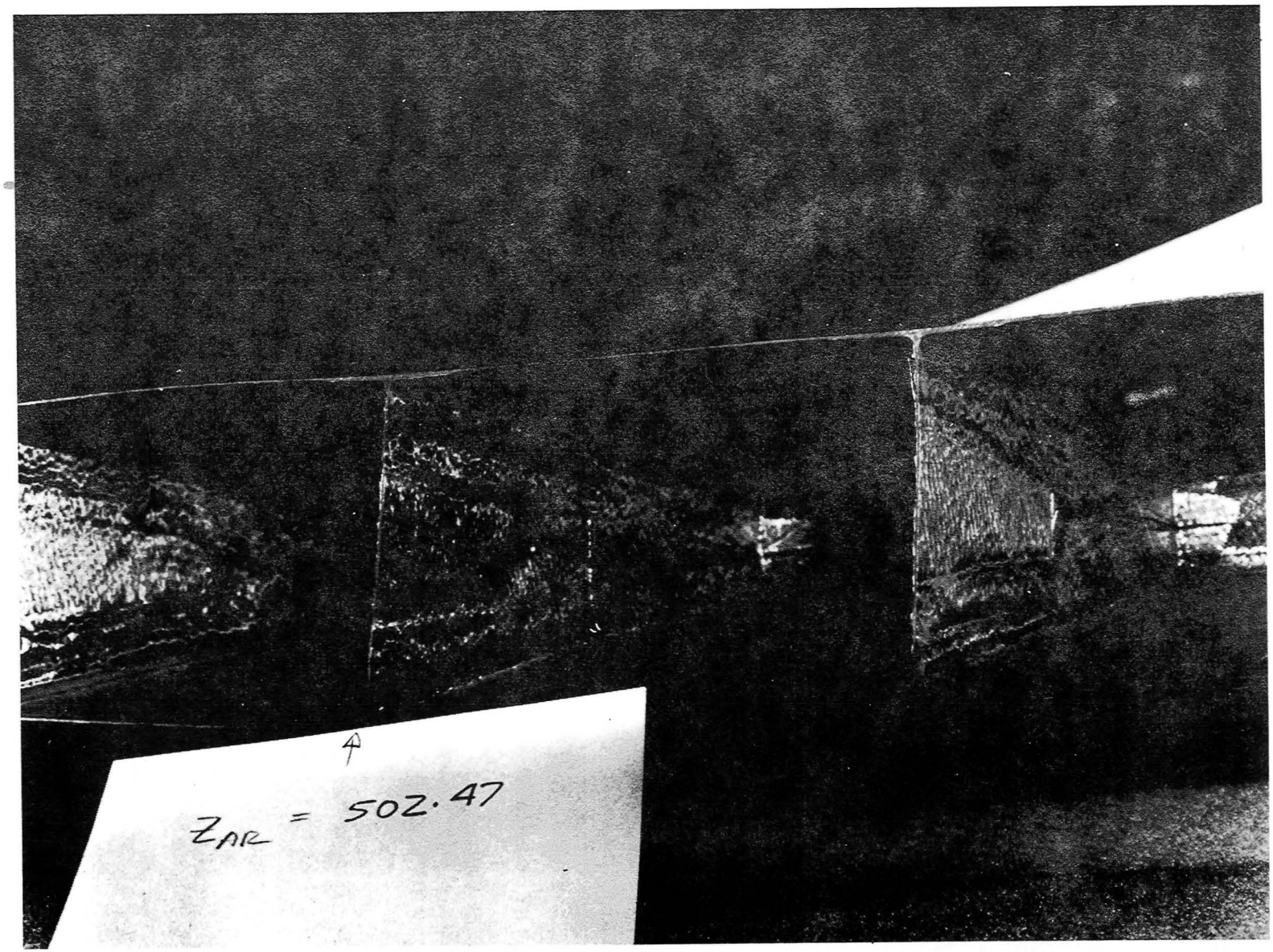

FIGURE 23. RIB WEB DAMAGE – STA Z_{AR} = 502.47

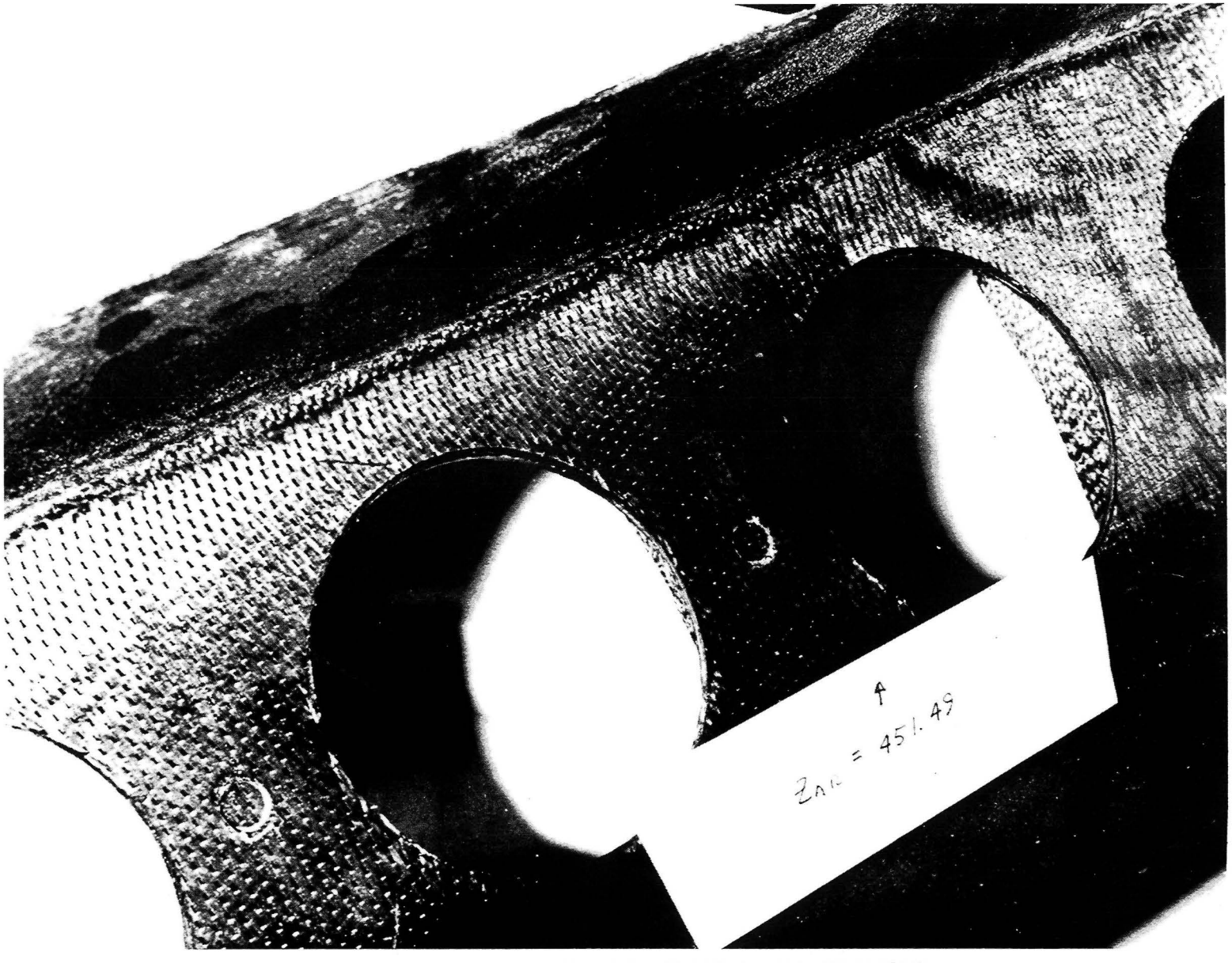

FIGURE 24. FRONT SPAR WEB THERMOCOUPLE INDENTATIONS

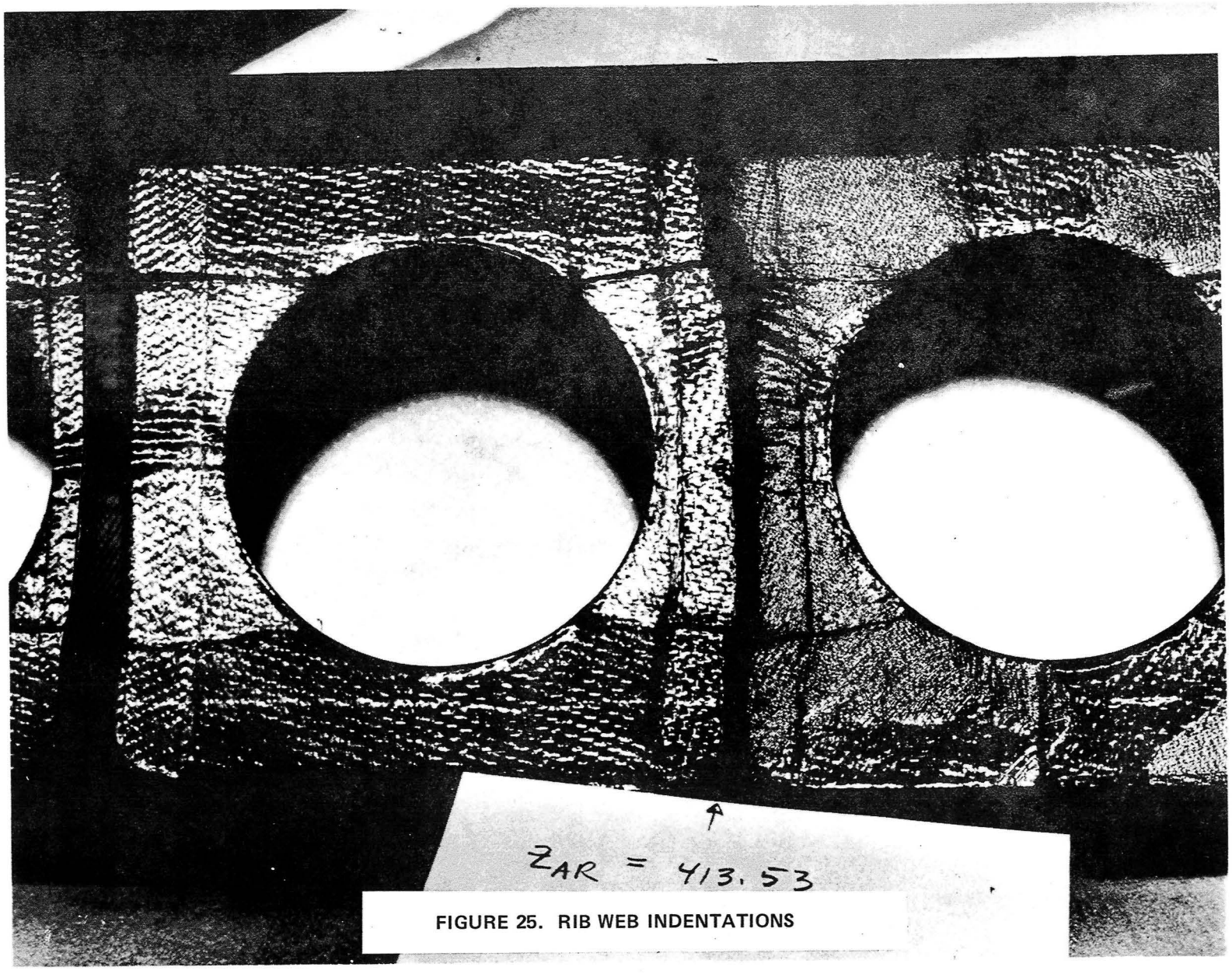

FIGURE 25. RIB WEB INDENTATIONS

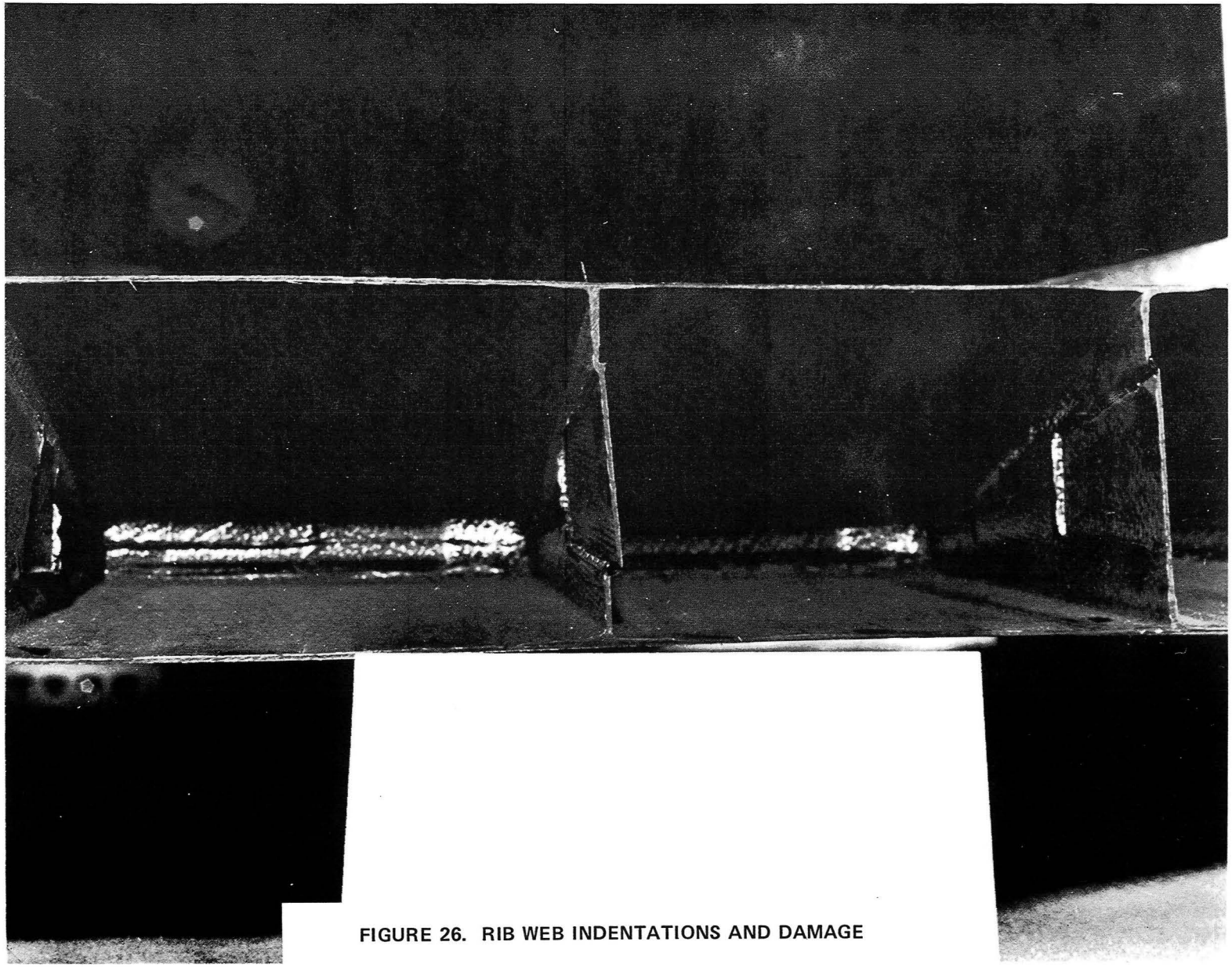

FIGURE 26. RIB WEB INDENTATIONS AND DAMAGE

Rib and front spar web failures (Problems 2 and 3 of Table 14) were caused primarily by the spring-back of the rudder box molding tool during tool cool-down. During heat-up, the trapped rubber expands and exerts considerable pressure on the PLM steel side plates. These plates deflect due to the rubber pressure and the rudder box skins gel against the steel side plates in this oversize condition. When the cure is complete, the cooldown phase commences. As the rubber pressure gradually reduces to zero, the steel side plates tend to spring back and exert pressures on the rudder box inside the steel molding tool. Gradually, the allowable compressive strains in the rib and front spar webs were exceeded, resulting in failure.

The thermocouple indentations (Problem 4 of Table 14) were between 0.254 mm (0.010 inch) and 0.381 mm (0.015 inch) deep and occurred in the forward face of the front spar web at a critical section (midway between the front spar web access holes and an equal distance from the left and right front spar flanges). The front spar locator is not supported continuously; therefore, during a cure cycle, the rubber pressure produces a bending deflection of the front spar locator. In this condition, the thermocouple support pins penetrate a little above the front spar locator and indent the front spar (see Figures 20 and 24). These indentations occur at a relatively critical front spar section.

SECTION 6
RECOVERY INVESTIGATION

The recovery investigation task was organized to determine the underlying reasons for the unsuccessful attempt to mold the composite rudder box for the test rudder. In addition, it was decided that this investigation should attempt to penetrate deeper into the sensitivity of trapped rubber molding to place it on a sound engineering basis. The following is a list of tasks or investigations undertaken:

1. Resin and void content tests (test rudder box)
2. Shrinkage of DAPCO 38-3 silicone rubber rectangular slabs
3. Mold release spray tests
4. Looseness of internal metal spikes after the test rudder cure
5. Front spar web thermocouple indentations
6. Rubber mandrel oversize investigation
7. Rib web indentations (test rudder box)
8. Coefficient of thermal expansion (DAPCO 38-3 silicone rubber)
9. Bulk modulus tests (DAPCO 38-3 silicone rubber)
10. Resin gel temperature determination
11. Dummy part fabrication and size determination
12. New rubber mandrel casting
13. Front spar reinforcement to resist tool spring-back effects
14. Endurance of rubber mandrels

Task 1 — Resin and Void Content Tests (Test Rudder Box)

Tests to determine the resin and void content values for specimens obtained from the unsuccessful rudder box were carried out. The results are given in Table 15. These values lie within the requirements of DPS 1.621-2 (Douglas Process Specification) and are satisfactory.

TABLE 15
RESIN AND VOID CONTENT – TEST RUDDER BOX

	SKIN	SPAR	RIB WEB	SPAR WEB	DPS J-621-2
PERCENT RESIN CONTENT (PERCENT BY WEIGHT)	23.57	23.08	22.70	24.36	21 TO 31
PERCENT VOID CONTENT (PERCENT BY VOLUME)	0.07	–0.15	0.06	2.08	2 (MAX)
FIBER VOLUME (PERCENT)	70.18	70.90	71.19	67.87	
DENSITY (GM/CU CM)	1.5978	1.6039	1.6026	1.5613	

Task 2 — Shrinkage of DAPCO 38-3 Silicone Rubber Rectangular Slabs

This test was devised to permit comparison of the shrinkage of rectangular slabs of DAPCO 38-3 silicone rubber subjected to various cure cycles.

Molded rubber slabs were cast using DAPCO 38-3 silicone rubber with the addition of 5 percent thinner and 5 percent catalyst. Four castings were made and four different cycles were used to cure them. A description of each rubber slab and each cure cycle is given in Table 16.

Each cured rubber specimen was subjected to three separate heat cycles of 450°K (350°F) for 4 hours. The specimens were unrestrained during these heat cycles. Dimensional measurements were made after each cycle was completed and the specimens had cooled down to room temperature (see Table 17).

The results of this test clearly indicate the advantage of rubber cure cycle No. 2, since shrinkage due to cure cycles No. 1 and 2 shows a reduction from 0.002 m (0.080 in.) to 0.0003 m (0.010 in.) (Table 17, Column 5).

TABLE 16

DAPCO 38-3 SPECIMENS AND CURE CYCLE DESCRIPTION FOR SHRINKAGE TEST

	SPECIMEN			
	NO. 1	NO. 2	NO. 3	NO. 4
	PLAIN RUBBER (OLD CURE CYCLE) (HOURS)	PLAIN RUBBER (NEW CURE CYCLE) (HOURS)	PLAIN RUBBER (NEW CURE CYCLE) (HOURS)	RUBBER WITH METAL SCREENING (NEW CURE CYCLE) (HOURS)
	CAST SILICONE RUBBER SPECIMENS AND CURE IN MOLD			
R.T. (HOURS)	48	48	96	48
65.6°C (IN (150°F) MOLD)	2	2	2	2
	REMOVE FROM MOLD FOR POSTCURE			
93.3°C (200°F)	–	4	4	4
121.1°C (250°F)	2	4	4	4
148.9°C (300°F)	–	4	4	4
176.7°C (350°F)	2	4	4	4

TABLE 17

DAPCO 38-3 SPECIMEN SHRINKAGE VERSUS TIMES AT 176.7°C (350°F)

①	②	③	④	⑤	⑥	⑦	⑧	⑨	⑩
		SPECIMEN DIMENSION							
SPECIMEN	DIMENSION	ORIGINAL CASTING	AFTER ORIGINAL CURE	SHRINKAGE DUE TO CURE	AFTER HEAT CYCLE NO. 1	AFTER HEAT CYCLE NO. 2	AFTER HEAT CYCLE NO. 3	SHRINKAGE DUE TO HEAT CYCLING m, (IN.) TOTAL	PER UNIT
NO. 1	h	0.423 (16.655)	0.421 (16.575)	0.002 (0.080)	0.420 (16.550)	0.420 (16.534)	0.420 (16.530)	0.001143 (0.045)	0.00270
	w	–	0.0833 (3.280)		0.0830 (3.268)	0.083 (3.270)	0.0829 (3.265)	0.000381 (0.015)	0.00457
	t	–	0.0391 (1.540)		0.0389 (1.530)	0.0388 (1.528)	0.0386 (1.520)	0.000508 (0.020)	0.0130
NO. 2	h	0.422 (16.610)	0.422 (16.600)	0.0003 (0.010)	0.420 (16.550)	0.420 (16.550)	0.420 (16.550)	0.001270 (0.050)	0.00301
	w	–	0.0815 (3.210)		0.0810 (3.190)	0.0815 (3.210)	0.0815 (3.210)	0	0
	t	–	0.0401 (1.578)		0.0395 (1.555)	0.0395 (1.555)	0.0394 (1.552)	0.000660 (0.026)	0.0165
NO. 3	h	0.421 (16.588)	0.421 (16.572)	0.0004 (0.016)	0.420 (16.550)	0.418 (16.475)	0.418 (16.475)	0.002464 (0.097)	0.00585
	w	–	0.0826 (3.250)		0.0824 (3.245)	0.0824 (3.245)	0.0824 (3.245)	0.000127 (0.005)	0.00154
	t	–	0.040 (1.560)		0.0392 (1.545)	0.0392 (1.545)	0.0392 (1.545)	0.000381 (0.015)	0.00962
NO. 4	h	0.421 (16.585)	0.421 (16.575)	0.0003 (0.010)	0.421 (16.575)	0.421 (16.575)	0.421 (16.575)	0	0
	w	–	0.0841 (3.310)		0.0841 (3.310)	0.0841 (3.310)	0.0841 (3.310)	0	0
	t	–	0.0391 (1.540)		0.0384 (1.510)	0.0384 (1.510)	0.0381 (1.500)	0.00102 (0.04)	0.0260

Task 3 — Mold Release Spray Tests

With a view to reducing the amount of bulk inside the PLM, it was proposed that mold release spray be substituted for the 0.0762-mm-thick (0.003-inch-thick) Teflon tape used in the manufacture of the first ten rudders for protecting the rubber mandrels and providing a nonstick surface. Ease of applying a liquid release agent as compared with Teflon tape was the basic consideration. Sample sprayed-on coats of 0.0508/0.0762 mm (0.002/0.003 inch) thick were tried. The samples were cured for

16 hours minimum	at room temperature
2 hours	at 339°K (150°F)
2 hours	at 394°K (250°F)

The release agent worked well as a release for rubber mandrels used in a mold. However, its inability to slide against itself made it inappropriate for application to the rudder rubber mandrels.

Task 4 — Looseness of Internal Metal Spikes After the Test Rudder Cure

The looseness of the internal metal spikes and the difficulty of removing the rudder and front spar locator from the molding tool, as described in Table 14, were attributed to the 6.35-mm (0.25-inch) Teflon plate at the base of each metal spike (Figure 18). These were replaced by aluminum plates of equal thickness and size. During a subsequent trial assembly of the molding tool, it was discovered that the rubber mandrels used for the unsuccessful rudder cure did not fit well with the newly assembled metal mandrels. Thus, it was resolved that new rubber mandrels would have to be cast before an attempt was made to cure another rudder box as it would be too difficult to orient the metal mandrels to fit the existing rubber.

Task 5 — Front Spar Web Thermocouple Indentations

The thermocouple indentations (Figures 20 and 24) were between 0.254 and 0.382 mm (0.010 and 0.015 inch) deep and occurred in the forward face of the

front spar web at a critical section (midway between the front spar web access holes and an equal distance from the front spar flanges). This problem was eliminated by threading the support pins and adding jamb nuts under the front spar locator (see Figure 27). A height adjustment nut was also added at the base of each thermocouple pin.

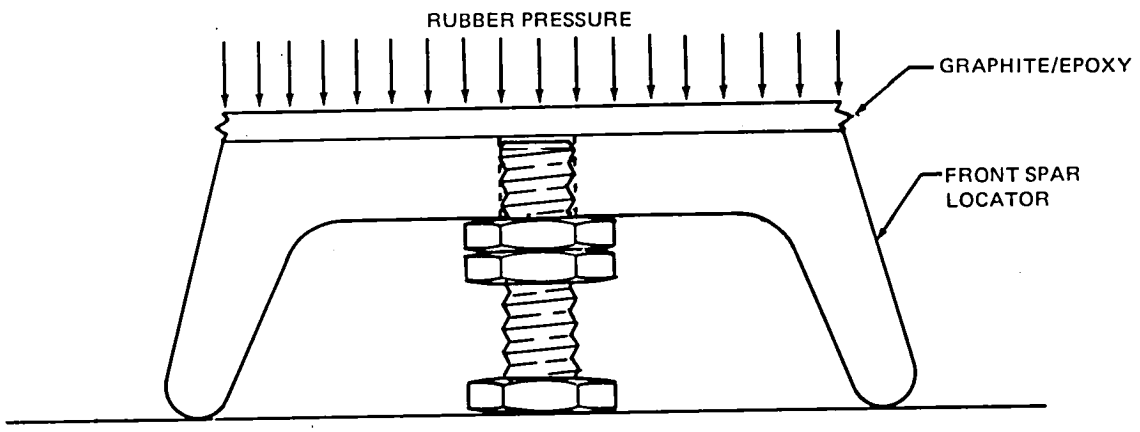

FIGURE 27. MODIFICATION OF THERMOCOUPLE PIN INSTALLATION TO PREVENT F/S INDENTATIONS

Task 6 — Rubber Mandrel Oversize Investigation

The extensive front spar and rib cracks (see Figures 21 to 26) in the unsuccessful rudder box were indicative of very high rubber pressure, which meant that the rubber mandrels were oversize. This led the investigators to theorize that the rudder thickness may be oversize since the molding tool side plates would deflect excessively under high rubber pressure. Measurements of the height of the front spar indicated a possible oversize of 3.30 mm (0.130 inch). Calculations based on this oversize front spar produced a computed rubber pressure of 5.28 MPa (766 psi) (see Appendix B).

Subsequent investigations revealed that the front spar locator, which was used to locate the dummy part for casting the front spar rubber mandrels, was 4.064 mm (0.160 inch) oversize. Because the front spar rubber mandrels were used to locate the dummy part for casting the internal rubber mandrels, the resulting internal mandrels were cast 4.064 mm (0.160 inch) oversize at the front spar and tapered down to the proper size at the rear spar.

It was resolved that new rubber mandrels would be needed for the next rudder cure and that the new rubber mandrels would be thoroughly inspected

before use to avoid the possibility of a size error. The measurements resulting from this inspection are described in Task 12 and also in Appendix P.

Task 7 — Rib Web Indentations (Test Rudder Box)

It is clear that the size of the rubber mandrels and the B-stage woven graphite/ epoxy details must be as small as possible for proper loading of the PLM. Thus, for the next loading of the PLM, the graphite/epoxy details were predensified very close to their final thickness. This densification was done at 394°K (250°F) and vacuum pressure for 30 minutes.

Task 8 — Coefficient of Thermal Expansion (DAPCO 38-3 Silicone Rubber)

Accurate values of the thermal coefficient of expansion for DAPCO 38-3 silicone rubber were necessary to enable the rubber pressure inside the rudder box molding tool to be calculated. Therefore, tests were conducted to determine the linear thermal coefficient of expansion for DAPCO 38-3 silicone rubber with and without embedded wire mesh. A complete description of these tests and the results is given in Appendix F. A summary of the results is given in Table 18.

TABLE 18

RESULTS OF THERMAL EXPANSION COEFFICIENT TESTS DAPCOCAST 38-3 SILICONE RUBBER

SPECIMEN DESCRIPTION	SPECIMEN NO.	(1) α_L^R ($\times 10^6$ m/m/°K) SPECIMEN DIMENSION 0.0254 m (1 IN.)	0.0762 m (3 IN.)	0.1524 m (6 IN.)	(2) α_C^R ($\times 10^6$ m/m/°K) PER SPECIMEN	AVERAGE
DAPCO 38-3 WITH EMBEDDED METAL MESH	1	479	185	108	772*	565
	3	293	178	80	551	
	5	331	172	76	579	
DAPCO 38-3 ONLY	2	182	187	179	548	528
	4	152	179	177	508	
	6	155	185	189	529	

*IRREGULAR TEST RESULT (REF: APPENDIX F)

(1) α_L^R : SYMBOL FOR THE RUBBER LINEAR COEFFICIENT OF THERMAL EXPANSION

(2) α_C^R : SYMBOL FOR THE RUBBER CUBIC COEFFICIENT OF THERMAL EXPANSION

It is assumed that the cubic expansion coefficient, α_C^R, should be the same for the two types of specimens:

$$\alpha_C^R = 546.5 \times 10^{-6} \ (m^3/m^3/^oK)$$

$$= 303.6 \times 10^{-6} \ (in.^3/in.^3/^oF)$$

The specimens for the thermal expansion coefficient tests were made from Dapcocast 38-3 silicone rubber, three with expanded-metal mesh and three without. These specimens were cured as described for specimen No. 2 (Table 16). Specimen dimensions are shown in Figure 28. It should be noted that metal screening used with three of the specimens was placed in the middle of the specimen with the longitudinal direction in line with the 0.1524-meter (6-inch) dimension. This metal screening is described as 2.5 black metal lath, 0.79- by 1.27-cm diamonds, 26-gauge steel.

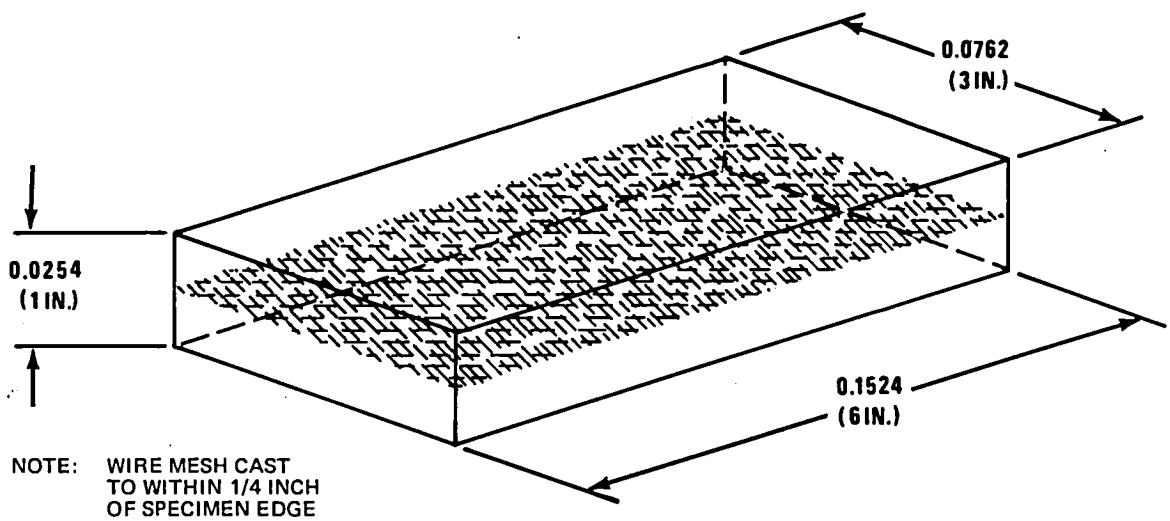

FIGURE 28. SPECIMEN – THERMAL EXPANSION COEFFICIENT TEST – DAPCOCAST 38-3 SILICONE RUBBER

The DAPCO 38-3 silicone rubber was prepared in the following manner: Add 5-percent DAPCO 38-3 thinner by weight. Thoroughly mix with 5-percent catalyst. Deaerate in vacuum chamber for 10 to 15 minutes. Rubber will remain fluid for about 3 hours. Cure the rubber specimen as follows:

Room Temperature	24 hours
333°K (140°F)	2 hours
394°K (250°F)	4 hours
450°K (350°F)	4 hours

Task 9 — Bulk Modulus Tests (DAPCO 38-3 Silicone Rubber)

A knowledge of the bulk modulus properties for DAPCO 38-3 silicone rubber is required to compute trapped rubber pressure. A description of these tests and the results are given in Appendix J. The final bulk modulus properties (i.e., the average values for the relationship between rubber pressure and bulk strain) are given in Figure 29.

Additional tests were then conducted to demonstrate the ability to utilize the bulk modulus properties for predicting rubber pressure due to the application of heat to a specimen of rubber trapped in an enclosure. These tests were successful and are described in Appendix K.

The number of cure cycles for which rubber mandrels may be used is not known. However, the bulk modulus properties of a rubber specimen which had undergone 43 heat cyles were determined in Test 97 of Appendix J. These properties are plotted in Figure 29 and show excellent agreement with the average properties in this figure. It can thus be concluded that rubber mandrels are usable for greater than 43 heat cycles provided the rubber pressure is kept below 2.07 MPa and the temperature below $450^{o}K$.

Task 10 — Resin Gel Temperature Determination

In view of the importance of providing 0.69 MPa (100 psi) rubber pressure before resin gel occurs during the rudder box cure cycle, it is important to establish the temperature of the rubber mandrels (during the cure cycle) when gel occurs. The gap size of rubber mandrels must be designed to provide 0.69 MPa at the gel temperature.

The first step consisted of determining the gel temperature for a particular heat rise rate for T300/N5208 graphite/epoxy woven broadgoods. The test method to acquire this data is described in Appendix H. The gel temperature results of these tests are given in Table H-1. The gel temperature is presented as a region in Figure H-1 rather than as a definite temperature, since this test method only produced data for the $0.56^{o}K$/minute ($1^{o}F$/minute) heat rise gel temperature within $5.6^{o}K$ and the $0.83^{o}K$/minute heat rise gel temperature within $11.1^{o}K$.

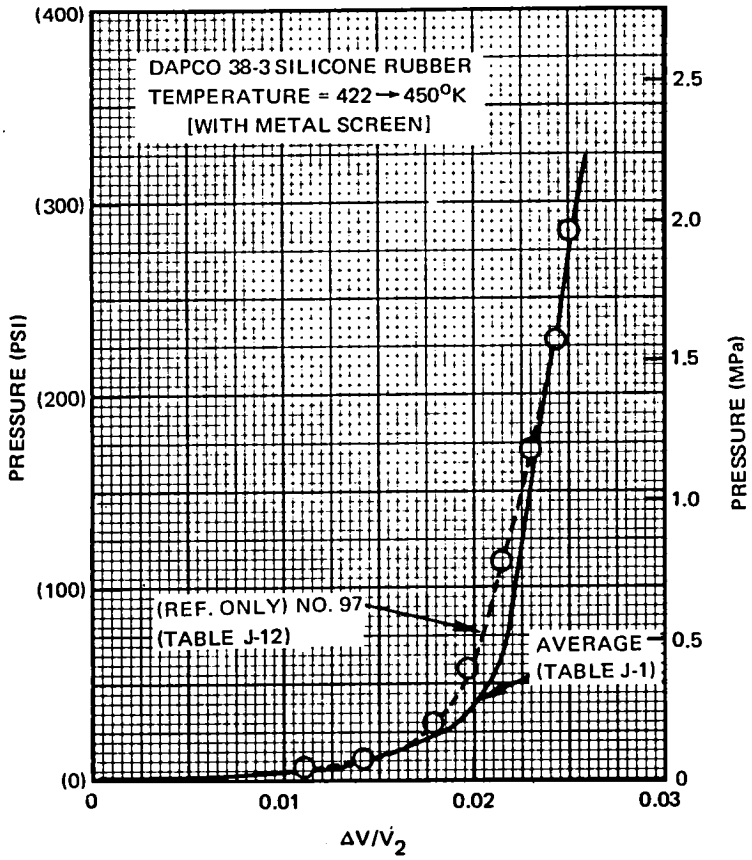

FIGURE 29. RELATIONSHIP OF PRESSURE VERSUS BULK STRAIN (DAPCO 38-3 SILICONE RUBBER)

The second step consisted of preparing the graphs in Figures H-2 to H-7. These graphs contain seven lines radiating from the room temperature, zero-time origin, where each line represents a heat rise rate from 0.56 to 0.89°K per minute. An upper and a lower gel temperature line was drawn to intersect each radial line using data from Figure H-1. Then, thermocouple data from the teletype records of the test rudder cure cycle (Table C-2) were plotted on these graphs. Each graph contains the data from one thermocouple. Judgment is used to replace the thermocouple data curve by an average heat-up rate line. The intersection of the average heat-up rate line with a gel temperature line gives the theoretical gel temperature and time to gel. The actual gel temperature is the thermocouple data value at the time to gel. These values are displayed on each graph in Appendix C.

These graphs for the purpose of estimating the gel temperature were prepared for six thermocouple readings located at three rudder stations (Z_{AR} = 413.53, 476.94, and 555.47). A summary of the estimated gel temperatures at each rudder station is given in Table H-2.

Table H-2 actually gives the temperature range during which gel occurs at the three rudder locations. Since it has been agreed that it is necessary to have a minimum of 0.69-MPa (100-psi) rubber pressure at the gel temperature, the rubber gap will be designed to provide a minimum of 0.69 MPa just before gel occurs. These design criteria are given in Table H-3. The temperatures for which the rubber should produce a minimum of 0.69 MPa are derived from Table H-2. The temperature for which the rubber pressure should not exceed 2.07 MPa (300 psi) is the nominal peak temperature of the cure cycle.

Task 11 — Dummy Part Fabrication and Size Determination

Previous dummy parts consisted of fiberglass bonded on a sheet of plywood backing, which represented the left- and right-hand dummy skins. There were also 31 dummy ribs and the dummy front spar of aluminum sheet. These items constituted the dummy part and were assembled into the PLM to form a shape suitable for casting the internal rubber mandrels.

This dummy part was designed so that the rubber mandrels cast would provide a 0.508-mm (0.020-inch) gap between the mandrels and the inner surface of the cured composite rudder box. Natural shrinkage of the rubber mandrels during the rubber cure procedure (Table 17, specimen No. 4) was compensated for by wrappings of 0.089-mm (0.0035-inch) Teflon tape as a protective coat on the sectioned rubber mandrels. This rubber gap was empirically developed under Contract NAS1-12954 and it worked successfully for the cure of 11 rudders.

It was established in Task No. 6 and Appendix B that the internal rubber mandrels used in the cure of the test rudder were oversize and that a new set of mandrels would have to be cast. The plywood base used for constructing the dummy part skins was suspected of warping during the rubber cure procedure. Also, the flatness tolerance of plywood was considered insufficient for the fabrication of future dummy parts.

Replacement dummy part side skins were fabricated using 6.35-mm (0.25-inch) aluminum plate as a base in place of the plywood. These dummy skins were laid up to provide a rubber gap of 0.508 mm (0.020 inch). The left-hand side dummy skin was cured under vacuum pressure and was near design gauges. The right-

hand side dummy skin, however, was cured under 0.35-MPa (50-psi) pressure and resulted in an undersize part. An undersize dummy skin could produce rubber mandrels with reduced gap.

A survey of the left- and right-hand dummy skin thicknesses was made and a record is given in Appendix D. An estimate of the gap allowances was also made (Appendix L). There was considerable variation in these gap allowances. Figures L-6 and L-7 were prepared to permit a judgment to be made concerning the rubber gaps that would result from casting rubber mandrels with the dummy skins. The shaded area of these figures shows what rubber gaps are acceptable to provide a satisfactory rubber pressure during graphite/epoxy rudder box cure cycle. On this basis, the dummy skins were judged to be acceptable.

The dummy ribs were fabricated from 1.60-mm (0.063-inch) and 2.03-mm (0.080-inch) standard aluminum sheet for the secondary and hinge ribs, respectively. This choice was based on the following information:

1. The desired rubber gap per rib face after casting, curing, sectioning, and Teflon wrapping should be 0.508 mm (0.020 inch).

2. Rubber shrinkage due to cure equals 0.005 cm per cm.

3. Teflon tape used for wrapping the rubber sections is 0.076 mm (0.003 in.).

Task 12 — Cast New Rubber Mandrels

Preparations were made to cast new rubber for the front spar flange and also new internal rubber mandrels for the next rudder cure. The wire screen reinforcement for the front spar forward flange rubber was installed in the PLM and is shown in Figure P-1. The front spar forward flange dummy parts, which were sized to provide a 0.508-mm (0.020-inch) rubber gap, were placed in position on the PLM (Figure P-2) and made ready for the rubber pour. The front spar forward flange rubber was poured and subjected to a 2-day room temperature cure followed by 4 hours at $339^{o}K$ ($150^{o}F$). At this time, measurements of the rubber gap dimensions were made at various Z_{AR} stations and are recorded in Table P-2.

Postcuring out of the tool up to 450°K (350°F) was accomplished later along with the curing of the main rubber mandrels. Cylindrical test specimens (11.9 cm diameter by 2.5 cm thick) were cast using the same rubber mixture and cured up to 450°K (350°F). The excessive shore hardness values (65) of these specimens lead to the discovery that:

1. Six percent curing agent had been mixed with the Dapco 38-3 silicone rubber received from the vendor.

2. The vendor's Dapco 38-3 already contained 9-percent thinner.

The desired rubber composition was the one used to cast all the specimens used for the Dapco 38-3 silicone rubber properties investigation reported in Appendix J. That mixture was as follows:

1. Dapco 38-3 pure silicone rubber

2. Thinner (5 percent of pure rubber)

3. Curing agent or catalyst (5 percent of pure rubber).

However, specimens from the 6-percent curing agent composition were tested and indications were that the physical properties of this rubber were not significantly different from the properties given in Appendix J.

The rubber mixture used to pour the main internal rubber mandrels was formulated by adding 4-1/2 percent* curing agent by weight to Batch 257 of Dapco 38-3, which contained 9-percent thinner. This mixture was degassed under vacuum conditions and poured into the assembled dummy parts and PLM, which is described below.

---

*Batch 257 of Dapco 38-3 contained 9 percent thinner
Silicone rubber content = 91 percent
Therefore 5 percent catalyst = 0.05 x 91 percent = 4.55 percent of Batch 257.

Preparations were made to cast the main internal rubber mandrels. The dummy front spar web was laid on the front spar locator. Four breakaway metal mandrels were mounted on each heater spike. Six strips of metal screening were attached to each metal mandrel and spacers were used to keep each strip about 0.64 cm (1/4 inch) off each metal mandrel (see Figures C-3, C-4, and C-5). When this was completed, the dummy skins and dummy ribs were placed in position

on the PLM (see Figure C-5). The 5.08-cm-thick steel PLM side plates were clamped on the outer sides of the dummy skins to stiffen the dummy skins and keep them properly located.

After the mold assembly was filled with the silicone rubber mixture, the following cure took place:

In the dummy part mold

36 hours at room temperature

4 hours at 339°K

With the dummy skins and ribs removed

4 hours at 366°K

4 hours at 394°K

4 hours at 422°K

4 hours at 450°K

After completion of the cure cycle, the main rubber mandrels were removed from the PLM and trimmed of excess rubber flashing. A preliminary dimensional check of mandrels 4, 11, 20, and 27* was compared with drawing rudder dimensions, and indications were that a satisfactory rubber gap existed. Then the rubber mandrels, which are pyramid-shaped on the outside with a pyramid hollow on the inside, were sectioned into six pieces similar to the section view in Figure 30.

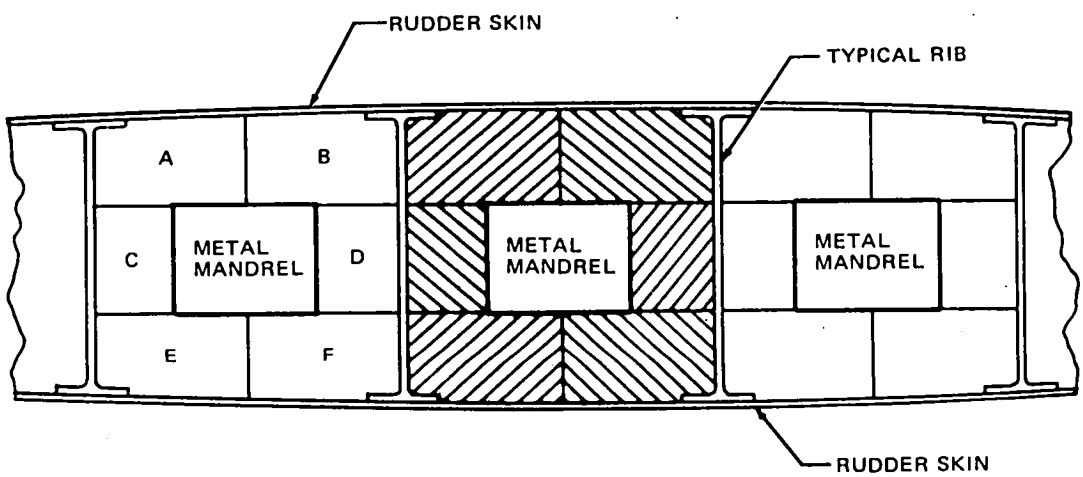

FIGURE 30. CROSS SECTION OF RUBBER MANDREL SECTIONS

*The internal rubber mandrels are numbered from 1 to 30, one for each rib-bay starting from the large end of the rudder. The mandrels for each bay (1-30) are further subdivided into 1A, 1B, 1C, 1D, 1E, and 1F, etc., to 30A, 30B, 30C, 30D, 30E and 30F.

The volume of each of six sections of mandrels 4, 11, 20, and 27 was measured by immersing the sections in a container of water and measuring the amount of overflow. The resulting rubber mandrel volumes are given in Table P-3. The purpose of measuring the volume of the rubber mandrels of rudder bays 4, 11, 20, and 27 was to verify that the rubber was sized properly. To accomplish this, it was necessary to estimate the following quantities per rudder bay at room temperature:

1. Rubber mandrel volume
2. Metal mandrel volume
3. Composite material volume
4. PLM tool inside volume.

The rubber mandrel volumes were obtained by the method described above. The metal mandrel and the PLM tool inside volumes were obtained by linear dimension measurement. The composite material volumes were estimated using PLM tool inside dimensions and layup nominal postcure thicknesses. The results of these estimates are given in Table P-4 of Appendix P. The maximum and minimum rubber gap estimates emerged from the computations of maximum and minimum tool bay volumes. This resulted from the location of the dummy ribs in the oversize slots in the dummy skins (due to the tolerance requirements of placing 30 dummy ribs in 30 slots in the left- and right-hand dummy skins during the rubber casting effort).

The desired rubber gap after one layer of 0.076-mm (0.003-inch) Teflon tape is wrapped around each rubber mandrel section was 0.508 mm (0.020 inch) although the gaps in the "adequate gap" range of Figures L-6 and L-7 would be satisfactory. Columns 11 and 12 of Table P-4 give the maximum and minimum of the estimated rubber gap for the sectioned main rubber mandrels.

Taking into consideration the accuracy of these measurements and estimates, it was concluded that the gaps between the main rubber mandrels and the side plates of the PLM tool were satisfactory for the curing of another rudder box.

Task 13 — Front Spar Reinforcement to Resist Tool Spring-Back Effects

Rib and front spar web failures (Problems 2 and 3 of Table 14) are caused primarily by the spring-back of the rudder box molding tool during tool cooldown.

Stiffening of the tool side plates was one method taken into consideration for reducing front spar and rib compressive strains due to tool spring-back. Preliminary calculations indicated that the tool side plates would have to be stiffened about four times their present stiffness to alleviate the possibility of tool spring-back crushing (Figure 31). This was considered impractical.

It was decided to remedy the crushing of the composite rudder box during tool cooldown by reinforcing the front spar web. It was anticipated that the internal rubber mandrels would be cast so that the internal pressure during a rudder cure cycle would not exceed 2.07-MPa (300-psi) pressure. Thus, the front spar web was reinforced to support the tool spring-back loads resulting from a maximum of 2.07-MPa rubber pressure.

The distribution of reinforcing layers added to the front spar web is shown in Figures M-1 and M-2. These additional layers were designed to provide sufficient strength to halt the tool side plate spring-back before the front spar web compression deformation exceeded 8000 μm/m (8000 μin./in.). These front spar reinforcing layers are oriented perpendicular to the hingeline to prevent any significant increase in rudder stiffness. A typical calculation and the results for three rudder sections are given in Appendix M and Figures M-4, M-5, and M-6.

Task 14 — Endurance of Rubber Mandrels

One little known factor was the ability of the rubber mandrels to produce consistent pressure during many repetitions of cure cycles. The results of Test 97 recorded in Appendix J indicated that a cylindrical specimen of Dapco 38-3 silicone rubber performed very well after 43 heat/pressure cycles, but these cycles did not accurately simulate an actual rudder box cure cycle.

It was considered desirable to monitor the rubber pressure during the anticipated production of 11 rudder boxes. The use of pressure gages mounted in the PLM side plates was considered unreliable and expensive. Therefore, it was decided that this job could be done simply and inexpensively by bonding strain gages on the outer face of the PLM side plates and recording the readings throughout the cure cycle. This was done at Station Z_{AR} = 461 midway between the front and rear spars on the left- and right-hand side plates.

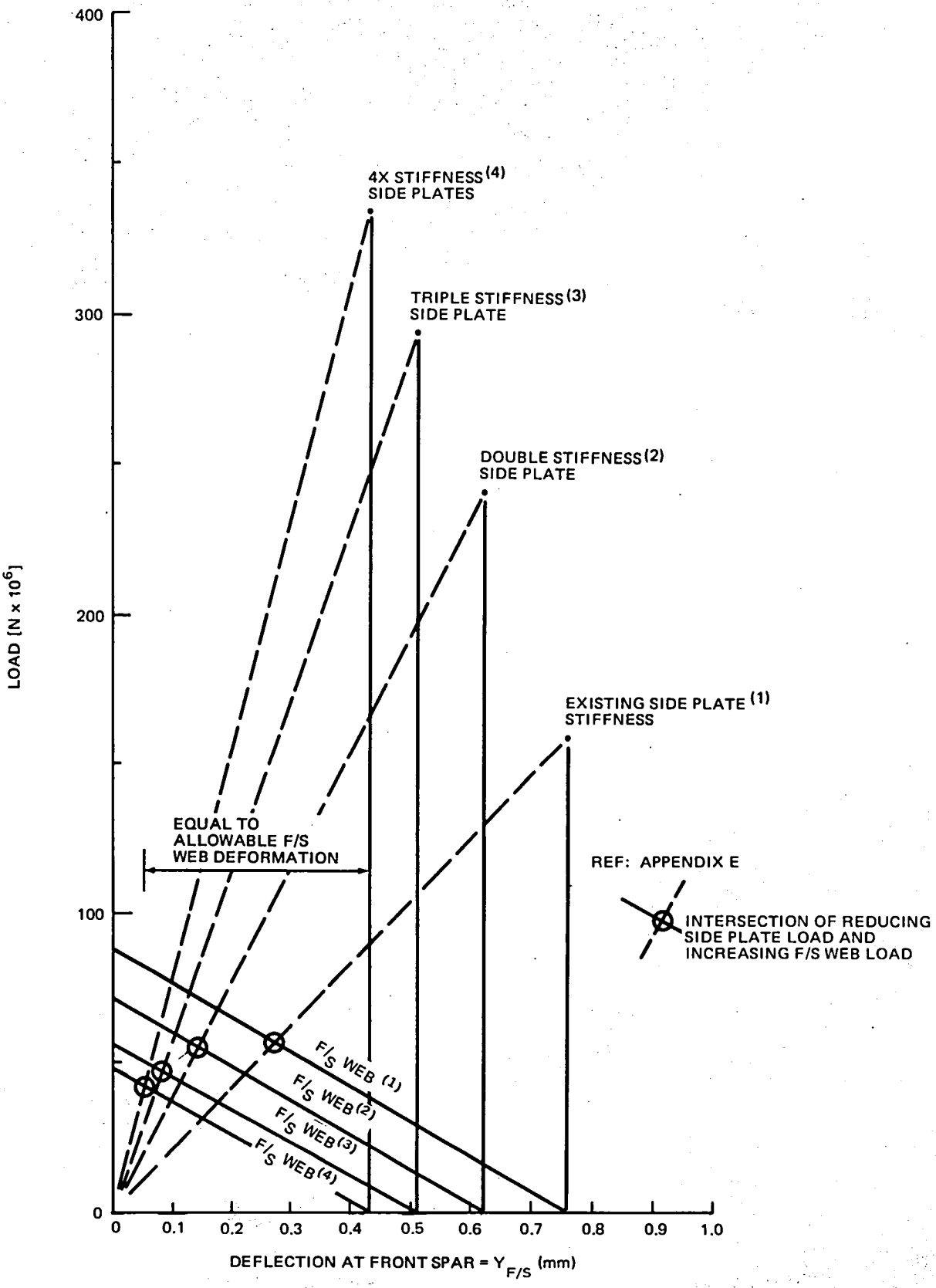

FIGURE 31. F/S LOAD VERSUS DEFLECTION DURING COOL-DOWN

During a cure cycle, the pressure from the internal rubber mandrels would deflect the PLM side plates and produce strains. These side plate strains were compared with the results from beam theory calculations and an estimate of the rubber pressure was obtained. The relationship between the PLM side plate strains and internal rubber pressure (namely, that plate strain of 716 μm/m represents 2.07-MPa (300-psi) rubber pressure) are given in Appendix E. The results of this survey, through the curing of 11 rudder boxes, are shown in Figure E-1.

SECTION 7
RUDDER PRODUCTION

The new rubber mandrels were declared to be satisfactory (Section 6, Task 13). A complete set of laid-up parts were predensified for 30 minutes at 394°K (250°F) at vacuum pressure. These parts were loaded into the PLM to fabricate the replacement test rudder and subjected to the cure cycle which consisted of:

- Room temperature to 450 ± 8°K at 0.55 to 1.1°K per minute (350 ± 15°F at 1 to 2°F/minute).
- Hold at 450°K (350°F) nominal with no thermocouple exceeding 461°K (370°F), for 3 hours starting with the first thermocouple to reach 436°K (325°F).
- Cool below 339°K (150°F) for all thermocouple readings before opening the mold.

After the replacement test rudder box was cured, the visual inspection revealed that the skins and front and rear spares were fine, but that more than half of the ribs had splintery cracks and three of the ribs had 7.6- to 10.2-cm breaks. Numerous ribs were indented moderately (see Figure 19). The faulty ribs were situated in the lower two-thirds of the replacement test rudder. Thus, it appeared that the shake test specimen, which makes use of the upper 1.2 m of the rudder box, could be fabricated from the replacement test rudder.

Moisture Contamination

The rib problem was attributed to the following. The ribs for the No. 2 test rudder box had been stored in the freezer for 9 months. When removed from the freezer, they exhibited a dull gray, very dry appearance and lacked tackiness after thawing out. They were quite limp even though they had been originally stored in the predensified condition. It was suspected that the postcure condition of these ribs could be attributed to moisture contamination. Tests on a precured rib indicated that the desired fresh tacky appearance and stiffness could be restored by subjecting the rib to a repeat predensification cycle without adversely affecting the time-to-gel property of the resin. It was then

decided that graphite/epoxy items that had been stored in the freezer for several months would be subjected to a second predensification cycle before being used for the curing of the production rudders.

With this decision made, the prospects for the fabrication of an improved rudder box appeared very favorable. Therefore, the next rudder box (identified as the No. 1 production rudder) was loaded into the PLM and subjected to the standard cure cycle. After the rudder box had completed the cure cycle and had been removed from the tool, the visual inspection revealed that the skins, ribs, and spars were of good quality.

Molding Tool (PLM) Modification

During the cure of the first production rudder, considerable difficulty was experienced because of the unreliable readings of many of the thermocouples that the microprocessor used for controlling the output of the internal electric heaters. Improper functioning of the thermocouples was attributed to worn and damaged wiring. The heater and thermocouple wiring was accumulated into bundles, which were permanently attached to the PLM and had to be moved in and out of the oven with the PLM. Furthermore, during the loading and unloading of the PLM, the wire bundles were vulnerable to damage from foot traffic.

Since the proper functioning of the microprocessor during a rudder cure was dependent on the receipt of good, reliable thermocouple information, it was considered essential to improve the thermocouple and heater wiring connections before the next rudder box was cured. A thermocouple and heater improvement effort was conducted to provide quick disconnects at the PLM. Thus, the wire bundles would remain in the oven throughout the rest of the rudder fabrication program and remain connected to the Doric Digitend 220 μP multiplexer. This would reduce the probability of damage to the Doric during the connect/disconnect operation originally required for each rudder cure effort. The wiring with the fiberglass insulation was retained. The fiberglass insulation has a tendency of becoming dry and brittle with use in the oven and requires regular inspection and repair. An attempt was made to rewire with kapton-insulated wiring, but the required lead time to obtain delivery was unacceptable.

Rudder Production

With the PLM modification complete, rudder fabrication resumed. The rudder production was divided into six operations:

1. Detail Fab: Subcomponent lay-up and predensification.
2. Fab Box: Load the PLM, cure in oven, remove from PLM, drill and trim box.
3. Inspection: Visual and ultrasonic.
4. AJ1: Install rudder box in the first assembly jig, attach hinge and crank fittings.
5. AJ2: Install rudder box in the second assembly jig, locate and drill attach holes for fiberglass subcomponents.
6. FA: Final assembly, countersink holes, and attach the fiberglass subcomponents.

The schedule called for performing operation No. 2 at the rate of one per week, which was maintained through the fabrication of all the remaining rudders. For operations No. 1 to 6, the schedule allowed 8 weeks for the first five rudders and 7 weeks for the second five rudders. Table 19 shows the comparison between the scheduled time span and the actual time span to perform operations No. 2 to 6.

Weight Summary

A summary of the weight estimates for the rudder and subcomponents is given in Appendix G. The summary includes a comparison with the original tape rudder. Table 20 summarizes the comparison between estimated and actual weights for production rudder units No. 9 and 10.

Front Spar Web Wrinkles

Inspection of the front spar web of rudder box unit No. 3 revealed numerous wrinkles. These front spar wrinkles were attributed to the excessive

TABLE 19

TIME TO COMPLETE RUDDER FAB OPERATIONS NO. 2–6

RUDDER NO.	SCHEDULE TIME (WEEKS)	ACTUAL TIME (WEEKS)
1	6	6
2	6	4
3	6	7*
4	6	3-1/2
5	6	5
6	5	7*
7	5	6
8	5	5
9	5	5
10	5	5

*SOME REPAIRS CARRIED OUT

TABLE 20

WEIGHT SUMMARY

RUDDER NO.	RUDDER BOX Kg, (LB)		COMPLETE RUDDER LESS PAINT Kg, (LB)	
	ESTIMATE	ACTUAL	ESTIMATE	ACTUAL
9	15.36 (33.86)	14.15 (31.2)	27.60 (60.85)	27.90 (61.5)
10	15.36 (33.86)	14.15 (31.2)	27.60 (60.85)	27.90 (61.5)
REFERENCE	APPENDIX G		APPENDIX G	

use of force when fitting the front spar web onto the 30 access hole metal discs. Lack of fit at some of the access holes due to tolerance buildup required the use of force to make the front spar web sit down on the front spar locator. X-ray examination revealed that voids existed in the front spar web at some of the wrinkles and it was decided to secondary bond additional reinforcement to strengthen the entire length of the web. It was also resolved to avoid the wrinkle problem by custom trimming the access holes in the front spar web before curing the remaining rudder box units so that the web would fit onto all the access hole metal discs without the use of force.

Rib-to-Skin Joints

The NDI (nondestructive inspection) for the No. 1 production rudder was done using the digital ultrasonic thickness tester. This revealed many 1.3-cm-wide disbond indications at the rib-to-skin joints centered at the licorice stick location (Figure 32). This is considered acceptable for strength as the remaining joint area provides an ample margin of safety for the applied loads involved.

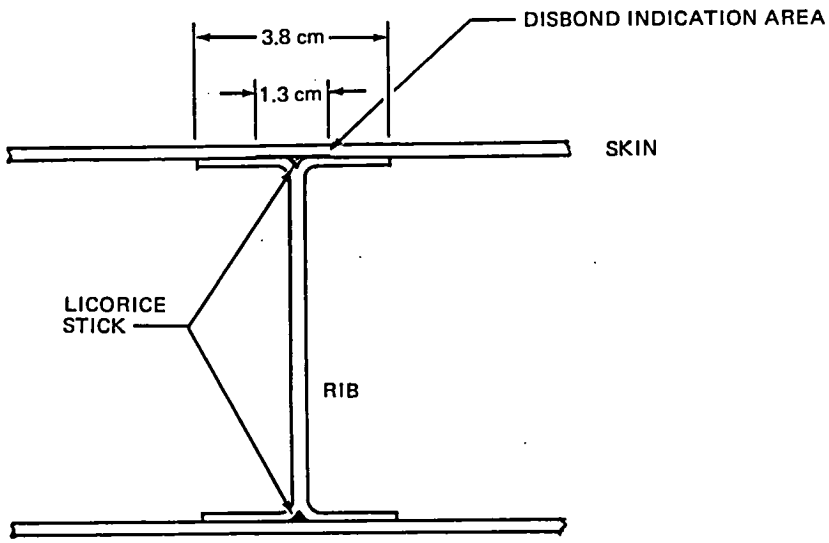

FIGURE 32. RIB TO SKIN JOINT

It was theorized that the problem of disbonding between the rib flanges and the skins was related to the gelling of the rudder box before the curing temperature of 450°K was reached during the oven cure cycle. Assuming the gel temperature is 422°K, as the temperature continues to rise during the heat-up portion of the cure cycle, the trapped rubber pressure continues to increase causing the PLM to expand in conjunction with the thermal expansion of the tool. The gelled rudder skins within the PLM are easily forced to conform to the expanding shape of the PLM. However, the rudder gelled box ribs and spars experience little forced or thermal expansion and so retain their 422°K gelled size. Thus, the forces in the ribs attempting to restrain the skins cause the skin-to-rib separation at the licorice stick area. It was theorized that an improved rudder box could be obtained if the gelling of the rudder box occurred at the final cure temperature or during the constant cure temperature portion of the heat cycle.

In keeping with the above theory, the PLM was heated up more rapidly for the curing of No. 8 rudder box than for previous rudder box cures. In this way, gel might occur at a temperature closer to the cure temperature. The oven is 6.1 m high and it was thought sufficient to increase the opening of the lower hot air ducts located on the left-hand side of the oven. This resulted in the PLM and rudder box left-hand skins heating up somewhat more quickly than the right-hand skins. When ultrasonic inpsection was conducted, it was seen that there were considerably less disbond indications on the left-hand side than on the right-hand side.

As a consequence of this test, it appears that the rudder side that heats up fastest achieves a more advanced cure than the side that heats up more slowly. When the disbond forces build up sufficiently, the side with the more advanced cure remains intact while the other side tends to experience the rib-to-skin disbonds.

In an attempt to improve quality of the rib-to-skin joints, as shown by the ultrasonic inspection of disbond indications between the rib flange licorice sticks and the mating skin surface, four ribs of the sixth rudder box layup were supplied with larger than usual licorice sticks. Normally, the rib licorice sticks are made of 2.54-cm-wide strips of graphite/epoxy tape, which are held at one end while the other end is twisted by an electric drill. Thus, for the sixth rudder box, two ribs were given licorice sticks of 3.18-cm tape, two ribs were given licorice sticks of 3.81-cm tape and the remaining ribs were laid up with the usual 2.54-cm tape licorice stick. After the sixth rudder box was cured, it was determined during the ultrasonic inspection that the wider tape did not alter the disbond indication situation.

Misplaced Licorice Stick

Prior to the curing of the rudder box unit No. 7, it was observed that at a few ribs, the licorice stick might be misplaced from its proper location. This misplacement could result in a reduced corner radius (see Figure 33). It was resolved to pay very close attention to the licorice stick location during the loading of the molding tool for the curing of the remaining rudders. Improperly placed licorice sticks were relocated or, if the existing one was not movable, an extra one was added.

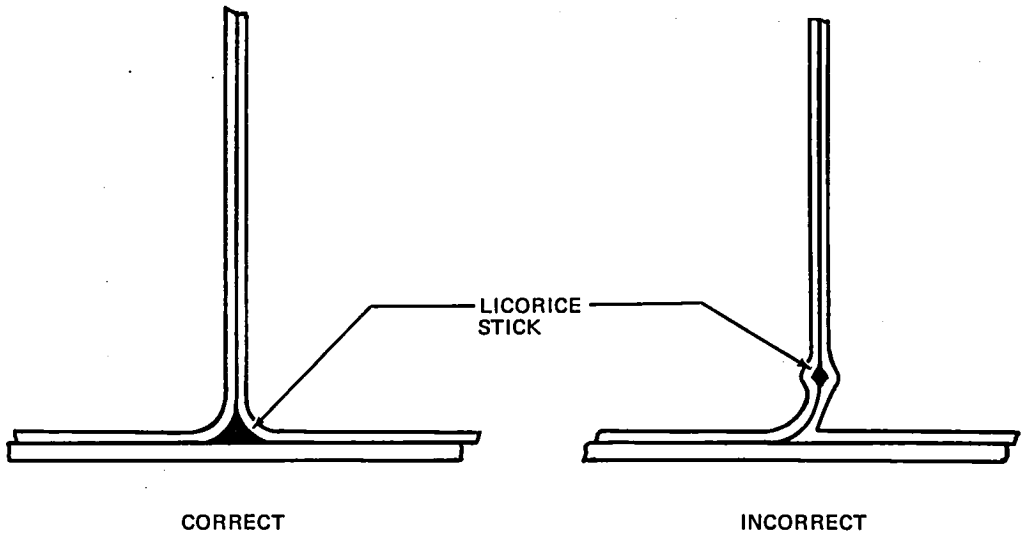

FIGURE 33. EFFECT OF MISPLACED LICORICE STICK

Woven Broadgoods

The follow-on program for the second set of 10 composite rubbers has employed the use of biwoven and uniwoven graphite/epoxy prepreg materials in lieu of the 7.62-cm-wide unidirectional tape previously used on the initial program. It was estimated that utilization of broadgoods versus tape would constitute a 30- to 50-percent man-hour savings in layup time, primarily due to the material's width (1.07 m) and the fact that layup of biwoven material would be equal to two plies of tape. The rationale for substituting broadgoods for tape to save costs appeared to be extremely sound and realistic; however, it did not prove as effective as expected in this program.

The following observations were made and experiences encountered during the routine layup of graphite/epoxy prepreg materials (broadgoods) for the second set of 10 production rudders:

1. Broadgood material received from Narmco was extremely tacky (within specification limits) and quite difficult to remove from the rolls. Also material was of nonuniform quality due to vendor's manufacturing process. The rolls had many defects that required cutting care prior to layup.

2. Removal of polyethylene separator film was difficult, thus lending itself to wrinkling of preplied materials.

3. Overall handling was more difficult than with the 7.62-cm-wide tape, probably due to the 1.07-m width of the broadgoods.

4. Prior to layup use, 2.54 to 3.81 cm of salvage had to be trimmed from both edges of the material. This led to extra man-hours in handling.

5. Material waste has been excessive, in some cases as high as 50 percent, due to ply orientation and detail configuration. Equivalent tape material waste is less than 5 percent.

6. Forming of individual details (i.e., ribs) has been more difficult with woven broadgoods than with unidirectional tape. Also, the material tends to bridge in corner areas as evidenced in the cured part. This phenomenon was minimal with the tape rudders.

Woven broadgoods are not recommended for use in future composite rudder fabrication unless improvements are made in the quality of the materials which will allow reductions in layup time to be realized. However, this type of material may easily prove to be efficient for large, simple types of components.

Rubber Pressure

The rubber pressure during a cure cycle was estimated by measuring the axial strain in the PLM 5.08-cm-thick steel side plates and comparing with computed values. The monitored strain values of two of the rudder box cures are given in Figures E-2 and E-3. The maximum readings recorded during each rudder box cure and the corresponding estimated rubber pressure at the strain gage station are shown in Figure E-1. The first use of the rubber for the replacement rudder box produced a maximum pressure of 2.17 MPa. The maximum pressure produced during the curing of the 10th rudder was 1.86 MPa. This shows that the rubber mandrels are a reasonable, reliable means of producing pressure for this process with a useful service life.

The strain gage values given in Figure E-2 show that the rubber started to produce pressure shortly after the oven was turned on, and the maximum strain was reached in 3-1/2 hours. The maximum strain of 750 μmm/mm corresponds to a maximum rubber pressure of 2.17 MPa (Figure E-1), which shows that the goal of not exceeding 2.07 MPa to avoid yielding the rubber has not been significantly

exceeded considering the steep slope of the pressure versus bulk rubber strain of Figure J-12.

Another goal of this cure was to provide a minimum of 0.69-MPa (100-psi) rubber pressure when the resin gelled. The 0.69-MPa (100-psi) rubber pressure corresponds to 716/2.07 x 0.69 = 239 μmm/mm of strain (Page E-2), which occurred at about 1.05 hours after the oven was started. However, the information of Figure H-4 indicates that the gel temperature of 430^{o}K was achieved at the heat-up rate of 0.73^{o}K/minute or (430 - 297) x 1/0.73 x 1/60 = 3.03 hours after the oven was started. This indicates that the gel point was reached when the rubber pressure was 2.07/716 x 720 = 2.08 MPa (Figures E-1 and E-2).

APPENDIX A
CURE CYCLE
TEMPERATURE
CONTROL SYSTEM

SECTION A-1
HARDWARE DESCRIPTION

The Composite Rudder Temperature Controller functions as an automatic means of measuring 97 part and tool temperatures and turning on or off 31 electrical heaters during the cure cycle. This is accomplished using a thermocouple multiplexer, a microcomputer with a resident control program, and a heater modulator. A block diagram of this system in its final configuration is shown in Figure A-1.

The multiplexer is a Doric Digitrend 220-µp Data Logger. The multiplexer accepts iron-constantan thermocouple inputs and performs cold junction compensation, analog-to-digital conversion, and linearization in addition to its switching functions. The switching is accomplished using field-effect transistors rather than the conventional reed switches. It also contains a digital clock which is synchronized with a 60-Hertz power line. Each temperature scan requires approximately 5 seconds and is initiated by the computer. Each scan produces the time of day, a self-test value, and 99 temperatures. Each element is a Binary Coded Decimal (BCD) number consisting of up to five digits and is furnished to the computer on an interrupt basis with no "handshaking." An open circuited thermocouple is digitized as all nines.

The computer (Figure A-2) is an Intel 8020 single-board type using an 8080A central processing unit (CPU). This board has 2048 (2K) eight-bit words (bytes) of read-write memory (RAM) and provisions for 4096 (4K) bytes of read-only memory (ROM). The input-output (I/O) capacity of this board, 48 lines, was insufficent for the task so the I/O capability was expanded to 96 lines with an Intel SBC 104 I/O expander board. This action also added 4K bytes of RAM and provisions for adding 4K bytes of ROM. As the software design evolved, this ROM capacity became insufficient and an Intel 416 memory expander board was added. This resulted in having a total ROM capacity of 16K bytes. Additional features of these boards, such as interval timers, a programmable interrupt controller and a universal synchronous, asynchronous

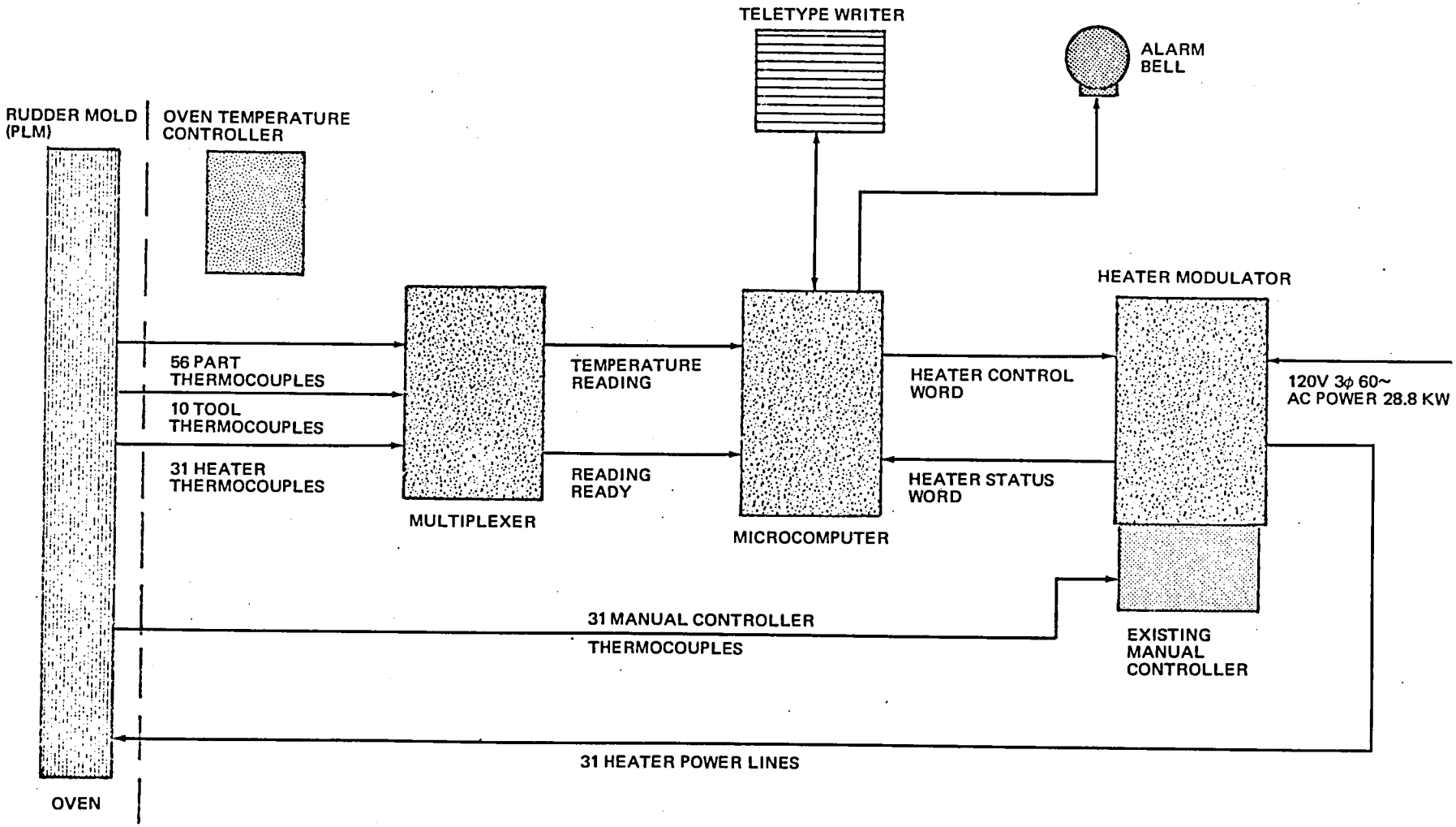

FIGURE A-1. TEMPERATURE CONTROL SYSTEM BLOCK DIAGRAM

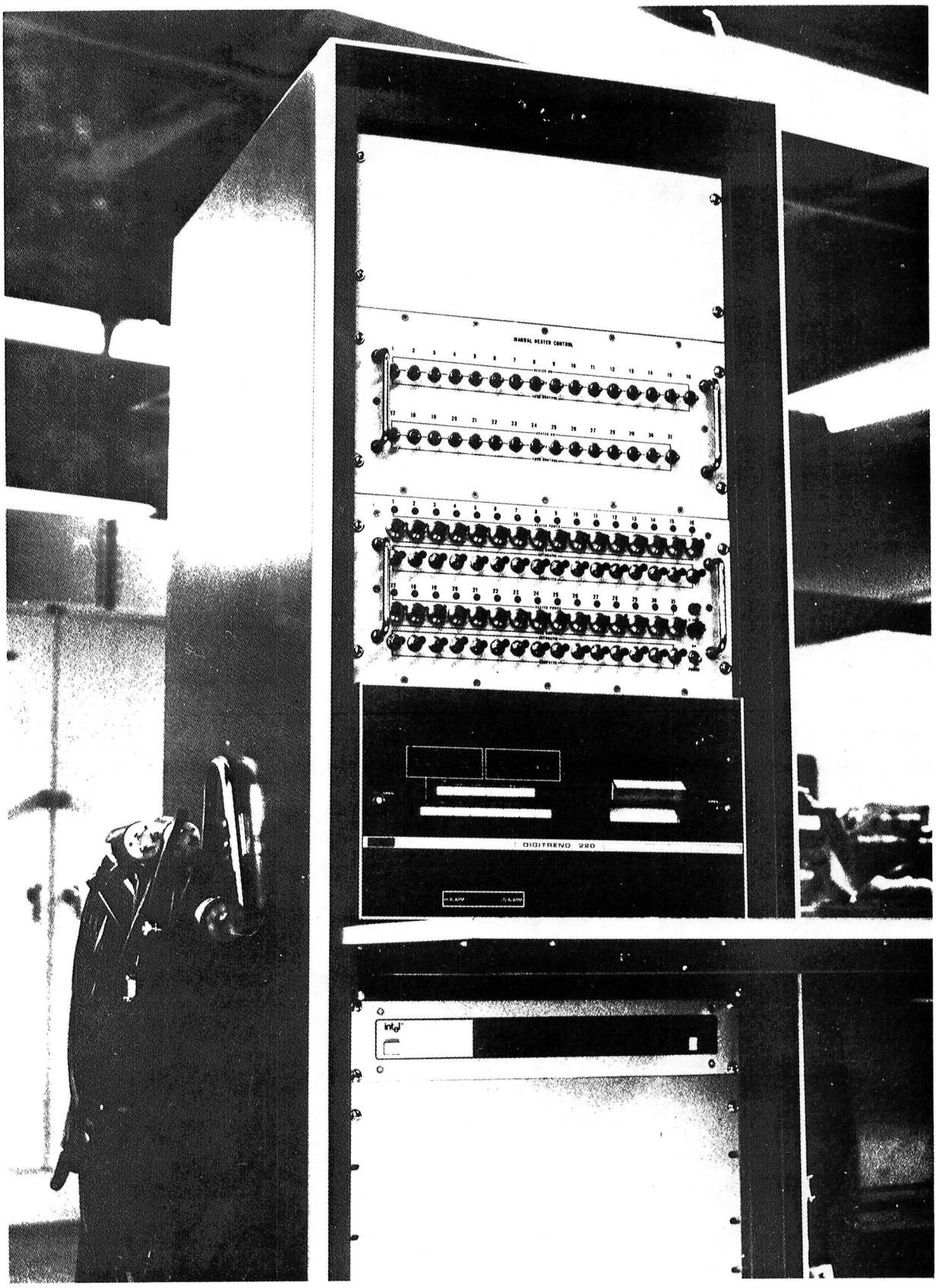

FIGURE A-2. MICROCOMPUTER PROCESS CONTROLLER FOR THE RUDDER CURE CYCLE

receiver/transmitter (USART), were advantageously used. The temperature control system program is resident in the computer as firmware. It consists of 14 Intel 2708 erasable programmable read-only memories (EPROM). The computer external interfaces are the Doric data logger, the heater modulator, a teletype writer, an alarm bell, and an output line that was to be used as an oven temperature controller.

The heater modulator used to cure the original 10 rudders contained 31 TRIAC solid-state switches with potentiometers that control their firing angles. These potentiometers were manually adjusted during the cure of the rudder box to vary the heater voltage for faster or slower internal heating. The plan was to incorporate these TRIAC switches in the present temperature control system. The computer manufacturer recommended against this, however, due to the noisy electrical power environment these switches created when they were switched on. They were replaced with simple zero-crossing solid-state swiches and the heater temperatures were controlled by turning the heaters on or off for short intervals. The heater modulator and the computer communicate with one another by means of a 31-bit heater control word and a 31-bit heater status word. Using temperature readings from the Doric Data Logger, the computer computes a desired temperature for each heater and compares this with the actual heater temperature. It then informs the heater modulator by means of the heater control word which heaters should be on and which should be off. A few milliseconds after receiving this information the heater modulator will have turned on or off all 31 heaters. (The heaters are almost equally distributed on a 3-phase 120-volt service so that they do not all turn on or off simultaneously.) It then returns the actual on-off status of each heater to the computer by means of the heater status word.

The 31 home-made set point controllers, used to control the TRIAC switches during the cure of the first 10 rudders, were incorporated into the heater modulator as a backup system to be used in the event of a computer failure. These controllers were never used. A completely manual system, consisting of manual on-off switches that bypassed the solid-state switches, was also incorporated. This system was to be used in the event of a solid-state switch failure. No switch failures were ever encountered; however, these switches

were occasionally used to good effect when it was desired to have a part temperature a little higher and this condition was beyond the computer's intelligence.

The teletypewriter (TTY) is used to record a temperature history of the entire heatup and cure process for quality assurance purposes. A temperature profile of the internal heaters, spar and skin temperatures, as well as oven air temperature, is printed every 10 minutes. The TTY is also used to call attention to conditions that may require human intervention. The alarm bell is rung concurrently with the printing of the message to attract that attention.

The control of the oven was never implemented due to budget constraints; and all oven temperature settings were made by hand using the manual oven controller. The computerized control was to have consisted of one output line that would have energized a solenoid which in turn would drop the follower on the oven programmable temperature controller to a lower setting. This control would have been limited to temperature decreases only, i.e., oven temperature reduction to $450^{o}K$ at start of cure and reduction to $322^{o}K$ (minimum controller setting) at end of cure.

SECTION A-2
SOFTWARE DESCRIPTION

Introduction

The Graphite Composite Rudder Cure Cycle Control Program is a microprocessor program which monitors thermocouples and controls heaters attached to the curing tool while the composite material is in the oven. Its primary inputs are 99 temperature readings supplied by the Doric Digitrend 220-μP data logger. Its primary outputs are carried on control lines to 31 heaters located along the length of the tool. It also displays data on a teletype, both automatically and in response to an inquiry, and sounds a loud bell in case of an abnormal condition.

The program includes a self-test mode that verifies the correct operation of the thermocouples and heaters before beginning a cure. Once the heatup cycle is begun, the program can run without human intervention, except when manual action is required to reduce the oven temperature and to correct serious errors.

Program Specification

General — The program operates in two basic modes: hardware self-test and cure cycle control. In the self-test mode, the program and the user together verify that the thermocouple inputs and heater control outputs are functioning properly. In the control mode, the program (1) monitors the temperatures, (2) determines outputs and verifies heater controls, (3) determines when to reduce the oven temperature, (4) responds to inquiries, (5) detects and reports error conditions, and (6) in case of a serious error which the program cannot overcome, sounds the loud bell and relinquishes control to a manual backup system.

When the restart button is pressed, the user has the opportunity to do the self-test zero or more times. When the user tells the program that the hardware is functioning properly, the cure cycle control module is entered and continues executing until either power is turned off or the restart button is pressed again.

Self-Test Mode — The self-test mode has two parts: thermocouple test and heater test.

At the start of the thermocouple test, the program asks the test supervisor to manually read the temperatures. Then the program reads the temperatures using the Doric temperature multiplexor. The program verifies (1) that the self-test temperature (temperature No. 0) is between 1128°K and 1133°K, (2) that no thermocouple is open, (3) that all temperatures are feasible, and (4) that the Doric unit responds as expected. If necessary, error messages are typed out. The temperatures are then typed out and the supervisor is asked to compare them to those recorded earlier. If the test was not successful, it is repeated; otherwise the supervisor is asked to prepare for the heater test.

The heater test is conducted for each of the 31 heaters. A heater is turned on until its temperature rises and then turned off. An error message is printed if (1) the heater fails to turn on, (2) additional heaters come on, (3) the heater temperature fails to rise, (4) the heater fails to turn off, or (5) the heater temperature continues to rise significantly after the heater is turned off. If the program cannot turn off a heater or if a heater temperature is rising abnormally, the program sounds the loud bell.

Cure Cycle Control Mode — In the control mode, the program operates without human intervention except for errors which cause the program to sound the loud bell to call for manual control.

Approximately every 6 seconds, the program completes a scan of all thermocouple temperatures. Using the heater temperatures just input and the most recently computed desired heater temperatures, the program decides whether to turn each heater on or off. If the desired temperature is higher than the actual heater temperature, the heater is turned on; otherwise it is turned off.

Approximately every minute the program computes the desired heater temperatures. The goal of the computation is to set the heaters such that each spar temperature is close to its neighboring skin temperature while maintaining each spar temperature close to the average spar temperature. In order to prevent destroying the rubber, the heaters must never exceed 477°K. During the cure cycles, the heater temperatures must be maintained between 444 and

455^{o}K so that temperatures remain within the 442 to 458^{o}K cure range. After the cure, the desired heater temperatures are zero so that the heaters are always off.

During the heat-up phase, the program checks whether it is time to reduce the oven temperature from 505 to 450^{o}K by forecasting the expected temperatures at the end of the 20 minutes required for the oven temperature decrease. At the appropriate time, the "reduce oven temperature" line is turned on and a message is printed.

Also during the heat-up phase, the program checks for the start of the cure phase, which is defined as the time when all of the composite temperatures (spar, skin, rear spar, and leading edge thermocouples) are at least at the minimum cure temperature (442^{o}K). When it detects this condition, the program types a message and then remembers the time, so that at the end of the cure cycle (2 hours later) it can command the oven to turn off.

About every 10 minutes the program types out the current temperature of each thermocouple. To get temperatures at other times, or to get additional information from the program, the program responds to a few simple inquiries which are described in the users' guide.

When the program detects an error condition, it prints an error message. If the problem is so severe that the program is no longer able to function properly, the loud bell is rung to signal that manual control is required. The error messages are listed in the users' guide.

If it is apparent to a human observer that a particular thermocouple is giving an erroneous reading, it is possible to tell the program to ignore that thermocouple and treat it as if it were open. This means that an average of neighboring values is used in place of the erroneous reading.

Memory Addresses – The assignment of addresses to memory, input/output devices and interrupt vectors follows:

ADDRESS RANGE	FOUND ON UNIT	MEMORY TYPE
0000 - 0FFF (4K)	80/20	EPROM (erasable programmable read-only memory)
1000 - 1FFF (4K)	104	EPROM
2000 - 33FF (5K)	416	EPROM
3800 - 3FFF (2K)	80/20	RAM (random access memory)
4000 - 4FFF (4K)	104	RAM

Other memory addresses are not available.

Program Overview

Methodology — The cure cycle control program (including the self-test mode) is written in PL/M using the INTEL MDS (Microcomputer Development System). The program is designed as a set of highly modular subroutines with a restricted use of common ("PUBLIC" in PL/M) data. Almost all communication between separately compiled modules is via passed arguments. PUBLIC data is used for data to which the inquiry module must have access.

Because the program resides in ROM, it is not possible to use the INITIAL attribute to initialize data. Instead, each module which requires that some of its data be initialized has an initialization procedure which must be called prior to calling any other procedure of the module.

A file of abbreviations for commonly used PL/M words and phrases has been used in every module via the $INCLUDE option. This file also gives alternate names to the basic data types to indicate how a variable is used (for example, BOOL for a BYTE variable containing a TRUE or FALSE value).

The $INCLUDE option is also used to include small files for the declaration of external procedures, input/output port assignments, data structures, etc. This reduces the amount of text within a module and makes it easier to change the included text than if the text were repeated in each module.

Only two subroutines, both small, are written in assembly language rather than PL/M. They perform functions which are straightforward in assembly language but which would be very clumsy and large in PL/M.

Library Structure — In order to minimize the time-to-run library updates, the object modules have been grouped into several libraries. The library name to which the object module belongs is the extension of the source file name. The libraries follow the hierarchical structure of the program; that is, a mdoule must only call modules in the same or lower libraries.

The libraries are: CC1, CC2, CC3, CC4, CC5, PUT, and UTL.

Libraries PUT and UTL contain general purpose routines which may be used in future PL/M programs.

Algorithm for Ideal Heater Temperature Computation — The computation has two potentially conflicting goals: (1) to make the spar temperature match the adjacent skin temperatures, and (2) to make the spar temperatures uniform along the length of the part. The computation algorithm finds temperatures at which to set the heaters, thereby giving each of the two goals equal weight.

The algorithm is derived from equations of current, past and future temperatures, and heat transfer coefficients.

Several assumptions were made in order to use simple equations. Most important is that the temperature at a spar thermocouple is a function solely of its current temperature and of the temperatures at the two closest heaters, and that the temperature at a skin thermocouple is a function solely of its current temperature and of the temperature of the corresponding point on the outside of the plate. It is assumed that the temperature on the outside of the plate will not change within the period projected in the computation (about 1 minute). Also it is assumed that the heater can respond quickly to reach the computed ideal temperature. However, since the heaters in fact cool rather slowly, it was necessary to prevent high heater temperature which might cause overheating of the part.

It is further assumed that the heat transfers from the heaters to the spars and from the plates to the skins are linear functions. This means that there is a "skin coefficient" which measures the rate of heat change at the skins as a function of the plate temperatures, and a "spar coefficient" which measures the rate of heat change at the spars as a function of the skin

temperatures. These coefficients are not known in advance but are computed by the program based upon the most recent sets of temperatures.

In defining the equations, a simplified situation is used in which there is only one heater, one spar, one skin, and one plate thermocouple. In the real situation the equations are more complicated because there are many of each type; the heaters are between the spars rather than a one-to-one correspondence between heaters and spars; and the heaters and spars are in the center with skins and plates on both sides. The simplified situation permits a clearer presentation of the essence of the equations.

Symbols used in the equations are:

SK_0 = current skin temperature

SK_1 = skin temperature expected 1 minute from now

P_0 = current (and future) plate temperature

SP_0 = current spar temperature

SP_{1A} = spar temperature 1 minute from now which would satisfy the goal of keeping the spar temperature close to the skin temperature

SP_{1B} = spar temperature 1 minute from now which would satisfy the goal of keeping the spar temperatures even along the length of the part

SP_1 = desired spar temperature 1 minute from now

H = heater temperature to which the heater will be set during the following minute

A = heat transfer coefficient between plate and skin

B = heat transfer coefficient between heater and spar

M = number of spars along the length of the part

N = number of minutes over which a current difference between spar temperature and skin temperature and between a spar and the average spar will be corrected

The heat transfer coefficients are defined such that they are always at least 1 (where 1 represents perfect heat conductivity) so that integer values

can be used in the program for the coefficients. Therefore, the coefficients are defined by the equations:

$$SK_1 = SK_o + (P_o - SK_o)/A$$

$$SP_1 = SP_o + (H - SP_o)/B$$

Therefore,

$$D_{SK} = SK_1 - SK_o = (P_o - SK_o)/A$$

The goal of keeping the spar temperature close to the skin temperature is met by changing the spar temperature at the same rate as the skin temperature while correcting any current difference within N minutes:

$$SP_{1A} = SP_o + D_{SK} = \frac{SK_o - SP_o}{N}$$

The goal of maintaining uniform spar temperatures is met by trying to match the average of SP_{1A} over the length of the part within N minutes:

$$SP_{1B} = SP_o + \frac{(\Sigma SP_{1A}/M) - SP_o}{N}$$

The two goals are combined by taking their average:

$$SP_1 = \frac{SP_{1A} + SP_{1B}}{2}$$

Solving for H gives:

$$H = B(SP_1 - SP_o) + SP_o$$

The computed heater temperatures are subject to limit constraints. During the heat-up phase, the maximum permitted temperature is between 461 and 472^{o}K depending on the location of the heater. During the cure phase, all heater temperatures are restricted to 444 to 455^{o}K. During the cool-down phase, all heaters are turned off (0^{o}). Also the heater temperature may not be greater than that temperature which will cause a 1.67^{o}K per minute change in the spar

temperature. This restriction dampens severe osciallations of computed heater temperatures which occasionally occur.

Of course, the coefficients must be computed before the foregoing equation can be used. The coefficients used in the program are the average of the most recently computed coefficients, where the individual coefficients are computed as follows:

let

SK_{-1} = skin temperature one time interval ago

P_{-1} = plate temperature one time interval ago

SP_{-1} = spar temperature one time interval ago

H_o = current heater temperature

$$1/A = \frac{SK_o - SK_{-1}}{P_{-1} - SK_{-1}}$$

$$1/B = \frac{SP_o - SP_{-1}}{H_o - SP_{-1}}$$

Note that the inverses of the coefficients are computed by the program, which uses scaling to prevent loss of accuracy. If $P_{-1} = SK_{-1}$ or $H_o = SP_{-1}$, no coefficient can be computed so the average coefficient will not include such cases in its average. Also if 1/A or 1/B is negative, the case is excluded. If 1/A or 1/B is >1, its value is reduced to 1 because the unusually high heat transfer rate implied should be an abberation.

Thermocouple Numbering Scheme — A consistent numbering scheme is used for thermocouple temperature readings in the program.

Heater thermocouples are numbered from 1 to 31. All other thermocouple groups are numbered from 0: spars from 0 to 31; left skins and right skins from 0 to 7; left plates and right plates from 0 to 2; and left oven air, right oven air, left leading edge, right leading edge, left rear spar and right rear spar from 0 to 1.

Brief History of System Problems — The first rudder was cured using the computerized temperature control system. The 8080A central processing unit (CPU) was removed from the control system and the ICE-80 In-Circuit Emulation feature of the Microcomputer Development System was substituted. This in essence allows a person to stand inside the CPU, observe all that is transpiring, look at or change any memory location, and change the program (not recommended) while the control system is controlling the process.

The Temperature Control System software performance was generally satisfactory. However, eight changes of a minor nature were deemed necessary. These are:

1. Add ability to selectively ignore thermocouples by user input.
2. Reduce maximum allowable heater temperatures at small end (top of rudder) of tool.
3. Correct program abort on "TEMP > 532.6^{o}K.
4. Increase the length of time the alarm bell rings.
5. Set the desired heater temperatures to zero degrees at end of cure cycle.
6. Allow user override of start of cure time.
7. Check for oven temperature in the neighborhood of 450 degrees Kelvin after "REDUCE OVEN TEMPERATURE TO 450 DEGREES" message as well as an immediate drop in temperature.
8. Give error messages a higher interrupt priority to enable them to print through normal output.

Change 3 above reflects a change in a basic concept. It was originally thought that if some conditions were to occur, such as a heater that would not turn off or a temperature that exceeded some set limit, the computer could not cope with these situations and would call for human intervention, and relinquish control. Humans would then control the process in a manual mode. During the cure of the first rudder, a temperature reading in excess of 533 degrees Kelvin was encountered four times and the program quit each time. It was

obvious the condition was momentary and no valid explanation could be offered. Each time the program quit, the point in the process was lost, and all process history was lost. In view of this, it was decided to have the computer call for help and explain the problem it encountered, but the decision to abort the automatic mode and enter the manual mode would be left to a human being. The computer will persevere in spite of all obstacles.

After curing the second rudder, the following additional changes were made to the software:

1. Flag all ignored thermocouples on the temperature profile output by printing an asterisk after the temperature.

2. Remove ignored thermocouples from part temperature spread.

3. Test for possible incorrect thermocouple reading and flag same for user evaluation. This was accomplished by testing for a five-degree temperature drop when temperatures were expected to be in a steady state or increasing.

4. Make selective ignorance of thermocouples a general case; allow user to ignore adjacent thermocouples.

After these changes were made, only one additional change was made. This was to refine and increase the accuracy of the "oven cutback to 450 degrees" algorithm.

Hardware malfunctions were infrequent. The first seven rudders were cured with no CPU installed in the computer; ICE and the 80 feature were used instead. The reason for this was the malfunctioning of the prom programmer. It was impossible to program the read-only memories and it was necessary to use the program that was on a floppy disk in the microcomputer development system (MDS). During this time the 8080A CPU was in a desk drawer and numerous people had handled it with no precautions against static electricity. When the firmware was finally programmed and installed and No. 8 rudder was cured, the CPU was found to have an intermittent fault. It was replaced with a new one which was also found to be faulty. It was replaced with no further problems.

The Doric data logger malfunctioned twice; once during a cure and the other time was during a test prior to putting the tool into the oven. One channel suddenly started to display a temperature indication that was 22 degrees Kelvin too low. This channel would respond to a heat gun applied to the thermocouple junction but was continuously 22 degrees Kelvin in error. After about two hours of troubleshooting, with no cause determined, the malfunction vanished. The heat-up of production rudder No. 3 (rudder box assembly No. 5) was progressing satisfactorily with all part temperatures above 436 degrees Kelvin with the exception of one which was 1.1 degrees low. The computer started a temperature profile printout. This requires about four minutes. When the printout was concluded, the computer, by means of the TTY, was asked for an up-to-date temperature reading. It was reading about 380 degrees, about 56 degrees low. We immediately began receiving error messages and this continued until the computer had reported that every thermocouple may be giving false information. This was confirmed by the next temperature profile. It was apparent the Doric had developed a fatal malfunction. The temperature control system has no parallel path or backup for the loss of temperature information so the oven was set at 450 degrees Kelvin and the 4-hour cure period was started without the temperature system in operation. When the Doric started giving false heater temperatures, the computer had turned on all heaters which initiated an over-temperature condition. The control system had to be shut down. A check of the equipment determined that a clamping field effect transistor had shorted on Channel 88 of the multiplexer circuitry. The junctions of all the thermocouples are tied to a common point; thus a malfunction of this type on one channel affects all channels. It was discovered that disconnecting this one thermocouple made all other channels operative. The defect was repaired and all who were involved in the curing of the rudder boxes were informed of the quick-fix method used for isolating the faulty channel.

Numerous problems were caused by the thermocouple leads. These wires were the same wires that had been used on the previous contract and were beginning to show their age. To extend the life of these wires, standard thermocouple disconnects were installed at the mold, so the cable could be disconnected during mold loading operations. This type of connector had been used on the mandrel No. 31 tool with no problems experienced during the cure of 14 rudder boxes on the previous contract and one on present contract.

However, the oven temperature during the heat-up phase of these rudders was 505 degrees Kelvin. The heat-up temperature was changed to 533 degrees Kelvin beginning with the test article rudder. This additional 28 degrees caused oxidation of the constantan contact of the connectors which made them very difficult to disconnect and caused intermittent open circuits. The use of Silicone grease (Dow Corning No. 4) successfully alleviated the disconnecting problem. However this grease contributed to the intermittent contact problem. The oven floor consists of a refractory material and is always covered with a light dust. The silicone grease in the female contacts was soon contaminated with this dust which further hindered good contact. Cleaning the connector contacts with small wire brushes prior to each cure was time consuming, and still did not prevent the loss of some thermocouples during heat-up and cure. No satisfactory solution to this problem was ever devised. One candidate solution would be use of an insulated box integral to the mold, ventilated with plant air in which these connections could be made. They only need to be kept at a temperature below the oxidation point.

The most serious thermocouple problem encountered was not discovered to be a thermocouple problem until after the cure of production rudder No. 9. It manifested itself in the early stages by jitter in Doric readings and a slower than normal scan time on one group of 20 channels. Also one spar thermocouple would rapidly rise to 605 degrees Kelvin when everything else including oven air temperature was at about 367 degrees Kelvin. Then it would slowly decrease as the rest of the mold heated up. After all expertise in attempting to correct this trouble had been exhausted, the Doric customer service was contacted and it was unsuccessful also. There was a production schedule to maintain so it was decided to try to live with the problem.

During the heat-up phase of No. 8 rudder, the right-hand side of the tool lagged the left-hand side, including the oven air temperature thermocouple, by as much as 22 degrees Kelvin. The right-hand side is downstream with respect to air flow in the oven and it was thought that the mold was blanketing itself. To counteract this, the inlet louvers on the left-hand side of the oven were readjusted in an attempt to get better hot air distribution around the tool. The key to the problem was that all thermocouples on that side of the tool were together in one cable assembly.

The problem came to a head during the heat-up and cure of rudder No. 9. After about 20 minutes into the heat-up phase of this rudder, 13 thermocouples were on the computer's ignore list and 11 more were obviously going bad. The trouble seemed to be confined to channels 39 through 61. The cure was aborted. These channels comprised the thermocouple leads making up one of the 5 separate cables connecting the Doric to the mold. These cables were taped with fiberglass tape with an adhesive of unknown composition to provide abrasion resistance. As stated before the oven floor consists of a refractory material and is very abrasive. The thermocouple wire insulation is also a fiberglass tape impregnated with an unknown resin system. This fiberglass tape was stripped from the cable in an attempt to discover the cause of trouble. It was noted that the wires were stained where they exited the oven conduit but at that time it was thought to be oil contamination caused by a diffusion vacuum pump that was in the vicinity. As the tape wrapping was removed the low temperature reading slowing started rising. Departments that might have thermocouple wire were canvassed as replacing the wire seemed to be the only remedy. When we returned to the oven with the borrowed wire, the readings had returned to normal and the stained area on the wire seemed to have dried out. This led to the conclusion that moisture, and not oil, was the cause of the trouble. To maintain schedule it was decided to again attempt to cure the rudder assembly even though it meant a second shift operation. The heat-up appeared to be normal except the right-hand side temperatures were lagging all others. The conclusion was that the change in the oven louver position was not producing the desired results. After about three hours elapsed time it was apparent that the right-hand skin was never going to reach cure temperature.

Jury rig baffling was set in place in the oven in an attempt to redirect the hot air flow. This did not cause any change in the right-hand temperatures. A separate thermocouple was substituted for the oven air thermocouple and taped to the bracket on the mold adjacent to the suspected junction. It registered a temperature reading of 454 degrees Kelvin in place of the 400 degrees Kelvin being reported by the regular thermocouple. Similar troubles were encountered during the aborted run. It was assumed that all temperatures being reported by the cable attached to the right-hand side plate were 55 degrees Kelvin in error. The computer was commanded to enter the cure cycle.

The next morning the tape wrapping was stripped from this cable and the same damp area was encountered. This time it was investigated more thoroughly. It had a strong odor of acetic acid and the cause of the trouble was now clear. The thermocouple insulation, wet with an acetic acid solution, caused the dissimilar wires of the thermocouple to act as a dry cell battery. Since copper-nickel alloys are positive with respect to iron, the resulting voltage generated by the current was in opposition to the thermal emf produced by the junction (the input impedance of the Doric is essentially an open circuit).

The moisture was evidently condensation since it only occurred at the external end of the oven conduit. This condensation somehow reacted with the adhesive or the fiberglass tape to produce the acetic acid solution. The tape was removed from all thermocouple cables and rudder No. 10 had no problems of this nature.

APPENDIX B
CALCULATION OF MAXIMUM RUBBER PRESSURE DURING FIRST RUDDER CURE

Height measurements of the front spar near the lower large end of the unsuccessful rudder indicated an oversize of 3.3 mm. This lead to the hypothesis that the rubber pressure was excessive during the cure cycle and deflected the molding tool side plates $\frac{3.3}{2}$ = 1.65 mm per plate.

The following work consists of deflection calculations of the molding tool side plates located at the front spar. Purpose of this work was to determine the rubber pressure which produced the excessive rudder size. These calculations were carried out for an assumed rubber pressure of 6.89 MPa acting on a 2.54-cm chordal strip of the molding tool side plate located between the rudder front spar and rear spar.

The side plates are modeled as a beam on four supports (see Figure B-1). Supports A and D are free ends bearing on hard points. Supports B and C are a line of 2.54-cm-diameter bolts used to assemble the molding tool.

The following steps were taken to determine the side plate deflection and the rubber mandrel pressure relationship.

The beam on four supports was divided into three beams (forward, middle, and aft) by cuts at support points B and C. Each beam is supported with the moments at supports B and C (i.e., M_B and M_C) treated as the redundant forces needed for the solution.

Solution of the redundant beam problem led to the result that

Deflection $Y_{F/S}$ = 2.16 mm (pressure = 6.89 MPa)

To produce $Y_{F/S}$ = 1.65 mm

$$\text{Pressure} = \frac{1.65}{2.16} \times 6.89 = \boxed{5.27 \text{ MPa}}$$

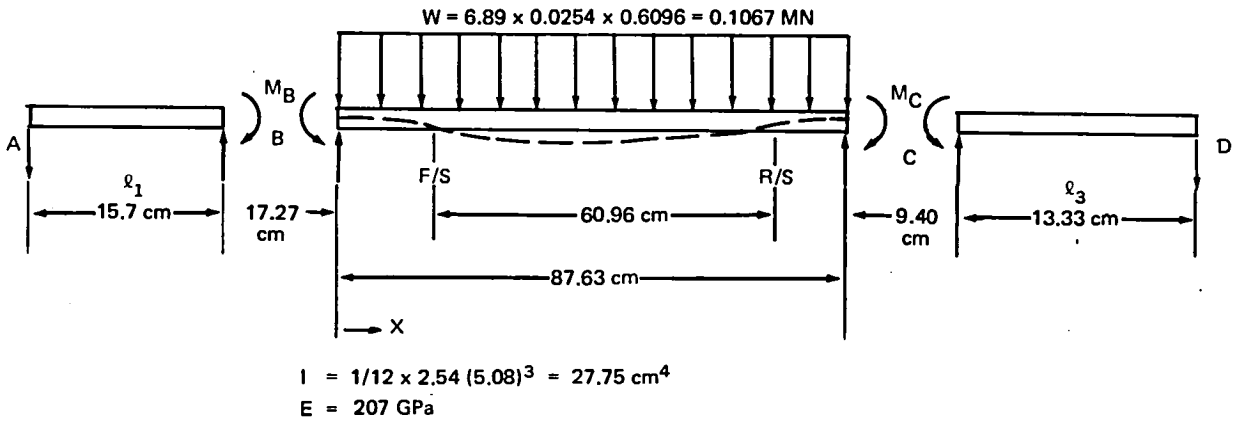

FIGURE B-1. BEAM MODELING OF THE RUDDER TOOL SIDE PLATES

APPENDIX C
THERMOCOUPLE SURVEY DURING THE FIRST RUDDER CURE

This appendix provides a survey of all the thermocouple readings taken during the test rudder cure. The heat-up and cure portions of the rudder cure cycle required a span of 387 minutes. The rudder cure cycle milestones were as follows:

Start of Heat-Up - 13:19:41	}	265 Minutes
Start of Cure - 17:44:36	}	122 Minutes
End of Cure - 19:46:36	}	

The test rudder was cured using the computerized temperature control system. The 8080A Central Processing Unit (CPU) was removed from the control system and the ICE-80 circuit emulation feature of the microcomputer development system was substituted. This allowed one to observe all that was transpiring, to look at or change any memory location, and to change the program while the control system is controlling the process.

Table C-1 shows the listing and the teletype printout format of the 99 thermocouples mounted on the rudder molding tool. The locations of these thermocouples are shown in Figure C-1.

Table C-2 gives a survey of all the rudder skin thermocouples at about half-hour intervals throughout the cure cycle. A plot of the average of thermocouples L78 and R80 at Station Z_{AR} = 476.94 is given in Figure C-2. This plot permits estimates to be made of skin heat-up rates. Typical values are 0.689 and 0.953^{o}K per minute.

About every 10 minutes, the program types out the most recent temperatures at each thermocouple. Five of these thermocouple surveys are given in Tables C-3 to C-7. These are typical surveys of the test rudder cure from the beginning through the end of the cure.

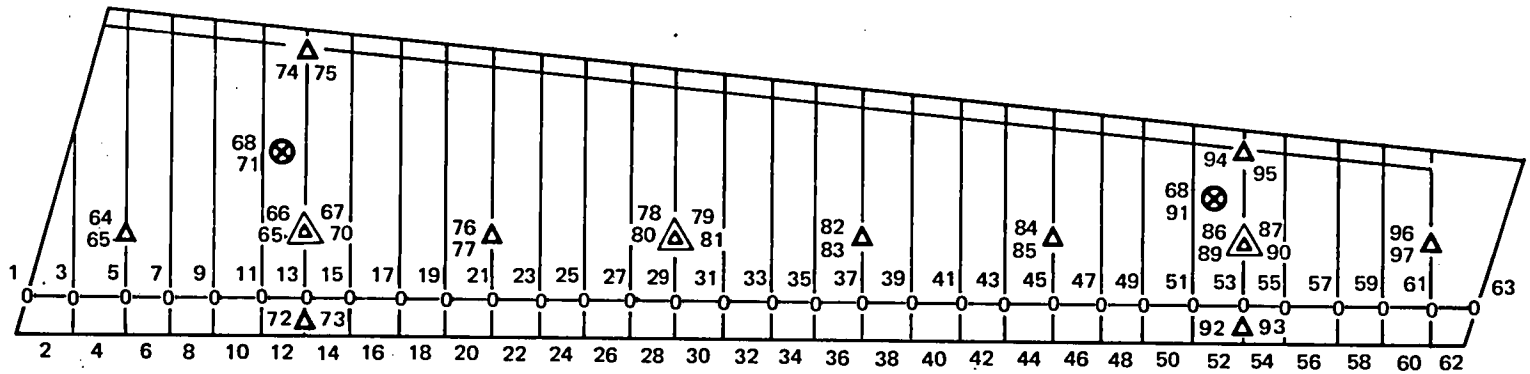

FIGURE C-1. GRAPHIC DISPLAY OF TEMPERATURE LOCATION CODE

TABLE C-1
THERMOCOUPLE LISTING FORMAT

L-ØA	L-RS	L-LE	L-PL	L-SK	HTR	SPAR	R-SK	R-PL	R-LE	R-RS	R-ØA
					2	1					
					4	3					
				64	6	5	65				
					8	7					
					10	9					
					12	11					
68	74	72	67	66	14	13	69	70	73	75	71
					16	15					
					18	17					
					20	19					
				76	22	21	77				
					24	23					
					26	25					
					28	27					
			79	78	30	29	80	81			
					32	31					
					34	33					
					36	35					
				82	38	37	83				
					40	39					
					42	41					
					44	43					
				84	46	45	85				
					48	47					
					50	49					
					52	51					
88	94	92	87	86	54	53	89	90	93	95	91
					56	55					
					58	57					
					60	59					
				96	62	61	97				
						63					

(SEE TABLES C-3 TO C-7)

NOTATION

LEFT	RIGHT	LOCATION
L – ØA	R – ØA	OVEN AIR
L – RS	R – RS	REAR SPAR
L – LE	R – LE	LEADING EDGE
L – PL	R – PL	PLATE (PLM SIDE PLATE)
L – SK	R – SK	SKIN
SPAR		FRONT SPAR
HTR		HEATERS (INTERNAL ELECTRIC)

TABLE C-2
SKIN THERMOCOUPLE SURVEY – TEST RUDDER CURE

TIME H:M:S	Z_{AR} MIN-UTES	TEMPERATURE (°K) 413.53 L_{64}	413.53 R_{65}	436.31 L_{66}	436.31 R_{69}	456.64 L_{76}	456.64 R_{77}	476.94 L_{78}	476.94 R_{80}	497.37 L_{82}	497.37 R_{83}	512.62 L_{84}	512.62 R_{85}	537.10 L_{86}	537.10 R_{89}	555.47 L_{96}	555.47 R_{97}
13:19:41	0																
13:20:35	1	297	297	297	298	297	297	297	297	297	297	297	297	297	298	297	299
13:31:12	11	300	299	299	300	299	299	300	300	299	300	299	301	300	302	298	303
13:41:51	22	306	304	305	305	304	305	306	307	305	307	306	308	307	311	308	313
14:02:50	43	324	320	322	322	319	321	322	325	322	325	323	330	325	335	328	339
14:23:53	64	345	338	340	342	338	340	342	346	343	347	344	353	346	360	352	365
14:45:06	85	366	358	359	360	356	359	360	365	362	367	364	375	367	384	376	390
15:06:09	106	384	374	377	376	373	376	377	380	380	385	383	392	386	402	398	411
15:37:52	138	407	390	399	400	396	400	401	398	404	410	408	407	412	424	425	432
15:58:41	159	420	400	413	414	409	413	414	412	418	423	420	415	426	433	438	435
16:30:28	191	438	418	432	432	428	432	432	429	435	440	439	434	444	448	455	448
17:02:15	222	446	427	441	439	437	434	441	438	445	448	448	440	453	450	460	454
17:34:01	254	447	431	444	440	443	444	445	442	448	448	450	437	455	451	463	452
*17:44:36	265	449	433	445	443	444	445	445	442	448	448	450	434	455	449	462	452
18:17:15	298	448	439	446	445	445	445	446	443	448	445	450	434	454	447	459	452
18:46:28	327	444	441	447	447	445	447	447	445	448	447	450	444	453	448	457	454
19:10:14	351	448	443	447	447	446	447	447	446	447	448	450	449	453	450	455	453
19:40:09	381	447	445	447	447	446	447	447	447	448	448	449	449	452	450	453	454
*19:46:36	387																

REF *START AND END OF CURE PERIOD

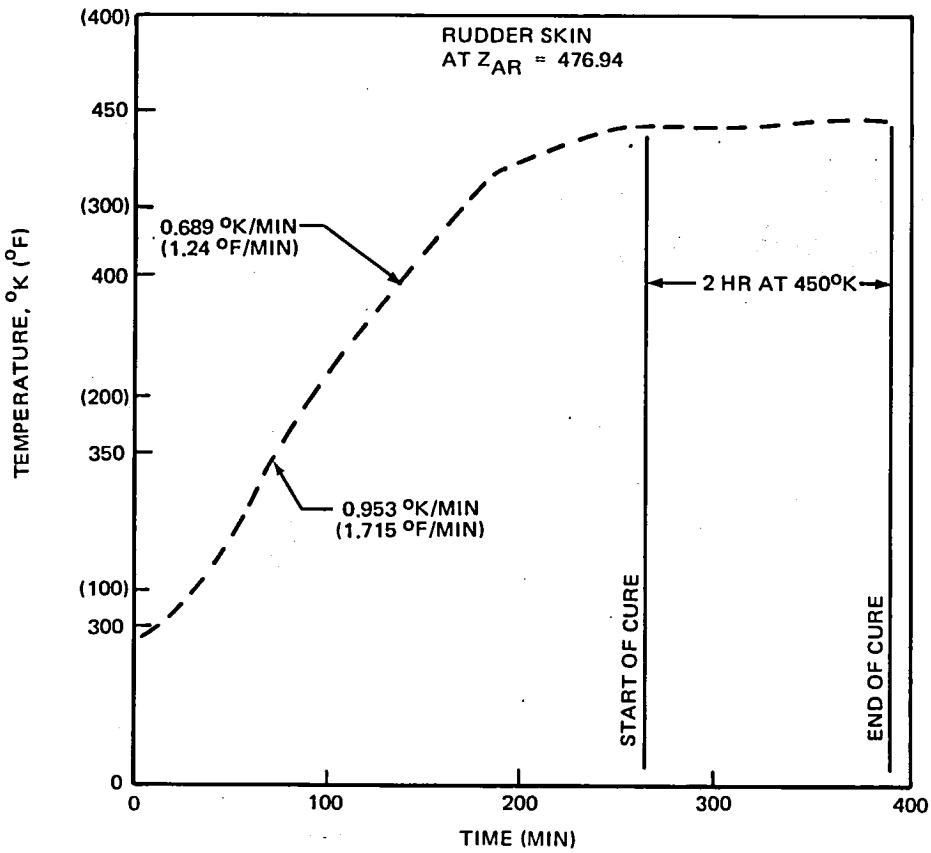

FIGURE C-2. PLOT OF SKIN THERMOCOUPLES NO. 78 AND 80

TABLE C-3
THERMOCOUPLE SURVEY, TIME = 13:20:35, TEST RUBBER CURE
(^{o}K)

13:20:35
SPAR, SKIN COEFF: 22 68

L-OA	L-RS	L-LE	L-PL	L-SK	HTR	SPAR	R-SK	R-PL	R-LE	R-RS	R-OA
					296.0	295.4					
						294.8					
					296.0						
				297.1		294.8	297.1				
					298.2						
						294.8					
					295.4						
						294.8					
					296.5						
						295.4					
					296.0						
310.4	297.6	295.4	301.5	296.5		294.8	297.6	303.2	297.6	298.2	311.5
					296.5						
						294.8					
					296.0						
						294.8					
					297.1						
						295.4					
					297.1						
				297.1		295.4	297.1				
					297.6						
						295.4					
					297.6						
						296.0					
					298.2						
						295.4					
					298.2						
			301.5	297.1		296.0	297.1	303.2			
					298.2						
						296.0					
					299.3						
						296.0					
					300.4						
						296.0					
					299.9						
				296.5		295.4	297.1				
					300.4						
						295.4					
					299.9						
						295.4					
					302.6						
						295.4					
					299.9						
				296.5		295.4	297.1				
					304.3						
						295.4					
					304.3						
						295.4					
					295.4						
						294.8					
					295.4						
310.4	297.6	296.5	301.5	297.1		295.4	297.6	302.6	297.1	298.2	311.5
					295.4						
						296.0					
					295.4						
						296.0					
					296.0						
						296.5					
					296.5						
				297.1		296.5	298.7				
					298.2						
						296.5					

TABLE C-4
THERMOCOUPLE SURVEY, TIME = 14:45:06, TEST RUDDER CURE
(°K)

14:45:06
SPAR, SKIN COEFF: 68 57

L-OA	L-RS	L-LE	L-PL	L-SK	HTR	SPAR	R-SK	R-PL	R-LE	R-RS	R-OA
						363.7					
					402.1	363.7					
					435.4	361.5	357.6				
				366.0	436.0	362.1					
					431.5	360.4					
					431.5	361.0					
					431.5	359.3					
489.9	369.3	356.5	407.6	359.3	431.0	360.4	359.8	409.8	358.2	370.4	498.7
					428.2	358.2					
					428.2	358.7					
					416.0	357.6					
				356.0	437.1	359.3	358.7				
					441.0	361.0					
					435.4	362.1					
					453.2	361.0					
			393.2	359.8	443.2	364.3	365.4	415.4			
					440.4	363.7					
					449.3	364.8					
					438.2	365.4	367.1				
					453.2	366.5					
					456.5	369.3					
					453.7	369.8					
					459.9	372.1	375.4				
				364.3	458.7	370.4					
					471.0	374.3					
					473.2	377.6					
					473.2	378.7	383.7	423.2	379.3	381.0	506.0
490.4	371.0	363.2	409.3	366.5	474.3	381.0					
					471.5	382.6					
					449.3	387.1					
					409.8	388.7	390.4				
				376.0	410.4	385.7					

TABLE C-5
THERMOCOUPLE SURVEY, TIME = 15:58:41, TEST RUDDER CURE
(^{o}K)

15:58:41

SPAR, SKIN COEFF: 48 171

L-OA	L-RS	L-LE	L-PL	L-SK	HTR	SPAR	R-SK	R-PL	R-LE	R-RS	R-OA
					441.5	417.6					
					455.4	417.6					
				420.4	463.2	415.4	397.8				
					463.2	416.0					
					464.3	413.2					
496.5	426.0	408.2	441.5	412.6	462.6	412.6	413.7	441.5	403.7	427.1	503.2
					468.7	402.6					
					467.6	402.1					
					464.3	401.5					
					465.4	411.5					
				409.3	468.7	409.3	413.2				
					456.5	409.8					
					458.2	411.5					
					458.2	412.1					
			433.2	413.7	452.6	409.3	411.5	448.7			
					447.1	414.3					
					464.3	415.4					
					463.2	417.6					
				418.2	468.2	418.7	422.6				
					453.7	414.8					
					453.2	418.7					
					445.4	417.6					
				420.4	447.1	417.6	414.8				
					466.5	419.3					
					461.5	423.7					
					462.6	427.6					
499.9	432.6	423.2	448.2	426.0	453.7	430.4	433.2	459.9	432.1	439.3	498.2
					462.1	431.5					
					439.3	432.6					
					439.3	434.3					
				437.6	457.1	436.0	434.9				
						436.0					

TABLE C-6
THERMOCOUPLE SURVEY, TIME = 17:44:36, TEST RUDDER CURE
(^{o}K)

17:44:36

SPAR, SKIN COEFF: 22 11

L-OA	L-RS	L-LE	L-PL	L-SK	HTR	SPAR	R-SK	R-PL	R-LE	R-RS	R-OA
					458.2	446.5					
					460.4	447.1					
				448.7	453.2	449.3	433.2				
					451.5	447.1					
					453.7	446.0					
					458.7	444.9					
447.6	452.6	442.1	446.5	445.4	458.2	446.5	443.2	442.6	432.1	452.6	444.3
					453.2	446.5					
					454.3	433.7					
					459.3	446.0					
				443.7	442.6	434.9	444.9				
					461.0	447.1					
					459.3	448.7					
					461.0	447.1					
			446.5	445.4	456.0	448.7	441.5	446.5			
					458.7	448.2					
					461.5	448.7					
					458.2	450.4					
				448.2	449.9	450.4	447.6				
					459.3	406.5					
					445.4	450.4					
					453.2	452.6					
				450.4	456.0	418.2	433.7				
					458.2	453.2					
					460.4	448.2					
					457.6	458.2					
448.2	458.2	454.3	452.6	454.9	459.9	460.4	448.7	449.3	457.1	456.0	433.2
					466.0	457.6					
					459.9	461.5					
					461.0	462.1					
				462.1	467.6	463.7	452.1				
						463.7					

TABLE C-7
THERMOCOUPLE SURVEY, TIME = 19:40:09, TEST RUDDER CURE
(^{o}K)

OVEN TEMP HAS NOT YET GONE DOWN 2.8^{o}K (5^{o}F)

19:40:09

SPAR, SKIN COEFF: 16 10

L-OA	L-RS	L-LE	L-PL	L-SK	HTR	SPAR	R-SK	R-PL	R-LE	R-RS	R-OA
					452.1	449.3					
					451.0	448.7					
				447.1	452.6	449.3	444.9				
					453.2	449.3					
					451.5	447.6					
					450.4	451.0					
447.6	446.0	445.4	447.1	446.5	453.2	447.6	446.5	446.5	433.7	448.2	444.3
					452.1	448.2					
					452.6	447.6					
					453.7	447.6					
				446.0	454.9	446.5	446.5				
					453.7	447.6					
					452.6	448.2					
					453.2	448.2					
			447.1	446.5	452.6	448.2	446.5	447.1			
					449.3	450.4					
					452.6	451.0					
					452.1	450.4					
				447.6	455.1	451.0	448.2				
					459.3	445.4					
					454.3	445.4					
					453.2	453.7					
				449.3	454.9	450.4	449.3				
					453.2	452.6					
					454.9	452.6					
					457.1	454.3					
447.1	451.5	451.0	449.9	451.5	454.9	454.9	449.9	450.4	446.0	451.0	448.9
					457.1	452.6					
					457.1	456.0					
					454.3	454.9					
				452.6	453.2	454.3	451.0				
						454.3					

19:46:36 CURE COMPLETE

APPENDIX D
DIMENSIONAL MEASUREMENTS OF DUMMY SKINS

The first set of dummy skins was used to cast internal rubber mandrels. These mandrels were used in the curing of the first composite rudder box (Section 5). However, this was an unsuccessful effort. Part of the fault was thought to lie in the use of a plywood base for the dummy skins because of an excessive thickness tolerance range. The first set of rubber mandrels was determined to be oversize (reference Section 6, Task 7) and the problem was resolved by fabricating a new set of dummy skins.

The fabrication of these dummy skins is described in Task 11 of Section 6. In place of the plywood, a 0.635-cm (1/4-inch) aluminum base plate was used for these new dummy skins in order to improve dimensional consistency. The right-hand dummy skin is shown in Appendix P (Figures P-3, P-4, and P-5). These photos were taken just prior to mounting the left-hand dummy skin which would close the mold for the internal rubber mandrels. The dummy skins were fabricated in such a manner so as to provide a rubber gap of 0.061 cm (0.024 inch). In order to avoid some of the previous dimensional problems, a survey was made of the dummy skin thicknesses. The results are shown in Tables D-1 and D-2. These tables also show the computation for the rubber gap allowance which would result from the use of these dummy skins. The results of the rubber gap calculations demonstrate the accuracy of the construction of the dummy skins and permit a judgment to be made on their suitability for casting usable rubber mandrels. This judgment is made in Task 11 of Section 6.

TABLE D-1
DUMMY PART DIMENSIONS FOR LEFT-HAND SKIN
(CORDAX READINGS)

AREA	TOTAL MEASURED THICKNESS (cm)	ALUMINUM PLATE THICKNESS (cm)	F/G DUMMY SKIN PLUS GAP PLUS 0.0762 SHROUD (cm)	SKIN PLUS GAP (cm)	ACTUAL G/E THICKNESS (cm)	ACTUAL GAP (cm)	AVERAGE GAP FOR NOTED AREA (cm)
OVERALL SKIN	0.864	0.652	0.213	0.137	0.091	0.046	0.053
	0.871	0.653	0.221	0.145	0.091	0.053	
	0.866	0.650	0.216	0.140	0.091	0.048	
	0.874	0.647	0.224	0.147	0.091	0.056	
	0.876	0.651	0.226	0.150	0.091	0.058	
	0.869	0.650 AVG	0.218	0.142	0.091	0.051	
	0.871		0.221	0.145	0.091	0.053	
	0.869		0.218	0.142	0.091	0.051	
6-PLY RIB FLANGE	0.927	0.650	0.277	0.201	0.142	0.058	0.053
	0.925	0.650	0.274	0.198	0.142	0.056	
	0.927	0.650	0.277	0.201	0.142	0.058	
	0.919	0.650	0.269	0.193	0.142	0.051	
	0.922	0.650	0.272	0.196	0.142	0.053	
	0.917	0.650	0.267	0.191	0.142	0.048	
	0.922	0.650	0.272	0.196	0.142	0.053	
	0.917	0.650	0.267	0.191	0.142	0.048	
	0.927	0.650	0.277	0.201	0.142	0.058	
8-PLY RIB FLANGE	0.935	0.650	0.284	0.208	0.160	0.048	0.061
	0.945	0.650	0.295	0.218	0.160	0.058	
	0.947	0.650	0.297	0.221	0.160	0.061	
	0.945	0.650	0.295	0.218	0.160	0.058	
	0.950	0.650	0.300	0.224	0.160	0.064	
	0.953	0.650	0.302	0.226	0.160	0.066	
	0.947	0.650	0.297	0.221	0.160	0.061	
	0.950	0.650	0.300	0.224	0.160	0.064	
	0.947	0.650	0.297	0.221	0.160	0.061	
	0.950	0.650	0.300	0.224	0.160	0.064	
REAR SPAR	0.947	0.650	0.297	0.221	0.183	0.038	0.038
	0.940	0.650	0.290	0.213	0.183	0.031	
	0.950	0.650	0.300	0.224	0.183	0.041	
	0.953	0.650	0.302	0.226	0.183	0.043	
	0.947	0.650	0.297	0.221	0.183	0.038	
FORWARD SPAR	1.092	0.650	0.442	0.366	0.318	0.048	0.051
	1.099	0.650	0.450	0.373	0.318	0.056	
	1.095	0.650	0.445	0.368	0.318	0.051	
	1.095	0.650	0.445	0.368	0.318	0.051	
HINGE BUILDUP	1.372	0.650	0.721	0.645	0.599	0.046	0.046
	1.328	0.650	0.678	0.602	0.559	0.043	0.043
SKIN BUILDUP	0.965	0.650	0.315	0.239	0.188	0.051	0.055
	0.965	0.650	0.323	0.246	0.188	0.058	

TABLE D-2
DUMMY PART DIMENSIONS FOR RIGHT-HAND SKIN (CORDAX READINGS)

AREA	TOTAL MEASURED THICKNESS (cm)	ALUMINUM PLATE THICKNESS (cm)	F/G DUMMY SKIN PLUS GAP PLUS 0.0762 SHROUD (cm)	SKIN PLUS GAP (cm)	ACTUAL G/E THICKNESS (cm)	ACTUAL GAP (cm)	AVERAGE GAP FOR NOTED AREA (cm)
OVERALL SKIN	0.856	0.649	0.208	0.132	0.091	0.041	0.043
	0.853	0.649	0.206	0.126	0.091	0.038	
	0.859	0.650	0.211	0.135	0.091	0.043	
	0.864	0.645	0.216	0.138	0.091	0.048	
	0.859	0.651	0.211	0.135	0.091	0.043	
	0.859	0.650	0.211	0.135	0.091	0.043	
	0.859	0.646	0.211	0.135	0.091	0.043	
	0.856	0.647	0.208	0.132	0.091	0.041	
	0.861	0.648 AVG	0.213	0.137	0.091	0.046	
	0.853		0.206	0.130	0.091	0.038	
6-PLY RIB FLANGE	0.902	0.648	0.254	0.178	0.142	0.036	0.041
	0.902	0.648	0.254	0.178	0.142	0.036	
	0.909	0.648	0.262	0.185	0.142	0.043	
	0.907	0.648	0.259	0.183	0.142	0.041	
	0.904	0.648	0.256	0.180	0.142	0.038	
	0.909	0.648	0.267	0.185	0.142	0.043	
	0.904	0.648	0.260	0.183	0.142	0.041	
	0.907	0.648	0.262	0.185	0.142	0.043	
	0.899	0.648	0.252	0.175	0.142	0.033	
	0.912	0.648	0.264	0.188	0.142	0.046	
	0.904	0.648	0.257	0.180	0.142	0.038	
SKIN BUILDUP	1.043	0.648	0.396	0.320	0.257	0.064	0.066
	1.046	0.648	0.399	0.323	0.257	0.066	0.066
8-PLY RIB FLANGE	0.925	0.648	0.277	0.201	0.160	0.041	0.041
	0.922	0.648	0.274	0.198	0.160	0.038	
	0.925	0.648	0.277	0.201	0.160	0.041	
	0.930	0.648	0.282	0.206	0.160	0.046	
	0.925	0.648	0.277	0.201	0.160	0.041	
	0.925	0.648	0.277	0.201	0.160	0.041	
	0.922	0.648	0.274	0.198	0.160	0.038	
	0.922	0.648	0.274	0.198	0.160	0.038	
	0.927	0.648	0.254	0.203	0.160	0.043	
	1.046	–	–	–	–	–	
REAR SPAR	0.925	0.648	0.277	0.201	0.183	0.018	0.023
	0.930	0.648	0.282	0.206	0.183	0.023	
	0.930	0.648	0.282	0.206	0.183	0.023	
	0.935	0.648	0.287	0.211	0.183	0.023	
	0.932	0.648	0.285	0.208	0.183	0.025	
	0.930	0.648	0.282	0.206	0.183	0.023	
FORWARD SPAR	1.069	0.648	0.422	0.345	0.318	0.028	0.041
	1.069	0.648	0.422	0.345	0.318	0.028	
	1.080	0.648	0.432	0.356	0.318	0.038	
	1.082	0.648	0.434	0.358	0.318	0.041	
	1.082	0.648	0.434	0.358	0.318	0.041	
	1.092	0.648	0.445	0.368	0.318	0.051	
	1.092	0.648	0.445	0.368	0.318	0.051	
	1.092	0.648	0.445	0.368	0.318	0.051	
	1.092	0.648	0.445	0.368	0.318	0.051	
HINGE BUILDUP	1.031	0.648	0.384	0.307	0.257	0.051	0.053
	1.031	0.648	0.384	0.307	0.257	0.051	
	1.034	0.648	0.386	0.310	0.257	0.053	

APPENDIX E
PLM SIDE PLATE STRAIN VERSUS RUBBER PRESSURE

Two uniaxial strain gages were bonded to the outer faces of the 5.08-cm steel side plates of the PLM in the chordal direction (one gage per side plate, midway between rib bays at Z_{AR} = 461.70 and Z_{AR} = 468.77 and midway between the front and read spars). These strain gages were installed to:

1. Provide a measure of the internal rubber pressure which would be indicated by deflection and strain in the side plates.

2. Provide an indication of how well the rubber mandrels perform during repeated use.

To achieve No. 1 above, it was necessary to compute a relationship between chordwise strain in the 5.08-cm sideplates and the internal rubber pressure in rib bay Z_{AR} = 461.70 to 466.77. This was based on the assumption that the PLM side plates act like an infinitely long plate since they are about 4.27 meters long and 0.914 meters wide.

The strain gage readings recorded during the cure of the replacement test rudder and the first production rudder are given in Figures E-1 and E-2. These are the greater of the two strain gage readings in each case. The maximum strain for each rudder cure as well as the corresponding rubber pressure were plotted in Figure E-3. A pressure-strain relationship was derived as an average of the strain calculated from the two PLM side plate idealizations depicted in Figure E-4. The relationship is that

716 μm/m strain is equivalent to 2.07 MPa (300 psi) rubber pressure.

Rubber was first used for the cure of the replacement rudder box and it produced a maximum pressure of 2.17 MPa (314 psi). A maximum pressure of 1.86 MPa (270 psi) was produced during the curing of the tenth rudder. This demonstrated that rubber mandrels (DAPCO 38-3 silicone rubber) are a reasonably reliable means of producing pressure for this process.

The strain gage values shown in Figure E-1 indicate that the rubber started to produce pressure shortly after the oven was turned on and the

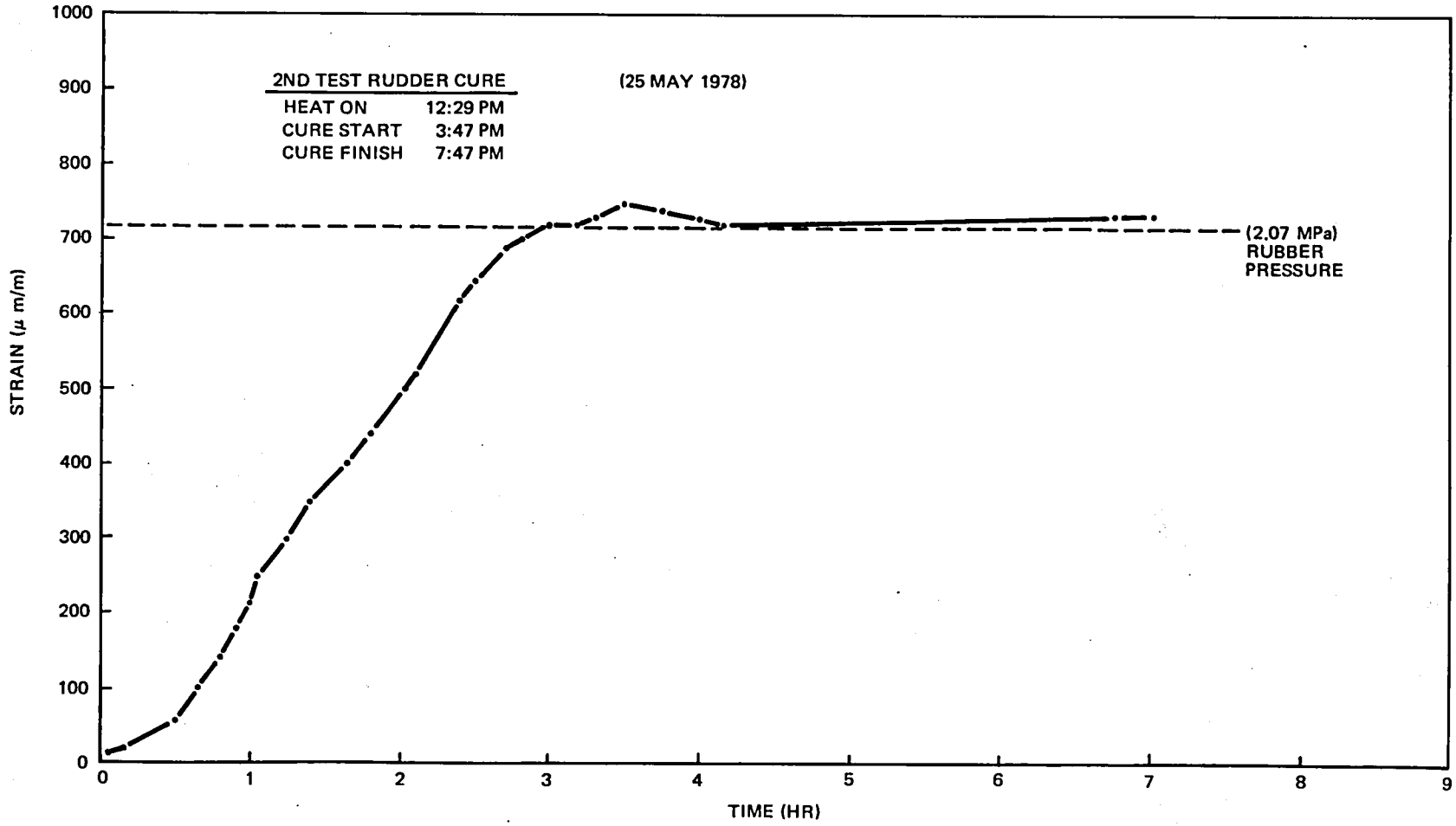

FIGURE E-1. STRAIN READINGS OF PLM 2-INCH SIDE PLATES AT STA Z_{AR} = 461 MIDWAY BETWEEN F/S AND R/S DURING TEST RUDDER CURE

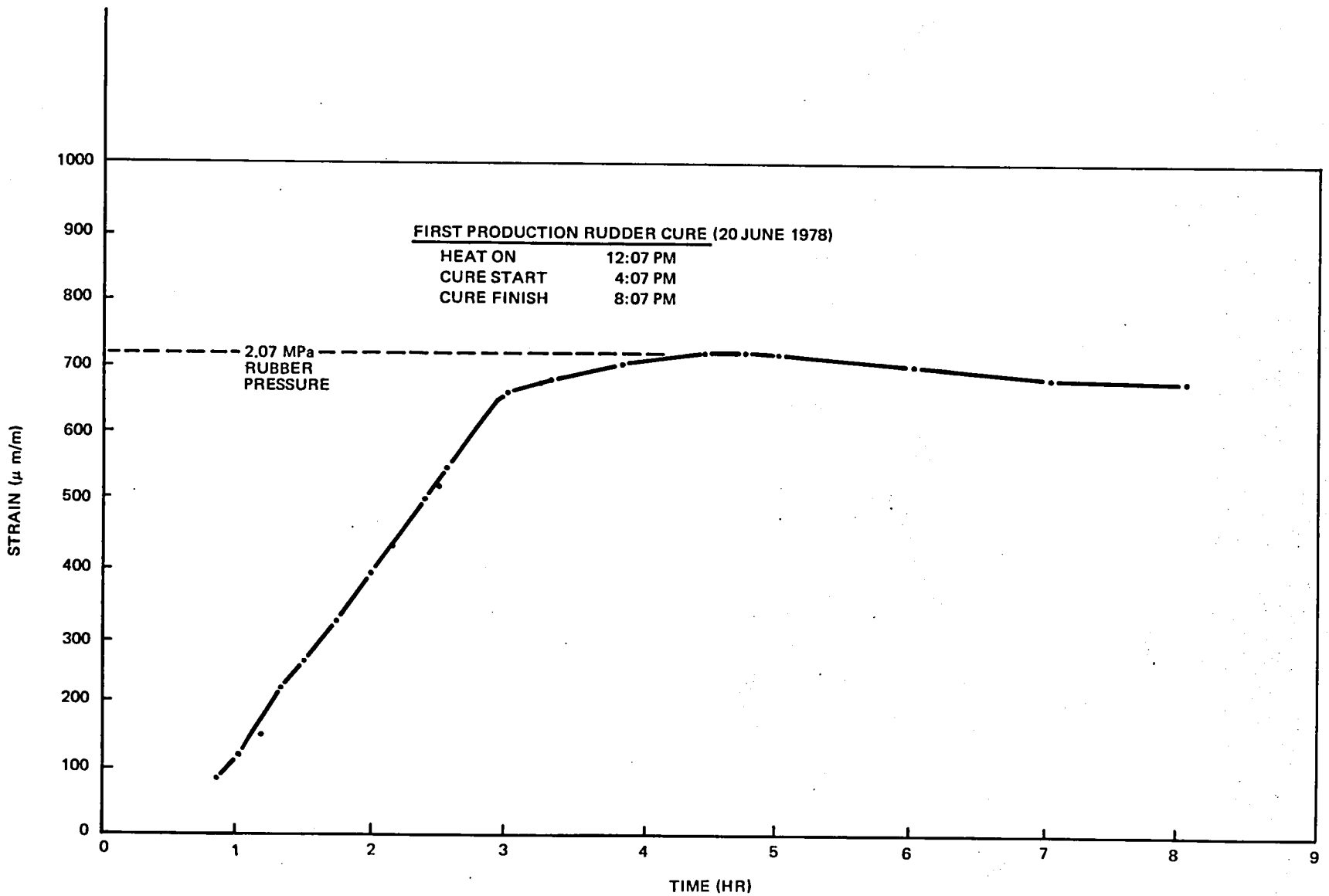

FIGURE E-2. STRAIN READINGS OF PLM 2-INCH SIDE PLATES AT STA Z_{AR} = 461 MIDWAY BETWEEN F/S AND R/S DURING FIRST PRODUCTION RUDDER CURE

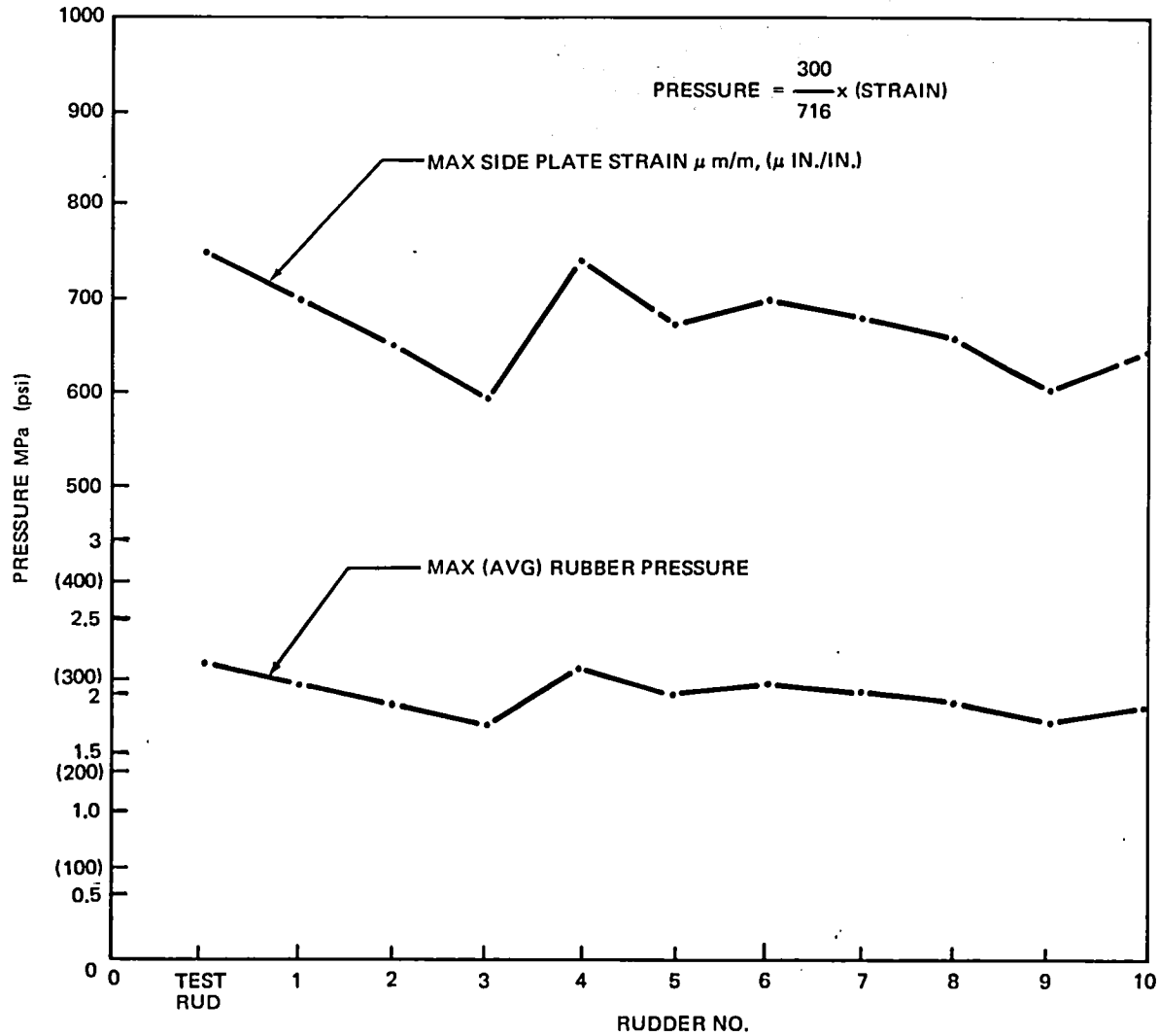

FIGURE E-3. SURVEY OF MAXIMUM SIDE PLATE STRAIN AND RUBBER PRESSURE DURING RUDDER CURE CYCLE (STA Z_{AR} = 461)

maximum strain was reached in 3-1/2 hours time. The maximum strain of 750 μ m/m corresponds to a maximum rubber pressure of 2.17 MPa (Figure E-3) which shows that the goal of not exceeding 2.07 MPa to avoid yielding the rubber has not been significantly exceeded considering the steep slope of Figure J-12 (Appendix J).

A prime goal of the cure cycle was to provide a minimum of 0.69 MPa (100 psi) rubber pressure when the resin gelled. The strain observations and the calculations in Section 7 demonstrate that this goal was achieved during the rudder cure cycles.

THREE BEAM, SIMPLE SUPPORT ASSUMPTION

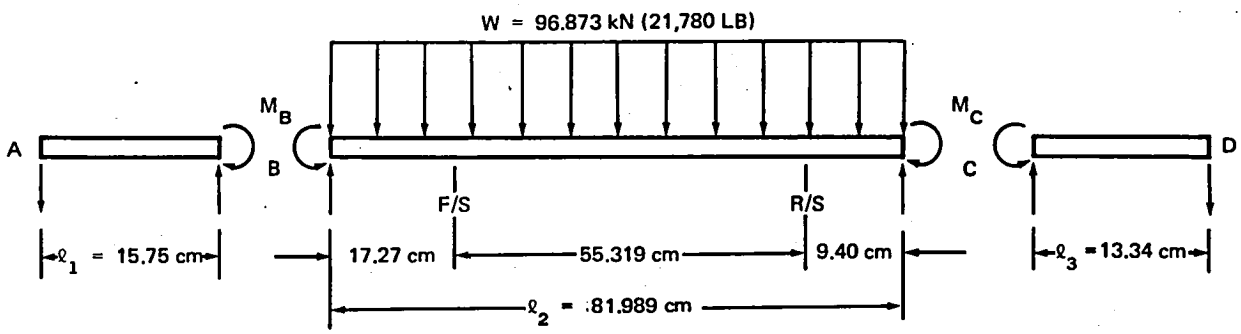

FULLY FIXED ASSUMPTION

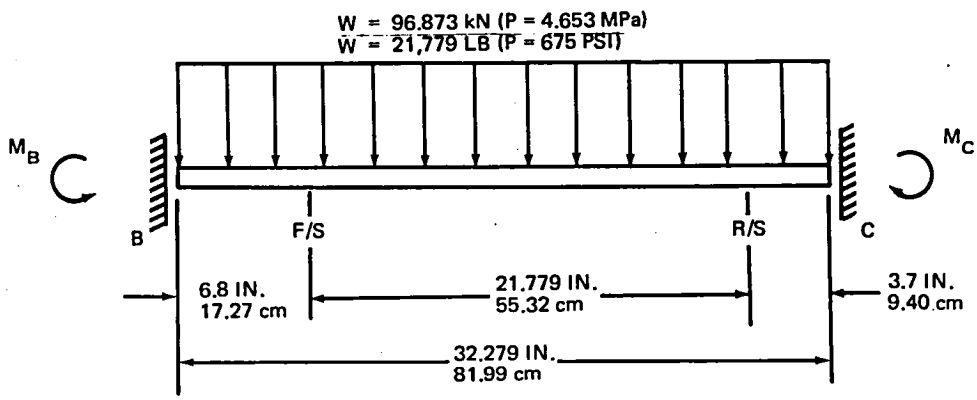

PLATE t = 5.08 cm (2 IN.)

PLATE E = 207 GPa (30 x 10^6 PSI)

FIGURE E-4. PLM SIDE PLATE IDEALIZATION DURING PRESSURIZATION CYCLE

APPENDIX F
LINEAR THERMAL COEFFICIENT MEASUREMENTS OF SILICONE RUBBER AND RUBBER-STEEL MESH COMPOSITE SAMPLES

Linear thermal coefficient measurements of three DAPCO 38-3 silicone rubber samples and three DAPCO 38-3 silicone rubber-steel mesh composite samples are described in this appendix. Size of these specimens and the method of curing are also described. These specimens were fabricated at the Douglas Aircraft Company and delivered to Geoscience, Ltd. of Solano Beach, California for measurement of the thermal expansion coefficients. A description of the results is presented in Table 18.

Geoscience was requested to make measurements ranging from room temperature to 450^{o}K. The sample blocks measured 2.54 cm thick, 7.62 cm wide, and 15.24 cm long. Measurements were made in all three dimensions. The following paragraphs outline the laboratory test method used and the results obtained.

Apparatus

The samples had to be utilized intact and were too large for a standard ASTM E 228-66A vitreous silica dilatometer. The ASTM apparatus was therefore modified. Figures F-1 and F-2 present a sketch and photograph of the apparatus used. The vitreous silica rods, which support the dial gage, are fastened securely into the aluminum base plate and slide in the alignment plate so that the aluminum can expand around the low-expansion silica rods without moving them. The base plate constitutes the reference surface for measurement.

The dial gage lowest scale markings are 2.54×10^{-4} cm and values can be interpolated to 7.62×10^{-5} cm. Temperatures are measured by two thermocouples, one in the oven for setting the temperature level, and the other taped securely to the sample.

Some of this apparatus was specially constructed for this set of measurements. It was therefore necessary to test the proper functioning of the instrument by measurement of thermal expansion of a sample of known material. This was done using a 7.62-cm sample of 1020 steel bar stock. The data obtained with this sample agree with the literature value within 1 percent.

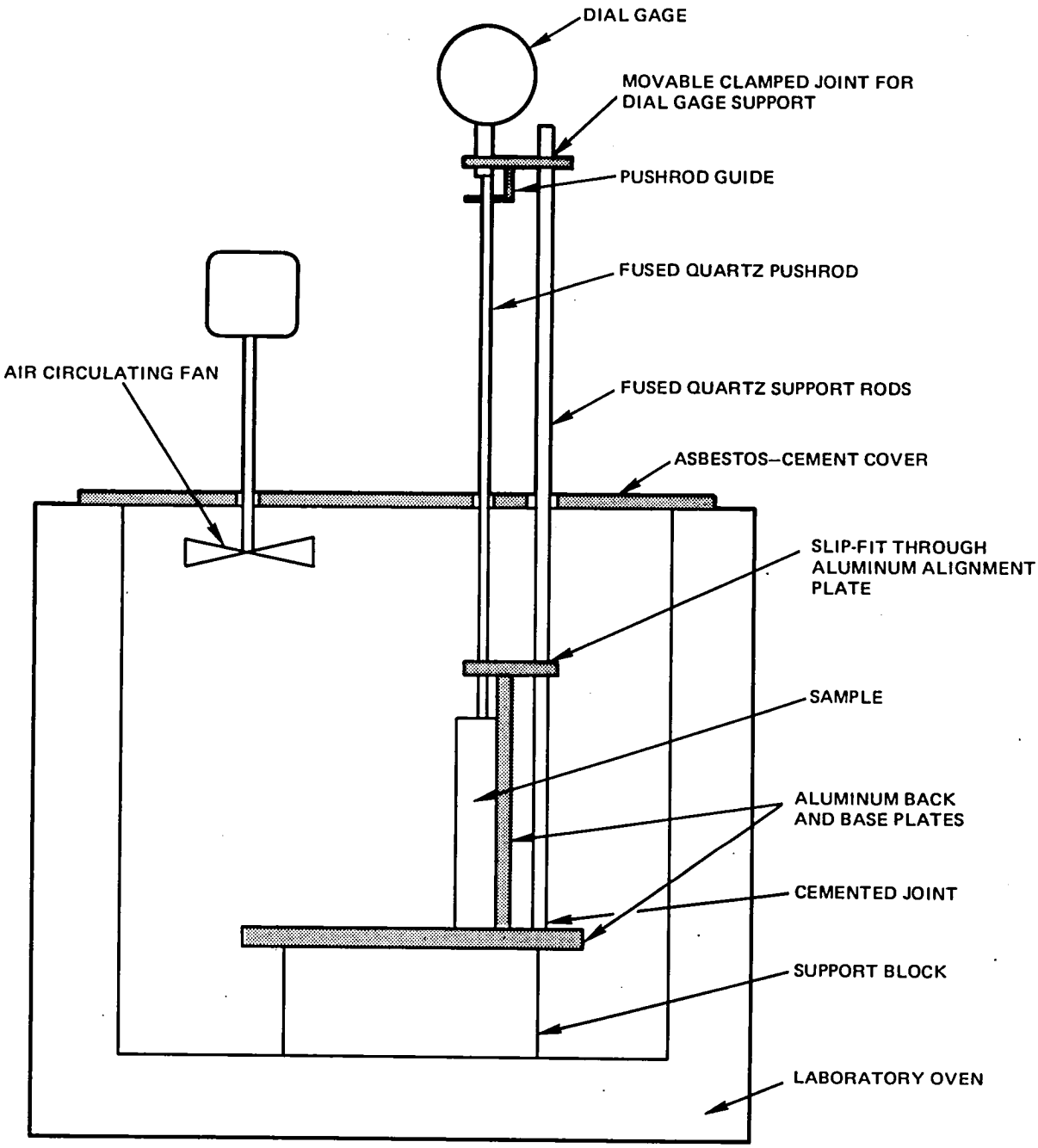

FIGURE F-1. SKETCH OF MODIFIED FUSED SILICA (QUARTZ) DILATOMETER

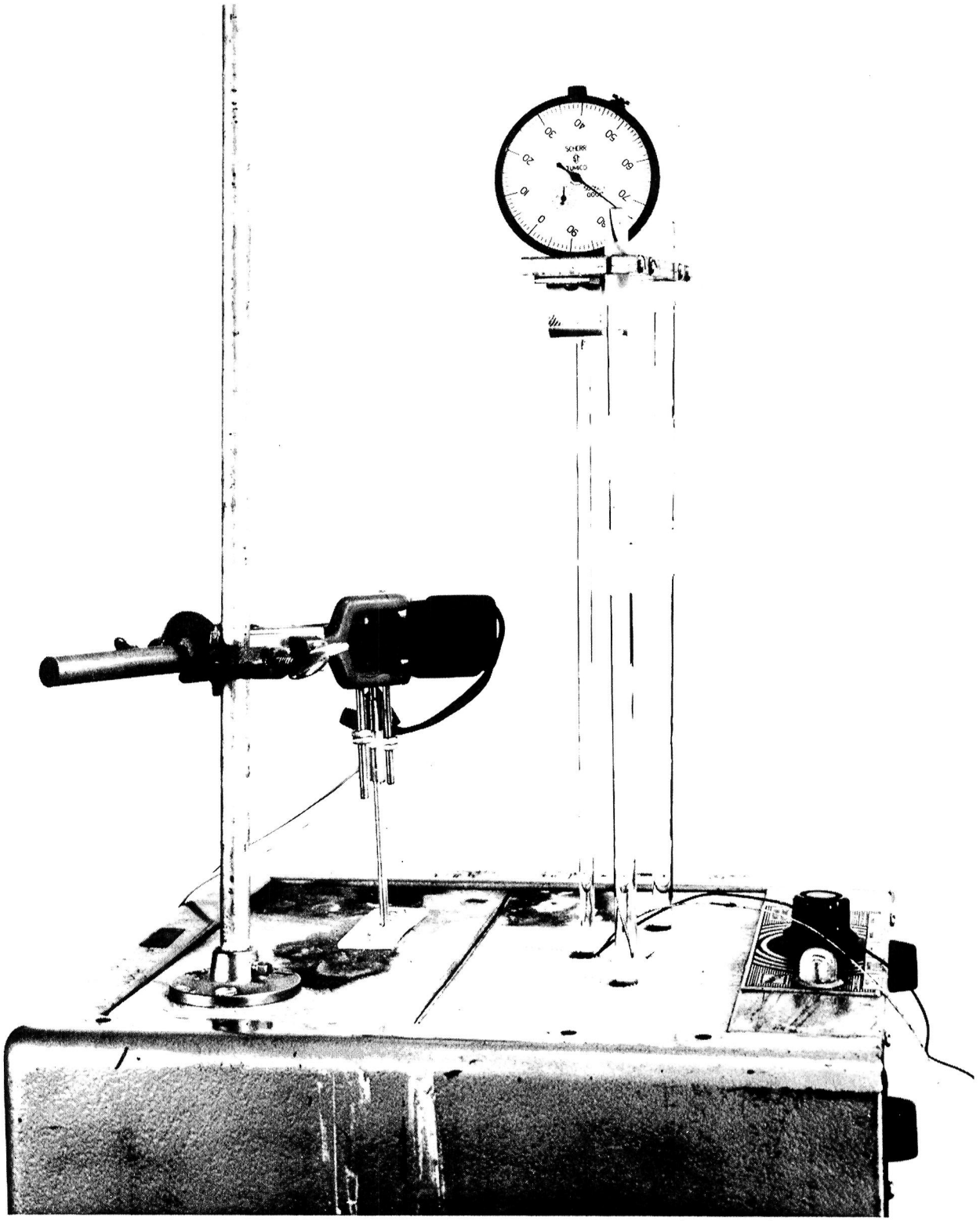

FIGURE F-2. PHOTOGRAPH OF THE MODIFIED DILATOMETER

Test Procedure

After an initial reading of the thermometer and dial gage, the oven power level was set to yield a chosen temperature, and the apparatus was allowed to equilibrate for 90 minutes. After this time, initial tests indicated that the temperature was sufficiently uniform throughout, as evidenced by a stable dial gage reading. Sample temperature and dial gage readings were then recorded and the oven power level changed to a new value. After taking readings at $450^{o}K$, the entire assembly was allowed to return to room temperature and the dial gage reading was recorded to ensure that the sample had not shifted. Readings were then taken at room temperature and at temperatures near $339^{o}K$, $394^{o}K$, and $450^{o}K$.

Results

The raw data for each sample are shown in Figures F-3 through F-8, and the average thermal coefficients of expansion over the temperature range are presented in Table 18.

The extreme variation in expansion coefficient with temperature level of some of the samples should be noted, along with the differences in coefficient exhibited by the same sample in different directions. In some cases, two points are shown for nearly equal temperatures. One point of these pairs was obtained on expansion, the other on contraction.

Discussion

All of the data from these samples exhibit more scatter than would be expected for the apparatus, which reproduces the coefficient of expansion for steel accurately despite the fact that steel expands an order of magnitude less than that of silicone rubber samples. This is thought to be caused by transient sample warping. During the heating cycle, the sample surface expands faster than the center, thus building up internal stresses which cause the sample faces to warp. This results in some shift in the apparatus.

The behavior of the samples containing steel mesh may be attributed to internal stresses. These stresses can affect the sample in at least three ways. If the slab is without internal stress at room temperature, then heating

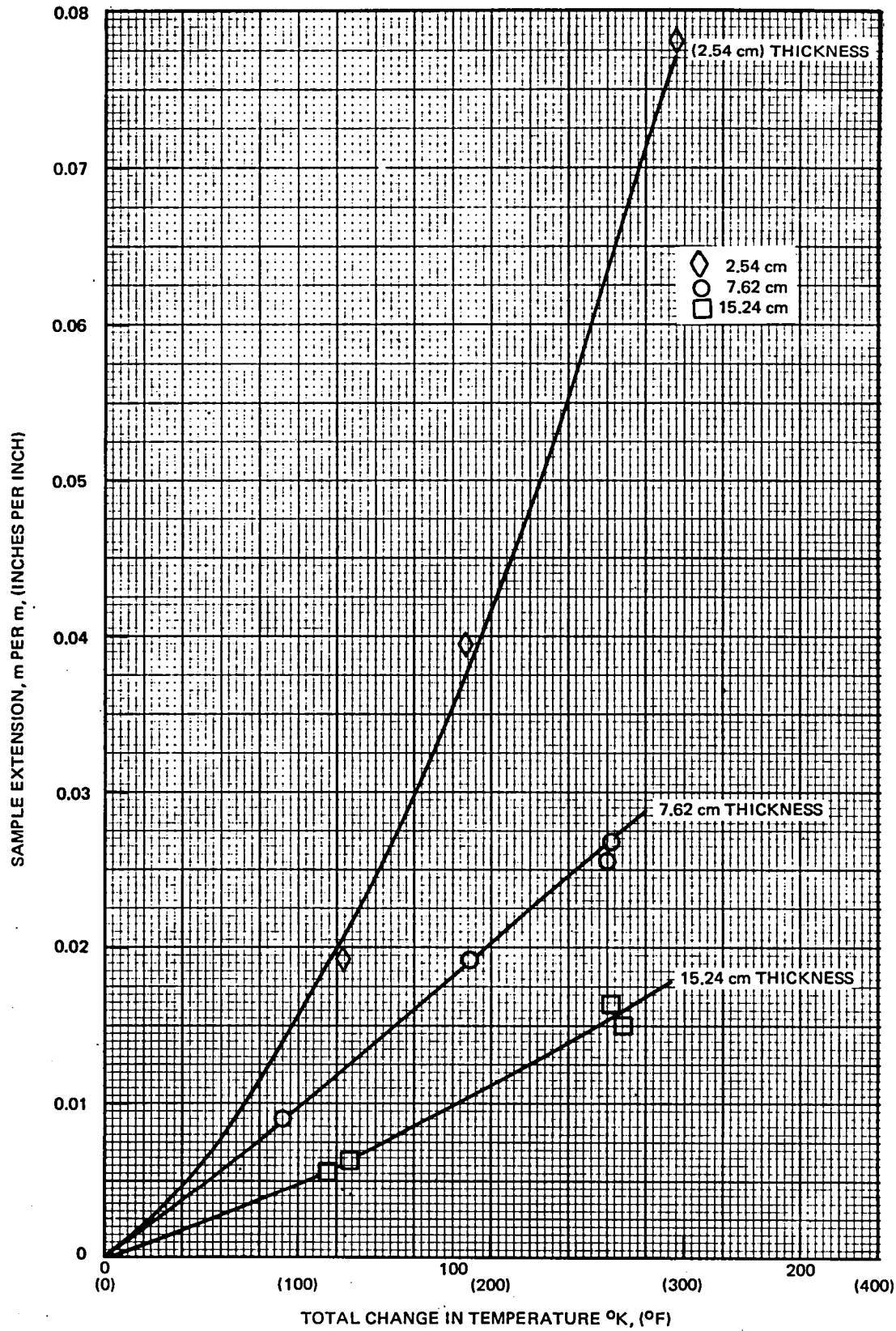

FIGURE F-3. SAMPLE NO. 1, 38-3 WITH EXPANDED METAL, 5 PERCENT THINNER

places the steel mesh in tension and the silicone rubber in compression. Since the steel is not uniformly distributed, the faces of the slab would be expected to warp, even though the internal temperature of the slab is uniform. If the steel does not lie on the neutral axis (considering the slab as a beam), the entire slab would be expected to bend exactly as does a bimetallic thermostat material. Finally, the volume of the sample increases with heating. Since the steel restrains the sample from expanding in the long direction, the short direction — which is unrestrained — expands a proportionately larger amount.

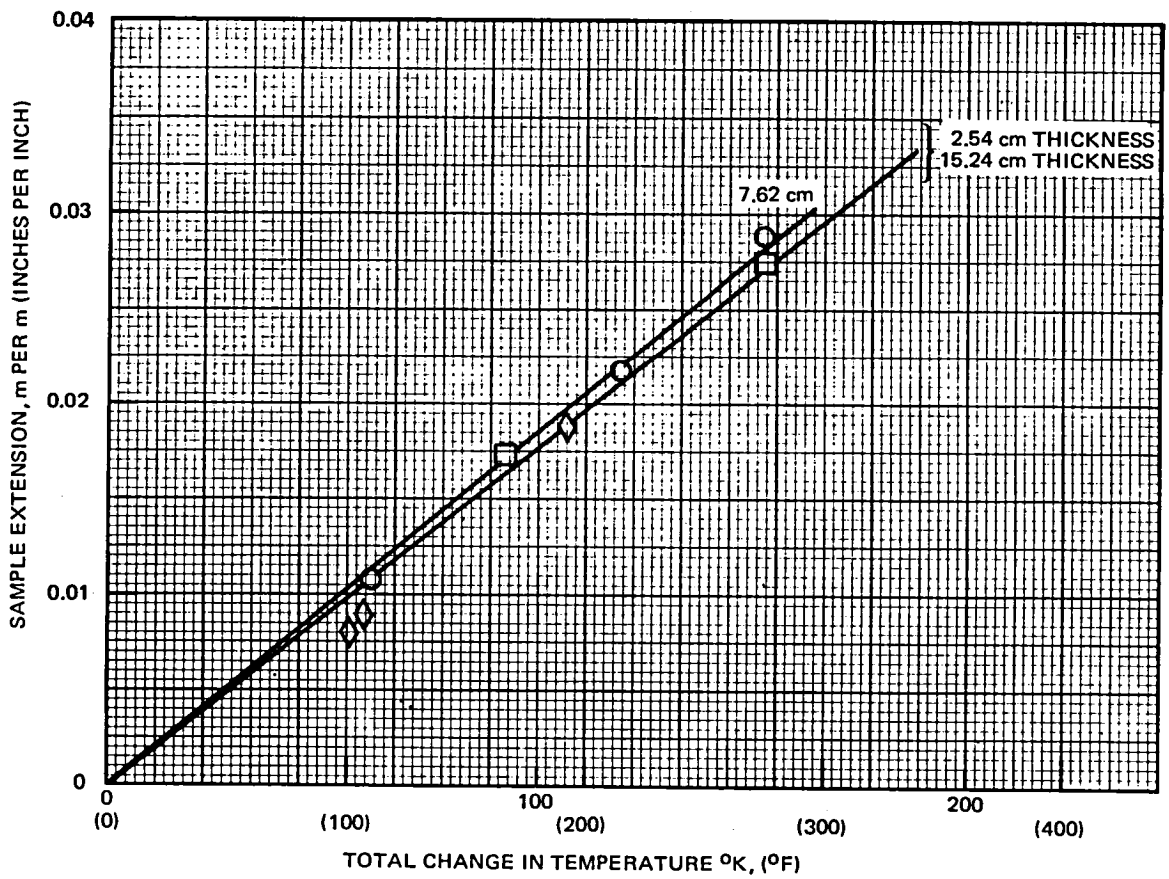

FIGURE F-4. SAMPLE NO. 2, 38-3, 5 PERCENT THINNER

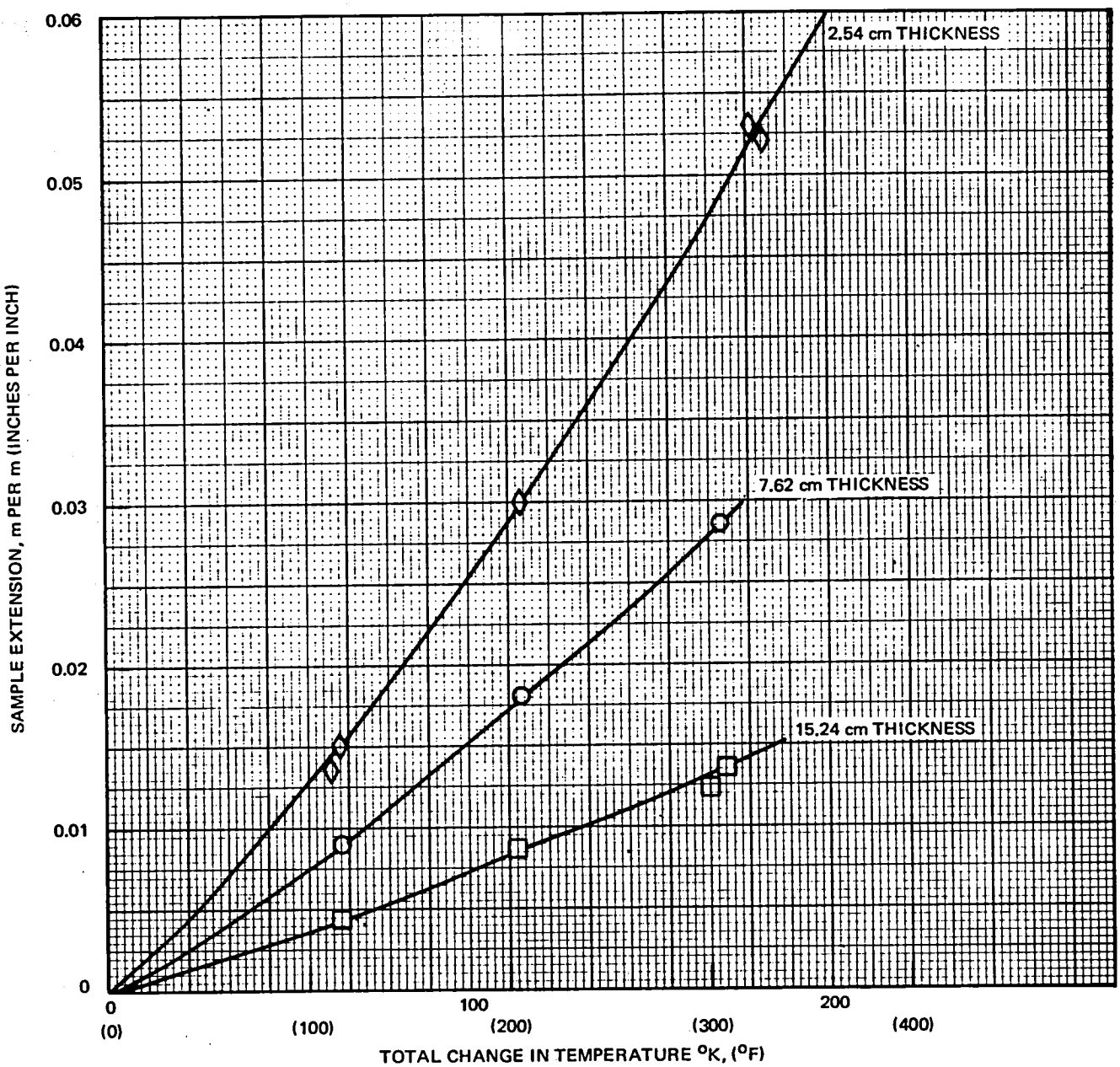

FIGURE F-5. SAMPLE NO. 3, 38-3 WITH EXPANDED METAL, 5 PERCENT THINNER

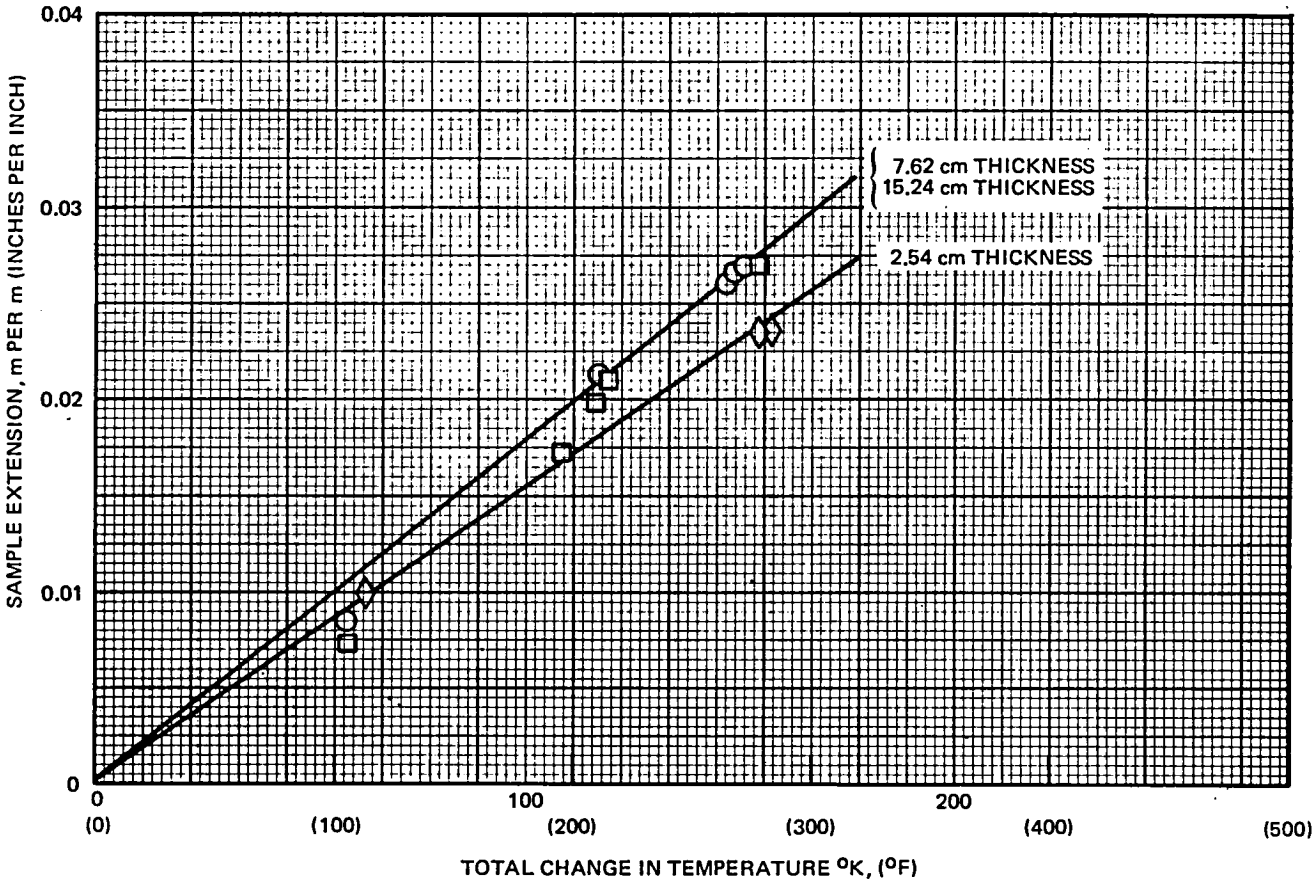

FIGURE F-6. SAMPLE NO. 4, 38-3, 5 PERCENT THINNER

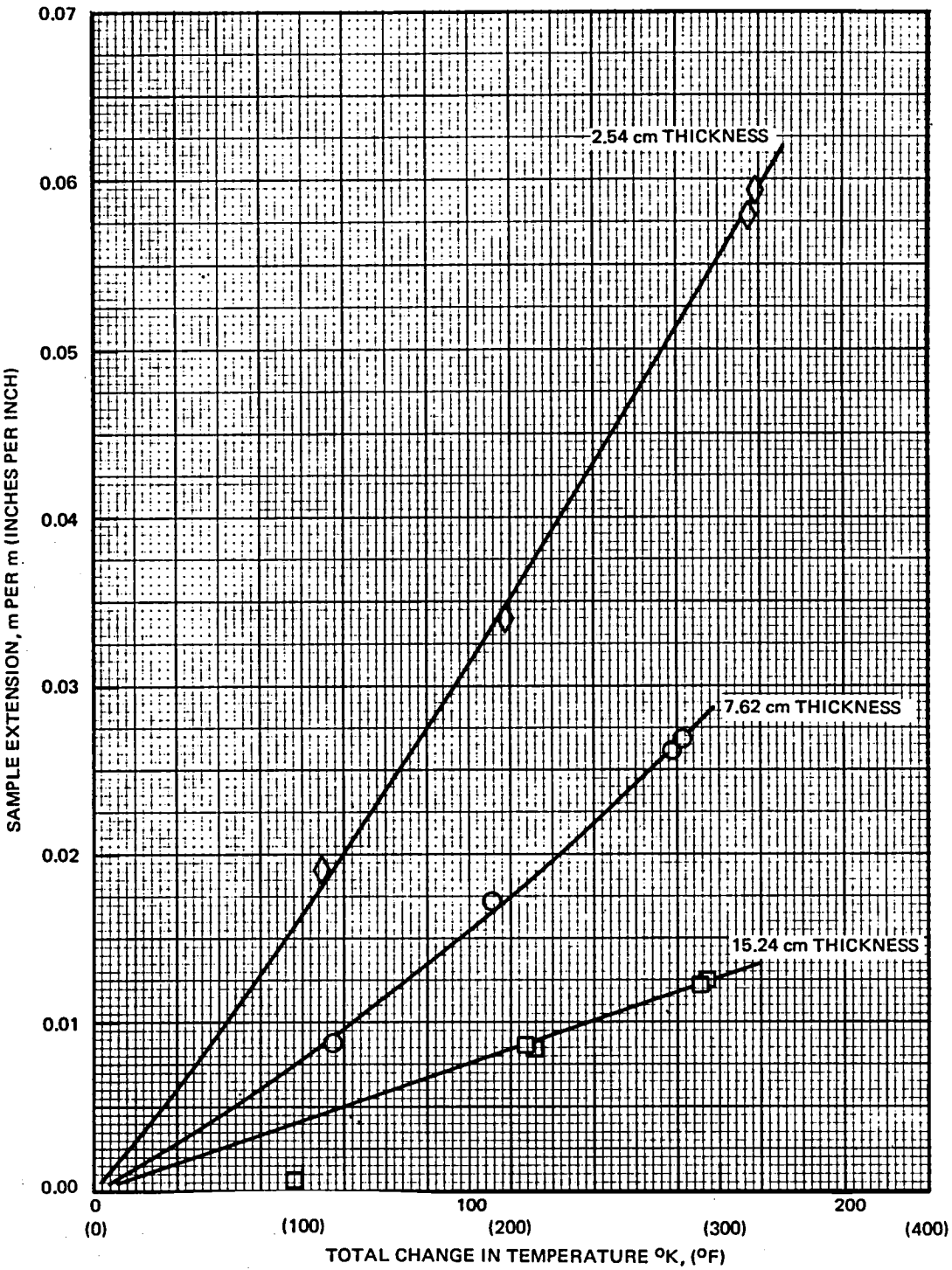

FIGURE F-7. SAMPLE NO. 5, 38-3 WITH EXPANDED METAL, 5 PERCENT THINNER

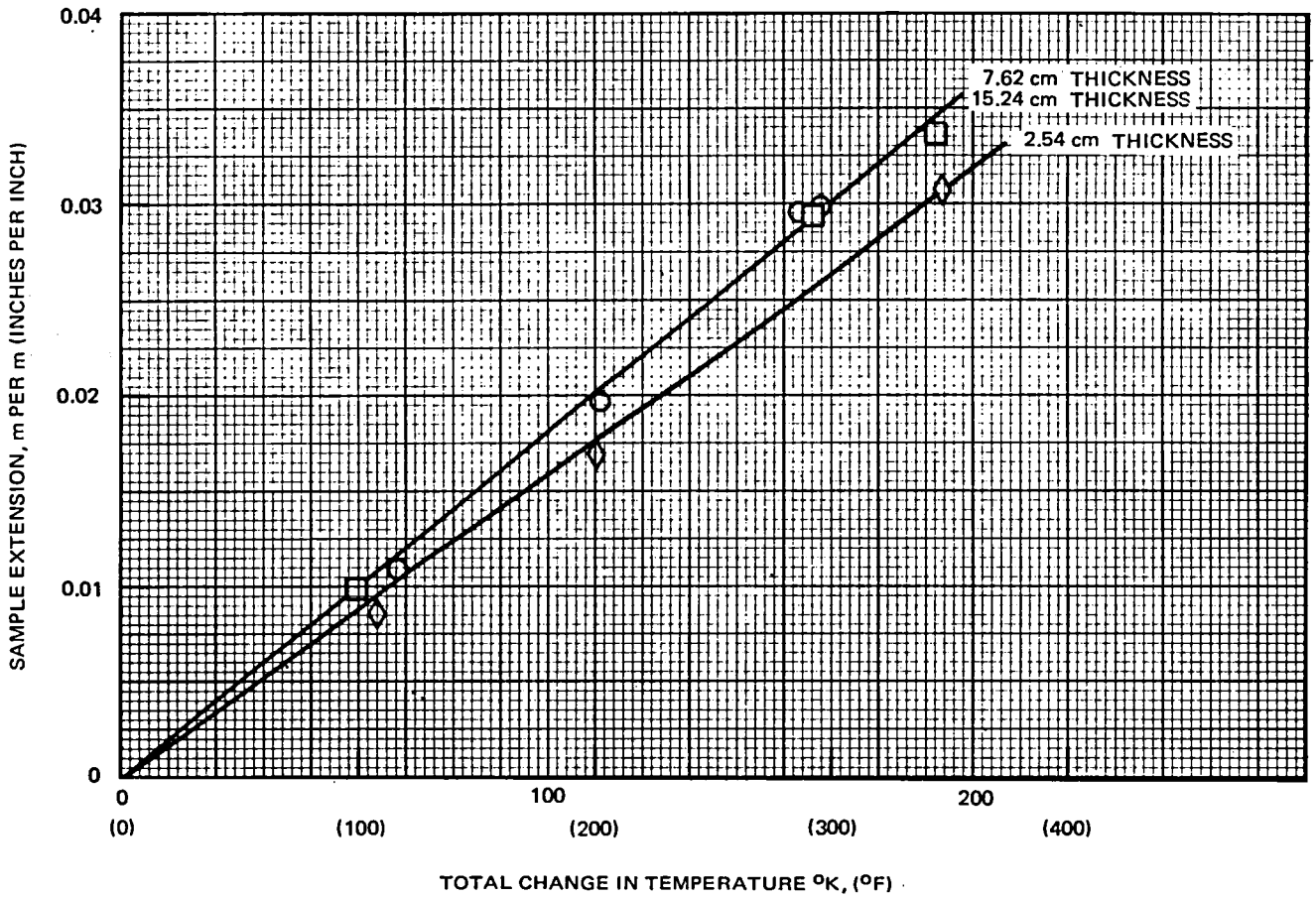

FIGURE F-8. SAMPLE NO. 6, 38-3, 5 PERCENT THINNER

APPENDIX G
RUDDER WEIGHT

This Appendix contains the estimated component and subcomponent weights for the woven broadgoods rudder and the 7.62-cm tape rudder which are listed in Table G-1.

TABLE G-1

WEIGHT COMPARISONS OF UPPER AFT RUDDER

CONVENTIONAL VERSUS ORIGINAL GRAPHITE COMPOSITE VERSUS NEW COMPOSITE

	METAL RUDDER WEIGHTS (kg)	COMPOSITE RUDDER WEIGHT (kg)						WEIGHT DIFFERENCE OF ORIG COMPOSITE RUDDER VERSUS NEW COMPOSITE RUDDER	REASON FOR WEIGHT CHANGE
		ORIGINAL COMPOSITE DESIGN			NEW COMPOSITE DESIGN				
		GRAPHITE	FIBER-GLASS	OTHER	GRAPHITE	FIBER-GLASS	OTHER		
SKIN	14.58	7.20			8.28			+1.08	INCREASED THICKNESS
RIBS	6.84	3.56			4.79			+1.23	INCREASED THICKNESS
FRONT SPAR	4.64	1.46			1.98			+0.53	INCREASED THICKNESS
REAR SPAR	3.00	0.23			0.30			+0.08	INCREASED THICKNESS
TRAILING EDGE	–		2.19	0.10		2.21	0.16	+0.08	ACTUAL VERSUS CALCULATED
TIP ASSEMBLY	0.49		0.43	0.05		0.43	0.05		
LEADING EDGE	6.30		4.35	0.14		4.14	0.14	–0.21	ACTUAL VERSUS CALCULATED
FAIRINGS	0.83		0.54			0.54			
FITTINGS	3.36			3.10			3.12	+0.02	ACTUAL VERSUS CALCULATED
ACCESS DOORS	0.17			0.13			0.13		
PAINT	0.68			2.68			2.68		
SEAL	0.49			0.48			0.48		
ADDITIONAL ITEMS	0.04			1.20			0.85	–0.35	BOOKKEEPING, CHANGES, MISC PARTS INCORPORATED UNDER MAJOR HEADINGS
TOTAL	41.42	12.44	7.52	7.87	15.36	7.32	7.60	+2.45	
		27.82			30.28				

APPENDIX H
DETERMINING THE RESIN (N5208) GEL TEMPERATURE

The gel temperature was determined for T300/5208 graphite/epoxy composite broadgoods for fresh material and two predensifications and two constant heat rise rates.

To determine the gel temperature for a particular constant heat rise rate, several samples of 0.635-cm by 0.635-cm preimpregnated material were placed in an oven at room temperature. The oven temperature was raised uniformly at the desired rate. Periodically, a sample was removed from the oven and placed on a hot plate heated to $450^{o}K$. The time-to-gel was noted in minutes and seconds. As the gel time grew shorter, the operator could determine the upper and lower limits of the gel temperature.

The gel time was determined using the following procedure:

1. Cut a randomly selected sample of prepreg approximately 0.635 cm by 0.635 cm in size.

2. Precondition a hot plate to $450^{o} \pm 1^{o}K$ ($350^{o} \pm 2^{o}F$).

3. Place a microcover glass on the hot plate, allowing 20 seconds for it to reach temperature equilibrium. Position a specimen at the center of the microcover glass and simultaneously commence timing. Within 5 seconds, place a second microcover glass over the specimen. After the resin softens and during the first 30 seconds, probe the top microcover glass and isolate a drop of resin. Observe the fluidity and color of the isolated resin drop periodically (continually as the end point approaches). The lateral (spreading) movement of the resin will decrease upon probing and the color shade will be altered as the gel point approaches. Stop the timer at the first indication of resin immobility and record elapsed time to the nearest second.

The results of the gel temperature tests are given in Table H-1 for heat rise rates of $0.556^{o}K$ per minute $0.833^{o}K$ per minute. The results for material previously densified for 30 minutes at $394^{o}K$ under vacuum pressure are also shown in Figure H-1.

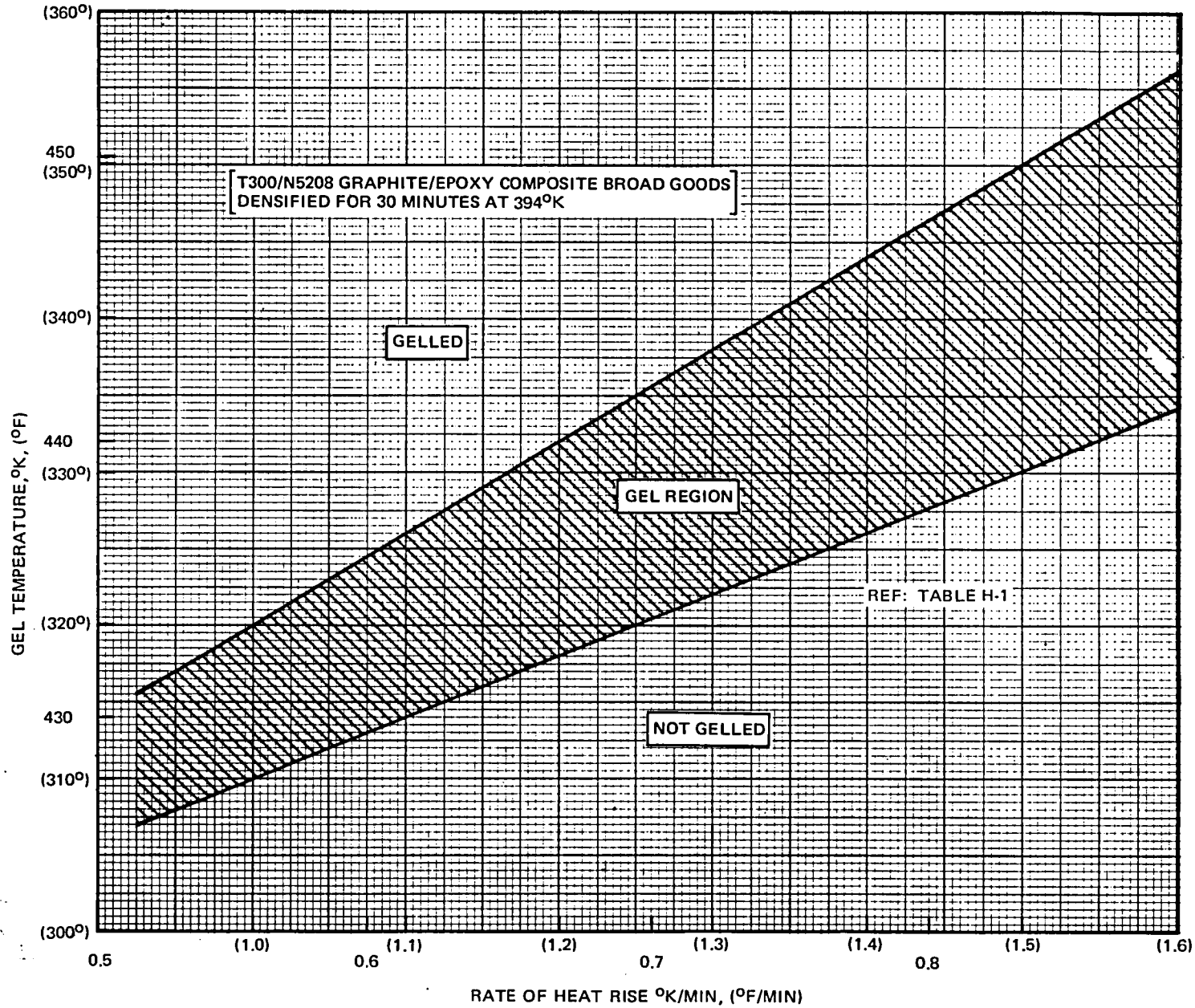

FIGURE H-1. RESULTS OF RESIN GEL TESTS

TABLE H-1
GEL TEMPERATURE AND TIME TO GEL AT 450°K FOR T300/N5208 GRAPHITE/EPOXY

T300/N5208	GEL TIME AT 450°K (MIN:SEC)	0.56°K HEAT RISE FROM AMBIENT TO 450°K		0.83°K HEAT RISE FROM AMBIENT TO 450°K	
		TEMP AT REMOVAL FROM OVEN (°K)	TIME TO GEL AT 450°K (MIN:SEC)	TEMP AT REMOVAL FROM OVEN (°K)	TIME TO GEL AT 450°K (MIN:SEC)
Fresh Material	20:32	411 428 433 439	10:20 4:30 1:20 0:0	433 450	10:15 1:20
Densified for 30 minutes at 394°K	12:06	400 428 433	9:40 1:30 0:0	411 439 450	8:05 1:24 0:20
Densified for 60 minutes at 394°K	10:26	400 417 422	5:00 1:00 0:0	389 422 444	9:05 1:19 0:0

In the design of the internal rubber mandrels, one of the prime design criteria considerations is to ensure that 0.689 MPa of rubber pressure is achieved inside the rudder box mold tool at the gel temperature of the graphite/epoxy composite material.

The gel temperature range for constant heat rise rates is given in Figure H-1. However, the heat rise rate during an actual rudder box cure cycle is not constant and varies from about 0^{o} to 0.97^{o}K per minute (Reference Figure C-2).

The gel temperature estimates at three rudder stations are shown in Figures H-2 through H-7 and the method of estimating is described in Task 11 of Section 6. The summary of rudder cure cycle gel temperatures is given in Table H-2 and the rudder cure cycle design pressure versus temperature design criteria is given in Table H-3.

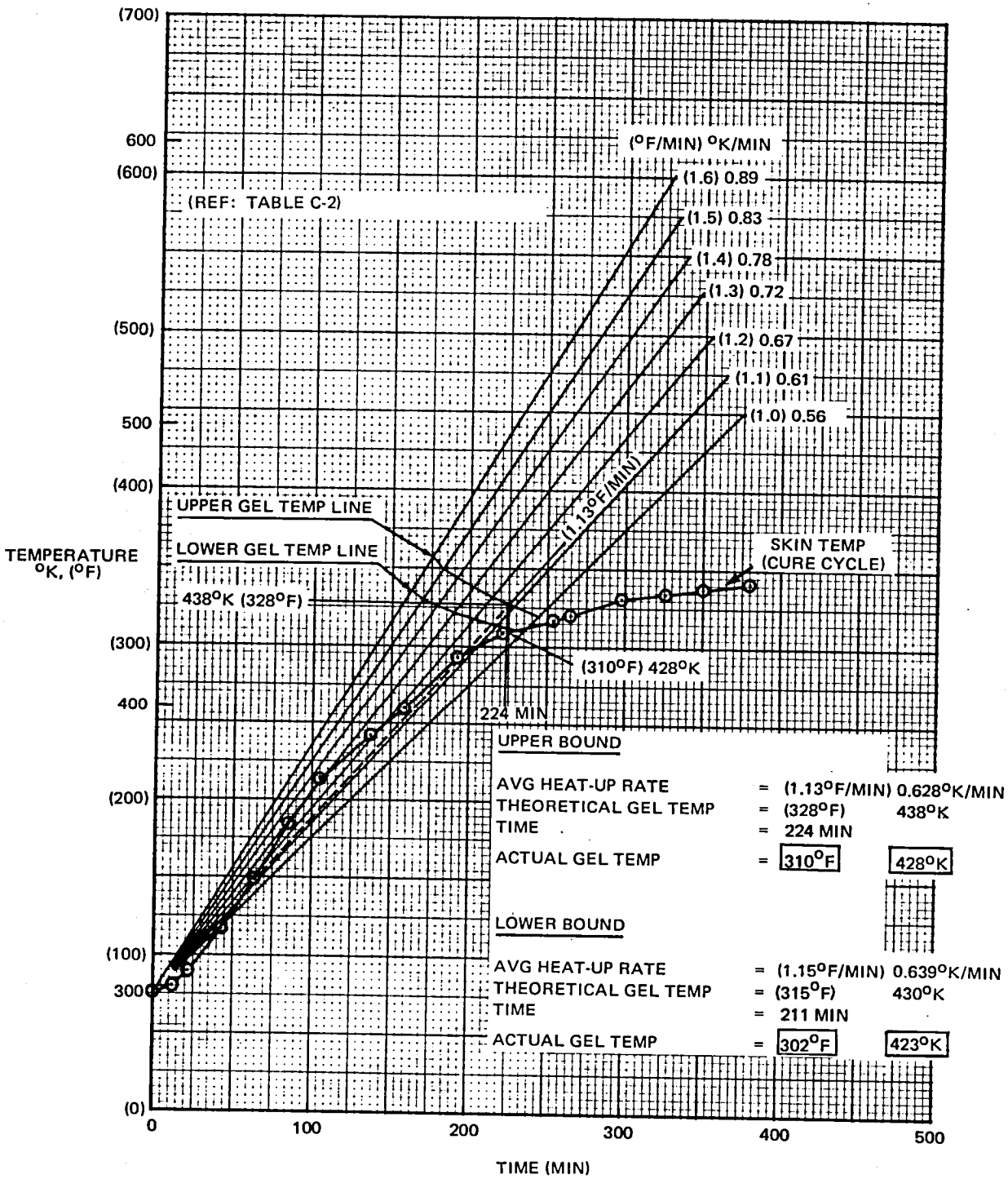

FIGURE H-2. GEL TEMPERATURE ESTIMATE AT SKIN THERMOCOUPLE NO. R65 (Z_{AR} = 416.25)

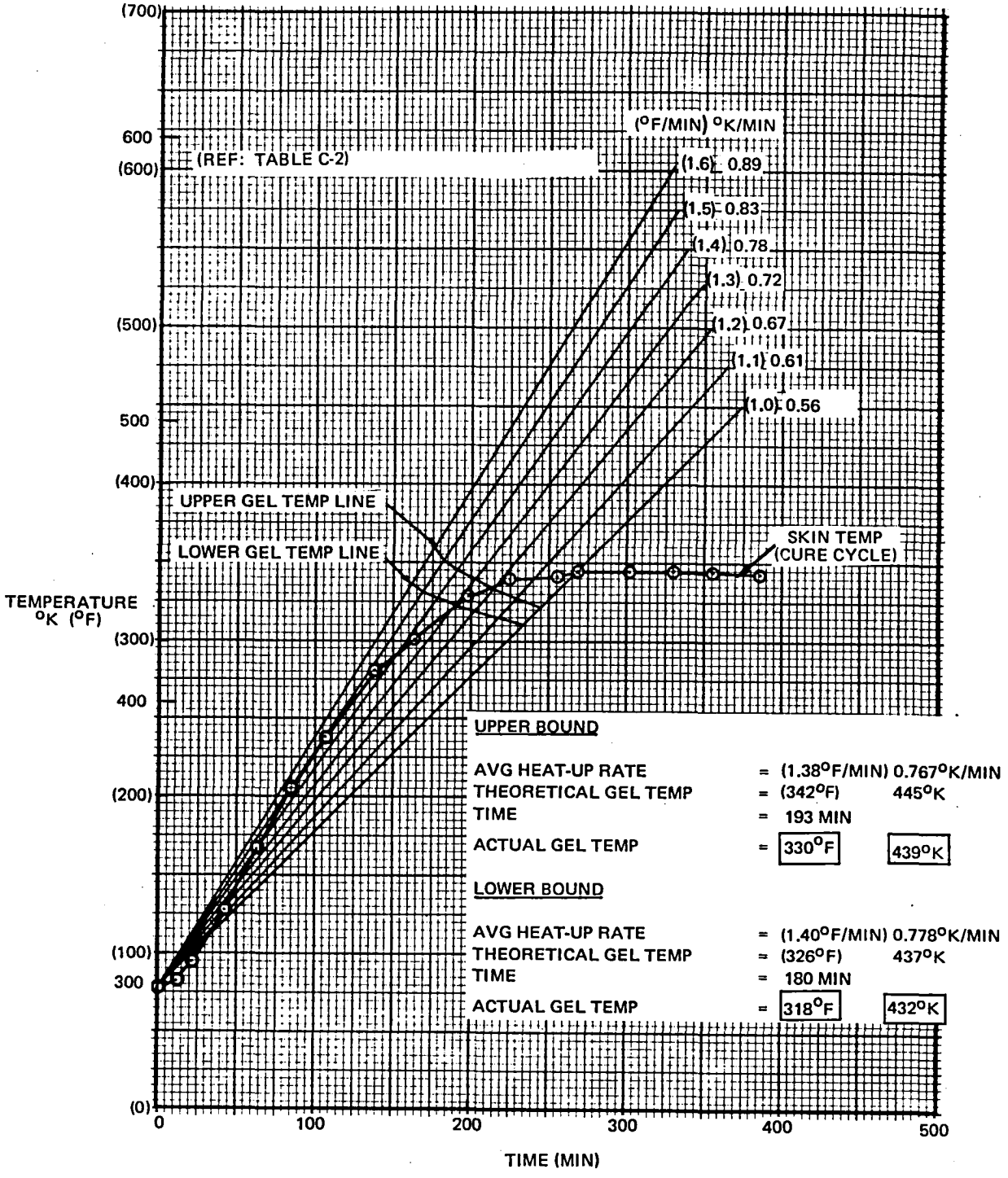

FIGURE H-3. GEL TEMPERATURE ESTIMATE AT SKIN THERMOCOUPLE NO. L64 (Z_{AR} = 416.25)

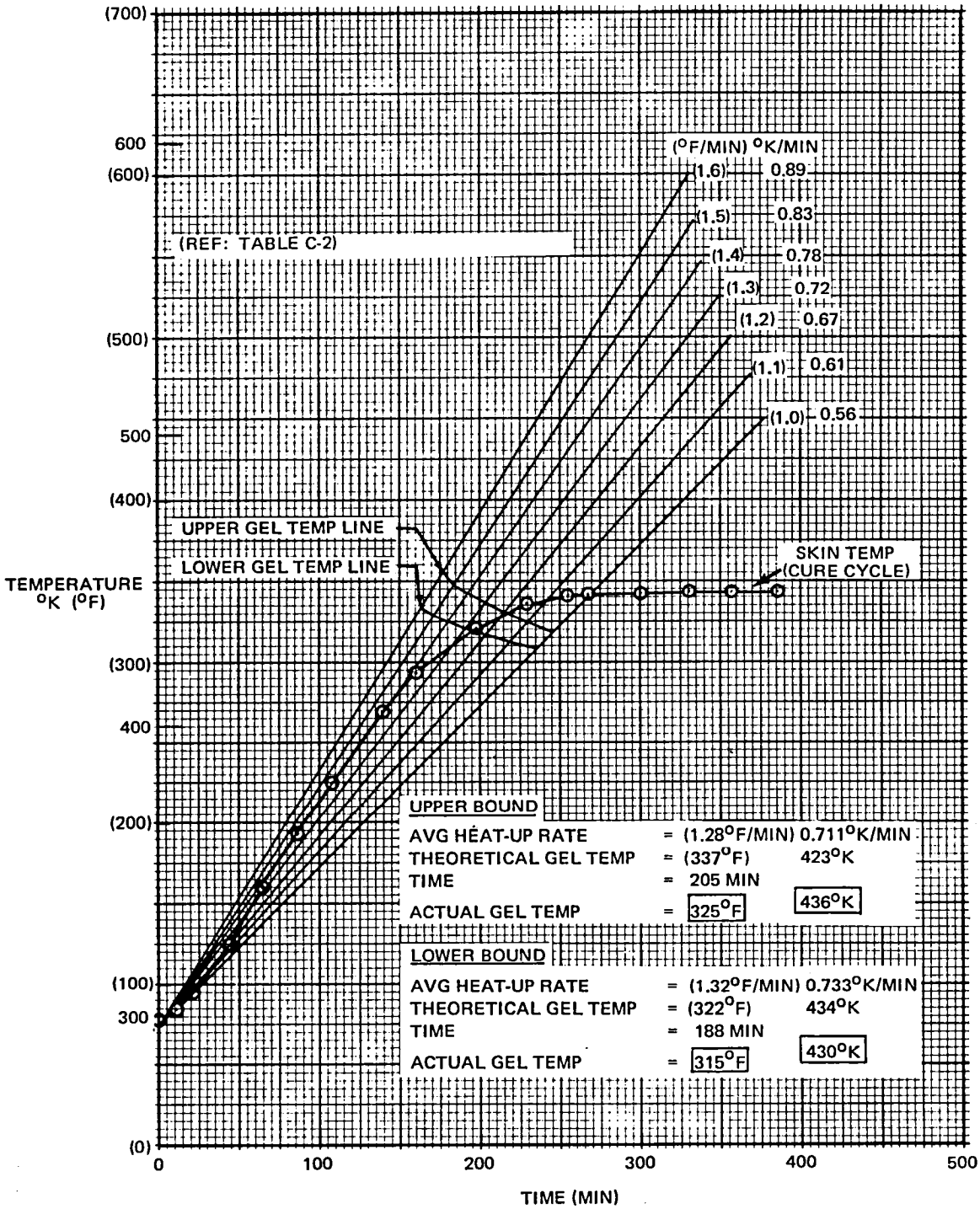

FIGURE H-4. GEL TEMPERATURE ESTIMATE AT SKIN THERMOCOUPLE NO. L78 (Z_{AR} = 476.94)

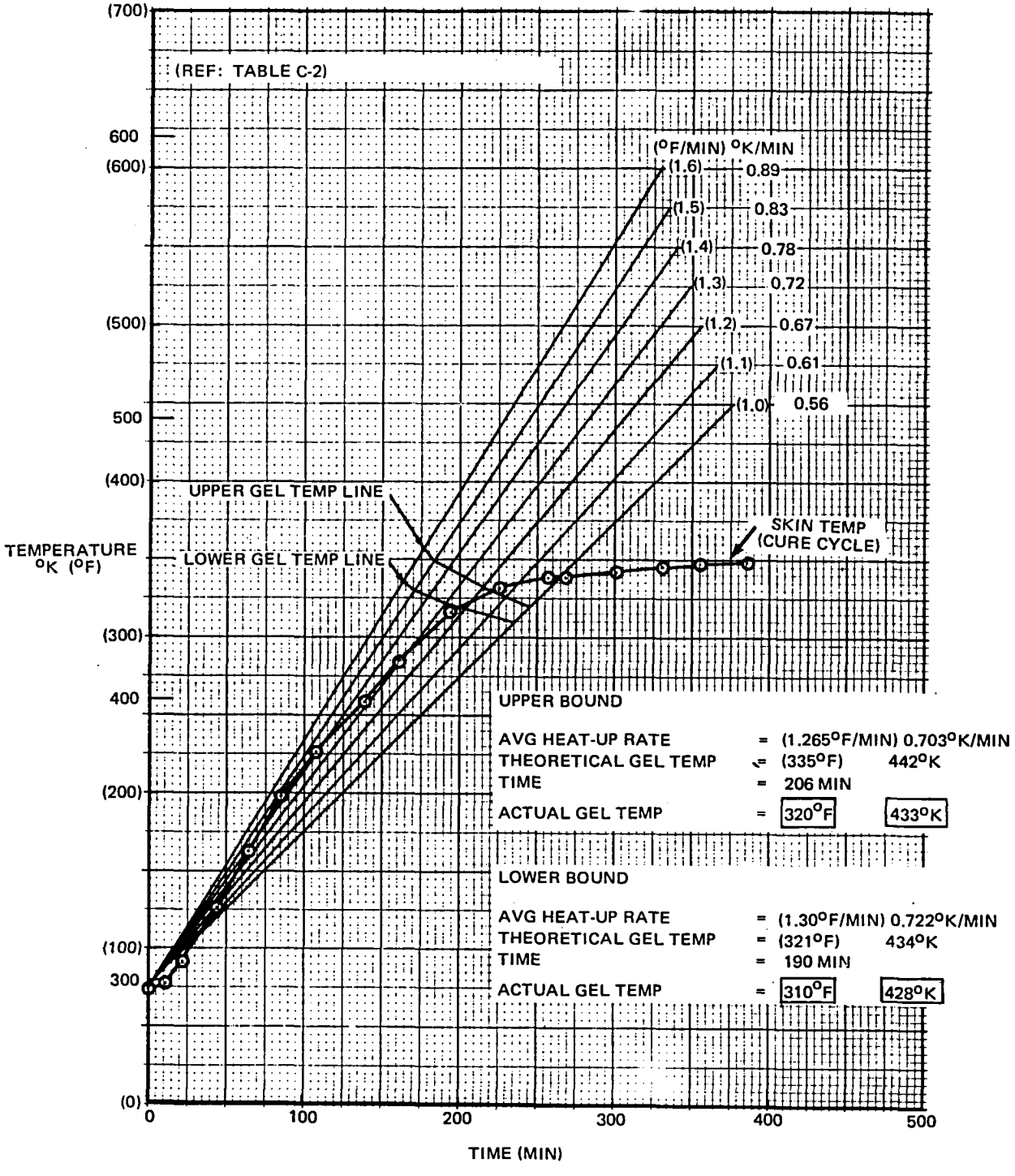

FIGURE H-5. GEL TEMPERATURE ESTIMATE AT SKIN THERMOCOUPLE NO. R80 (Z_{AR} = 476.94)

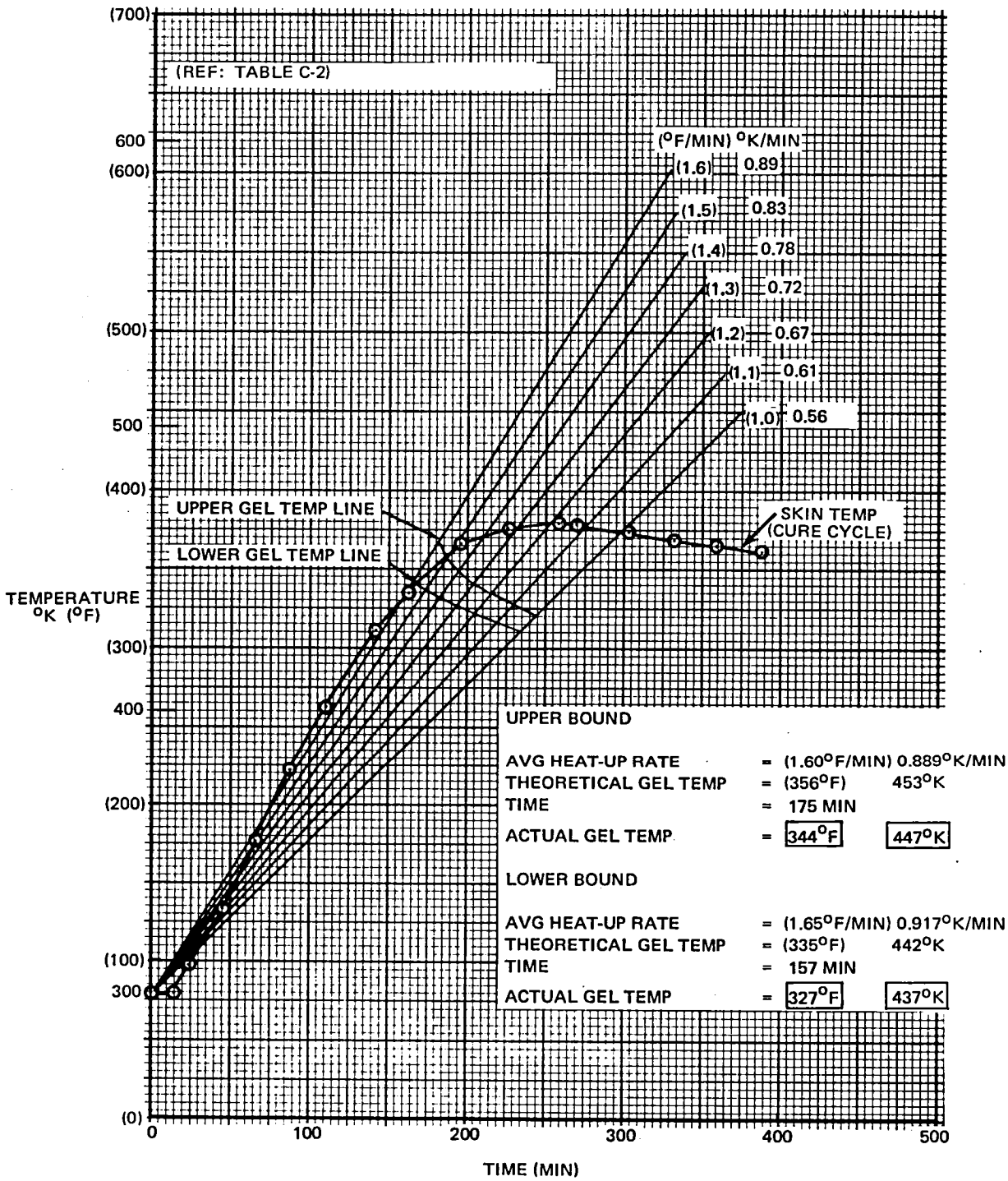

FIGURE H-6. GEL TEMPERATURE ESTIMATE AT SKIN THERMOCOUPLE NO. L96 (Z_{AR} = 555.47)

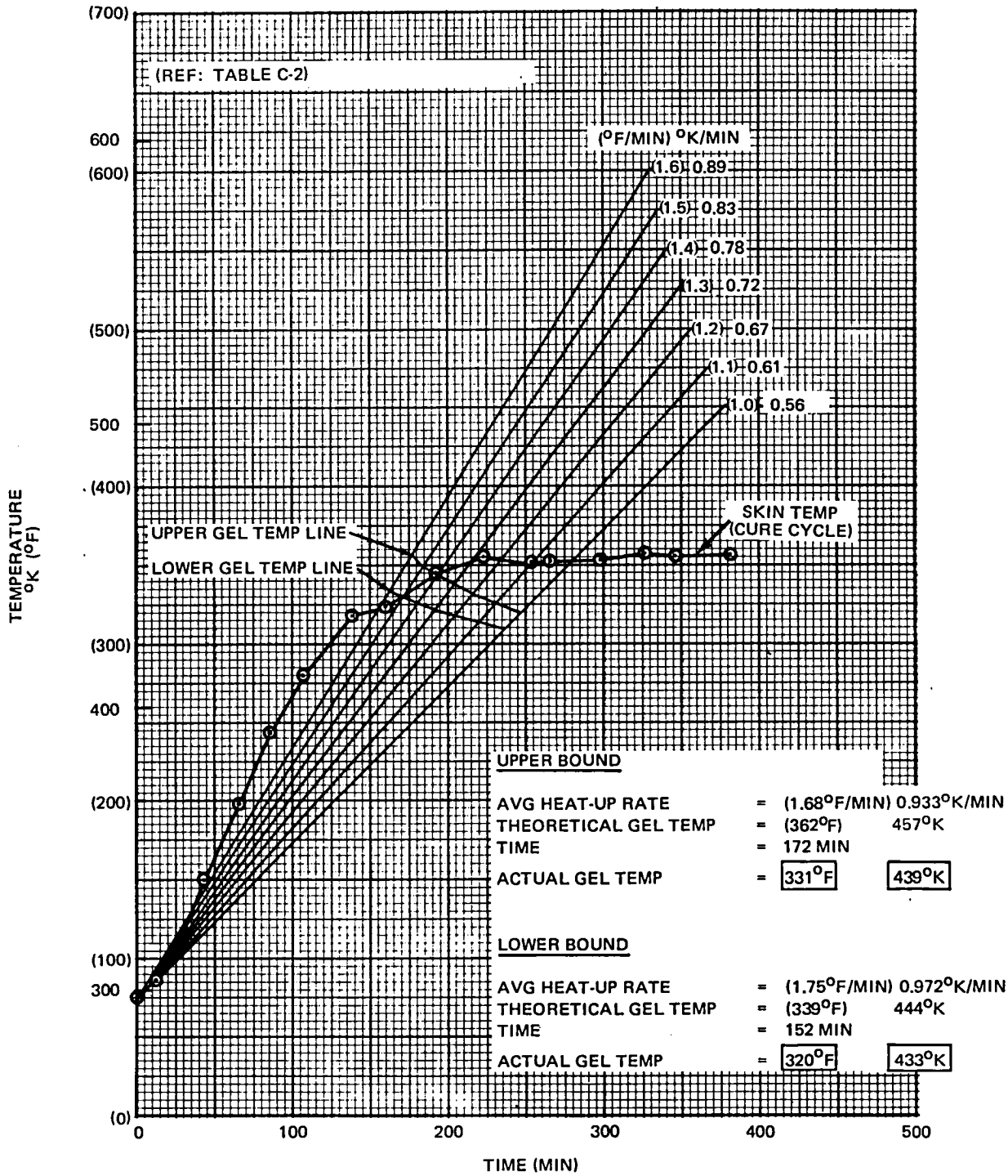

FIGURE H-7. GEL TEMPERATURE ESTIMATE AT SKIN THERMOCOUPLE NO. R97 (Z_{AR} = 555.47)

TABLE H-2
GEL TEMPERATURE SUMMARY – RUDDER CURE CYCLE

T300/N5208 GRAPHITE/EPOXY COMPOSITE BROADGOODS
DENSIFIED FOR 30 MIN AT 394°K

	TEMPERATURE (°K)					
	SMALL END Z_{AR} = 413.53		MIDDLE Z_{AR} = 476.94		LARGE END Z_{AR} = 555.47	
	LEFT SKIN	RIGHT SKIN	LEFT SKIN	RIGHT SKIN	LEFT SKIN	RIGHT SKIN
GELLED	447	439	436	433	439	428
NOT GELLED	437	433	430	428	432	423
FIGURE REF	H-6	H-7	H-4	H-5	H-2	H-3

TABLE H-3
DESIGN PRESSURES AT TEMPERATURE – RUDDER CURE CYCLE

	DESIGN TEMPERATURE (°K)		
	SMALL END Z_{AR} = 413.53	MIDDLE Z_{AR} = 476.94	LARGE END Z_{AR} = 555.47
2.07 MPa MAX*	447	447	447
0.689 MPa MIN**	433	428	422

*MAXIMUM CURE TEMPERATURE PRESSURE
**TABLE H-2 (NOT GELLED)

APPENDIX J
DAPCO 38-3 SILICONE RUBBER BULK MODULUS TESTS

This appendix describes the DAPCO 38-3 silicone rubber bulk modulus tests and the results of those tests. The majority of the tests were conducted on rubber specimens cast with an inner layer of expanded metal which is used to reinforce the actual rubber mandrels. These rubber specimens were cast undersize in a 11.43 cm (4-1/2-inch)-diameter by 2.86 cm (1-1/8-inch)-deep aluminum tool shown in Figure J-1. This permitted bulk modulus tests to be conducted in the casting tool while providing various gaps between the rubber specimens and the tool.

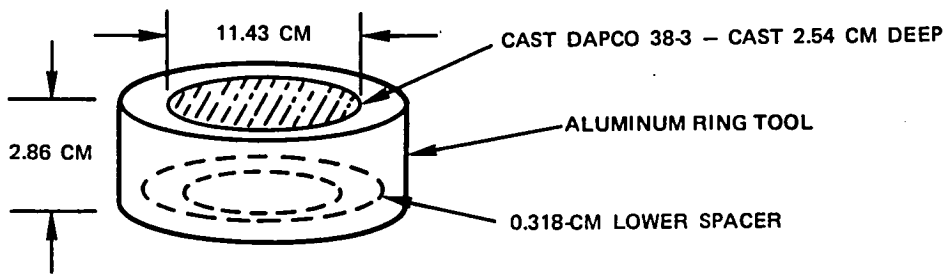

FIGURE J-1. CASTING TOOL

Basically, the equipment for these tests consisted of a sturdy aluminum ring tool (Figure J-1), a loading pad (Figure J-7), and a means of applying and recording load and deflection. Photos of the equipment are shown in Figures J-2 to J-6, and a simplified diagram of the test setup is shown in Figure J-7.

The cylindrical rubber specimens were cast undersize and cured per specimen No. 4 in Table 16. Aluminum and teflon shims were used to provide the gap when loaded into the aluminum ring. These rubber pressure-versus-deflection tests were conducted for temperatures from room temperature up to 450°K (350°F) and for rubber pressures from zero up to 4.14 MPa (600 psi).

The test results shown in Figure J-8 demonstrate the nonlinearity of the rubber. This specimen was DAPCO 38-3 silicone rubber with embedded screen mesh and the test was conducted at 394°K (250°F). The bulk modulus for this specimen is not a constant and the rubber specimen appears to experience

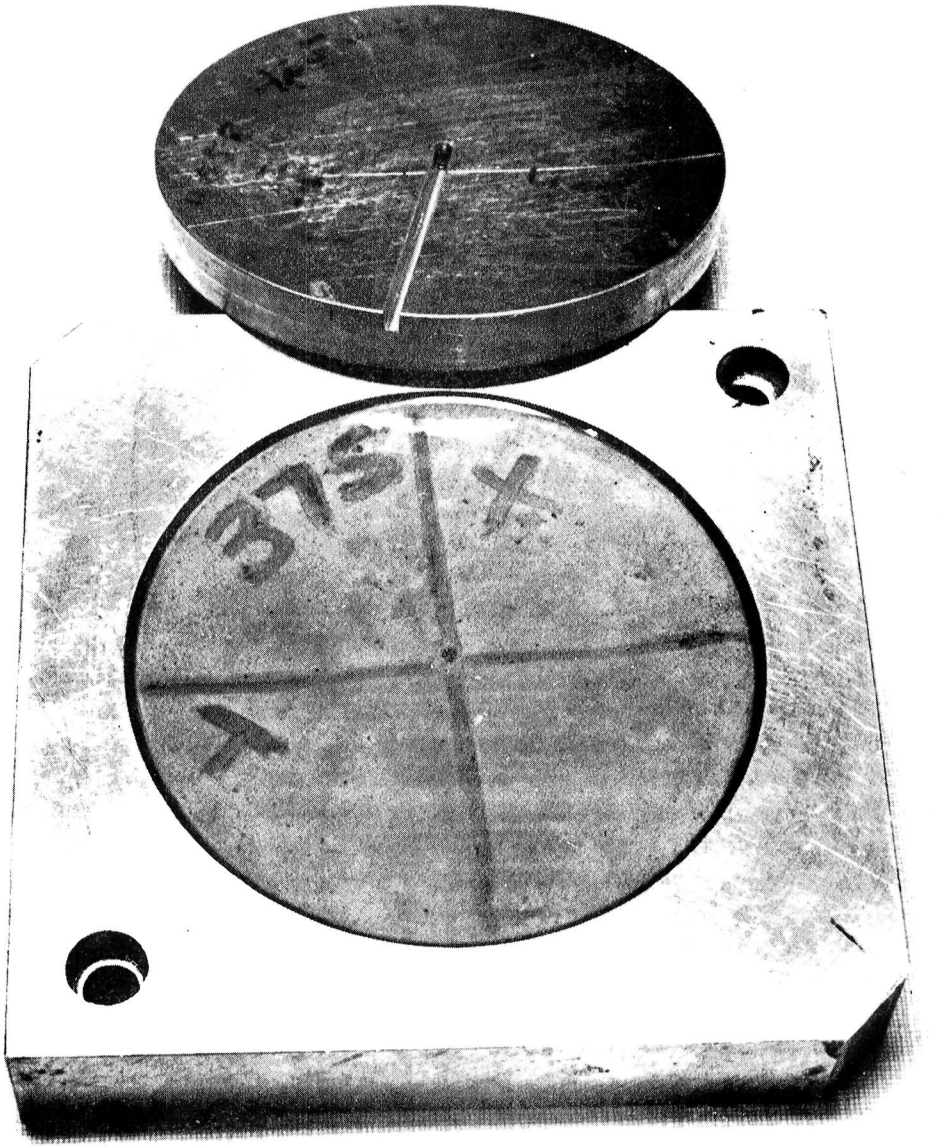

FIGURE J-2. RUBBER, RING, AND PRESSURE PLATE

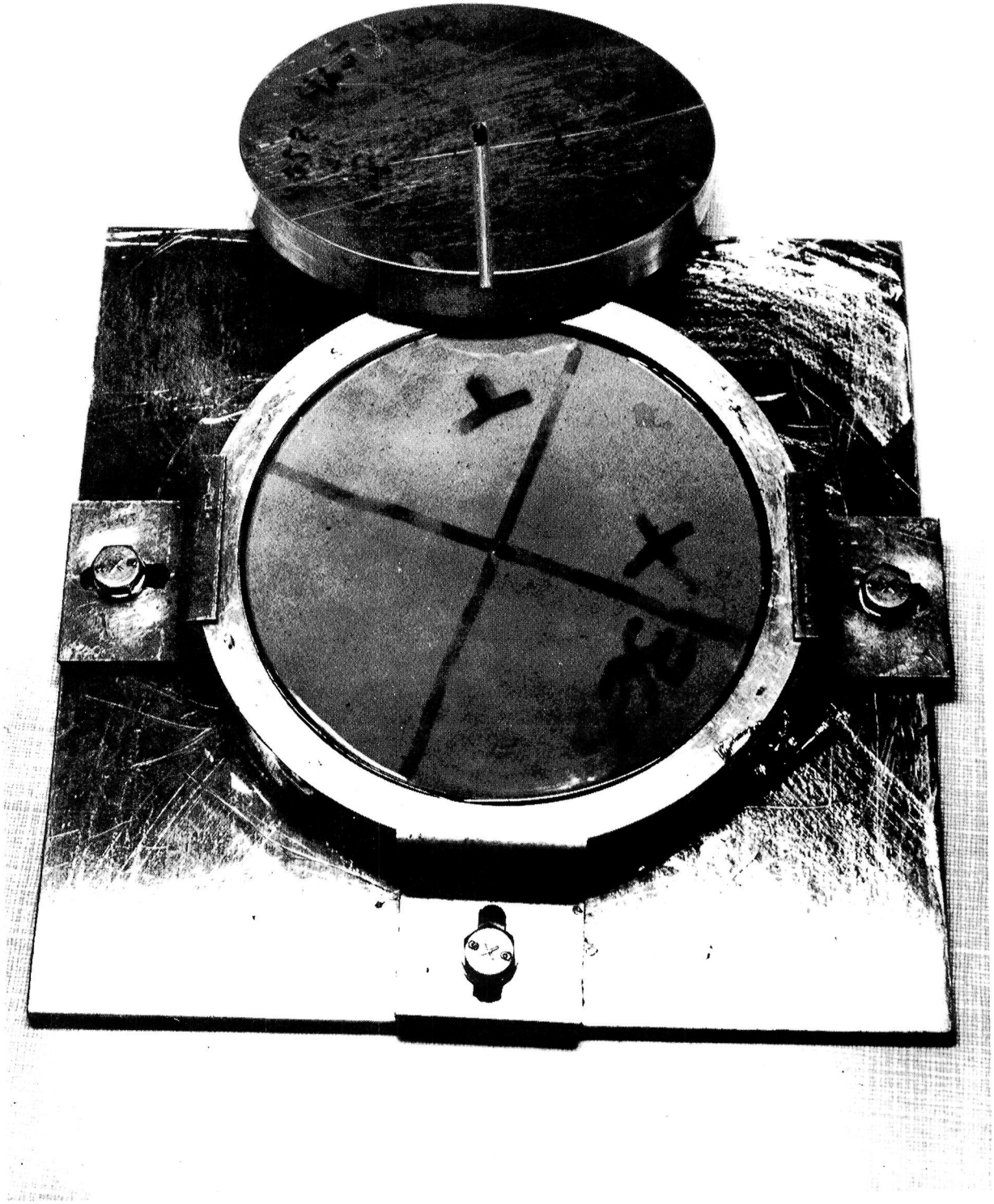

FIGURE J-3. RUBBER, HELD RING, AND PRESSURE PLATE

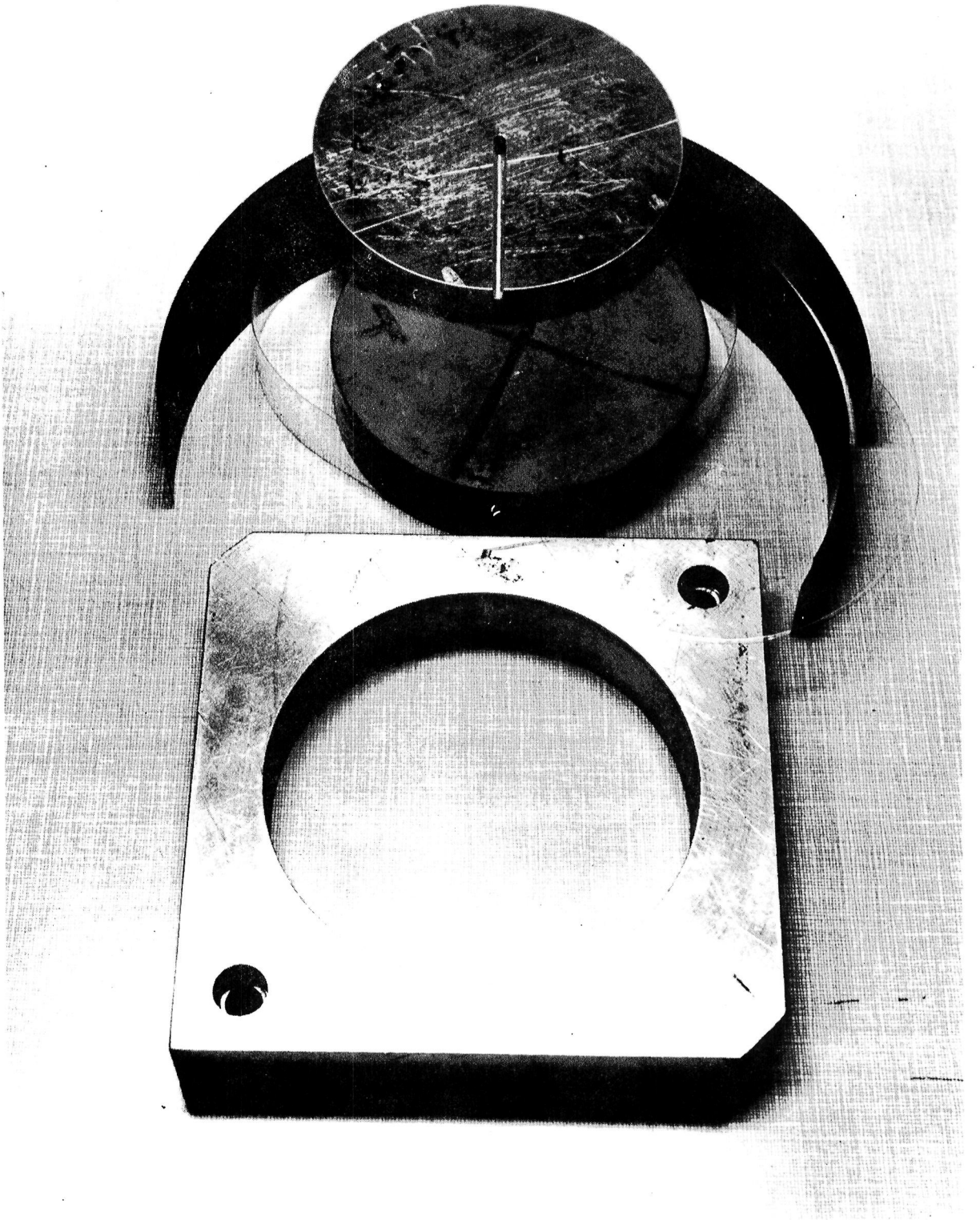

FIGURE J-4. RUBBER, RING, PRESSURE PLATE, AND METAL AND TEFLON SHIMS

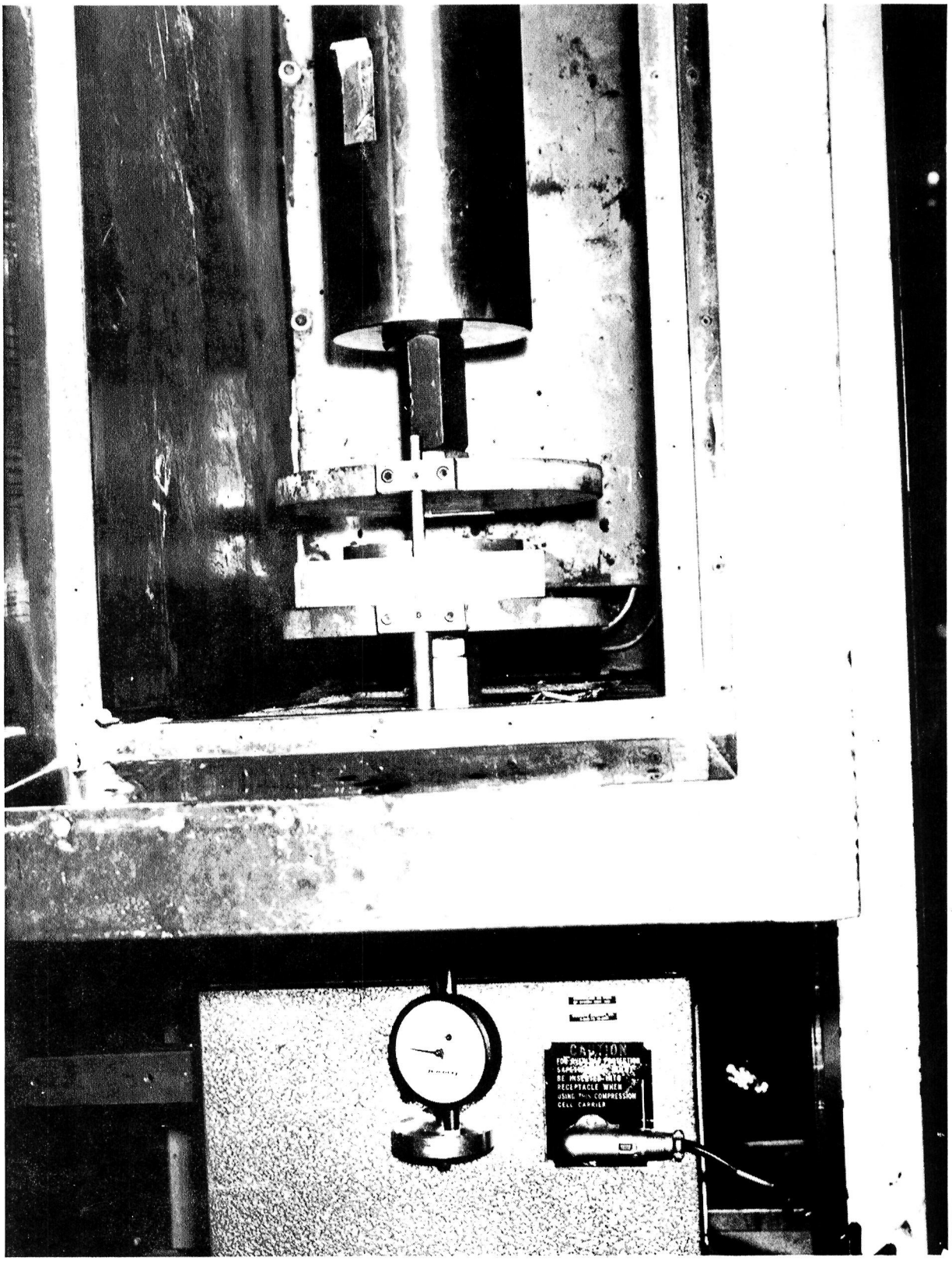

FIGURE J-5. PRESSURE MEASUREMENT SETUP IN OVEN

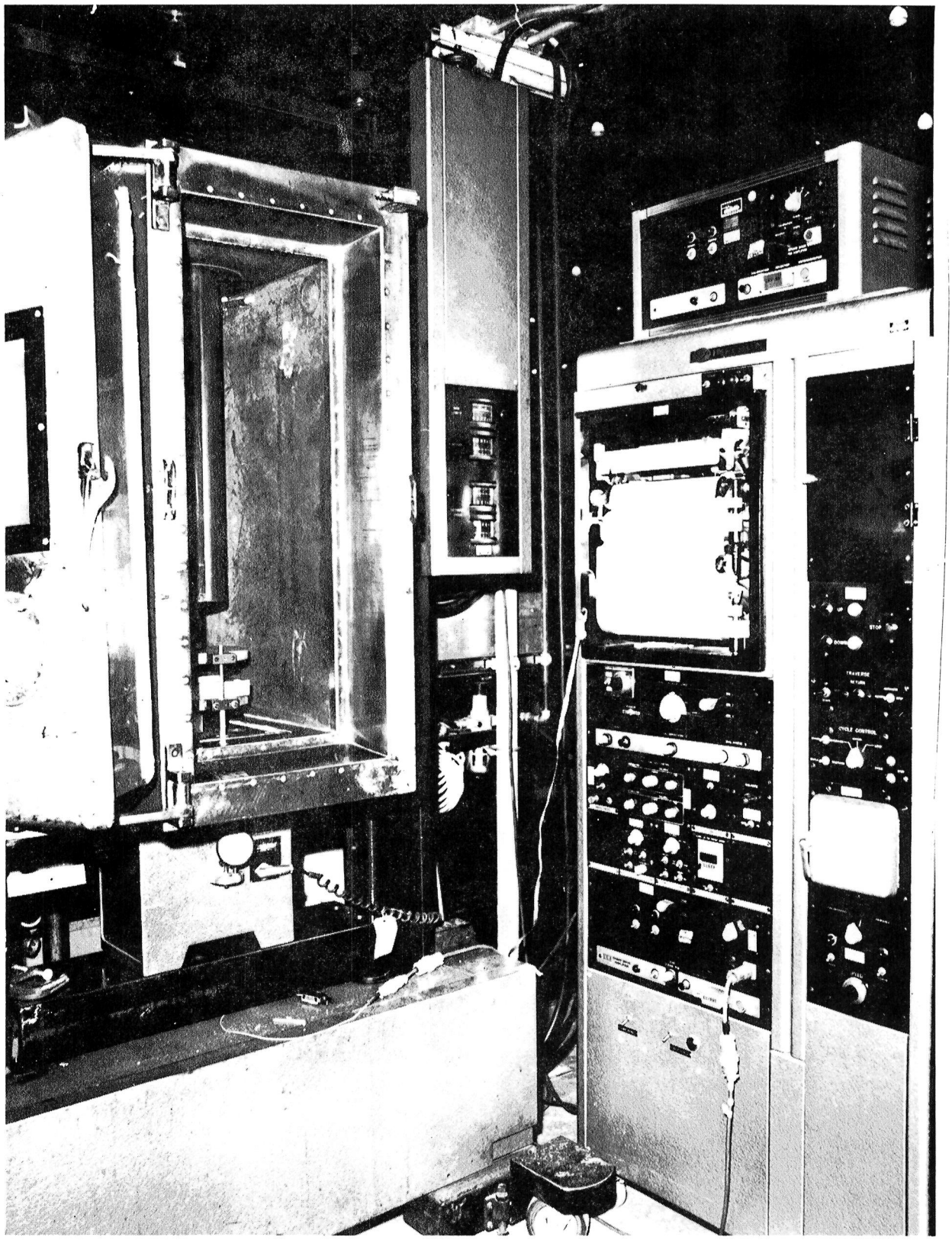

FIGURE J-6. OVEN AND INSTRON RECORDING AND CONTROL BOARD

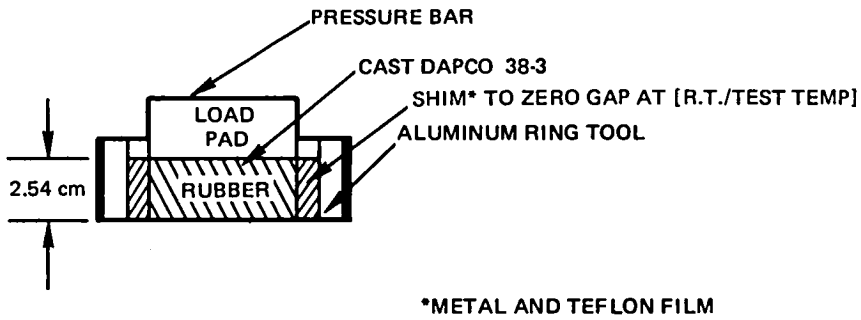

FIGURE J-7. TEST SETUP

yielding above 2.07 MPa (300 psi) followed by an apparent reduction in stiffness when the load returns to zero.

Figure J-9 is a plot of pressure versus deflection for a series of six tests conducted on one cylindrical rubber specimen (with metal screen). These tests were conducted with zero gap at room temperature. Each test was conducted up to near 4.14 MPa (600 psi) with intervals of from 1 to 3 days between tests to allow the rubber to recover from the effects of the preceding test. The rubber specimen appeared to exhibit less stiffness at each loading than was exhibited during the preceding test. Run No. 5 does not appear to conform to the above hypothesis, but this is attributed to faulty shimming (i.e., a small gap existed between the aluminum ring and the rubber specimen at room temperature).

Similar tests conducted on rubber specimens without embedded metal screen exhibited similar nonlinear and yielding properties as with the metal screen.

The bulk modulus test results thus far have indicated that the method of testing produced pressure-versus-deflection curves with widely varying values for different specimens of the same rubber. This was attributed to the apparent yielding of the rubber specimens at pressures above 2.07 MPa (300 psi). It was theorized that, if these bulk modulus tests were conducted at pressures below which rubber exhibited yielding, then the rubber specimens could be used repeatedly without a continual shift in physical properties.

Thus, the first step in establishing the bulk modulus properties was to determine the rubber yield pressure. Tests 67 and 69 were conducted for this purpose; these tests and their results are reported in this Appendix. A room

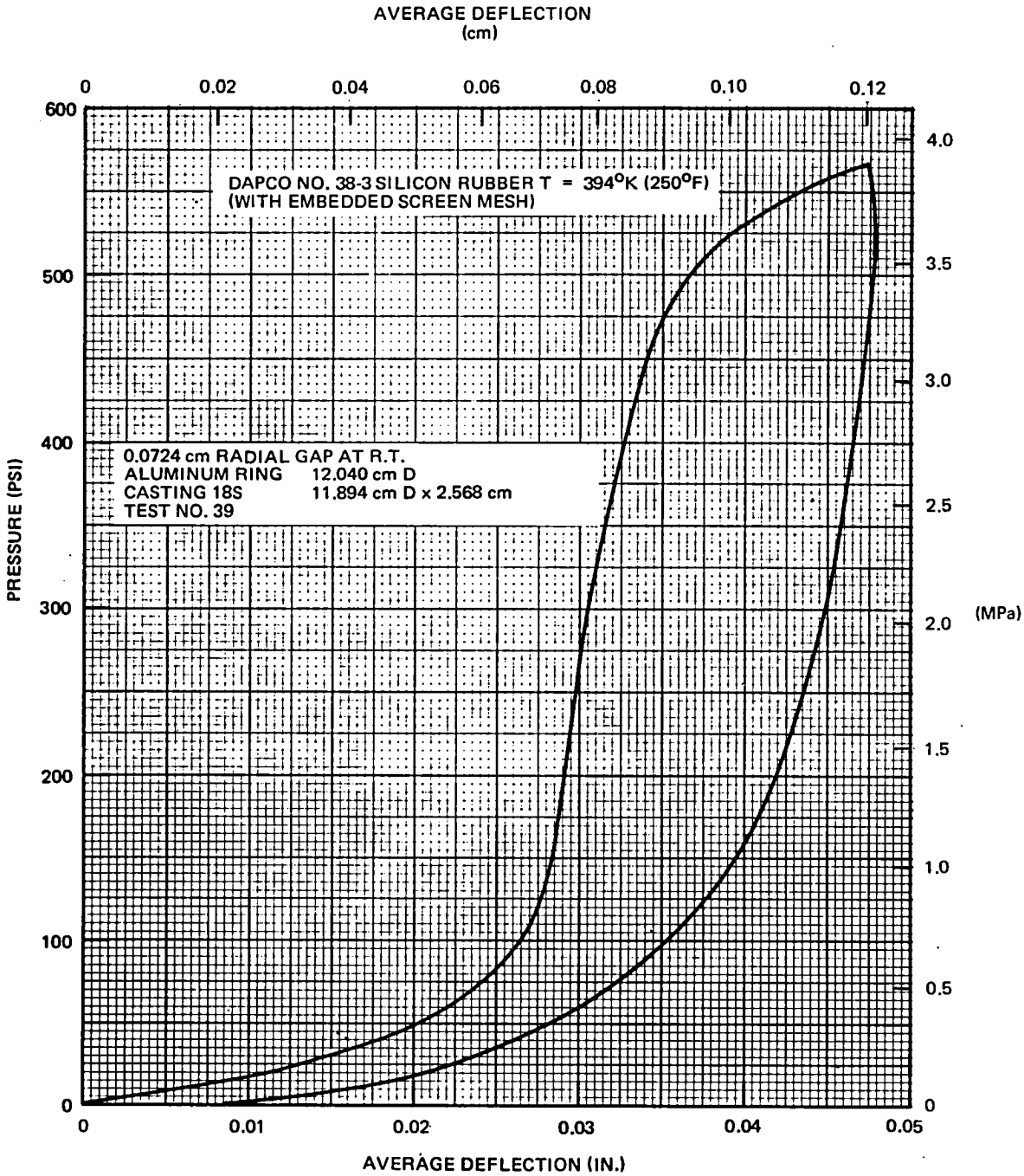

FIGURE J-8. PRESSURE VERSUS DEFLECTION

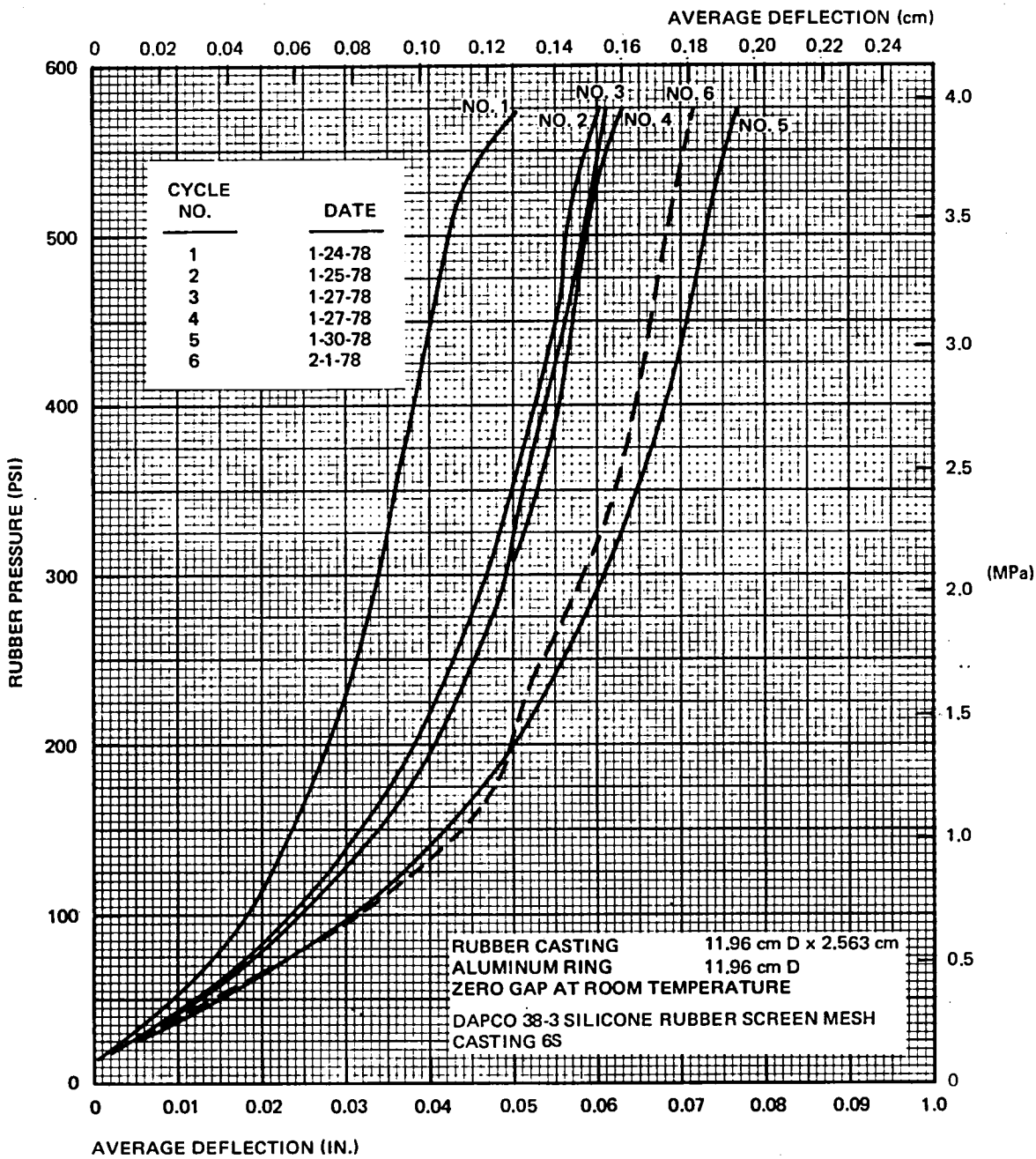

FIGURE J-9. REPEAT BULK MODULUS TEST – ROOM TEMPERATURE

temperature radial gap of 0.889 mm (0.035 inch) was provided between the ring and the rubber specimen after the rubber was wrapped with a layer of 0.127 mm (0.005-inch) Teflon strip. The rubber specimen was made to fill the aluminum ring (gap and all) by raising the rubber temperature to 433^{o}K (320^{o}F). The rubber specimen was then cycled at gradually increasing pressures to establish the highest pressure for which the rubber retains repeatable pressure-deflection properties. This pressure was established as 2.07 MPa (300 psi).

The bulk modulus properties of DAPCO 38-3 silicone rubber were established from the results of Tests 67, 69, and 71 of this appendix and given in Figure J-13. This appendix also contains the results of Test 97, which is the bulk modulus test for a rubber specimen previously subjected to 43 temperature/ pressure cycles. The results of Test 97 are plotted in Figure J-12 and show excellent agreement with the results of Tests 67, 69, and 71.

The tests for the bulk modulus of DAPCO 38-3 silicone rubber were conducted at room temperature, and at 394 and 450^{o}K (250 and 350^{o}F). In these tests, the rubber specimen is loaded in compression. However, the specimen did not deflect uniformly over the entire specimen due to the difficulty of centering the applied load. Thus, it was necessary to measure the pad deflection at two diametrically opposite pad locations in order to establish the average deflection of the rubber specimen for each loading.

The room-temperature tests were conducted by wrapping metal and teflon-shim material around the under diameter silicone rubber to fill the gap between the ring tool and the rubber specimen as shown in Figure J-7. Load was applied through a metal pressure pad sized to fit the rubber specimen and the compression load versus rubber deflection values were recorded.

The tests at 394 and 450^{o}K (250 and 350^{o}F) were conducted by wrapping shim material around the under diameter silicone rubber specimen so as to leave a calculated gap between the rubber and the retaining ring at room temperature. The gap was sized such that the rubber specimen would just fill the ring tool at the test temperature. Compression loads were applied to the rubber and the resulting rubber deflections were recorded. The test set up was similar to the setup shown in Figure J-7.

The tests have been grouped into:

1. Preliminary Tests: These tests included the rubber pressure-versus-deflection data given in Figures J-8 through J-11. They were not considered suitable for deriving useful bulk modulus data.

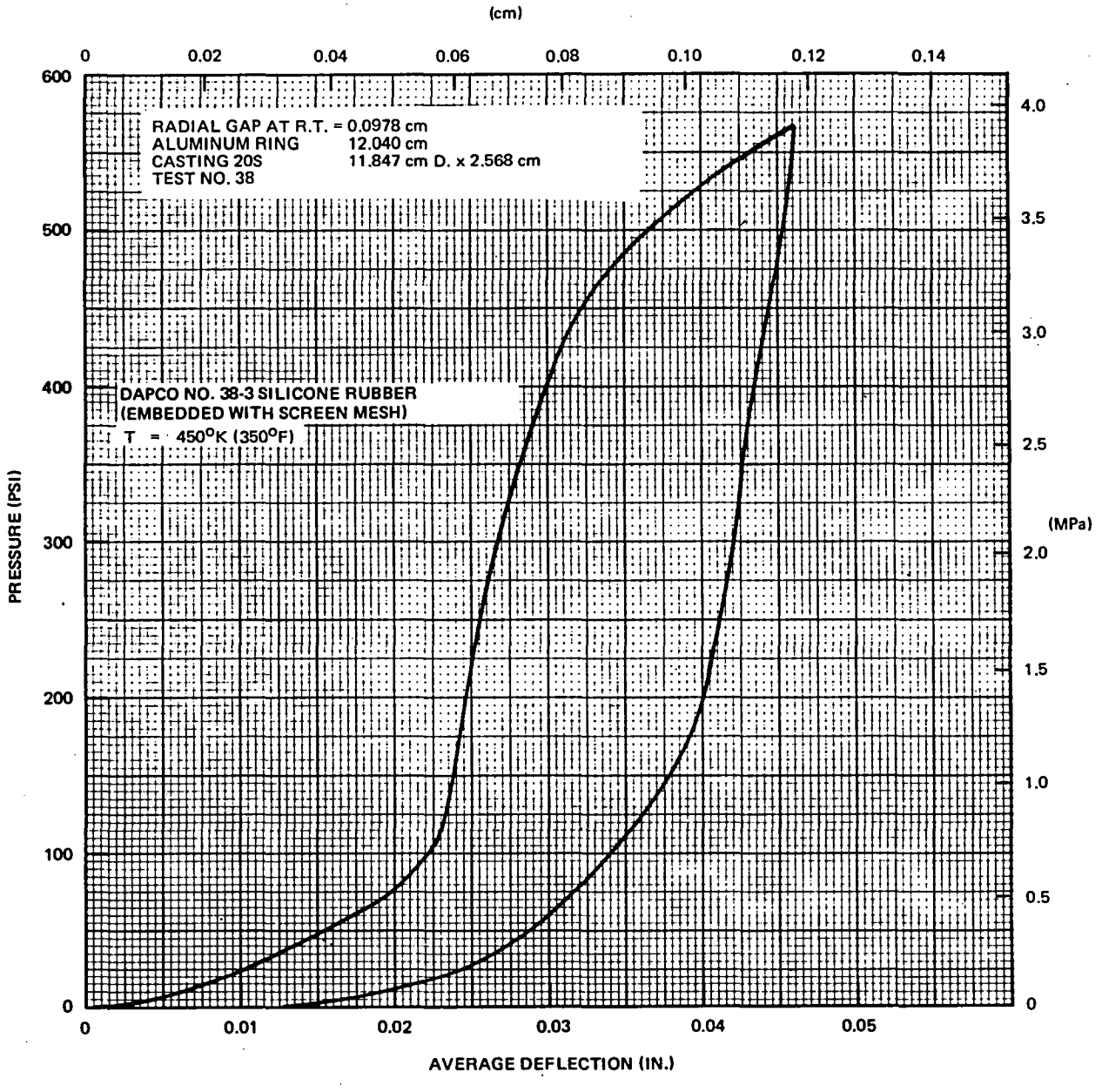

FIGURE J-10. PRESSURE VERSUS DEFLECTION – TEST NO. 38

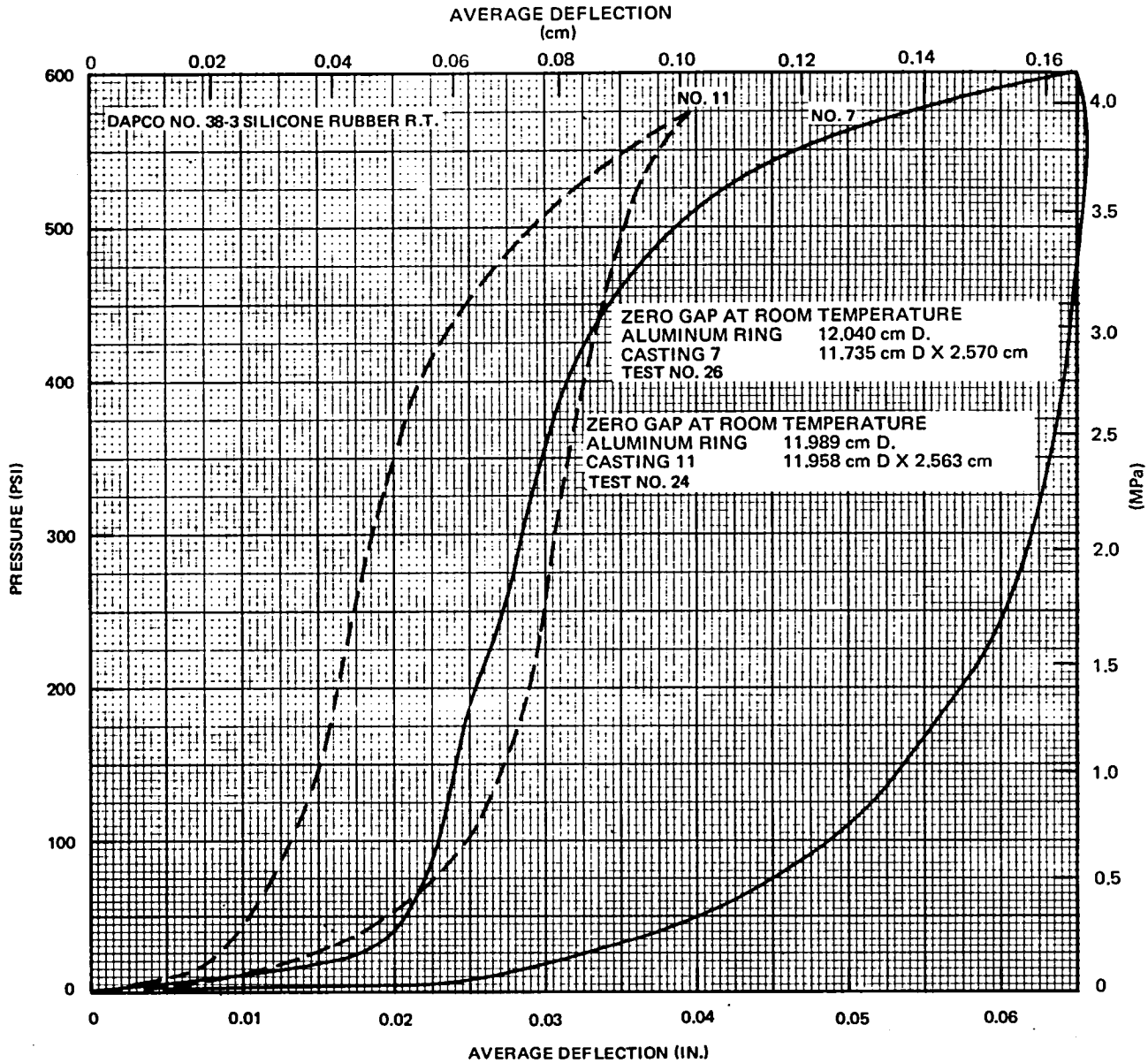

FIGURE J-11. PRESSURE VERSUS DEFLECTION (DAPCO 38-3, ROOM TEMPERATURE)

2. Final Tests: These included the load-versus-deflection tests No. 67, 69, 71, and 97. For rubber pressures below 2.07 MPa (300 psi) the results from these tests provided consistent and repeatable data which resulted in the bulk modulus data of Figures J-12 and J-13.

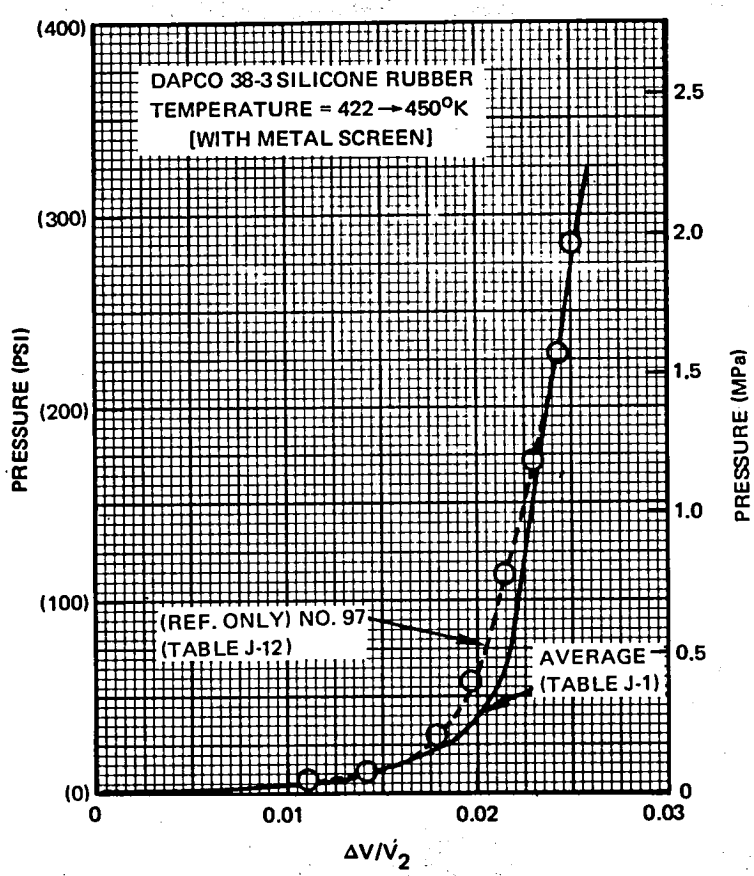

FIGURE J-12. RELATIONSHIP OF PRESSURE VERSUS BULK STRAIN (DAPCO 38-3 SILICONE RUBBER)

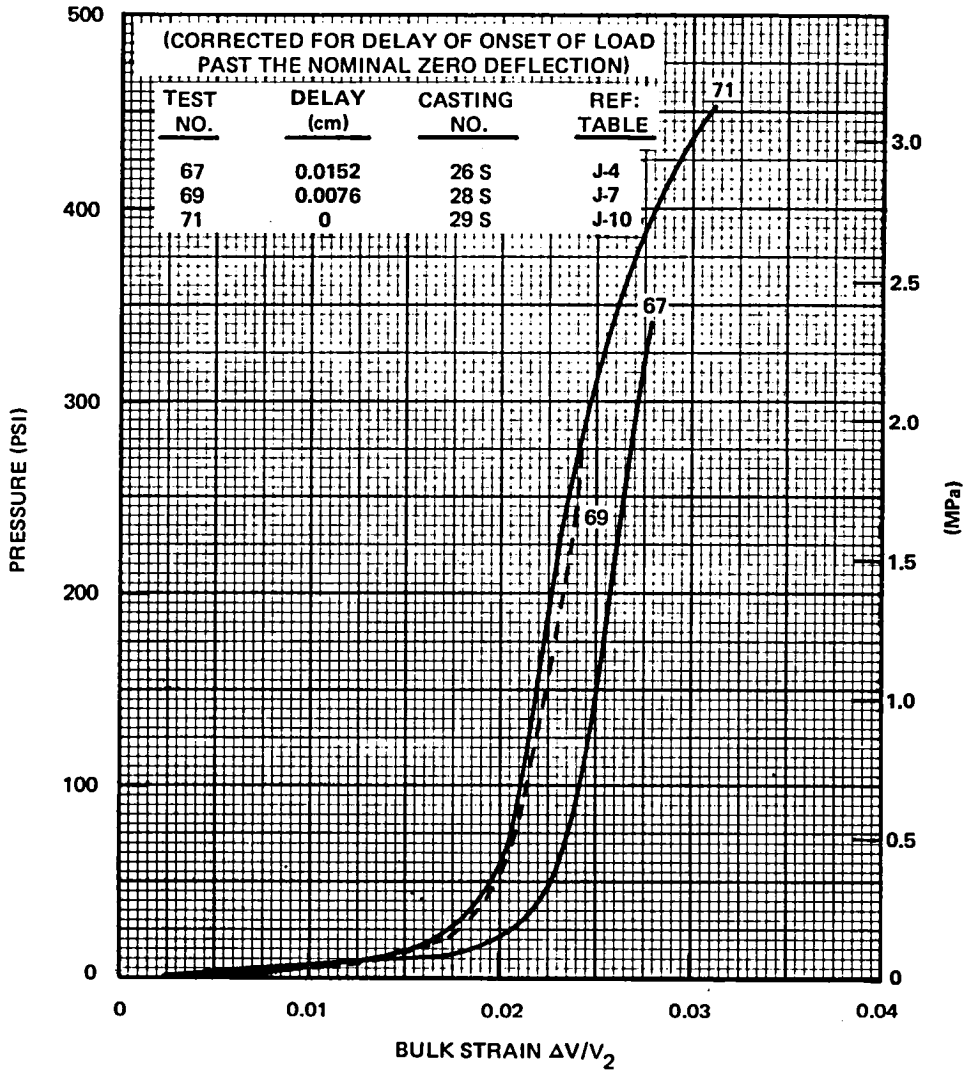

FIGURE J-13. COMPARISON: PRESSURE VERSUS BULK STRAIN

Preliminary Tests

These four tests were conducted up to rubber pressures greater than 560 psi and the yielding, which generally occurs at these high pressures, was considered responsible for the nonrepeatability of the results of these tests.

Figure J-8 is a plot of six pressure-versus-deflection tests conducted on one rubber specimen with metal screening. Rubber stiffness appears to reduce after each loading. The fact that No. 5 is out of order is attributed to inadequate shimming. Figures J-9 and J-10 are plots of pressure-versus-

deflection tests conducted on virgin rubber* specimens with metal screening. These figures show the typical yielding which generally begins to occur at pressures above 2.07 MPa (300 psi). These tests were conducted at 394 and 450°K (250 and 350°F), respectively. Figure J-11 is a plot of pressure-versus-deflection tests conducted on virgin rubber specimens with no metal screening.

Final Tests

The results of tests Nos. 67, 69 and 71 are given in Figure J-13. These data were averaged in Table J-1 and plotted in Figure J-12 and constitute the sought after relationship between rubber pressure and bulk strain.

TABLE J-1
AVERAGE VALUES FOR PRESSURE VERSUS BULK STRAIN DAPCO 38-3 SILICONE RUBBER
TEMPERATURE = 422° TO 450°K (300° TO 350°F)

PRESSURE (MPa)	BULK STRAIN ($\Delta V/V_2$)			
	TEST 67	TEST 69	TEST 71	AVERAGE
0.345	0.0227	0.0199	0.0196	0.0207
0.689	0.0241	0.0214	0.0211	0.0222
1.034	0.025	0.0224	0.0218	0.0231
1.379	0.0256	0.0236	0.0225	0.0239
1.724	0.0263	0.0239	0.0235	0.0246
2.068	0.0270	0.0246	0.0245	0.0254
2.241	0.0275	0.0253	0.0252	0.0260
REF		REF FIGURE J-7		

An additional purpose of tests Nos. 67 and 69 was to establish the rubber yield pressure. It is undesirable to exceed this pressure if the rubber is to maintain consistent properties during repeated use. This is the reason why each of these tests were repeated for six gradually increasing loads and the test was repeated three times for each load level. It was found that the rubber settled in better because of these repetitions and improved the consistency of the results. The rubber yield pressure was found to be 2.07 MPa (300 psi).

Test No. 97 was a bulk modulus test conducted on a rubber specimen which had been subjected to 43 temperature-pressure cycles. The results of the test were plotted in Figure J-12 and showed very good agreement with the average of tests Nos. 67, 69, and 71.

*"Virgin rubber .. is the term used to signify a cast rubber specimen that has been cured and heat-treated but not stressed beyond its yield pressure.

These bulk modulus tests Nos. 67, 69, 71 and 97 were carried out as described for test "2" (Reference page 182). It was intended to carry out these tests at about 450°K (350°F). Thus it was necessary to provide sufficient rubber gap at room temperature that would allow the rubber to expand at about 450°K (350°F) to just fill the cylindrical aluminum retaining tool. The rubber gap situation was as follows:

TEST NO.	ROOM TEMPERATURE RUBBER GAP (cm)	TEST TEMPERATURE (°K)	RADIAL GAP GROWTH AT TEST TEMPERATURE (cm)	REFERENCE PAGE
67	0.089	433	0.107	J-7
69	0.089	433	0.107	J-9
71	0.089	433	0.107	J-9
97	0.099	450	0.122	J-54

The calculations connected with the following bulk modulus tests for rubber specimen radial gap and rubber bulk strain take into account silicone rubber specimen and aluminum retaining ring thermal expansion.

Bulk Modulus Test No. 67 (T = 433°K (320°F)). — To establish the rubber yield pressure, this test was conducted for gradually increasing loads of 13.34, 17.79, 22.24, 26.69, 31.14 and 35.58 kN. The 13.34 and 17.79 kN tests were very valuable in settling the rubber into the ring; that is, the rubber appeared to produce more consistent results after being cycled through these relatively low loads. A minimum wait of 5 minutes was allowed between tests. The extensometer readings are plotted in Figures J-14 to J-16. Table J-2 gives the extensometer and dial gage readings and the average of these for the 26.69 kN load test.

The representative bulk modulus properties for this specimen are given in Tables J-3 and J-4. These properties are plotted in Figure J-13. Rubber yielding appears to start at a load of 23.13 kN in the first 26.69 kN load cycle in Figure J-15. This translates to a pressure of 23130/0.0113 = 2.05 MPa (297 psi). Typical calculations for bulk modulus are given below (Also see Table J-3):

TABLE J-2

TEST NO. 67 – BULK MODULUS TEST RESULTS (T = 433°K) – SECTION 4

LOAD (kN)	GAGE DEFLECTION (cm)								
	FIRST CYCLE			SECOND CYCLE			THIRD CYCLE		
	EXTENSOMETER	DIAL	AVG	EXTENSOMETER	DIAL	AVG	EXTENSOMETER	DIAL	AVG
0.045	0	0	0	0	0		0	0	
0.445	0.0406	0.0508	0.0457	0.0394	0.0508		0.0424	0.0521	
0.890	0.0508	0.0660	0.0584	0.0505	0.0660		0.0521	0.0660	
2.224	0.0643	0.0787	0.0716	0.0645	0.0787		0.0665	0.0787	
4.448	0.0747	0.0787	0.0767	0.0752	0.0787		0.0770	0.0787	
8.900	0.0869	0.0737	0.0803	0.0876	0.0749		0.0897	0.0747	
13.344	0.0960	0.0711	0.0836	0.0970	0.0711		0.0991	0.0711	
17.792	0.1036	0.0660	0.0848	0.1054	0.0686		0.1072	0.0686	
22.24	0.1105	0.0635	0.0869	0.1125	0.0660		0.1143	0.0660	
26.688	0.1194	0.0610	0.0902	0.1196	0.0635		0.1214	0.0635	
22.24	0.1184	0.0610	0.0897	0.1191	0.0622		0.1204	0.0622	
17.792	0.1138	0.0610	0.0874	0.1148	0.0635		0.1161	0.0627	
13.344	0.1085	0.0635	0.0859	0.1092	0.0635		0.1110	0.0635	
8.900	0.1016	0.0635	0.0826	0.1021	0.0648		0.1041	0.0650	
4.448	0.0904	0.0686	0.0795	0.0914	0.0686		0.0935	0.0686	
2.224	0.0813	0.0711	0.0762	0.0826	0.0711		0.0838	0.0711	
0.890	0.0655	0.0699	0.0676	0.0655	0.0686		0.0686	0.0699	
0.445	0.0521	0.0610	0.0564	0.0508	0.0584		0.0559	0.0610	
0.045	0	0	0	0	0		0	0	
REF	FIG J-8			FIG J-9			FIG J-9		

TABLE J-3

TEST NO. 67 – PRESSURE VERSUS STRAIN – FIRST 26.69 kN LOADING CYCLE
DAPCO 38-3 SILICONE RUBBER

LOAD (kN)	AVERAGE DEFLECTION (cm)	PRESSURE (MPa)	Δ VOLUME (cu cm)	BULK STRAIN ($\Delta V/V_2$)
0.045	0	0.0069	0	0
0.445	0.0457	0.0414	5.14	0.0171
0.890	0.0584	0.0758	6.56	0.0219
2.224	0.0716	0.1999	8.05	0.0268
4.448	0.0767	0.3930	8.62	0.0287
8.896	0.0803	0.7859	9.03	0.0301
13.344	0.0836	1.1789	9.40	0.0313
17.792	0.0848	1.5718	9.53	0.0323
22.240	0.0869	1.9717	9.77	0.0325
26.688	0.0902	2.3646	10.14	0.0338
22.240	0.0897	1.9717	10.08	0.0335
17.792	0.0874	1.5718	9.82	0.0327
13.344	0.0859	1.1789	9.66	0.0321
8.896	0.0826	0.7859	9.28	0.0309
4.448	0.0795	0.3930	8.94	0.0297
2.224	0.0762	0.1999	8.56	0.0285
0.890	0.0676	0.0758	7.60	0.0253
0.445	0.0564	0.0414	6.34	0.0211
0.045	0	0.0069	0	0
REF	TABLE J-2	LOAD/11.29	112.4 (AVG DEFL)	ΔV/302.8

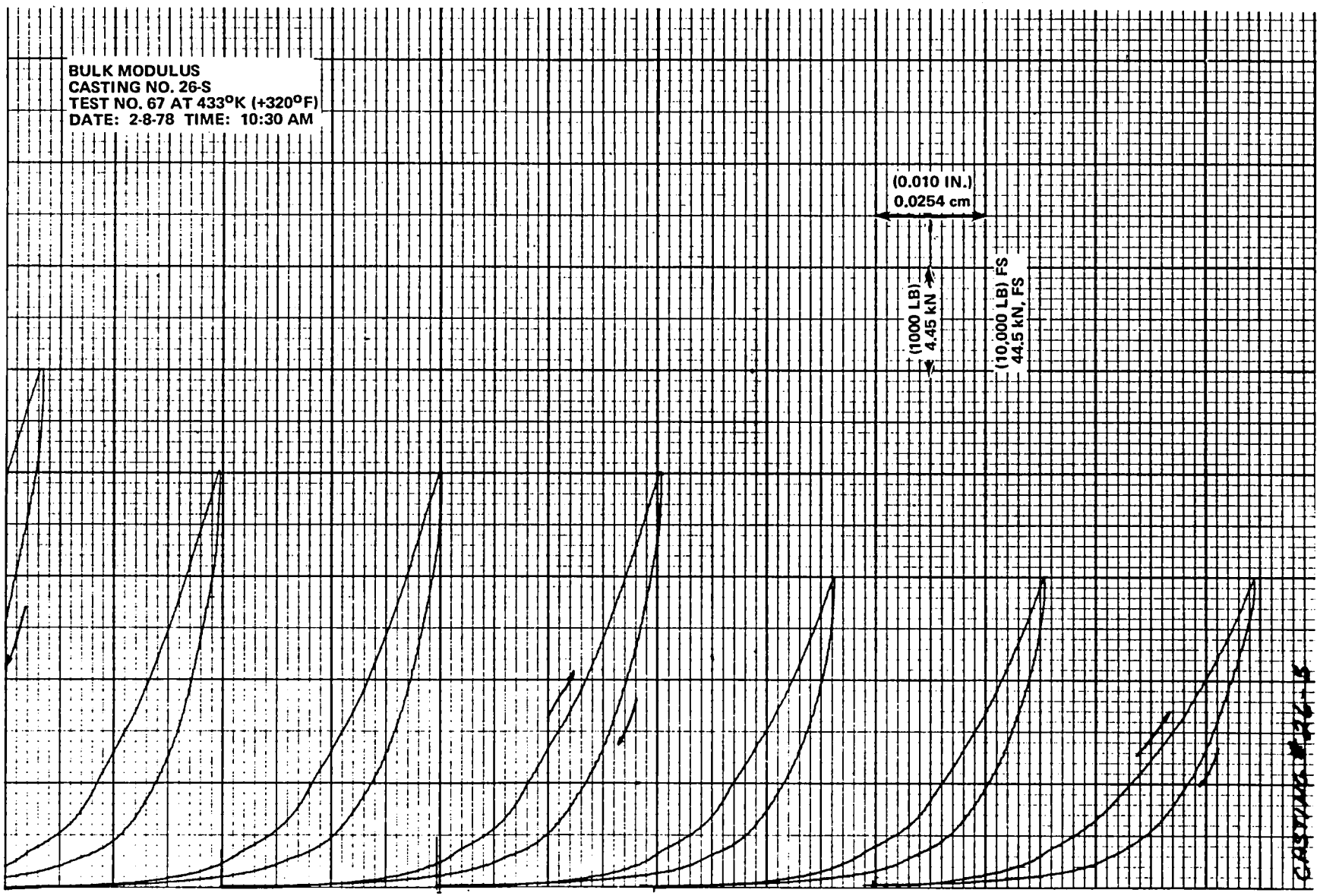

FIGURE J-14. TEST NO. 67 – EXTENSOMETER READING PLOTS, SECTION 1

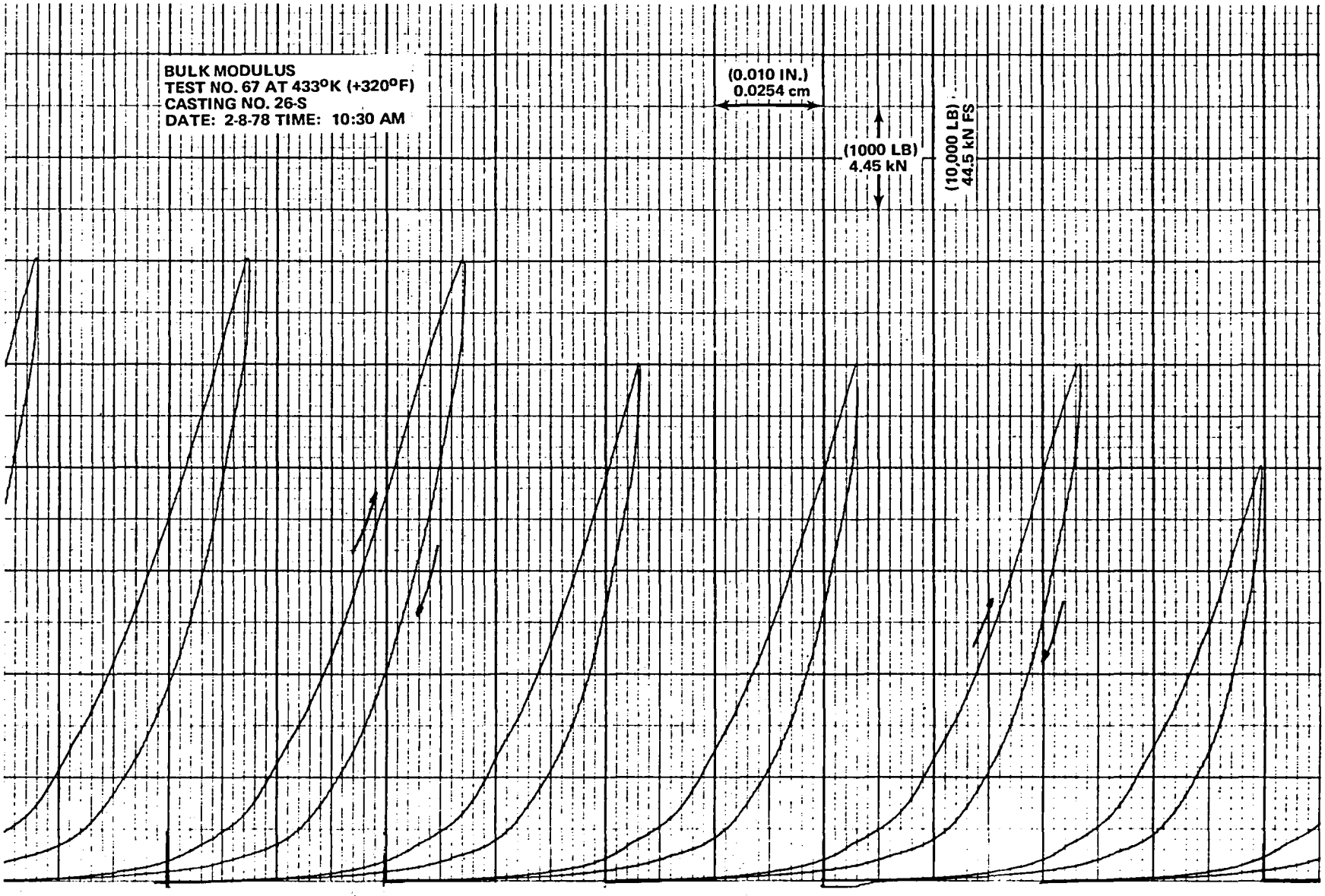

FIGURE J-15. TEST NO. 67 – EXTENSOMETER READING PLOTS, SECTION 2

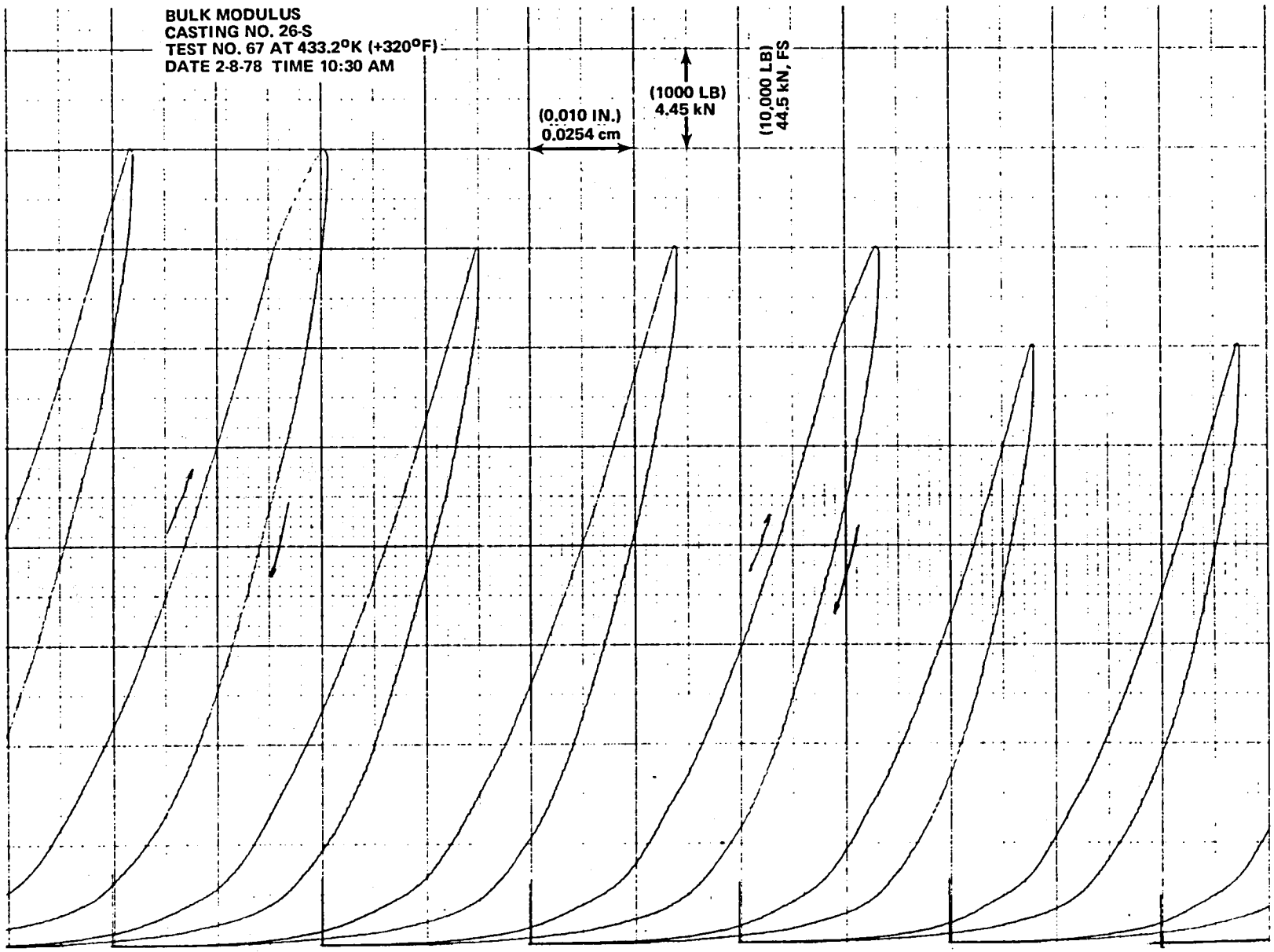

FIGURE J 16. TEST NO. 67 – EXTENSOMETER READING PLOTS, SECTION 3

Rubber Casting No. 26S (with expanded metal screening)

RT average dia = 1/2 (11.81 + 11.76) = 11.786 cm

RT height = 2.578 cm

Pressure Pad (aluminum), RT dia = 11.956 cm

Aluminum ring, RT ID = 11.989 cm

RT Radial gap = 1/2 (11.989 - (11.786 + 0.025))
= 0.089 cm

*One wrap of (0.0127 cm) Teflon tape

(RT) Pressure Pad Area = $(\frac{11.956}{2})^2$ = 112.266 sq cm

433°K Pressure Pad Area = 112.266 (1 + 46.8 x 10^{-6} x 136)
= 113.0 sq cm

α_L^{AL} = 23.4 x 10^{-6} m/m/°K

α_A^{AL} = 46.8 x 10^{-6} m/m/°K

ΔT = 433 - 297 = 136°K

(433°K Rubber Casting Radial Growth = 1/2 x 11.786 x 127 x 10^{-6} x 136

= 0.1067 cm (0.042 in.)

AVG α_L^R = 1/2 (175 + 78) x 10^{-6}
= 127 x 10^{-6} m/m/°K

(in plane of expanded metal screening, see Appendix F)

(RT) Rubber Casting Volume = π (11.786/2)^2 x 2.578 = 279.86 cu cm

(433°K) Rubber Casting Volume (V_2) = 279.86 (1 + 565 x 10^{-6} x 136)
= 300.44 cu cm

(433°K) Rubber Casting Area = π(11.786/2 + 0.0889)^2 = 112.41 sq cm

The load versus deflection curve for the first 26.69 kN loading cycle indicates that the onset of load occurred about 0.015 cm later than the nominal zero deflection (see Figure J-15). Therefore, the values for the average deflection from Table J-3 will be adjusted to correlate the onset of deflection with the onset of load. These corrections are given in Table J-4. Table J-4 also contains corrected bulk strain values which are in Figure J-13.

TABLE J-4
TEST NO. 67 – PRESSURE VERSUS CORRECTED BULK STRAIN –
FIRST 26.69 kN LOADING CYCLE – DAPCO 38-3 SILICONE RUBBER

①	②	③	④	⑤	⑥
LOAD (kN)	NOMINAL AVERAGE DEFLECTION (cm)	CORRECTED AVERAGE DEFLECTION (cm)	PRESSURE (MPa)	CORRECTED Δ VOLUME Δ V (cu cm)	CORRECTED BULK STRAIN ($\Delta V/V_2$)
0.045	0	−0.0152	0.0069	−1.708	−0.0057
0.445	0.0457	0.0305	0.0414	3.428	0.0114
0.890	0.0584	0.0432	0.0758	4.856	0.0162
2.224	0.0716	0.0564	0.1999	6.339	0.0211
4.448	0.0767	0.0615	0.3930	6.913	0.0230
8.896	0.0803	0.0651	0.7859	7.317	0.0243
13.344	0.0836	0.0684	1.1789	7.688	0.0256
17.792	0.0848	0.0696	1.5718	7.823	0.0260
22.240	0.0869	0.0717	1.9717	8.059	0.0268
26.688	0.0902	0.0750	2.3646	8.430	0.0280
REF	TABLE J-3	②−0.0152	TABLE J-3	112.4 ③	⑤ /302.8

Bulk Modulus Test No. 69, T = 433°K (320°F) – This test was a repeat of test No. 67. Again, rubber yielding appears to start at a load of 23.13 kN (approximately 2.07 MPa (300 psi)).

The extensometer readings are plotted in Figures J-17 and J-18. Table J-5 gives the extensometer and dial gage readings and their average values for the 26.69 kN load test.

The representative bulk modulus properties for this specimen are given in Tables J-6 and J-7.

The load versus deflection curve for the first 26.69 kN loading cycle indicates that the onset of load occurred about 0.0076 cm after the nominal zero deflection (see Figure J-18). Therefore, the values for the average deflection from Table J-6 will be adjusted to correlate the onset of deflection with the onset of load. Values of pressure versus corrected bulk strain are computed in Table J-7 and plotted in Figure J-13.

Bulk Modulus Test No. 71, T = 433°K (320°F) – This is a bulk modulus test setup, as shown in Figure J-7. The rubber was settled in first by performing three loading cycles to a maximum load of 13.34 kN to obtain results consistent with tests 67 and 69. A minimum of 5 minutes was allowed between tests.

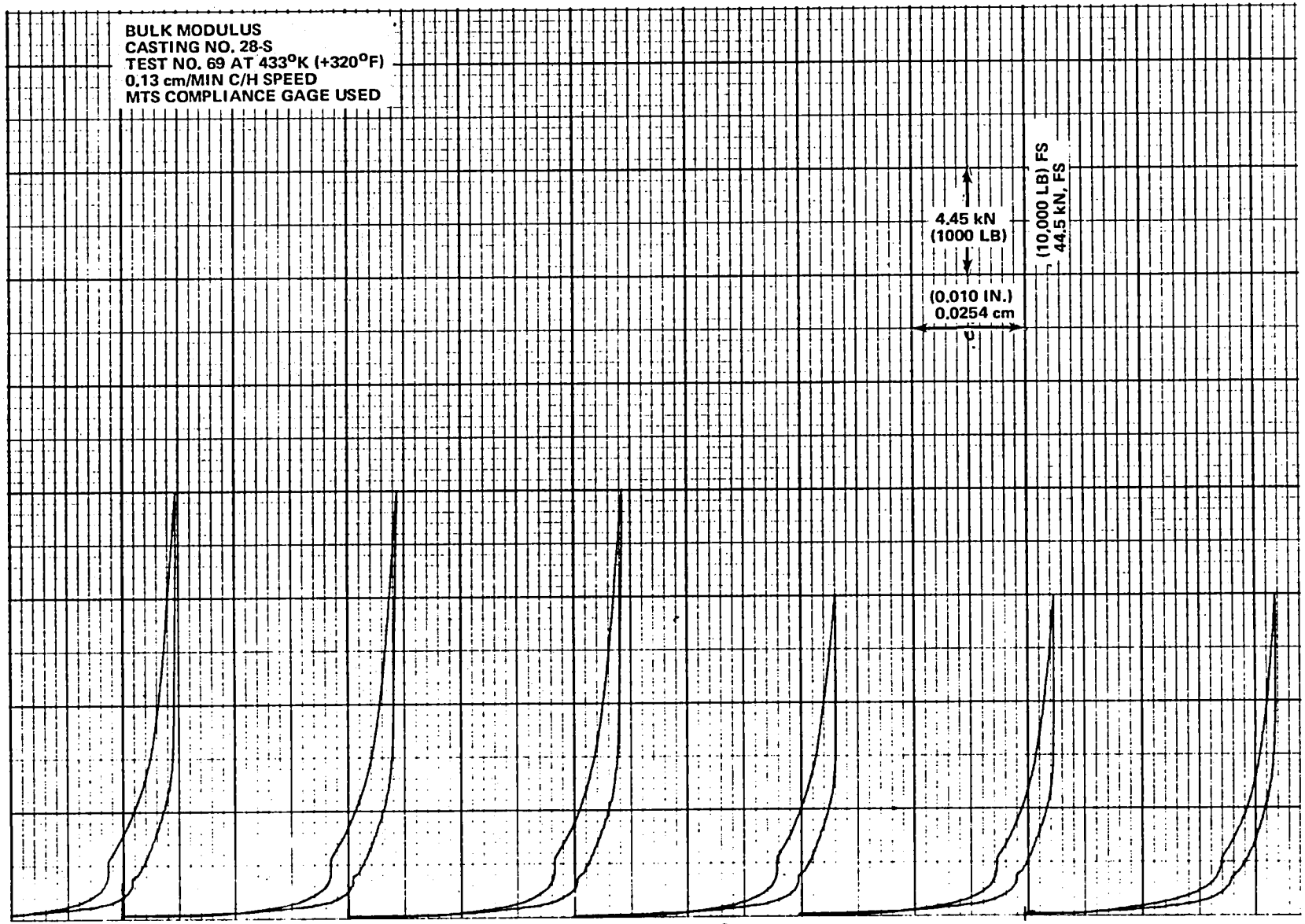

FIGURE J-17. TEST NO. 69 – EXTENSOMETER READING PLOTS, SECTION 1

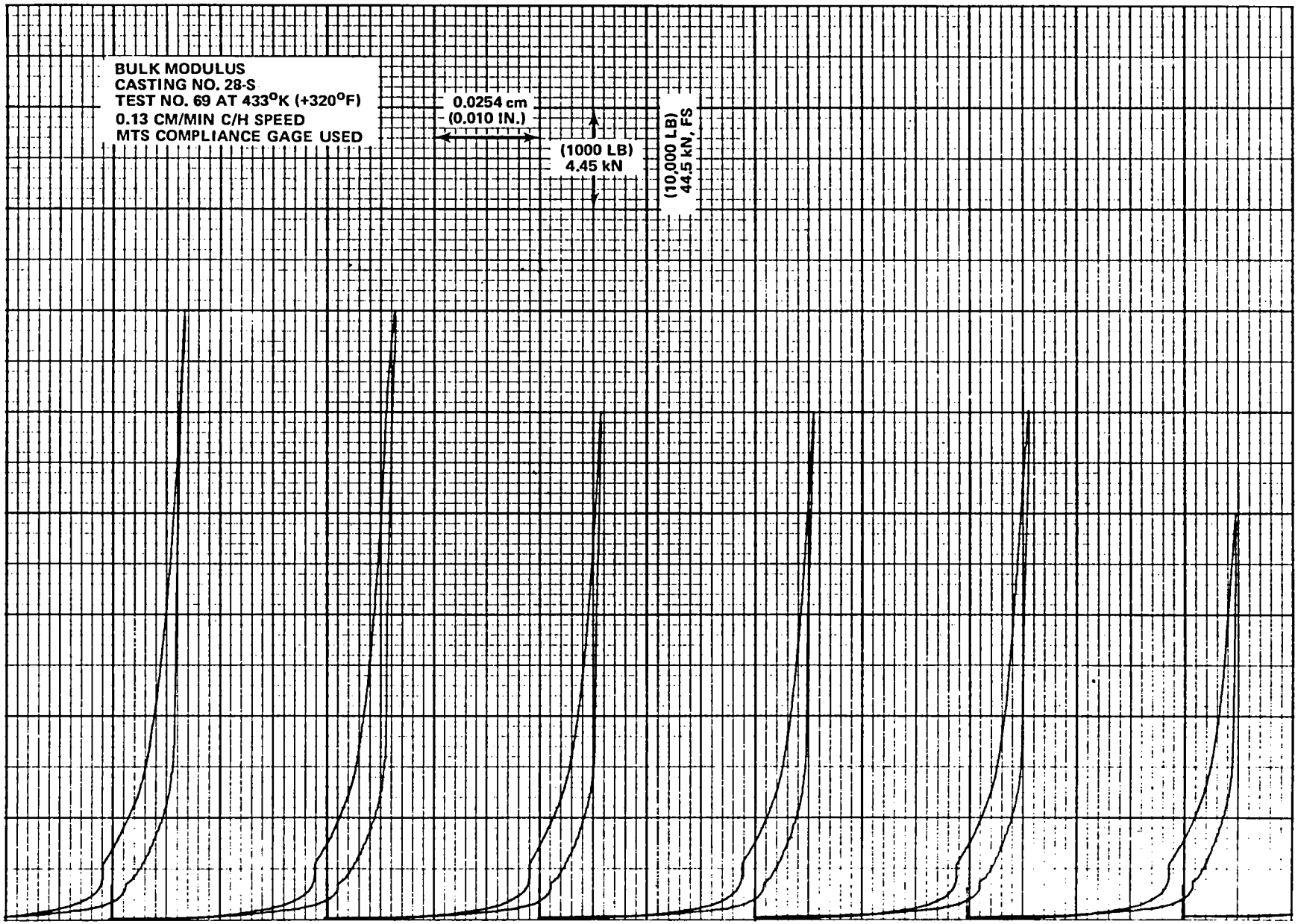

FIGURE J-18. TEST NO. 69 – EXTENSOMETER READING PLOTS, SECTION 2

TABLE J-5

TEST NO. 69 – BULK MODULUS TEST RESULTS (T = 433°K) – SECTION 4

LOAD (kN)	FIRST (3:08 P.M.)			SECOND (3:24 P.M.)			THIRD (3:36 P.M.)		
	EXTENSOMETER (cm)	DIAL (cm)	AVG (cm)	EXTENSOMETER (cm)	DIAL (cm)	AVG (cm)	EXTENSOMETER (cm)	DIAL (cm)	AVG (cm)
0.045		0	0		0				
0.445	0.0358	0.0305	0.0330	0.0368	0.0287		0.0366	0.0330	
0.890	0.0437	0.0437	0.0437	0.0442	0.0432		0.0439	0.0457	
2.224	0.0480	0.0650	0.0566	0.0483	0.0635	0.0559	0.0483	0.0648	0.0566
4.448	0.0538	0.0688	0.0615	0.0544	0.0673		0.0546	0.0686	
8.896	0.0592	0.0711	0.0650	0.0607	0.0701		0.0607	0.0711	
13.344	0.0617	0.0747	0.0683	0.0635	0.0739	0.0688	0.0635	0.0752	0.0693
17.792	0.0635	0.0782	0.0709	0.0650	0.0775	0.0714	0.0655	0.0787	0.0721
22.240	0.0645	0.0813	0.0729	0.0663	0.0813	0.0739	0.0665	0.0826	0.0747
26.688	0.0665*	0.0864	0.0765	0.0676	0.0853	0.0765	0.0681	0.0864	0.0772
22.240	0.0660	0.0864	0.0762	0.0663	0.0848		0.0665	0.0859	
17.792	0.0655	0.0833	0.0744	0.0660	0.0815		0.0663	0.0826	
13.344	0.0650	0.0795	0.0724	0.0658	0.0785		0.0660	0.0787	
8.896	0.0648	0.0749	0.0699	0.0655	0.0734		0.0658	0.0742	
4.448	0.0620	0.0699	0.0660	0.0627	0.0683		0.0625	0.0686	
2.224	0.0566	0.0681	0.0625	0.0572	0.0660		0.0572	0.0663	
0.890	0.0511	0.0538	0.0523	0.0518	0.0508		0.0521	0.0533	
0.445	0.0427	0.0406	0.0417	0.0427	0.0396		0.0429	0.0406	
0.045	0	0.0025	0.0013	0	0			0.0025	
REF	FIG J-11			FIG J-11			FIG J-11		

*APPARENT YIELD @ 23.13 kN

TABLE J-6

TEST NO. 69 – PRESSURE VERSUS BULK STRAIN (T = 433°K)
FIRST 26.69 kN LOADING CYCLE – DAPCO 38-3 SILICONE RUBBER

LOAD (kN)	AVERAGE DEFLECTION (cm)	PRESSURE (MPa)	Δ VOLUME ΔV (cu cm)	BULK STRAIN ($\Delta V/V_2$)
0.045	0	0.0069	0	0
0.445	0.0330	0.0414	3.709	0.0122
0.890	0.0437	0.0758	4.912	0.0162
2.224	0.0566	0.1999	6.362	0.0211
4.448	0.0615	0.3930	6.913	0.0228
8.896	0.0650	0.7859	7.306	0.0241
13.344	0.0683	1.1789	7.677	0.0254
17.792	0.0709	1.5714	7.969	0.0263
22.240	0.0729	1.9717	8.194	0.0271
22.688	0.0765	2.3646	8.599	0.0284
22.240	0.0762	1.9717	8.565	0.0283
17.792	0.0744	1.5714	8.363	0.0276
13.344	0.0724	1.1789	8.138	0.0269
8.896	0.0699	0.7859	7.857	0.0259
4.448	0.0660	0.3930	7.418	0.0245
2.224	0.0625	0.1999	7.025	0.0232
0.890	0.0523	0.0758	5.879	0.0194
0.445	0.0417	0.0414	4.687	0.0155
0.045	0.0013	0.0069	0.146	0.0005
REF	TABLE J-5	LOAD/11.29	112.4 (AVG DEFL)	ΔV/302.8

TABLE J-7
PRESSURE VERSUS CORRECTED BULK STRAIN – FIRST 26.69 kN
LOADING CYCLE – TEST NO. 69 – DAPCO 38-3 SILICONE RUBBER

①	②	③	④	⑤	⑥
LOAD (kN)	NOMINAL AVERAGE DEFLECTION (cm)	CORRECTED AVERAGE DEFLECTION (cm)	PRESSURE (MPa)	CORRECTED Δ VOLUME ΔV (cm^3)	CORRECTED BULK STRAIN ($\Delta V/V_2$)
0.045	0	-0.0076	0.0069		
0.445	0.0330	0.0254	0.0414	2.855	0.0094
0.890	0.0437	0.0361	0.0758	4.058	0.0134
2.224	0.0566	0.0490	0.1999	5.508	0.0182
4.448	0.0615	0.0539	0.3930	6.058	0.0200
8.896	0.0650	0.0574	0.7859	6.452	0.0213
13.344	0.0683	0.0607	1.1789	6.823	0.0225
17.792	0.0709	0.0633	1.5714	7.115	0.0235
22.240	0.0729	0.0653	1.9717	7.340	0.0242
26.688	0.0765	0.0689	2.3646	7.744	0.0256
REF	TABLE J-6	② -0.0076	TABLE J-6	†12.4 ③	⑤ /302.8

The extensometer readings are plotted in Figure J-19. Table J-8 gives the extensometer and dial gage reading and the average of these for the 36.34 kN load test.

The bulk modulus properties are given in Tables J-9 and J-10 and are plotted in Figure J-13. In Figure J-19, it is apparent that the rubber yielding starts at about 22.24 kN (1.98 MPa).

The load versus deflection curve for this test shown in Figure J-19 indicates that the onset of load occurred about 0.0102 cm after the nominal zero deflection. Therefore, the values for the average deflection from Table J-9 will be adjusted to correlate the onset of deflection with the onset of load..

Values of pressure versus corrected bulk strain are computed in Table J-10 and are plotted in Figure J-13.

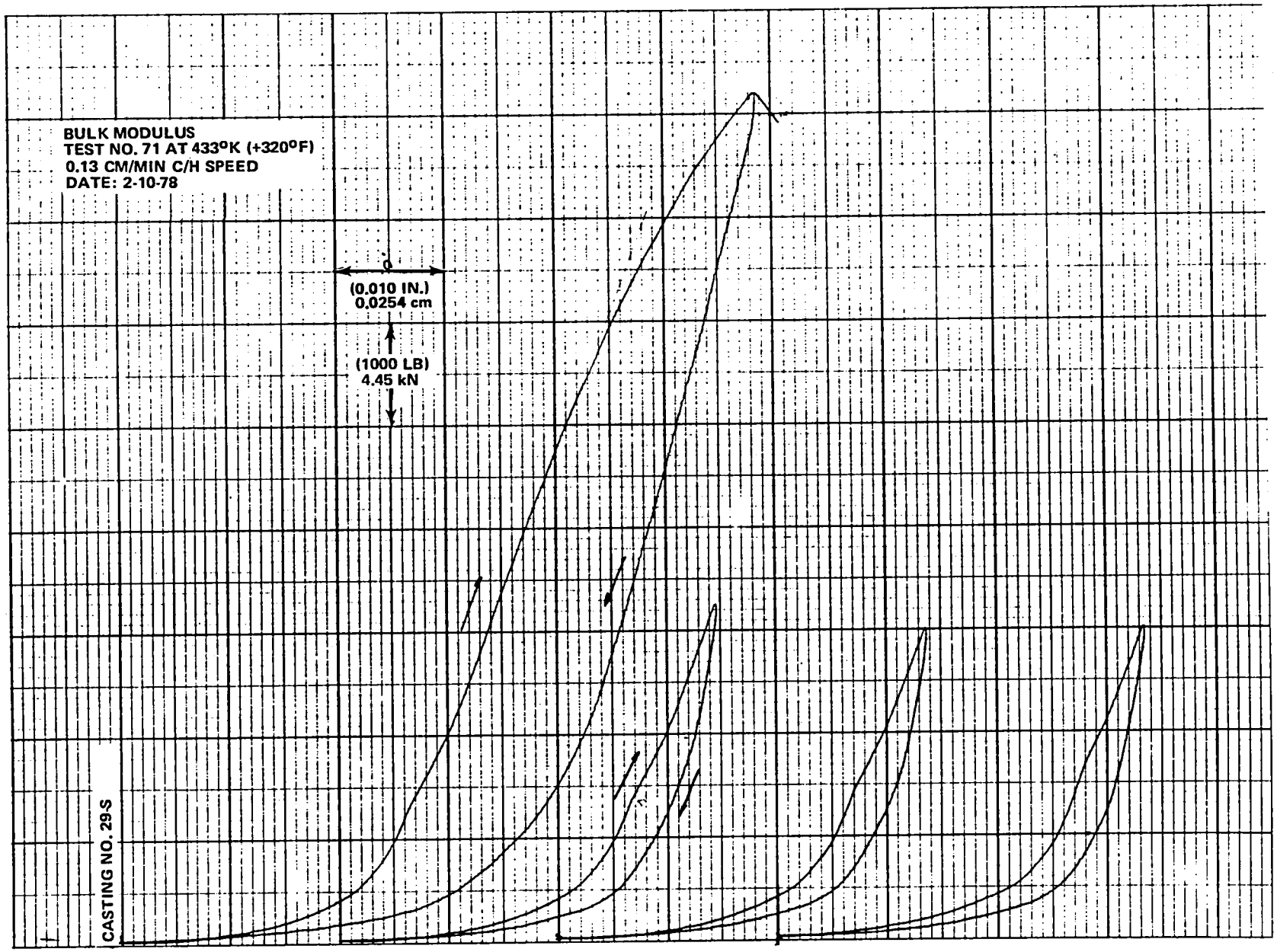

FIGURE J-19. TEST NO. 71 – EXTENSOMETER READING PLOTS

TABLE J-8

TEST NO. 71 – BULK MODULUS
TEST RESULTS (T = 433.2°K)

LOAD (kN)	GAGE DEFLECTION (cm)		
	EXTENSOMETER	DIAL	AVG
0.045	0	0	0
0.311	0.0257	0.0211	0.0234
0.756	0.0381	0.0318	0.0351
2.091	0.0541	0.0417	0.0478
4.315	0.0640	0.0432	0.0536
8.763	0.0762	0.0381	0.0572
13.211	0.0853	0.0330	0.0592
17.659	0.0945	0.0292	0.0620
22.107	0.1041	0.0257	0.0650
26.555	0.1148	0.0229	0.0688
31.003	0.1278	0.0203	0.0742
36.340	0.1486	0.0203	0.0843
REF	FIG J-19		

TABLE J-9

TEST NO. 71: PRESSURE VERSUS BULK STRAIN
(T = 433.2°K) DAPCO 38-3 SILICONE RUBBER

LOAD (kN)	AVERAGE DEFLECTION (cm)	PRESSURE (MPa)	Δ VOLUME ΔV (cm^3)	BULK STRAIN ($\Delta V/V_2$)
0.045	0	0.0040	0	0
0.311	0.0234	0.0277	2.629	0.0087
0.75	0.0351	0.0673	3.944	0.0127
2.091	0.0478	0.1860	5.371	0.0177
4.315	0.0536	0.3840	6.023	0.0199
8.763	0.0572	0.7798	6.428	0.0213
13.211	0.0592	1.1756	6.652	0.0220
17.659	0.0620	1.5715	6.967	0.0231
22.107	0.0650	1.9673	7.304	0.0242
26.555	0.0688	2.3631	7.731	0.0256
31.003	0.0742	2.7590	8.338	0.0276
36.340	0.0843	3.2340	9.473	0.0314
REF	TABLE J-15	LOAD/11.237	$112.37\left[\begin{smallmatrix}\text{AVG}\\ \text{DEFL}\end{smallmatrix}\right]$	$\Delta V/302.10$

TABLE J-10
TEST NO. 71 – PRESSURE VERSUS CORRECTED BULK STRAIN
DAPCO 38-3 SILICONE RUBBER

①	②	③	④	⑤	⑥
LOAD (kN)	NOMINAL AVERAGE DEFLECTION (cm)	CORRECTED AVERAGE DEFLECTION (cm)	PRESSURE (MPa)	CORRECTED Δ VOLUME ΔV (cu cm)	CORRECTED BULK STRAIN ($\Delta V/V_2$)
0.045	0	–0.0102	0.0040	–1.146	–0.0038
0.311	0.0234	0.0132	0.0277	1.483	0.0049
0.756	0.0351	0.0249	0.0673	2.798	0.0090
2.091	0.0478	0.0276	0.1860	3.101	0.0140
4.315	0.0536	0.0434	0.3840	4.877	0.0162
8.763	0.0572	0.0470	0.7798	5.281	0.0175
13.211	0.0592	0.0490	1.1756	5.506	0.0182
17.659	0.0620	0.0518	1.5715	5.821	0.0193
22.107	0.0650	0.0548	1.9673	6.158	0.0204
26.555	0.0688	0.0586	2.3631	6.585	0.0218
31.003	0.0742	0.0640	2.7590	7.192	0.0238
36.340	0.0843	0.0741	3.2340	8.327	0.0276
REF	TABLE J-16	② –0.0102	TABLE J-16	112.37 ③	ΔV/302.10

Bulk Modulus Test No. 97, T = 450°K (350°F) – Test No. 97 was performed on rubber casting No. 37S after it had been subjected to 43 temperature/pressure cycles described in Appendix K.

The intention was to determine any change in the bulk modulus properties of DAPCO 38-3 silicone rubber after numerous cure cycles (see Figure J-12).

This test was conducted for three maximum loads: 13.34 kN, 17.79 kN, and 22.24 kN, and cycled three times at each maximum load. The initial cycling parallels the loading sequence of the previous bulk modulus tests. It settles the rubber in the tool and should provide better comparable data. A minimum wait of 5 minutes was allowed between tests.

The extensometer readings are plotted in Figure J-20. Table J-11 gives the extensometer and dial gage readings and the average of these. The bulk modulus properties are given in Table J-12 and are plotted in Figure J-12.

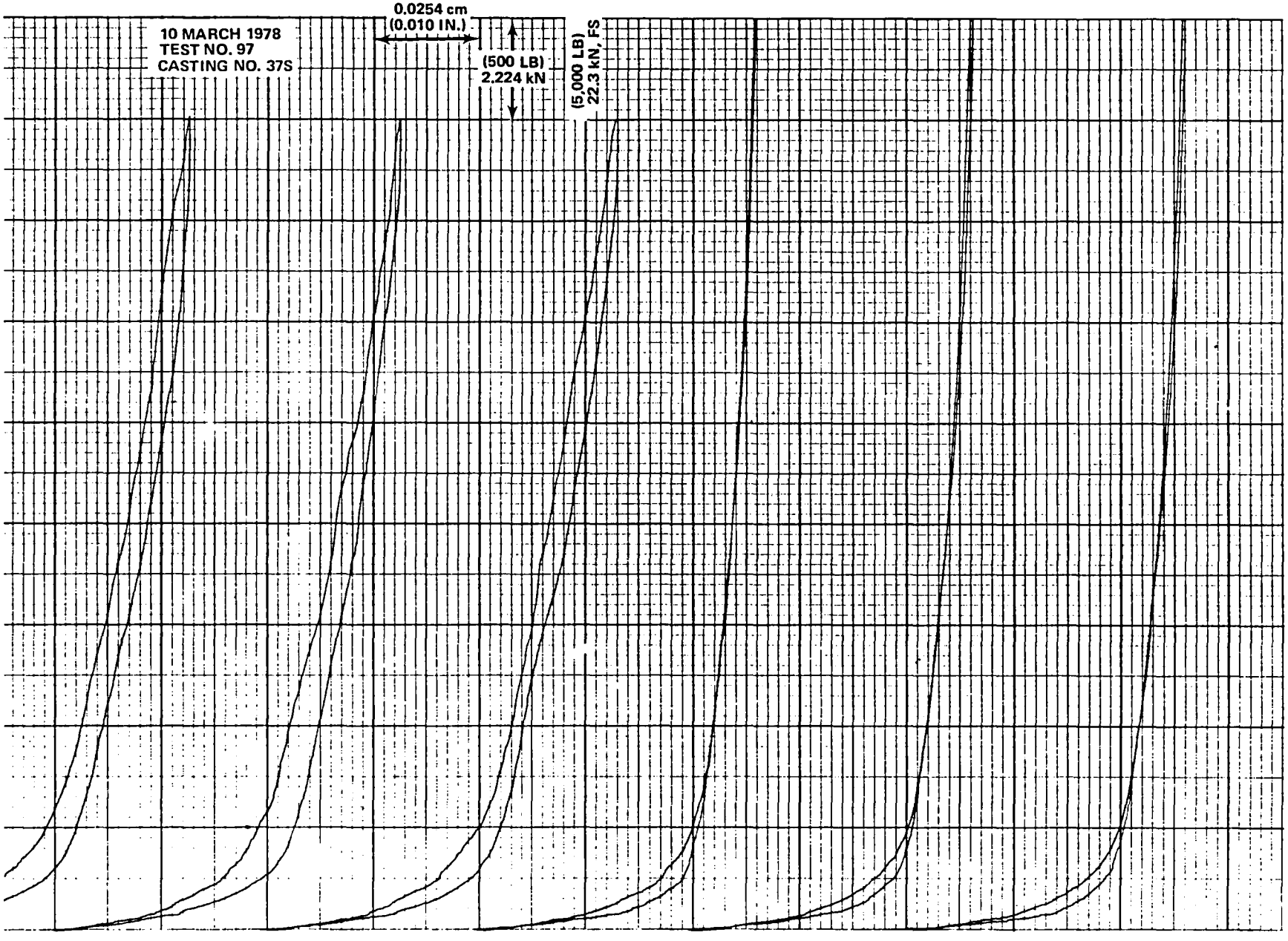

FIGURE J-20. TEST NO. 97 – EXTENSOMETER READING PLOTS, SECTION 2

TABLE J-11
TEST NO. 97 – BULK MODULUS TEST RESULTS (T = 450°K) – SECTION 3

LOAD (kN)	GAGE DEFLECTION (cm)								
	FIRST CYCLE			SECOND CYCLE			THIRD CYCLE		
	EXTENSOMETER	DIAL	AVG	EXTENSOMETER	DIAL	AVG	EXTENSOMETER	DIAL	AVG
0	0	0	0	0	0	0	0	0	0
0.445	0.0295	0.0305	0.0300	0.0302	0.0305	0.0304	0.0295	0.0305	0.0300
0.890	0.0404	0.0356	0.0381	0.0406	0.0368	0.0386	0.0394	0.0381	0.0386
2.224	0.0508	0.0457	0.0483	0.0511	0.0457	0.0483	0.0508	0.0457	0.0483
4.448	0.0556	0.0508	0.0533	0.0556	0.0508	0.0533	0.0551	0.0508	0.0528
8.896	0.0599	0.0559	0.0579	0.0605	0.0559	0.0582	0.0599	0.0572	0.0584
13.344	0.0632	0.0610	0.0620	0.0635	0.0610	0.0622	0.0630	0.0610	0.0620
17.792	0.0648	0.0660	0.0655	0.0653	0.0660	0.0655	0.0648	0.0660	0.0655
22.240	0.0660	0.0699	0.0681	0.0668	0.0711	0.0691	0.0660	0.0711	0.0686
17.792	0.0650	0.0686	0.0668	0.0660	0.0686	0.0673	0.0655	0.0686	0.0671
13.344	0.0635	0.0660	0.0648	0.0640	0.0610	0.0650	0.0635	0.0660	0.0648
8.896	0.0599	0.0635	0.0617	0.0605	0.0635	0.0620	0.0599	0.0635	0.0617
4.448	0.0556	0.0584	0.0569	0.0556	0.0584	0.0569	0.0551	0.0584	0.0569
2.224	0.0521	0.0533	0.0528	0.0521	0.0521	0.0521	0.0516	0.0521	0.0518
0.890	0.0457	0.0457	0.0457	0.0450	0.0457	0.0452	0.0447	0.0457	0.0452
0.445	0.0371	0.0381	0.0376	0.0368	0.0381	0.0376	0.0376	0.0381	0.0378
0	0		0	0	0	0	0	0	0
REF	FIG J-20			FIG J-20			FIG J-20		

TABLE J-12
TEST NO. 97 – PRESSURE VERSUS BULK STRAIN (T = 450°K)
FIRST 22.24 kN LOADING CYCLE – DAPCO 38-3 SILICONE RUBBER

LOAD (kN)	AVERAGE DEFLECTION (cm)	PRESSURE (MPa)	Δ VOLUME ΔV (cu cm)	BULK STRAIN ($\Delta V/V_2$)
0	0	0	0	0
0.445	0.0300	0.0393	3.386	0.0111
0.890	0.0381	0.0787	4.301	0.0141
2.224	0.0483	0.1967	5.452	0.0179
4.448	0.0533	0.3934	6.017	0.0198
8.896	0.0579	0.7868	6.536	0.0215
13.344	0.0620	1.1803	6.999	0.0230
17.792	0.0655	1.5737	7.394	0.0243
22.240	0.0681	1.9671	7.687	0.0252
REF	TABLE J-18	LOAD/11.306	112.88 (AVG DEFL)	ΔV/304.4

APPENDIX K
ANALYSIS VERIFICATION TESTS

The tests described in Appendix K had a two-fold purpose. One purpose was to provide a demonstration of the relationship between temperature and pressure for specimens of trapped rubber with a variety of gaps between the rubber specimen and the enclosing structure. The other purpose was to show the degree of accuracy in predicting the trapped rubber pressure using the bulk modulus properties of Figure J-12.

Tests 72, 74, 76, 77, and 78 are typical temperature-versus-trapped-rubber-pressure tests with gaps ranging from zero to 0.635 mm (0.025 inch) at the top and sides of the specimen. Graphs of temperature versus pressure show reasonable agreement between tests and analysis values, considering the possible scatter of rubber material and dimensional properties.

The rubber specimen used for Test 78 (gap = 0.635 mm (0.025 inch)) produced 2.14 MPa (310-psi) rubber pressure at 450^{o}K (350^{o}F). This specimen was temperature/pressure-cycled 43 times with an 0.635-mm (0.025-inch) gap. Tests 81, 86, 90, and 95 were performed at the 6th, 13th, 21st, and 43rd cycles. On completion of these tests, bulk modulus Test 97 was conducted on the same rubber specimen, and its bulk modulus properties at that time showed excellent agreement with average properties of Figure J-12.

To illustrate that rubber expands as a volume due to temperature, Test 89 was conducted with the gap on one face of the rubber only. The gap volume for Test 89 was the same as for Test 78, where the gap was on the face and sides of the specimen. A comparison of the temperature/pressure observation for Tests 89 and 78 (Figure K-10) is given in this appendix. The results are remarkably similar.

Test 93 is a duplication of Test 77 after a lapse of 23 days. These tests were performed with the same rubber specimen to determine the effects of aging. The results of these tests were plotted in this appendix. These results are a reasonable comparison with the results of Test 93 being more compatible with analysis (Figure K-11).

The equipment for these tests was the same as that used for the bulk modulus tests described in Appendix J and shown in Figures J-1 through J-7. The cylindrical rubber specimens were cast of Dapco 38-3 silicone rubber with an inner layer of metal screening. These specimens were cured per specimen No. 4 in Table 20 (Section 6). The size of these specimens was the same as described in Appendix J and used for the bulk modulus tests. These analysis verification tests consisted of three general types which are described below.

The Dapco 38-3 silicone rubber specimens were cast slightly undersize and cured by standard procedures. The following tests were performed by enclosing the rubber specimens in cylinders with various gaps. They provided information on how much pressure resulted from the thermal expansion of silicone rubber and also an opportunity to compare test results with the values obtained by analysis, using bulk modulus, and thermal expansion coefficient information.

1. Zero Gap Tests - Metal shims were used to fill the gap around all the sides of the cylindrical rubber specimen when at room temperature while the pressure pad was brought down to contact the upper flat side of the rubber specimen inside an oven (see Figure K-1). The oven was turned on and the rubber pressure and temperature were measured and recorded while holding the volume constant.

2. Controlled Gap (0.254-, 0.0457-, and 0.0635-cm; (0.010-, 0.018-, and 0.025-inch)) Tests - Cylindrical Dapco 38-3 silicone rubber specimens were cast slightly undersize and cured by standard procedures. Metal shims (see Figure K-2) were used to achieve the desired gap (0.0254, 0.0457, and 0.0635 cm; (0.010, 0.018, and 0.025 inch)) between the sides of the rubber specimen and the enclosing metal ring. The pressure pad, attached to the loading machine, was used to provide the desired gap at the upper surface of the rubber specimen. With the holding container maintaining constant volume when placed in the oven, rubber pressure was measured as the rubber temperature increased.

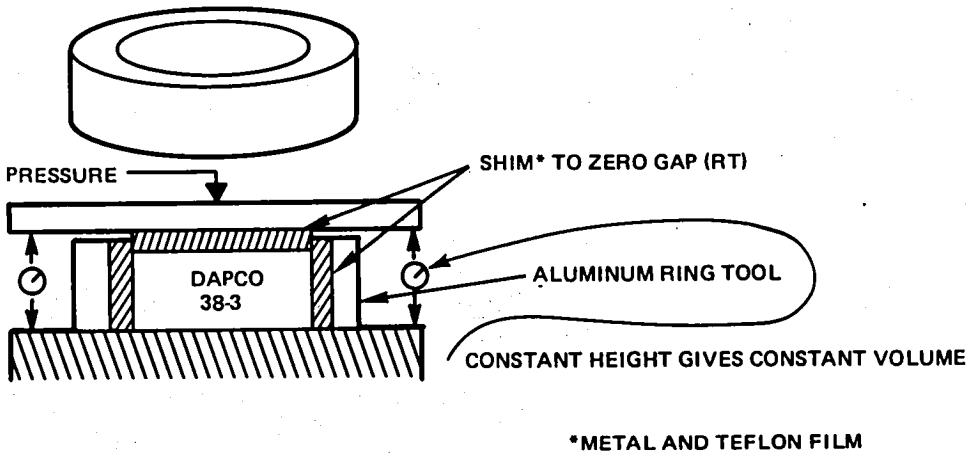

FIGURE K-1. TRAPPED RUBBER PRESSURE TEST SETUP
(NO INITIAL RUBBER GAP)

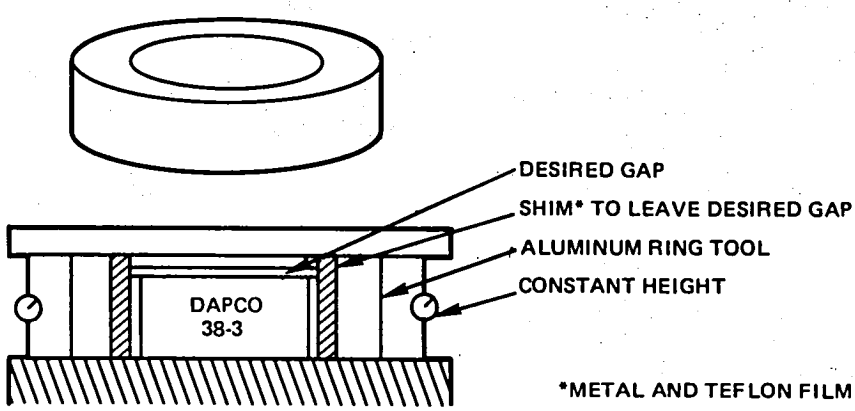

FIGURE K-2. TRAPPED RUBBER TEST SETUP
(SPECIFIED GAP)

3. Repeat Cycle Pressure Tests - A cylindrical Dapco 38-3 silicone rubber specimen was found to produce the maximum desirable pressure of approximately 2.068 MPa (300 psi) when placed in an enclosure providing an 0.0635-cm (0.025-inch) gap and then heated to 449.9^{o}K (350^{o}F). This setup was temperature-cycled 42 times in a plain oven. However, the 6th, 13th, 21st, and 42nd cycles were performed in the oven attached to the loading machine, and pressure versus temperature values were recorded up to 449.9^{o}K (350^{o}F). This test should provide useful information on the longevity of Dapco 38-3 silicone rubber when used as mandrels for the trapped rubber process.

During each of this series of tests a record is kept of the rubber temperature and pressure. Then, an analysis is made to estimate the rubber pressure for each test for the observed corresponding rubber temperature.

The analytical method for estimating the rubber pressure consists of the following steps:

1. Estimate the volume of the rubber specimen at its desired temperature if it were permitted to expand in an unrestricted manner.

2. Repeat Step 1 for the internal surface of the aluminum ring.

3. Subtract the result of Step 2 from that of Step 1.

4. If the result of Step 3 is a positive number, divide it by Step 2 to obtain the bulk strain.

5. Read off the rubber pressure from Figure J-12.

A step-by-step analysis using the above method is given in the following work for test No. 74 only. For the other tests, only the results are given in the tables and figures of this appendix.

Pressure Versus Temperature Test No. 72

A temperature versus trapped rubber pressure test with zero gap was conducted as described previously. Figure K-3 presents the rubber pressures resulting from test and analysis.

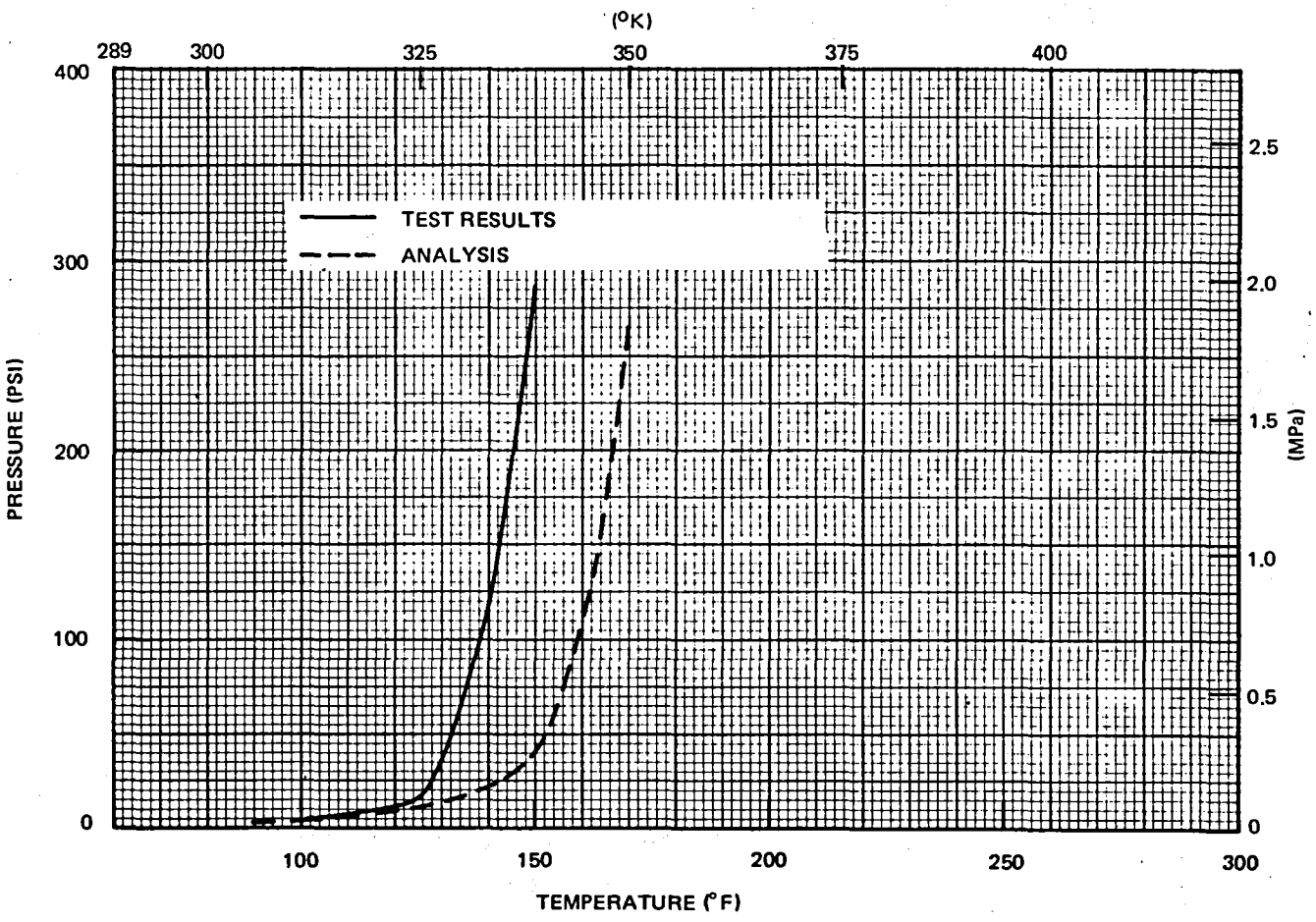

FIGURE K-3. TEST NO. 72 – PRESSURE VERSUS TEMPERATURE

Pressure Versus Temperature Test No. 74

This is a temperature versus trapped rubber pressure test with zero gap and was conducted per test No. 72. The rubber pressures resulting from testing and the following analysis are given in Tables K-1 and K-2 and plotted in Figure K-4. There is excellent agreement between test and theory.

RT Radial Gap = 0.00254 cm

RT Axial Gap = 0 cm

0.0127 cm Teflon: 2 wraps on side
1 wrap on top and bottom

Rubber Casting No. 33S

TABLE K-1
TEST NO. 74 – PRESSURE VERSUS TEMPERATURE ANALYSIS
ZERO GAP, DAPCO 38-3 SILICONE RUBBER

TEMP (°K)	ΔT (°K)	ΔV_C^R (cu cm)	V_2 (cu cm)	$\Delta V_C^R/V_2$	PRESSURE (MPa)
297.1	0	-0.25	289.89	0	0
305.4	8.3	0.936	291.19	0.0032	0.021
311.0	13.9	1.736	292.07	0.0060	0.028
324.8	27.8	3.723	294.24	0.0127	0.069
338.7	41.7	5.709	296.42	0.0193	0.221
344.3	47.2	6.495	297.28	0.0219	0.579
349.8	52.8	7.295	298.15	0.0245	1.655
351.5	54.4	7.524	298.40	0.0253	2.068
353.2	56.1	7.767	298.67	0.0260	2.241
355.4	58.3	8.081	299.01	0.0271	2.413
REF		$0.1429\Delta T$ -0.25	$0.1565\Delta T$ $+289.89$		FIG. J-12

TABLE K-2
TEST NO. 74 – PRESSURE VERSUS TEMPERATURE TEST RESULTS
ZERO GAP, DAPCO 38-3 SILICONE RUBBER

TEMP (°K)	LOAD (kN)	PRESSURE (MPa)
311.0	0.156	0.0138
316.5	0.245	0.0218
322.1	0.334	0.0297
327.6	0.489	0.0435
333.2	0.801	0.0713
338.7	1.601	0.1425
344.3	6.450	0.5739
349.8	17.347	1.5435
353.7	24.019	2.1371
REF		LOAD/11.239
*PRESSURE PAD AREA ≈ 112.39 cu cm		

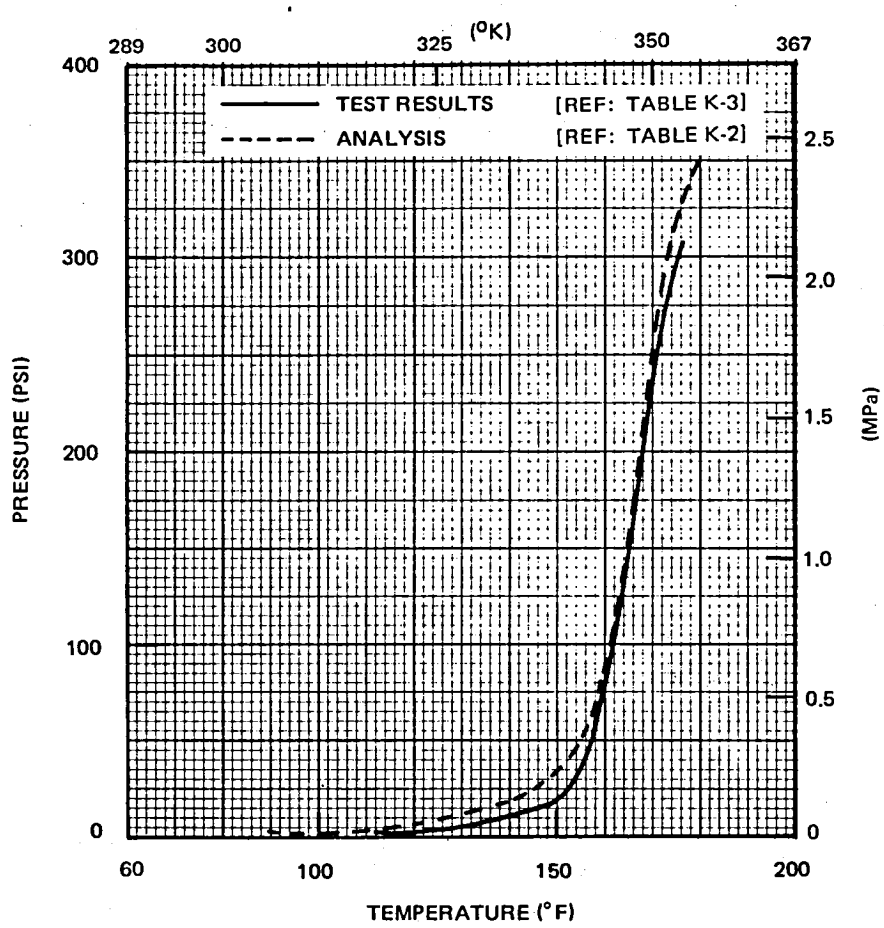

FIGURE K-4. TEST NO. 74 – PRESSURE VERSUS TEMPERATURE

RT Average Diameter = 11.984 cm

RT Height = 2.570 cm

Aluminum Ring, RT Diameter = 12.040 cm

Pressure Pad, RT Diameter = 11.956 cm

$$\text{RT Aluminum Ring Volume} = \pi\left(\frac{12.040 - 0.0508}{2}\right)^2 \times 2.570 = 290.14 \text{ cu cm}$$

$$(T^{o}K)\ \text{Aluminum Ring Volume Expansion} = 290.14 \times 46.8 \times 10^{-6} \times \Delta T = 0.0136\ \Delta T \text{ cu cm}$$

$$\text{RT Rubber Volume} = \pi(11.984/2)^2 \times 2.570 = 289.89 \text{ cu cm}$$

$$(T^{o}K)\ \text{Rubber Volume Expansion} = 289.89 \times 565 \times 10^{-6}\ \Delta T = 0.1638\ \Delta T \text{ cu cm}$$

($T^{o}K$) Rubber Volume (V_2) = 289.89 + 0.1638 ΔT cu cm

($T^{o}K$) Aluminum Ring Inner Volume = 290.14 + 0.0136 ΔT cu cm

Change from free rubber volume

$$\Delta V_C^R = 289.89 + 0.1638\ \Delta T - (290.14 + 0.0136\ \Delta T)$$

$$= 0.1502\ \Delta T - 0.25 \text{ cu cm}$$

Bulk Strain = $\Delta V_C^R / V_2$

Pressure Versus Temperature Test No. 76

This is a temperature versus trapped rubber pressure test with a 0.0254-cm (0.010-inch) rubber gap. Figure K-5 shows the rubber pressures that resulted from testing and analysis.

Pressure Versus Temperature Test No. 77

This is a temperature versus trapped rubber pressure test with a 0.0457-cm (0.018-inch) rubber gap. Figure K-6 shows the rubber pressures that resulted from testing and analysis.

Pressure Versus Temperature Test No. 78

This is a temperature versus trapped rubber pressure test with a 0.0635-cm (0.025-inch) rubber gap. Figure K-7 gives the rubber pressures resulting from testing and analysis.

Pressure Versus Temperature Tests No. 78, 81, 86, 90 and 95

Tests No. 78, 81, 86, 90, and 95 were all part of an overall test to determine the effect of subjecting a rubber specimen to many temperature-pressure cycles.

This testing started when it was determined by Test No. 78 that a gap of 0.0635 cm (0.025 inch) at the sides and top of rubber casting No. 37S produced a pressure of 2.14 MPa (310 psi) at 450^{o}K (350^{o}F) (See Figure K-7).

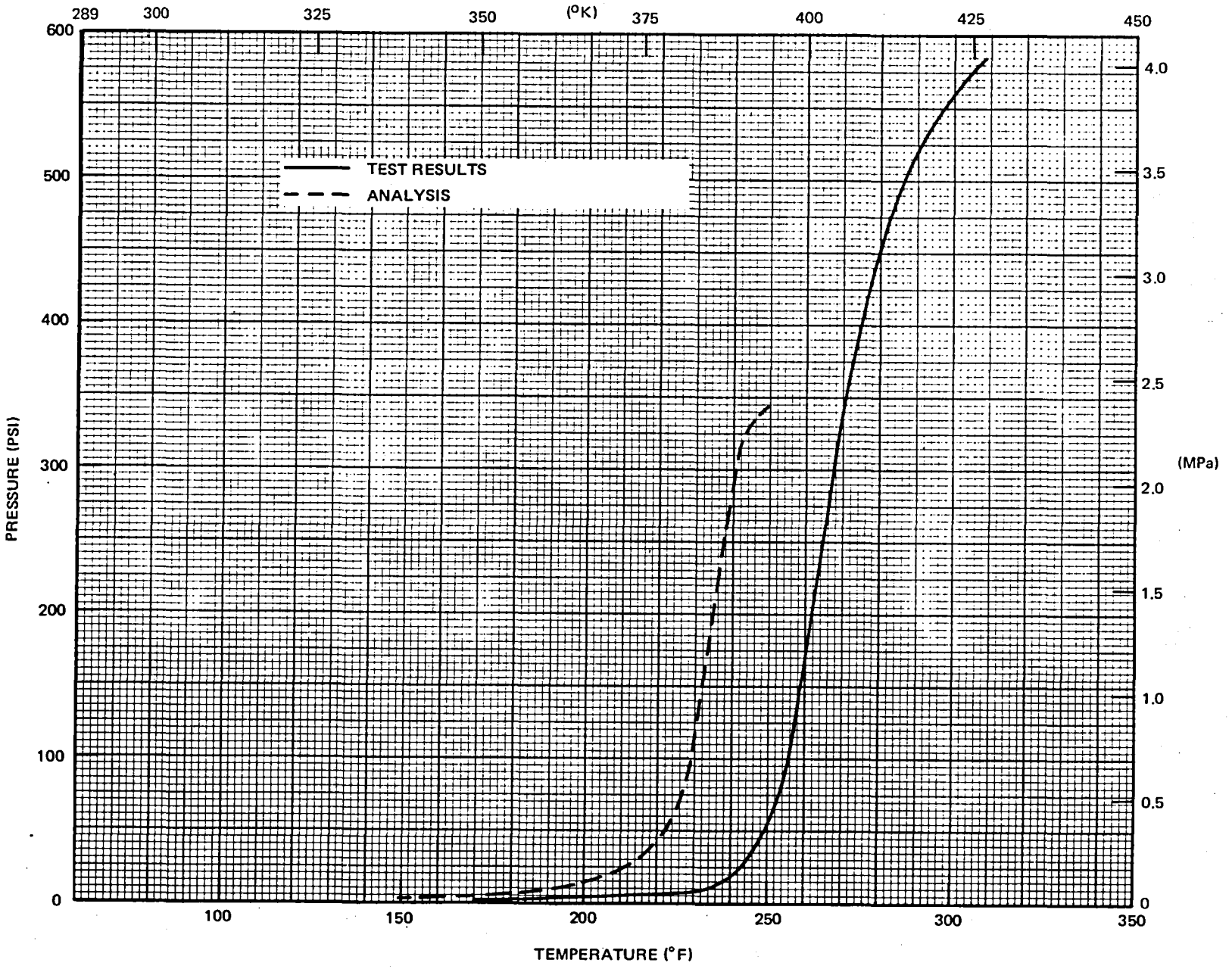

FIGURE K-5. TEST NO. 76 – PRESSURE VERSUS TEMPERATURE

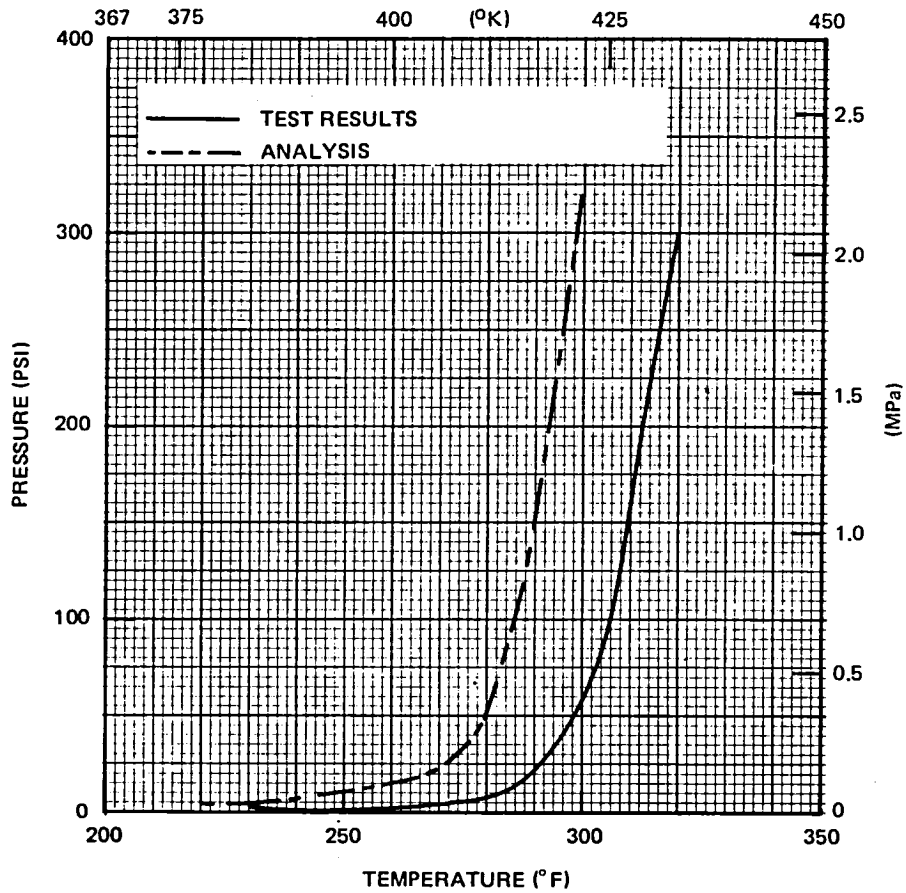

FIGURE K-6. TEST NO. 77 – PRESSURE VERSUS TEMPERATURE

Thus rubber casting No. 37S was placed in an enclosing aluminum cylinder with the same gaps as for test No. 78 and cycled between room temperature and 449.9°K (350°F) as indicated in Figure K-8.

Altogether there were 43 temperature-pressure cycles performed on casting No. 37S, with five of the cycles performed on a loading machine, as listed in Table K-4. The results of these tests are given in Figure K-9.

The pressure-temperature plots in Figure K-9 indicate that the rubber tends to soften during the first 13 cycles but stiffens during the later cycles. After the 43 cycles were performed, casting No. 37S was subjected to a bulk modulus test described in Appendix J under test No. 97.

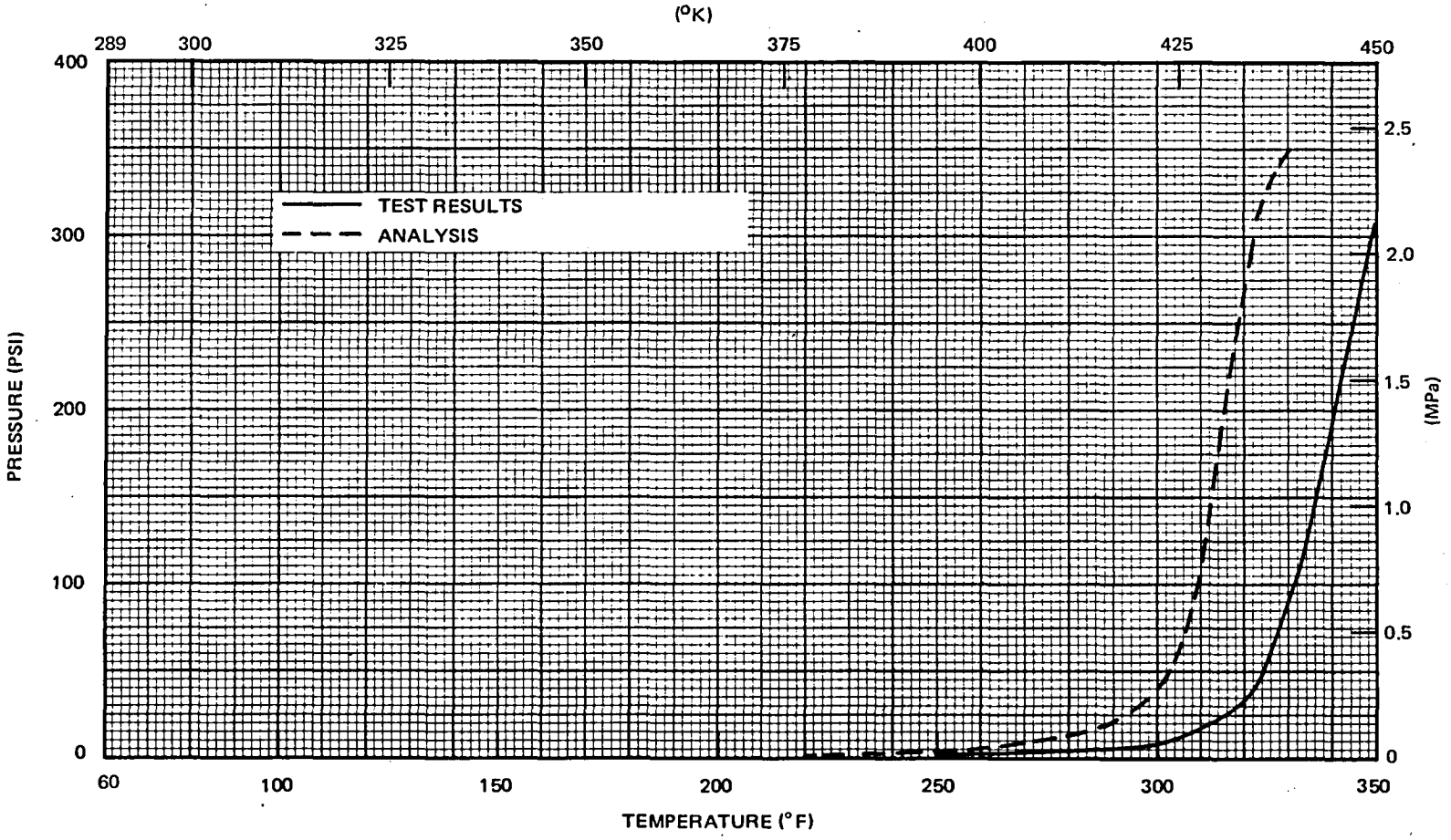

FIGURE K-7. TEST NO. 78 – PRESSURE VERSUS TEMPERATURE

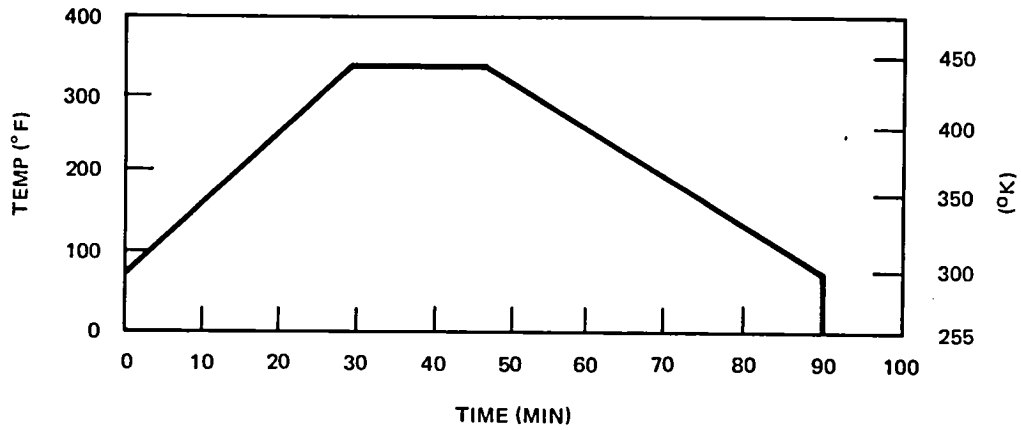

FIGURE K-8. TEMPERATURE – TIME CYCLE: RUBBER CASTING NO. 37S

TABLE K-3
PRESSURE VERSUS TEMPERATURE TESTS
DURING CYCLING OF CASTING NO. 37S

TEMP-PRESSURE CYCLE NO.	TEST NO.
1	78
6	81
13	86
21	90
43	95

Pressure Versus Temperature Test No. 89

The volume gap between the rubber specimen and the enclosing aluminum ring at room temperature for this test was designed to be similar to the volume gap for test No. 78. The purpose of this was to demonstrate whether or not rubber tended to expand as a volume. Although the two volume gaps were similar in quantity, they were different in shape. The volume gap for test No. 89 was on top only while the volume gap for test No. 78 was on the sides and top. A review of the comparison of the test results indicates that this rubber expanded as a volume (See Figure K-10).

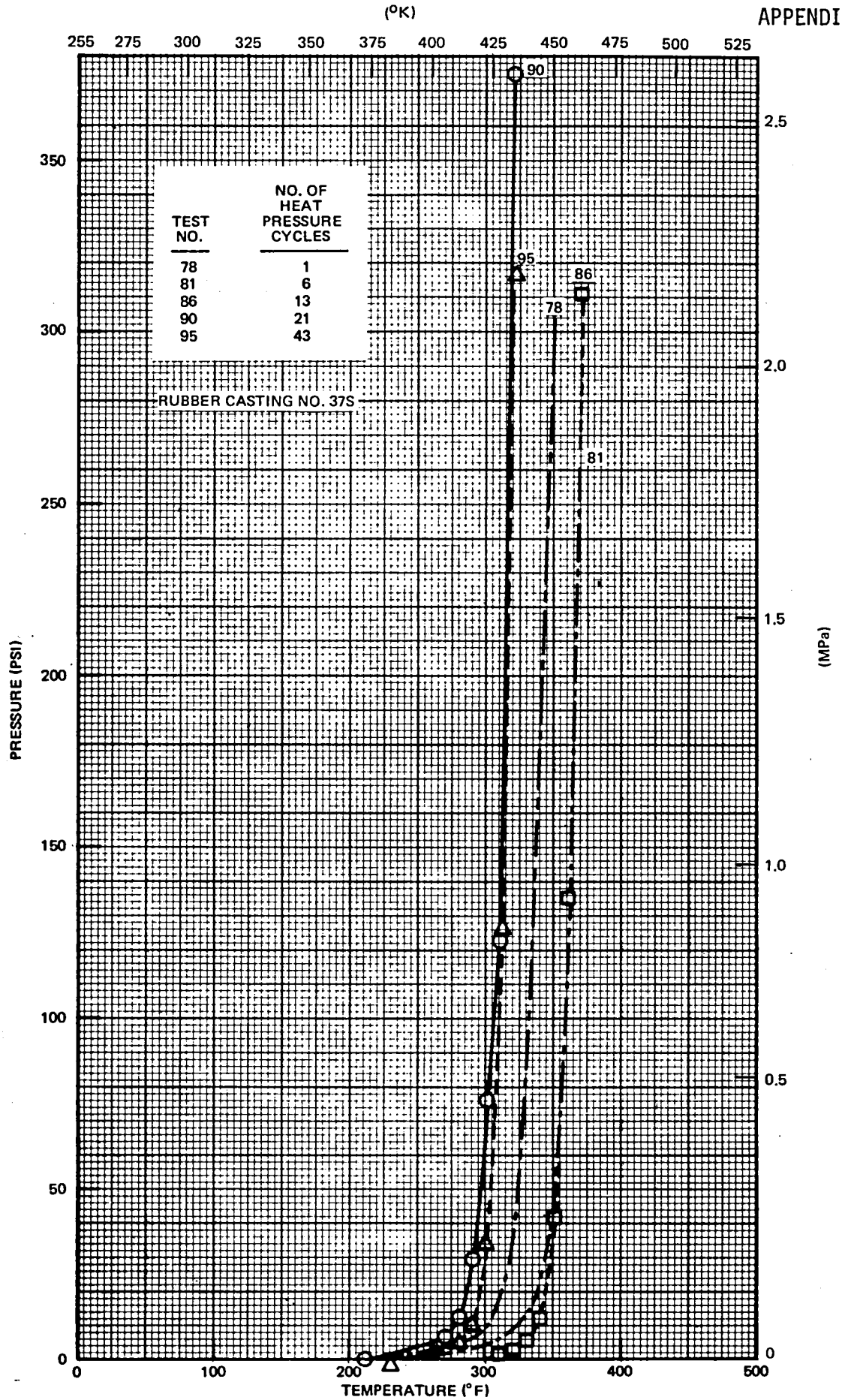

FIGURE K-9. TESTS 78, 81, 86, 90, AND 95 – PRESSURE VERSUS TEMPERATURE TEST RESULTS AFTER HEAT AND PRESSURE CYCLING

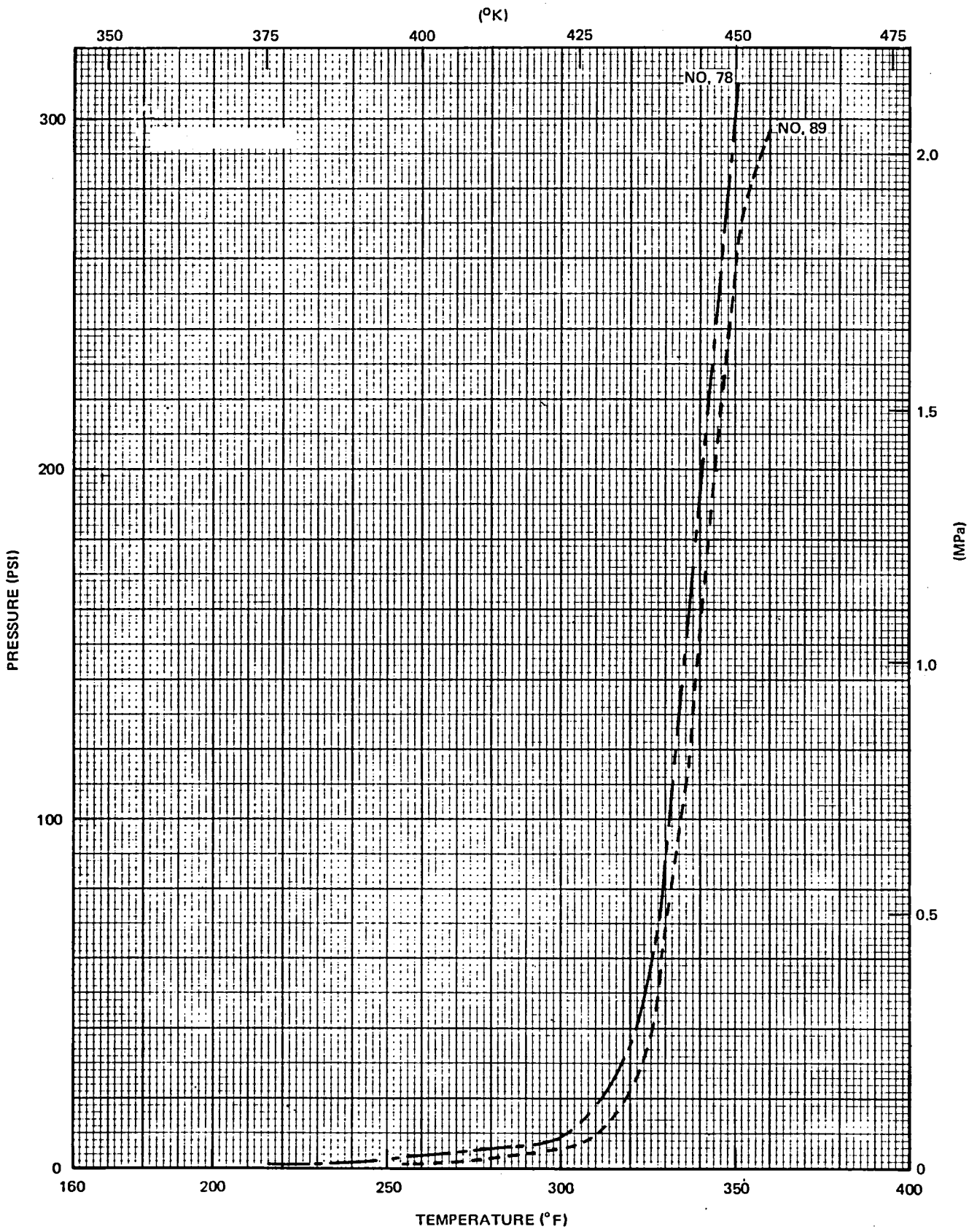

FIGURE K-10. TESTS NO. 89 AND 78 – PRESSURE VERSUS TEMPERATURE COMPARISON

APPENDIX L
DESIRED GAP BETWEEN RUBBER MANDRELS AND GR/EP LAYUP INSIDE THE PLM

This appendix presents the results of calculations to determine internal rubber pressure for various rubber gaps. The rubber pressures were computed for various rubber gaps at the gel temperatures derived in Appendix H. Sample calculations for the rib bay between ribs at Z_{AR} = 419.26 and 424.94 are given; calculations for other rib bays are similar. The basic theory is extracted from Reference 3 and the rubber characteristics used were taken from Appendices F and J.

In general it is desirable that the pressure, produced by the rubber mandrels during a cure cycle, range from 0.689 MPa (100 psi) at gel temperature to 2.068 MPa (300 psi) at cure temperature. With this in mind, Figures L-6 and L-7 were constructed from the calculations made herein to show the distribution of desired rubber gaps across the whole span of the rudder. Figures L-6 and L-7 are estimates produced for a cure cycle based on a 505^{o}K (450^{o}F) oven temperature setting and a 533^{o}K (500^{o}F) oven temperature setting, respectively. The use of the 533^{o}K (500^{o}F) oven during the heat up portion of the cure cycle results in a higher rudder temperature and pressure when gel occurs.

Figures L-6 and L-7 were developed from analyses carried out for three rudder bays:

Z_{AR} = 419.26 - 424.94

Z_{AR} = 461.70 - 466.77

Z_{AR} = 550.88 - 555.47

Only the calculations for rudder bay Z_{AR} = 419.26 - 424.94 are shown.

The basic geometric properties of the rib bay needed for the calculations are:

1. The rudder bay volume and the rudder bay outer surface area bonded by the outer surface of the skins, ribs, front and rear spar webs (Figure L-1).

TABLE L-1
RUBBER PRESSURE VERSUS RUBBER GAP –
RUDDER BAY Z_{AR} = 419.26-424.94

RUBBER GAP (cm)	RUBBER PRESSURE (MPa)	
	GEL TEMP $T_2 = 422.1^oK$	CURE TEMP $T_2 = 450^oK$
0.0508	0.593	1.241
0.0381	0.965	1.689
0.0254	1.372	1.999
REF PAGES		

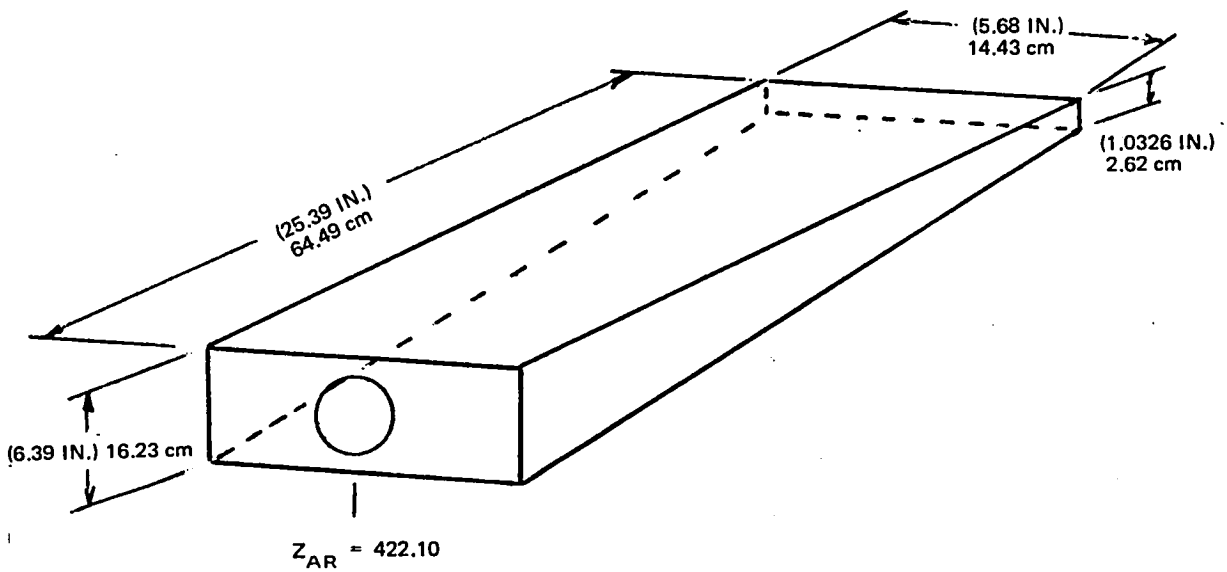

FIGURE L-1. RIB BAY, MOLD CAVITY GEOMETRY (Z_{AR} = 419.26-424.94)

2. The rudder bay graphite/epoxy structure volume.

3. The graphite/epoxy inner surface area.

4. The metal mandrel volume comprising the heater spikes and the breakaway metal mandrels (Figure L-2).

The calculations were carried out by a trial and error method due to the fact that the deflection of the molding tool side plates exerts a very substantial influence on the value of the internal rubber pressure. The steps

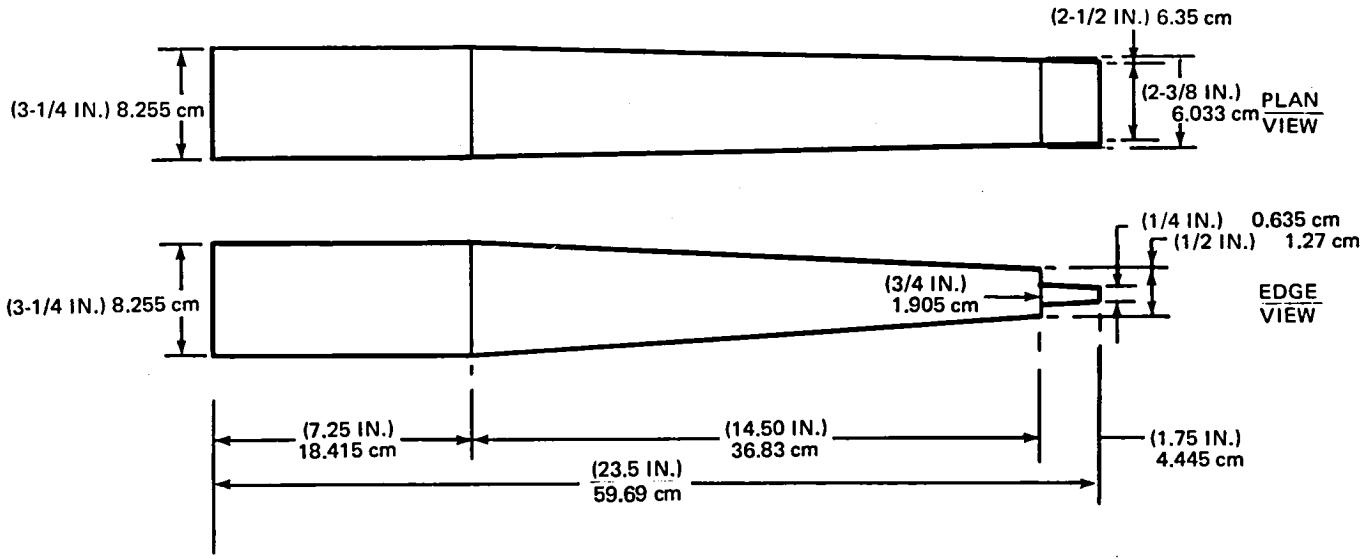

FIGURE L-2. METAL MANDREL GEOMETRY (Z_{AR} = 419.26 TO 424.94)

in the calculation of rubber pressure for rubber temperature T_2 and a rubber gap t were as follows:

1. Compute $\Delta T = T_2\ (^oK) - T_1\ (^oK)$

   where T_1 = room temperature

2. Compute V_1^R = volume of rubber mandrel at T_1

3. Compute V_2^R = volume of freely expanded rubber at T_2

4. Compute ΔV_c^R = compressed volume of freely expanded rubber

   $= V_2^R$ + metal mandrel volume at T_2

   + graphite/epoxy structure volume

   - rudder bay volume at T_2

5. Assume a value for the rubber pressure. Adjust the value for ΔV_c^R for the effects of tool plate deflection given in Table N-1.

6. Compute the bulk strain = $\Delta V_c^R / V_2^R$.

7. Read the rubber pressure P_1 (MPa) from the bulk modulus curve in Figure J-13.

8. Using the rubber pressure value P_1, readjust the value for ΔV_c^R for the effects of tool plate deflection as in Step 5.

9. Repeat Step 6.

10. Repeat Step 7 to obtain the rubber pressure P.

11. Repeat Steps 8, 9, and 10, n times (where n = 1, 2, $-\infty$) until P(n) = P(n-1).

Bay Volume at RT = $14.43\left(\frac{16.23 + 2.62}{2}\right)64.49$

= 8771.96 cm^3

Volume at 422^oK = 8771.96 (1 + 37.8 x 10^{-6} x 125.0) = 8813.41 cu cm

Volume at 450^oK = 8771.96 (1 + 37.8 x 10^{-6} x 152.8) = 8822.61 cu cm

Volume at 433^oK = 8771.96 (1 + 37.8 x 10^{-6} x 136.1) = 8816.76 cu cm

Volume at 446^oK = 8771.96 (1 + 37.8 x 10^{-6} x 148.9) = 8821.33 cu cm

Bay Surface Area (RIB BAY Z_{AR} = 419.26 - 424.94)

Right Skin = 930.417 sq cm

Left Skin = 930.417 sq cm

Lower Rib = 608.018 sq cm

Upper Rib = 608.018 sq cm

F/S Face = 234.200 sq cm

R/S Face = 37.839 sq cm

TOTAL 3348.903 sq cm

GR/EP Structure (RIB BAY Z_{AR} = 419.26 - 424.94)

Skin t = 6 x 0.0152 = 0.0914 cm

F/S Cap CSA = 0.762 x 1 x 0.0343 + 0.762 (2 x 0.0343 + 0.0152)

+ 0.762 (2 x 0.0343 + 4 x 0.0152)

= 0.0265 + 0.0639 + 0.0987 = 0.1890 sq cm

F/S Cap Reinforcement

CSA = 1.016 x 2 x 0.0152 + 1.016 x 4 x 0.0152 + 0.762 (4 x 0.0152 + 1 x 0.0343)

= 0.0310 + 0.0619 + 0.0723

= 0.1652 cm^2

Rib Cap

CSA = 1.905 [0.0152 + 0.0343] + 1.27 x 0.0152

= 0.0942 + 0.0194 = 0.1136 sq cm

R/S Cap and Web

CSA = 2 [0.762 x 0.0152 x 2 + 0.508 x 4 x 0.0152 + 0.4445 x 4 x 0.0152]

+ 0.4445 x 2 x 0.0152) +(2.623 - 2 x 0.0914) 0.19050

= 2 [0.0232 + 0.0310 + 0.0271 + 0.0136] + 0.0465

= 2 [0.0948] + 0.4645 = 0.654 sq cm

F/S Web

CSA = 0.381 x [16.233 - (10 x 0.0152 + 0.0343) 2] = 6.0426 sq cm

GR/EP Structure Volume (RIB BAY Z_{AR} = 419.26 - 424.94)

Left Skin Vol = 930.417 x 0.0914 + 0.1652 x 14.43 + 2 x 0.1135 x 64.49

= 85.0816 + 2.3761 + 14.6500 = 102.1077 cu cm

Right Skin Vol = = 102.1077 cu cm

Lower Skin Vol = 608.0181 [0.0152 + 0.0343] = 30.1194 cu cm

Upper Rib Vol = 30.1194 cu cm

Rear Spar Cap + Web Vol = 14.43 x 0.6542 = 1.463 cu cm

F/S Web Vol = 14.43 x 6.0426 = 87.1792 cu cm

Total Volume = 2 [102.1077 + 30.1194] + 1.463 + 87.1792

= 361.073 cu cm

$A_{V_G} t = \frac{361.073}{3348.903} = 0.1078$ cm

Rib Bay (Z_{AR} = 419.26 - 424.94)

GR/EP Structure Inner Surface Area (RIB BAY Z_{AR} = 419.26 - 424.94)

Right Skin = 14.275 x 64.341 = 918.450

Left Skin = = 918.450

Lower Rib = 1/2 (16.0807 + 2.470) 64.338 = 596.773

Upper Rib = 596.773

F/S Face = 14.275 x 16.0807 = 229.548

R/S Face = 14.275 x 2.470 = 35.264

Total =3295.258 sq cm

RT Mandrel Volume = $(8.255)^2$ x 18.415 + 1/2 [8.255 + 6.35 x 1.905] 36.83

+ 1/2 [6.35 x 1.27 + 6.033 x 0.635] 4.445

= 1254.888 + 1477.653 + 26.4323 = 2758.973 cu cm

(422.1^oK) Vol = 2758.973 [1 + 70.2 x 10^{-6} x 125.0] = 2783.177 cu cm

(449.9^oK) Vol = 2758.973 [1 + 70.2 x 10^{-6} x 152.8] = 2788.568 cu cm

(433.2^oK) Vol = 2758.973 [1 + 70.2 x 10^{-6} x 136.1] = 2785.340 cu cm

(446.0^oK) Vol = 2758.973 [1 + 70.2 x 10^{-6} x 148.9] = 2787.814 cu cm

Rib Bay (Z_{AR} = 419.26 - 424.94)

$T_2 = 422^oK$

Rubber Undersize t = 0.0508 cm (RIB BAY Z_{AR} = 419.26 - 424.94)

$\Delta T = 422^o - 297^o = 125^oK$

α_C^R = 540 x 10^{-6} $cm^3/cm^3/^oK$ (Page 53) (Approx)

V_1^R = 8771.955 - [273.893 + 2758.973 + 3295.255 x 0.0508] = 5571.695 cm^3

V_2^R = 5571.695 [1 + 540 x 10^{-6} x 125.0] = 5947.778 cu cm

ΔV_c^R = 5947.778 + 2783.177 + 273.893* - 8813.418 = 191.450 cu cm

$\Delta V_c^R / V_2^R$ = 191.450/5947.778 = 0.0322

P_2 = Large (Figure J-12)

Taking into account the associated deflection of the tool, assume rubber pressure. P_2 = 0.862 MPa

$\Delta V_c^R = 191.450 - \frac{0.862}{6.894} \times 702.677 = 103.615$ cu cm (Table N-1)

$\Delta V_c^R / V_2^R$ = 103.615/5947.778 = 0.0174

P_2 = 0.152 MPa

Assume rubber pressure P_2 = 0.600 MPa

$\Delta V_c^R = 191.450 - \frac{0.600}{6.894} \times 702.677 = 130.310$ cu cm

$\Delta V_c^R / V_2^R = 130.310/5947.778 = 0.0219$

P_2 = 0.593 MPa (Figure J12)

*GR/EP structure volume = 361.073 - 87.179 = 273.893 cu cm
(F/S is the aft face of the F/S web)

Rib Bay (Z_{AR} = 419.26 - 424.94)

$T_2 = 422^oK$

Rubber Undersize t = 0.0381 cm (RIB BAY Z_{AR} = 419.26 - 424.94)

$\Delta T = 422 - 297 = 125^oK$

$\alpha_c^R = 540 \times 10^{-6}$ cu cm/cu cm/^oK (Page 53) (Approx)

$V_1^R = 8771.955 - [273.893 + 2758.973 + 3295.255 \times 0.0381] = 5613.548$ cm^3

$V_2^R = 5613.548 [1 + 540 \times 10^{-6} \times 125] = 5992.466$ cm^3

$\Delta V_c^R = 5992.466 + 2783.177 + 273.893 - 8813.418 = 236.137$ cu cm

$\Delta V_c^R = 236.137/5992.466 = 0.0394$

P_2 = Large

Taking into account the associated deflection of tool assume rubber pressure

P_2 = 0.965 MPa

$\Delta V_c^R = 14.410 - \frac{0.965}{6.894} \times 702.677 = 137.766$ cm^3 (Ref Table N-1)

$\Delta V_c^R / V_2^R = 137.766/5992.466 = 0.0230$

P_2 = 0.965 MPa (Figure J-12)

Rib Bay (Z_{AR} = 419.26 = 424.94)

$T_2 = 422^{o}K$

Rubber Undersize t = 0.0254 (RIB BAY Z_{AR} = 419.26 - 424.94)

ΔT = 422 - 297 = $125^{o}K$

α_c^R = 540 x 10^{-6} cu cm/cu cm/^{o}K (Page 53) (Approx)

V_1^R = 8771.955 - [273.893 + 2758.973 + 3295.255 x 0.0254] = 5654.985 cu cm
= 5654.958 cu cm

V_2^R = 5654.958 (1 + 540 x 10^{-6} x 125) = 6036.661 cu cm

ΔV_c^R = 6036.661 + 2783.176 + 273.893 - 8813.41 = 280.333 cu cm

Taking tool deflection into account assume rubber pressure P_2 = 1.337 MPa

$\Delta V_c^R = 280.333 - \frac{1.337}{6.894} \times 702.677 = 144.009$ cu cm (Table N-1)

$\Delta V_c^R / V_2^R$ = 144.009/6036.661 = 0.0239

P_2 = 1.372 MPa (Figure J-12)

$T_2 = 450^{o}K$

Rubber Undersize t = 0.0508 cm (RIB BAY Z_{AR} = 419.26 - 424.94)

ΔT = 450 - 297 = $153^{o}K$

α_c^R = 540 x 10^{-6} cu cm/cu cm/^{o}K (Page 53) (Approx)

V_1^R = 5571.695 cu cm (Page 191)

V_2^R = 5571.695 (1 + 540 x 10^{-6} x 153) = 6031.352 cu cm

ΔV_c^R = 6031.352 + 2788.568 + 273.893 - 8822.607 = 271.206 cu cm

Taking Tool Deflection into account assume Rubber Pressure P_2 = 1.269 MPa

ΔV_c^R = 271.206 - 1.269/6.894 x 702.677 = 141.912 cu cm (Table N-1)

$\Delta V_c^R / V_2^R$ = 141.912/6031.352 = 0.0235

P_2 = 1.249 MPa (Figure J-12)

Rubber Undersize t = 0.0381 (RIB BAY Z_{AR} = 419.26 - 424.94)

V_1^R = 5613.548 cu cm (Page 192)

V_2^R = 5613.548 (1 + 540 x 10^{-6} x 153) = 6076.662 cu cm

ΔV_c^R = 6076.662 + 2788.568 + 273.893 - 8822.607 = 316.516 cu cm

Taking Tool Deflection into account assume Rubber Pressure P_2 = 1.648 MPa

ΔV_c^R = 316.516 - 1.648/6.894 x 702.677 = 148.58 cu cm (Table N-1)

$\Delta V_c^R / V_2^R$ = 148.581/6076.662 = 0.02445

P_2 = 1.689 MPa (Figure J-12)

Rib Bay (Z_{AR} = 419.26 - 424.94)

T_2 = 450°K (cont'd)

Rubber Undersize t = 0.0254 cm (RIB BAY Z_{AR} = 419.26 - 424.94)

V_1^R = 5654.958 cu cm (Page 193)

V_2^R = 5654.958 (1 + 540 x 10^{-6} x 153) = 6121.497 cu cm

ΔV_c^R = 5654.958 + 2788.568 + 273.893 - 8822.607 = 361.35 cu cm

Taking Tool Deflection into account assume rubber pressure P_2 = 2.034 MPa

ΔV_c^R = 361.351 - 2.034/6.894 x 702.677 = 154.055 cu cm (Table N-1)

$\Delta V_c^R / V_2^R$ = 154.055/5654.958 = 0.0252

P_2 = 2.000 MPa (Figure J-12)

	TEMP (°K)	RUBBER GAP (cm)	PRESSURE (MPa)	REF PAGE
505°K OVEN	422 (GEL TEMP)	0.0508	0.593	192
		0.0381	0.965	192
		0.0254	1.379	193
	450 (CURE TEMP)	0.0508	1.241	194
		0.0381	1.689	194
		0.0254	2.000	195
REF	TABLE H-3			

ACCEPTABLE PRESSURES AND CORRESPONDING GAPS	
GAP	0.0254→0.0508 cm
GEL PRESSURE	1.379 →0.586 MPa
CURE PRESSURE	2.000 →1.241 MPa

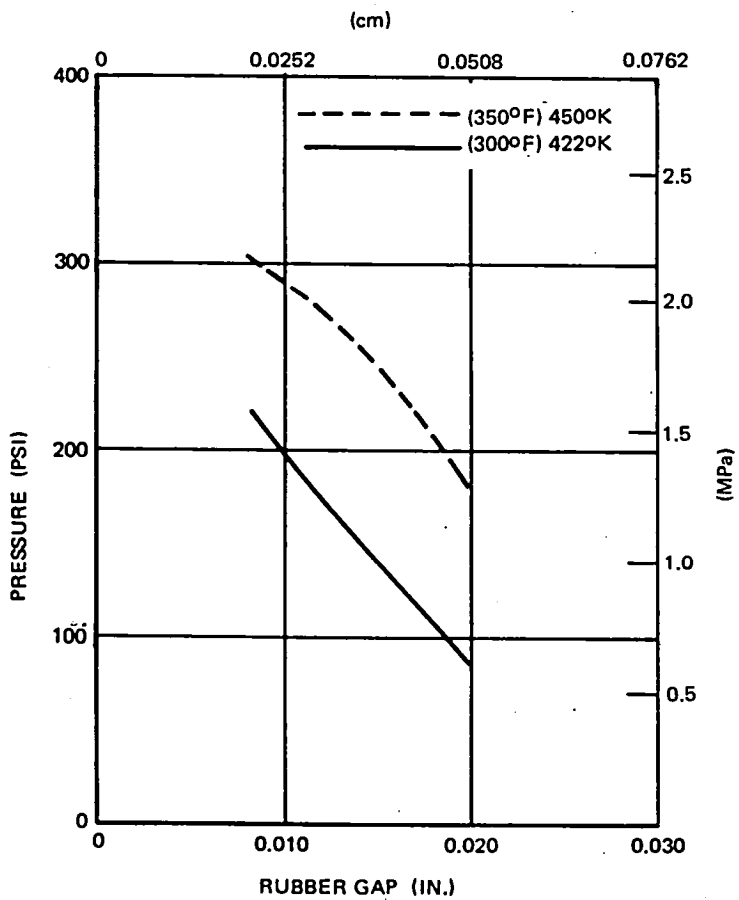

FIGURE L-3. PRESSURE VERSUS RUBBER GAP (Z_{AR} = 419.26 → 424.94)

	TEMP (°K)	RUBBER GAP (cm)	PRESSURE (MPa)
505°K OVEN	428 (GEL TEMP)	0.0635	0.379
		0.0508	0.862
		0.0381	1.351
	450 (CURE TEMP)	0.0635	1.000
		0.0508	1.517
		0.0381	2.027
REF	(TABLE) H-3		

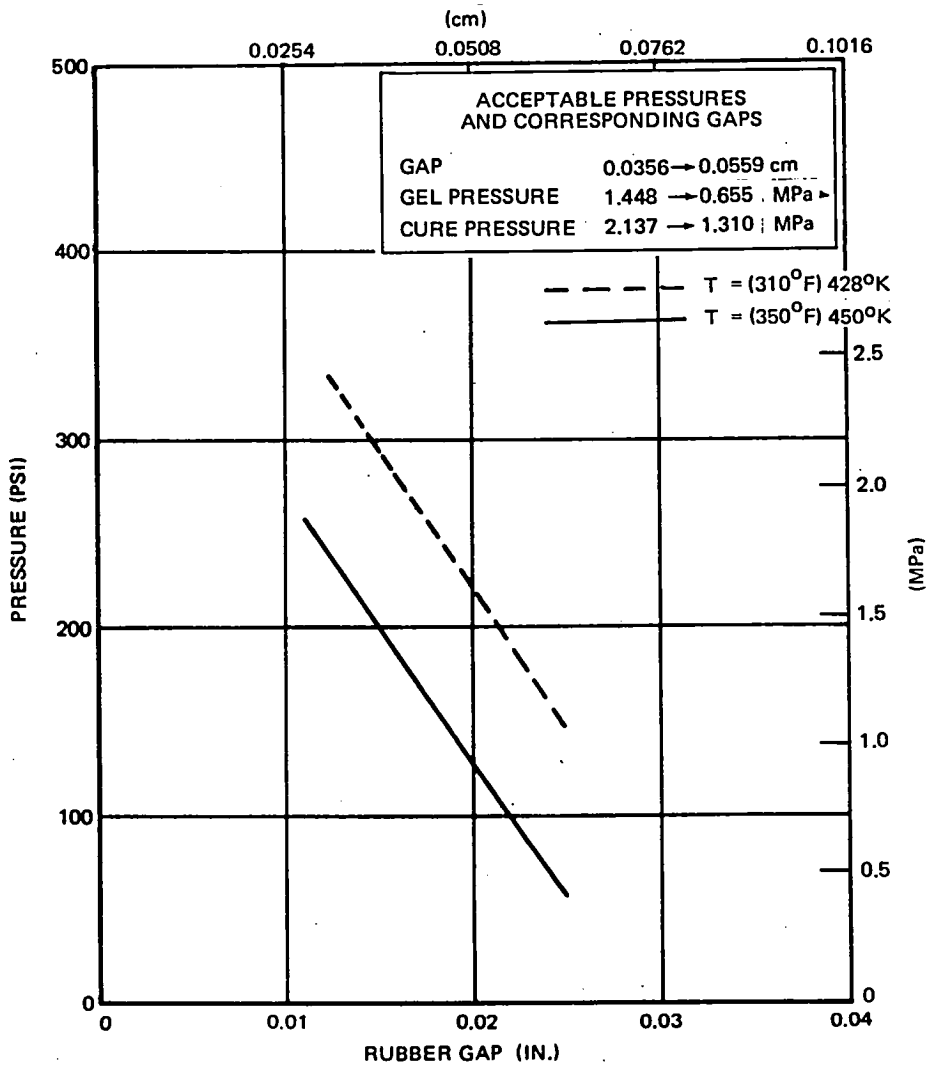

FIGURE L-4. PRESSURE VERSUS RUBBER GAP (Z_{AR} = 461.70 → 466.77)

	TEMP (°K)	RUBBER GAP (cm)	PRESSURE (MPa)
505°K OVEN	433 (GEL TEMP)	0.0635	0.083
		0.0508	0.758
		0.0381	1.896
	450 (CURE TEMP)	0.0635	0.538
		0.0508	1.627
		0.0381	2.551
REF	TABLE H-3		

ACCEPTABLE PRESSURES AND CORRESPONDING GAPS	
GAP	0.0432 → 0.0533 cm
GEL PRESSURE	1.379 → 0.620 MPa
CURE PRESSURE	2.172 → 1.413 MPa

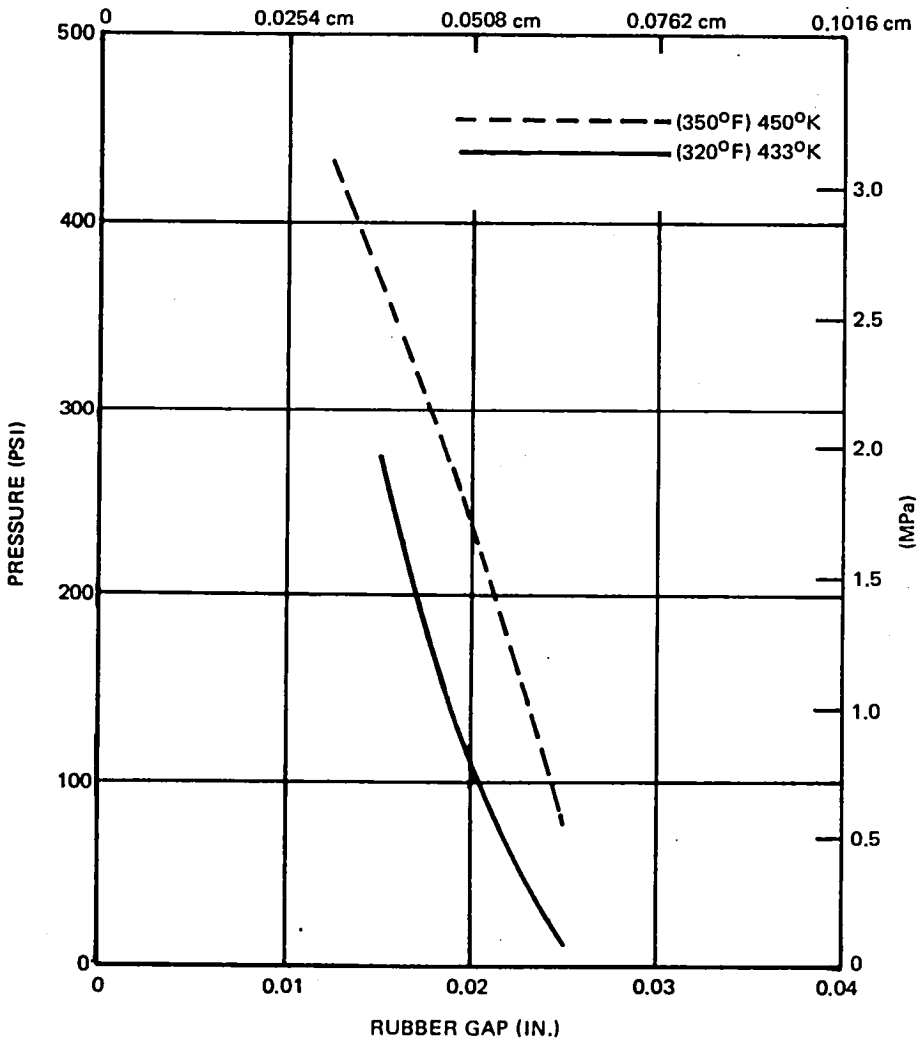

FIGURE L-5. PRESSURE VERSUS RUBBER GAP (Z_{AR} = 550.88 → 555.47)

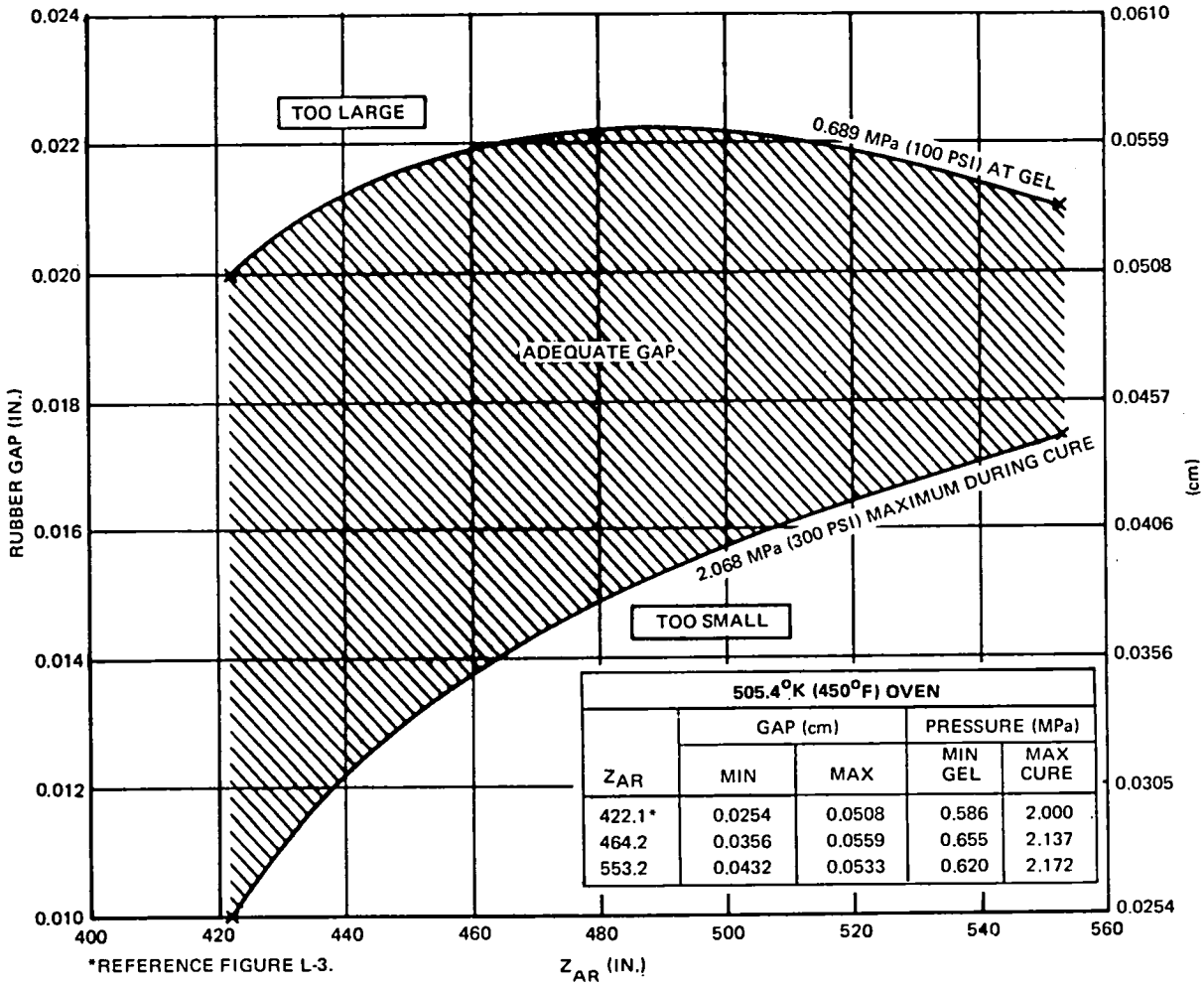

505.4°K (450°F) OVEN

Z_{AR}	GAP (cm) MIN	GAP (cm) MAX	PRESSURE (MPa) MIN GEL	PRESSURE (MPa) MAX CURE
422.1*	0.0254	0.0508	0.586	2.000
464.2	0.0356	0.0559	0.655	2.137
553.2	0.0432	0.0533	0.620	2.172

*REFERENCE FIGURE L-3.

FIGURE L-6. RUBBER GAP 505°K (450°F OVEN)

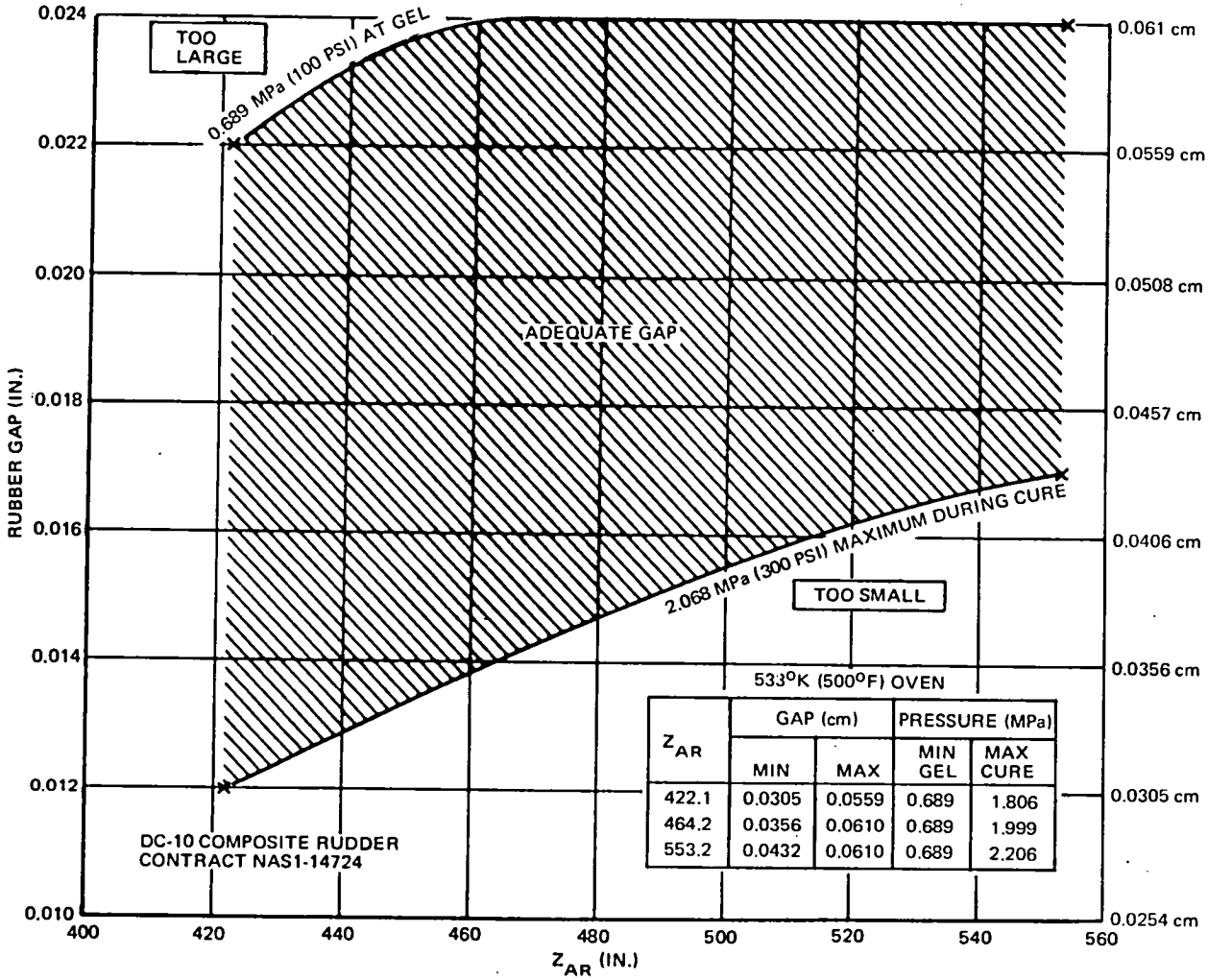

Z_{AR}	GAP (cm)		PRESSURE (MPa)	
	MIN	MAX	MIN GEL	MAX CURE
422.1	0.0305	0.0559	0.689	1.806
464.2	0.0356	0.0610	0.689	1.999
553.2	0.0432	0.0610	0.689	2.206

FIGURE L-7. RUBBER GAP 533°K (500°F OVEN)

APPENDIX M
FRONT SPAR WEB REDESIGN

In order to avoid a repeat of the front spar damage, due to tool spring back, such as occurred during the cure of the first test rudder (Reference Table 14), it was decided to reinforce the front spar web. It was anticipated that the rubber mandrel gap size would be designed to limit the rubber pressure to a maximum of 2.068 MPa (300 psi) during the next rudder cures. Therefore, the analysis described in this appendix was undertaken to size the front spar web reinforcement in order to permit it to support the tool spring back which results from 2.068 MPa (300 psi) of internal rubber pressure. Figure M-1 shows the distribution of unidirectional reinforcing plies.

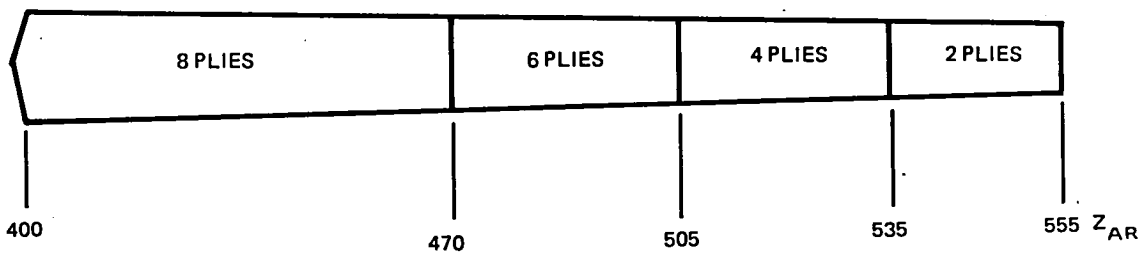

FIGURE M-1. FRONT SPAR REINFORCING PLIES

The layup location of the front spar web reinforcing plies (Layers A, B, C and D) is shown in Figure M-2. In order to strengthen the front spar web in the vicinity of the flange, reinforcing layers A and C were extended up into the flange 1.27 cm (0.50 inch) and 0.635 cm (0.25 inch), respectively. The distribution of reinforcing plies in Figure M-1 is obtained by dropping the D layers at Z_{AR} = 470, the C layers at Z_{AR} = 505, and the B layers at Z_{AR} = 535.

The relationship between the compressive strength of the front spar web and the spring back load of the PLM side plates at three critical sections of the front spar is shown in Figures M-4, M-5 and M-6. In these figures, the spring back load in the PLM side plates reduces as the deflection of the side plates reduces but the load on the front spar web increases at the same time. Equilibrium occurs when the side plates load line intersects the F/S web load line. The deflection of the F/S web when equilibrium is reached is compared with the allowable deformation of the F/S web to obtain a margin of safety.

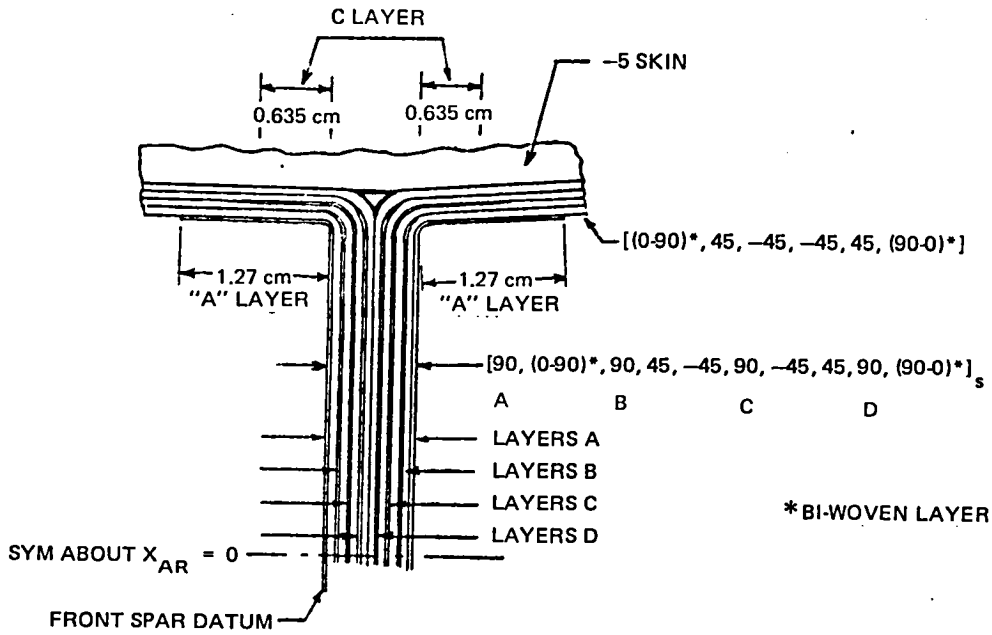

FIGURE M-2. REINFORCING PLIES LAY-UP, FRONT SPAR WEB

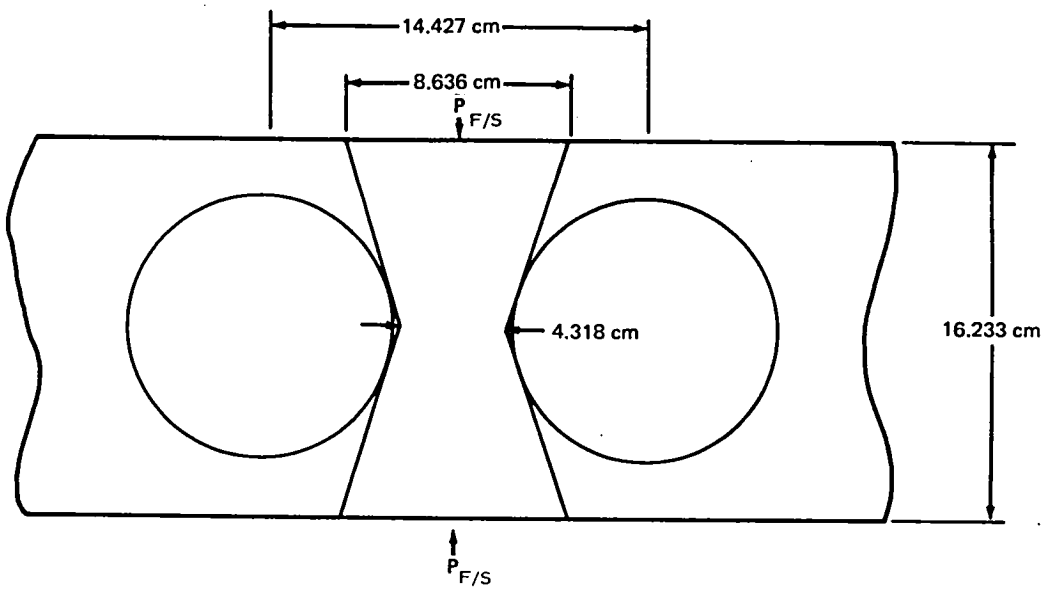

FIGURE M-3. FRONT SPAR WEB GEOMETRY, Z_{AR} = 419.26 → 424.94

	$P_{F/S}$* (kN)	$Y_{F/S}$ (cm)
(3 BEAM) HINGE + OVERHANG	217.3	0.1044
FIXED ENDS	238.0	0.0691
AVERAGE	227.7	0.0689

$$MS = \frac{0.0488^{(1)}}{0.0416} - 1 = +0.17$$

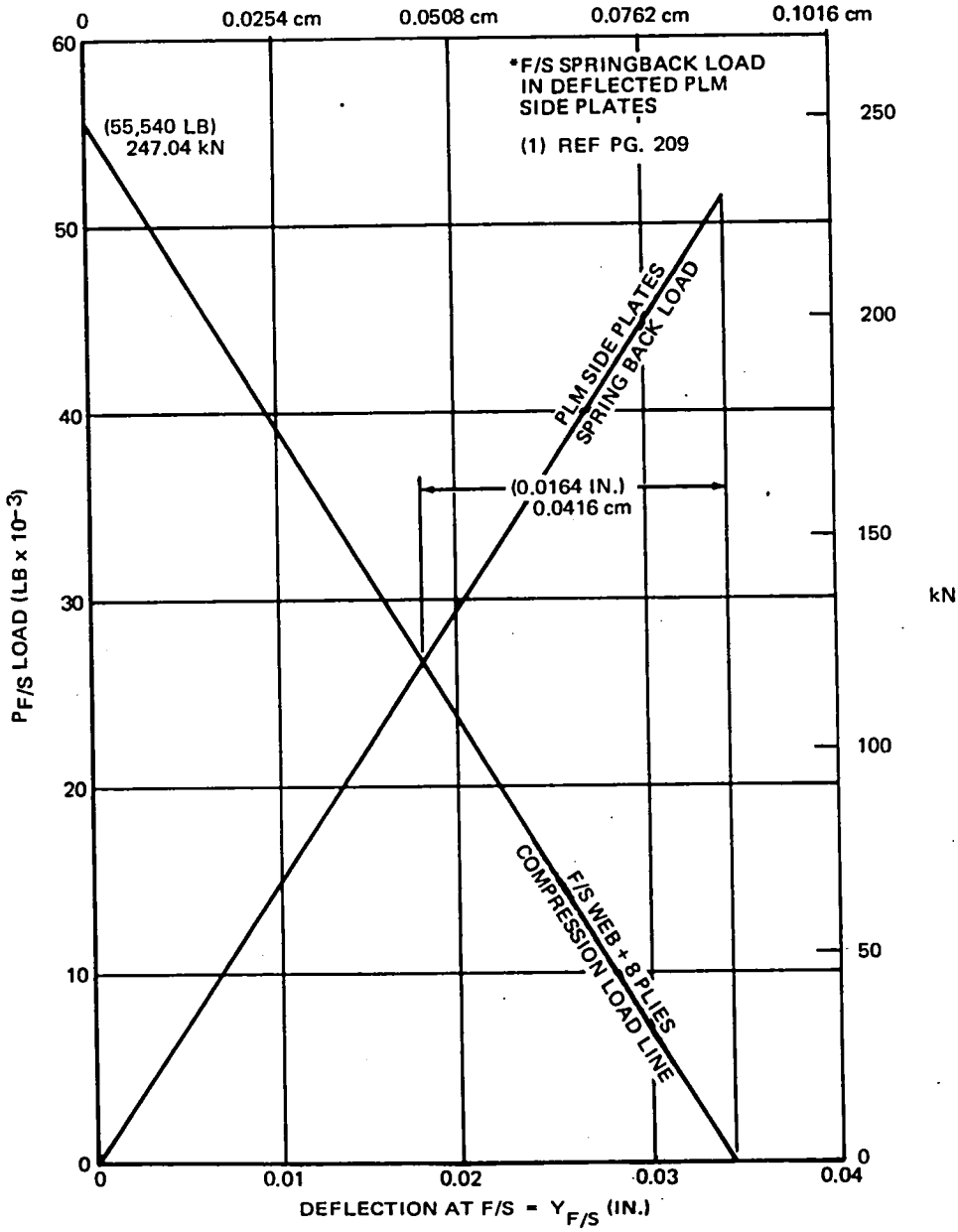

FIGURE M-4. F/S LOAD VERSUS DEFLECTION DURING COOLDOWN (Z_{AR} = 419.26 → 424.94) (AVERAGE SUPPORT)

	$P_{F/S}$* (kN)	$Y_{F/S}$ (cm)
(3 BEAM) HINGE + OVERHANG	178.9	0.0851
FIXED ENDS	186.2	0.0579
AVERAGE	189.2	0.0716

$$MS = \frac{0.0429}{0.0376} - 1 = +0.14$$

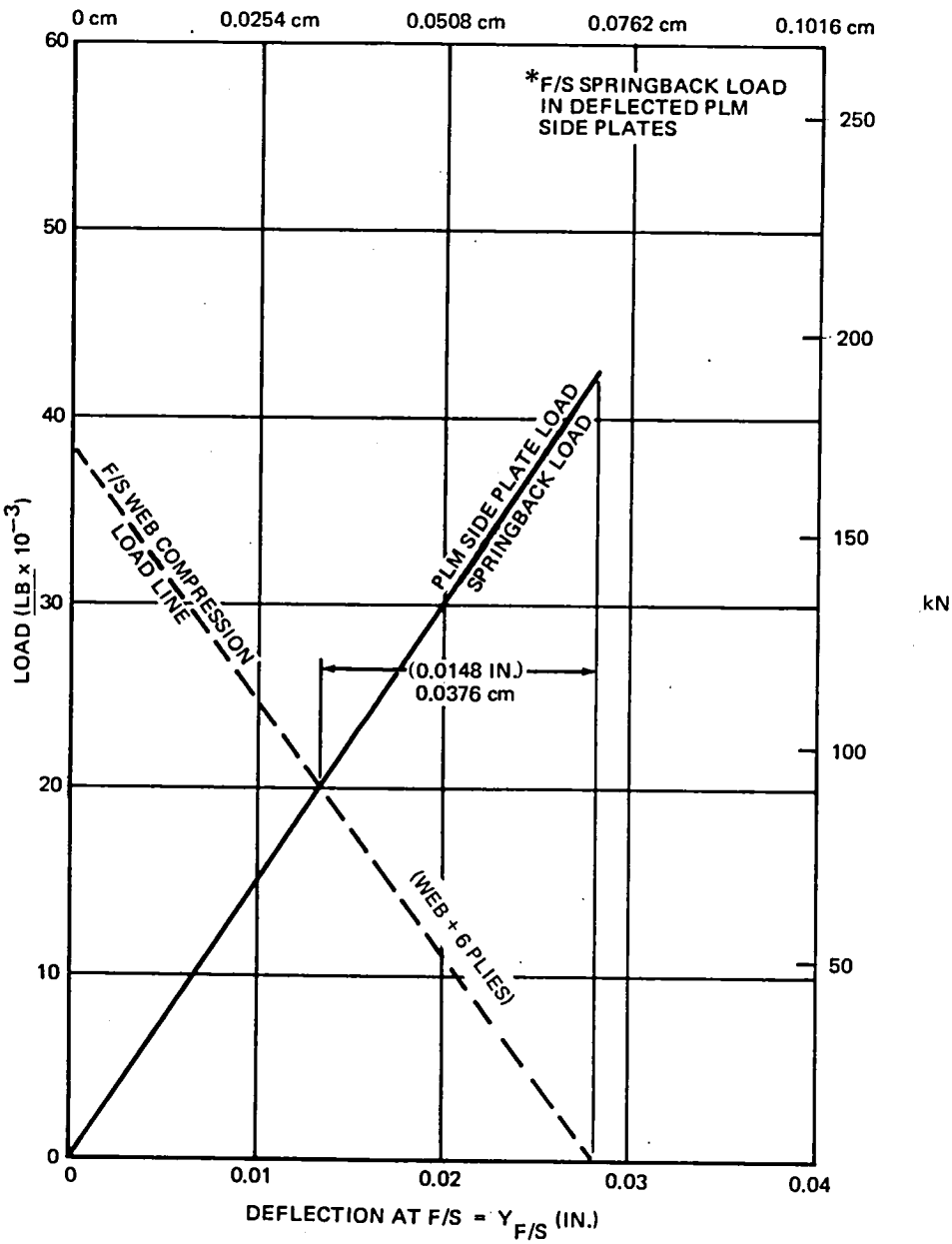

FIGURE M-5. F/S LOAD VERSUS DEFLECTION DURING COOLDOWN (Z_{AR} = 461.70 → 466.70) AVERAGE SUPPORT

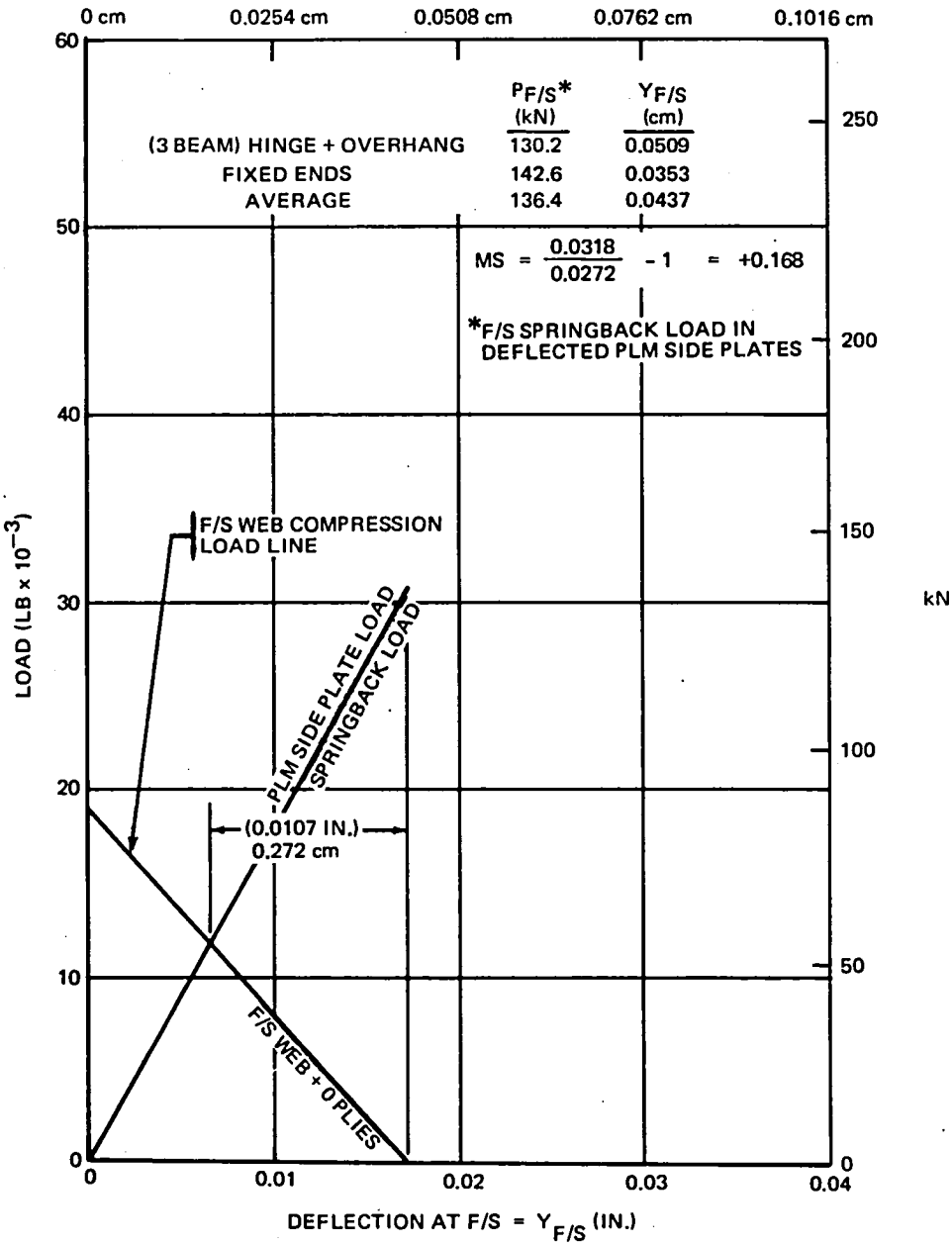

FIGURE M-6. F/S LOAD VERSUS DEFLECTION DURING COOLDOWN (Z_{AR} = 550.88 → 555.47) (AVERAGE SUPPORT)

The actual computations to show adequate strength for one critical front spar bay (Z_{AR} = 419.24 to 424.94) are shown on Pages 209 to 209. Basically, the assumption is made that only the front spar web absorbs all the tool spring back crushing forces. This is a conservative assumption since the ribs will actually assist the front spar. A description of the steps in the calculation is as follows:

1. Estimate the maximum rubber pressure (approximately 2.068 MPa (300 psi)).

2. For the Three-Beam Assumption (Appendix E), estimate the maximum deflection of a PLM side plate at the front spar location due to the maximum rubber pressure and thermal expansion.

3. Calculate the maximum crushing load exerted on the front spar web due to tool cool down to room temperature.

4. Repeat Steps 2 and 3 for the Fixed End Condition assumption (Appendix E).

5. Obtain the average maximum deflection of the PLM side plate and the average maximum crushing load on the front spar for the average end fixity.

6. Estimate the value for Young's Modulus and the average front spar web cross sectional area per rib bay.

7. Calculate the load versus strain data for the front spar web.

8. Plot a load versus deflection line for the PLM side plates at the front spar location.

   Plot a force versus strain line for the front spar web.

   The intersection point is where equilibrium is reached.

9. Calculate the front spar web margin of safety by comparing the equilibrium deformation with the permissible front spar web deformation.

The margins of safety for the reinforced front spar web at three front spar stations, due to the molding tool spring back loads, are given in Figures M-4, M-5 and M-6.

Maximum Rubber Pressure During Rudder Cure Cycle

Rudder Station Z_{AR} = 419.26 - 424.94

Assume Rubber Gap = 0.0381 ± 0.0127 cm (0.015 ± 0.005 in.)

Maximum Temperature = 450°K (350°F)

Maximum Rubber Pressure = 2.00 MPa (290 psi) (Figure L-3)

Front Spar Spring Back Force (Z_{AR} = 419.26 - 424.94)

1. Three Beam Assumption

$Y_{F/S}$ = Molding Tool Side Plate deflection at front spar

Due to Rubber Pressure

6.894 MPa (1000 psi) $Y_{F/S} = 0.2415 + \frac{0.1285}{2}$ (Table N-1)

$= 0.3058$ cm

2.00 MPa (290 psi) $Y_{F/S} = 0.3058 \times \frac{2.00}{6.894} = 0.0886$ cm

Due to Thermal Contraction

$$Y^{(1)}_{F/S} = 12.6 \times 10^{-6} \times 152 \times \frac{16.233}{2} = 0.0157 \text{ cm}$$

Total $Y_{F/S} = 0.0886 + 0.0157 = 0.1044$ cm

(Spring Back Force) $P_{F/S} = \frac{0.1044 \times 10^6}{0.480}$ (Table N-2)

$= 217.3$ kN (48,870 lb)

2. Fixed End Assumption

Due to Rubber Pressure

6.894 MPa (1000 psi) $Y_{F/S} = 0.1491 + \frac{0.0688}{2}$ (Table N-1)

$= 0.1836$ cm

2.00 MPa (290 psi) $Y_{F/S} = 0.1836 \times \frac{2.00}{6.894} = 0.0533$ cm

Total $Y_{F/S} = 0.0533 + 0.0157 = 0.0691$ cm

(Spring Back Force) $P_{F/S} = 0.0691 \times \frac{10^6}{0.290}$ (Table N-2)

$= 238.0$ kN (53,510 lb)

(1) Steel Coefficient of Thermal Expansion = 12.6×10^{-6} cm/cm/^{o}K (7×10^{-6} in./in./^{o}F)
ΔTemp = 450 - 297 = 153^{o}K (350 - 75 = 275^{o}F)
Spare Height = 16.233 cm (6.391 in.)
$Y_{F/S}$ = Tool steel side plate deflection at F/S location.

3. Average End Fixity

Total $Y_{F/S}$ = 1/2 (0.1044 + 0.0691) = 0.0869 cm

(Spring Back Force) $P_{F/S}$ = 1/2 (217,300 + 238,000)

= 227.7 kN (51,190 lb)

Permissible Strain in F/S Web

Maximum Permissible Strain = 8000 μm/m = ε_2

$$E_2 = \frac{P}{A_2 \varepsilon_2}$$

$$P = A_2 \ \varepsilon_2 \ E_2$$

$$\varepsilon_1 = \frac{P}{A_1 E_1}$$

$$= \frac{A_2 \ \varepsilon_2 \ E_2}{A_1 \ E_1}$$

$$= A_2/A_1 \ \varepsilon_2 \qquad \text{(since } E_1 = E_2\text{)}$$

Average Permissible Strain = 1/2 $(\varepsilon_2 + \varepsilon_1)$

$$= 1/2 \ (8000 + \frac{A_2}{A_1} 8000) \quad \mu m/m$$

$$= 8000 \left(\frac{A_1 + A_2}{2A_1}\right) \quad \mu m/m$$

Front Spar Web (Z_{AR} = 419.26 - 424.94)

GR/EP LAY-UP $[90, (0\text{-}90)^*, 90, 45, -45, 90, -45, 45, 90, (90\text{-}0)^*]_S$

Uni weave	t = 2 [8 x 0.0152]	0.244 cm
Bi weave	t = 2 [2 x 0.0343]	0.137 cm
		0.381 cm

$\pm 45^{o}$ plies	2 x 4 = 8	33.3 percent
90^{o} plies	2 x 6 = 12	50 percent
0^{o} plies	2 x 2 = 4	16.7 percent

$E_{(90^{o})}$ = 85,500 MPa (12.4 x 10^{6} psi)

Average width of effective compression material

= 1/2 [4.318 + 8.636] = 6.477 cm (Figure M-3)

Average C.S.A. = $6.477^{(1)}$ x 0.381 + $5.08^{(2)}$ x 0.0457 = 2.700 cm^{2}

Max F/S WEB LOAD (P) = $\frac{E\ A\ e}{\ell}$

$$= \frac{85{,}500 \times 2.700 \times 0.0869}{16.233/2} = 247.04 \text{ kN}$$

(1) 1/2 (8.636 + 4.318) = 6.477 cm (Figure M-3)

(2) Rib flange and rib web material

Permissible Deformation in Front Spar Web

Maximum Permissible Strain = 8000 μm/m.

Average Permissible Strain = $8000 \left(\frac{A_1 + A_2}{2A_1}\right)$ μm/m

$$= 8000 \left(\frac{8.636 + 4.318}{2 \times 8.636}\right)$$

= 6000 μm/m

Permissible F/S Web Deformation

$$= 6000 \times 10^{-6} \times \frac{16.233}{2} = \boxed{0.0488 \text{ cm}}$$

APPENDIX N
MOLD TOOL SIDE PLATE DEFLECTION AND TOOL VOLUME CHANGE

The calculation of rubber pressure during the composite rudder cure cycle requires an accurate estimate of the volume change in the molding tool during the cure cycle. This appendix consists of estimates of the molding tool volume change due to 6.894-MPa (1000-psi) rubber pressure in the following rudder bays:

$$Z_{AR} = 419.25 \rightarrow 424.94$$
$$Z_{AR} = 461.70 \rightarrow 466.77$$
$$Z_{AR} = 550.88 \rightarrow 555.47$$

The molding tool volume change under rubber pressure is due to the deflection of the side plates and the extension under pressure of the 2.54-cm (one-inch)-diameter bolts used to clamp the molding tool. The molding tool side plates are assumed to be divided into 2.54-cm (one-inch)-wide chordwise beams supported at the bolt lines. The beam-end conditions are assumed to be an average of the following support methods:

1. Three continuous beams on simple supports. (Appendix E)

2. Fixed-end supports. (Appendix E)

The summary of the results is given in Table N-1.

Molding tool springback produces crushing forces on the rudder during tool cooldown. The magnitude of the springback forces is related to the deflection of the molding tool side plates during the rudder cure cycle. The forces on the front spar resulting from molding tool side plate deflection are summarized for three rudder bays in Table N-2. These values are based on the conservative assumption that all the springback forces act on the rudder front spar. Table N-2 gives the front spar forces ($P_{F/S}$) for two different tool side plate beam end conditions:

1. Three-beam assumption where supports B and C are at the lines of 2.54-cm (one-inch)-diameter tool clamping bolts.

2. Fixed-end assumption.

TABLE N-1

SUMMARY OF SIDE PLATE DEFLECTION AND TOOL VOLUME CHANGE DUE TO 6.894 MPa (1000 psi) INTERNAL RUBBER PRESSURE

RUDDER BAY	SIDE PLATE DEFLECTION AT THE F/S (cm)				VOLUME CHANGE (cm^3)		
	DUE TO BENDING		DUE TO BOLT EXTENSION				
	THREE BEAM ASSUMPTION	FIXED END ASSUMPTION	THREE BEAM ASSUMPTION	FIXED END ASSUMPTION	THREE BEAM ASSUMPTION	FIXED END ASSUMPTION	AVERAGE
419.26 TO 424.94	0.2416	0.1491	0.1285/2	0.0688/2	823.12	582.23	702.68
461.70 TO 466.77	0.1775	0.0805	0.0777/2	0.0541/2	480.436	304.636	392.536
550.88 TO 555.47	0.0752	0.0447	0.0447/2	0.0282/2	109.433	63.942	86.688
REF. PAGE							

TABLE N-2

SUMMARY OF RELATIONSHIP BETWEEN A CONCENTRATED FRONT SPAR LOAD AND THE MOLD SIDE PLATE DEFLECTION AT THE FRONT SPAR

RUDDER BAY ZAR	$P_{F/S}$ = CONCENTRATED FRONT SPAR LOAD (MN)	
	3 BEAM ASSUMPTION	FIXED END ASSUMPTION
419.22-424.94	$\frac{Y_{F/S}}{0.4797}$	$\frac{Y_{F/S}}{0.2897}$
461.70-466.70	$\frac{Y_{F/S}}{0.4757}$	$\frac{Y_{F/S}}{0.2903}$
550.88-555.47	$\frac{Y_{F/S}}{0.3981}$	$\frac{Y_{F/S}}{0.2476}$

NOTE: $Y_{F/S}$ = cm

APPENDIX P
RUBBER MANDREL FABRICATION AND SIZE MEASUREMENT

The major steps taken to prepare for pouring of the front spar rubber mandrels (Figures P-1 and P-2) and the main internal rubber mandrels (Figures P-3, P-4, and P-5) are described in this appendix.

A comparison between the design requirements for the thicknesses of the dummy front spar web versus the achieved thicknesses is given in Table P-1. The dummy front spar web gages were fabricated identically to the rudder front spar web gages. Hence, a chordwise rubber gap of zero was used in the pouring operation. The final desired chordwise rubber gap was achieved from shrinkage during the high-temperature cure procedure.

Gap measurements of the front spar forward flange rubber were made following the initial cure of 36 hours at room temperature and 4 hours at 339^{o}K (150^{o}F). The results are given in Table P-2. These rubber gaps were considered satisfactory.

Measurements of rubber gaps built into the dummy side skins are shown in Appendix D. Following the casting of the front spar flange rubber mandrels, the dummy F/S web, metal mandrels, metal screening, and dummy front spar skins and ribs were assembled on the PLM tool and the main internal rubber mandrels were poured. After the rubber was cured at temperatures up to 450^{o}K (350^{o}F), the entire rubber mandrel was dimensionally checked at rudder bays No. 4, 11, 20, and 27 and found to be satisfactory. Following this, the rubber mandrels were sectioned into six parts. The volume of these sectioned pieces for rudder bays No. 4, 11, 20, and 27 were measured by immersion in water and the results recorded in Table P-3. The volumes of the rubber and metal mandrels, the composite material, and the PLM tool at rudder bays No. 4, 11, 20, and 27 were computed and recorded in Table P-4. These values were used to estimate the existing rubber gap tolerance range which in turn were used to judge the adequacy of the main rubber mandrels for use in curing graphite/composite rudders (Task 13 of Section 6).

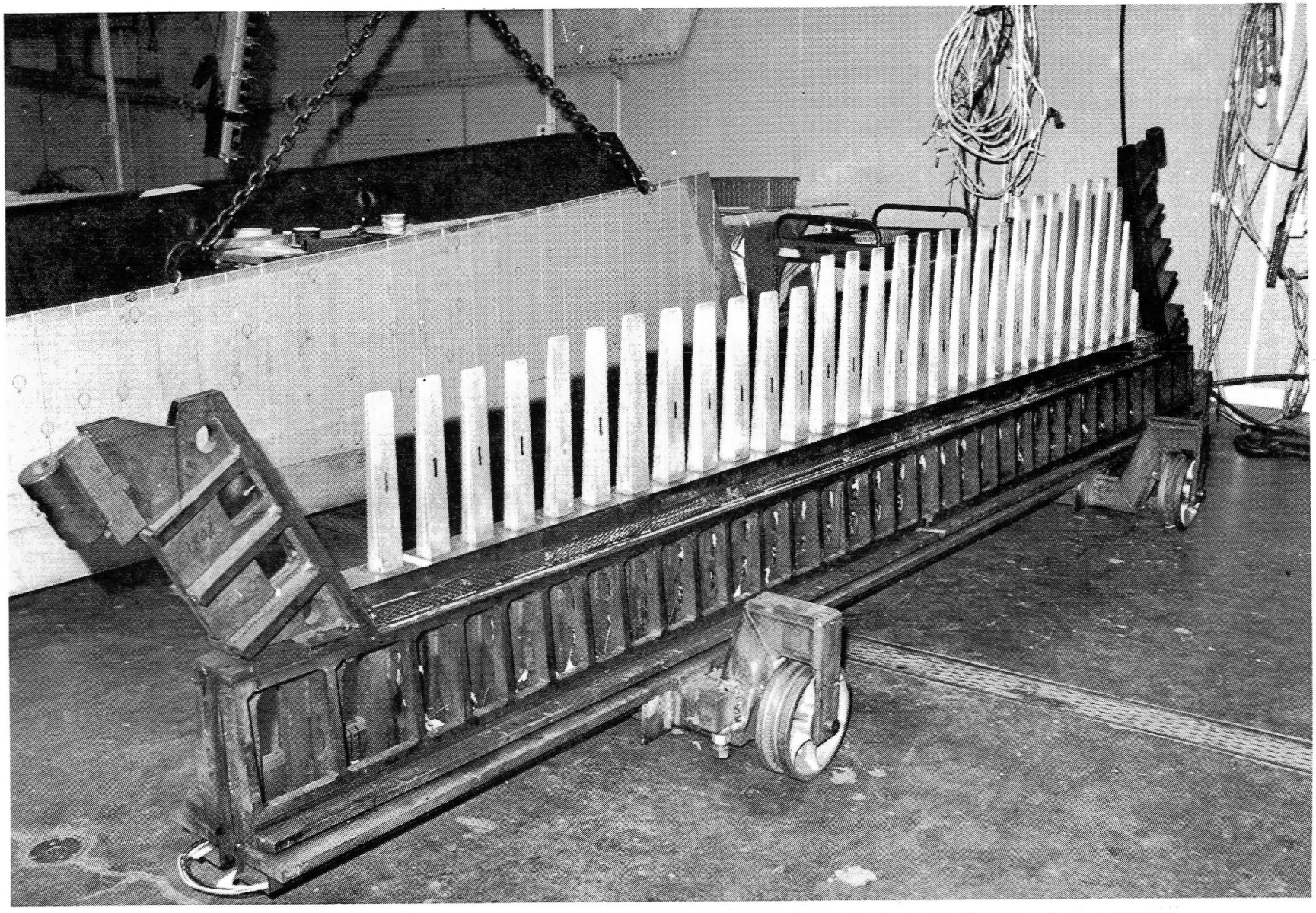

FIGURE P-1. METAL SCREEN REINFORCEMENT FOR FRONT SPAR FORWARD FLANGE RUBBER MANDRELS

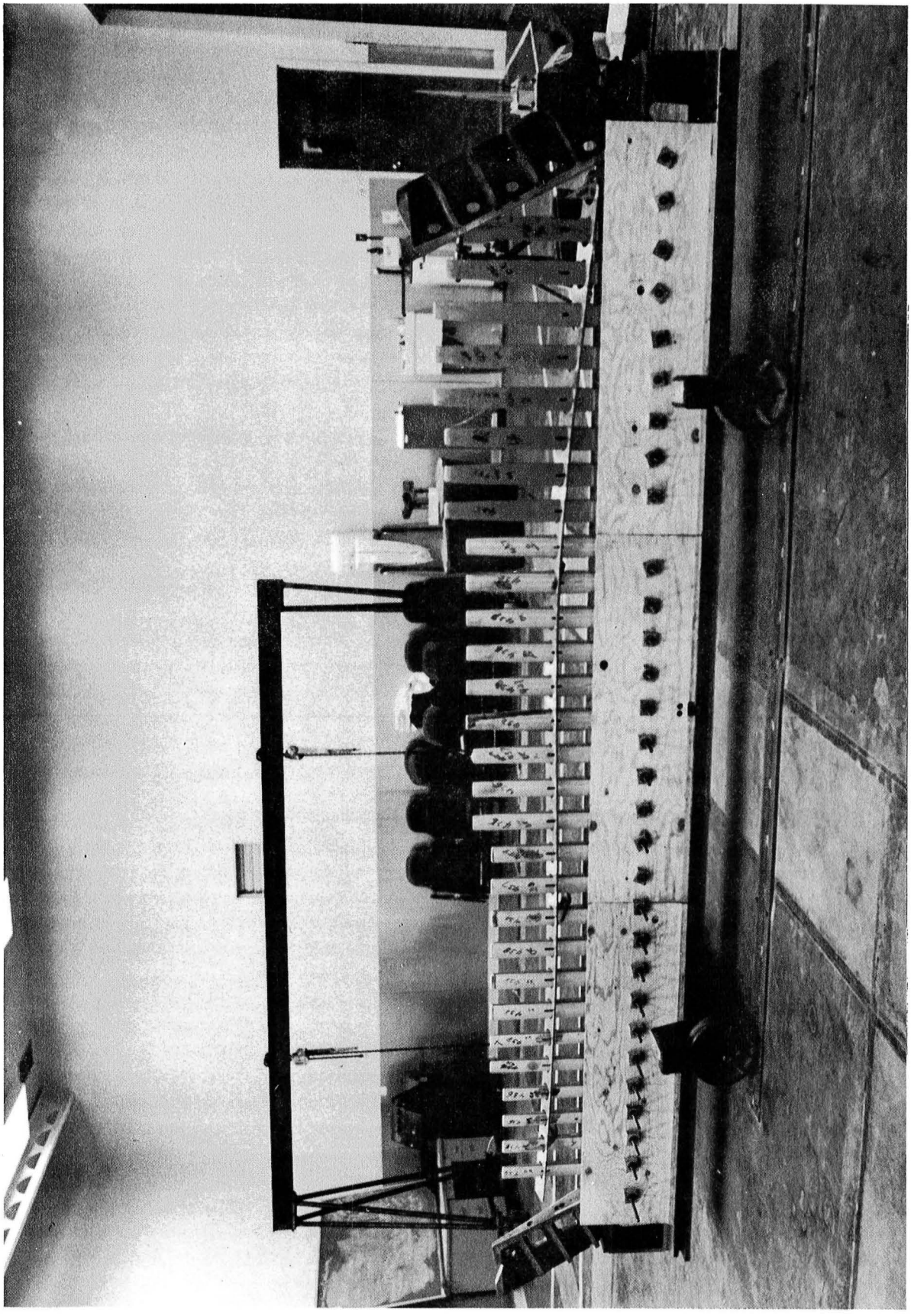

FIGURE P-2. FRONT SPAR FORWARD FLANGE DUMMY PART ASSEMBLED ON PLM

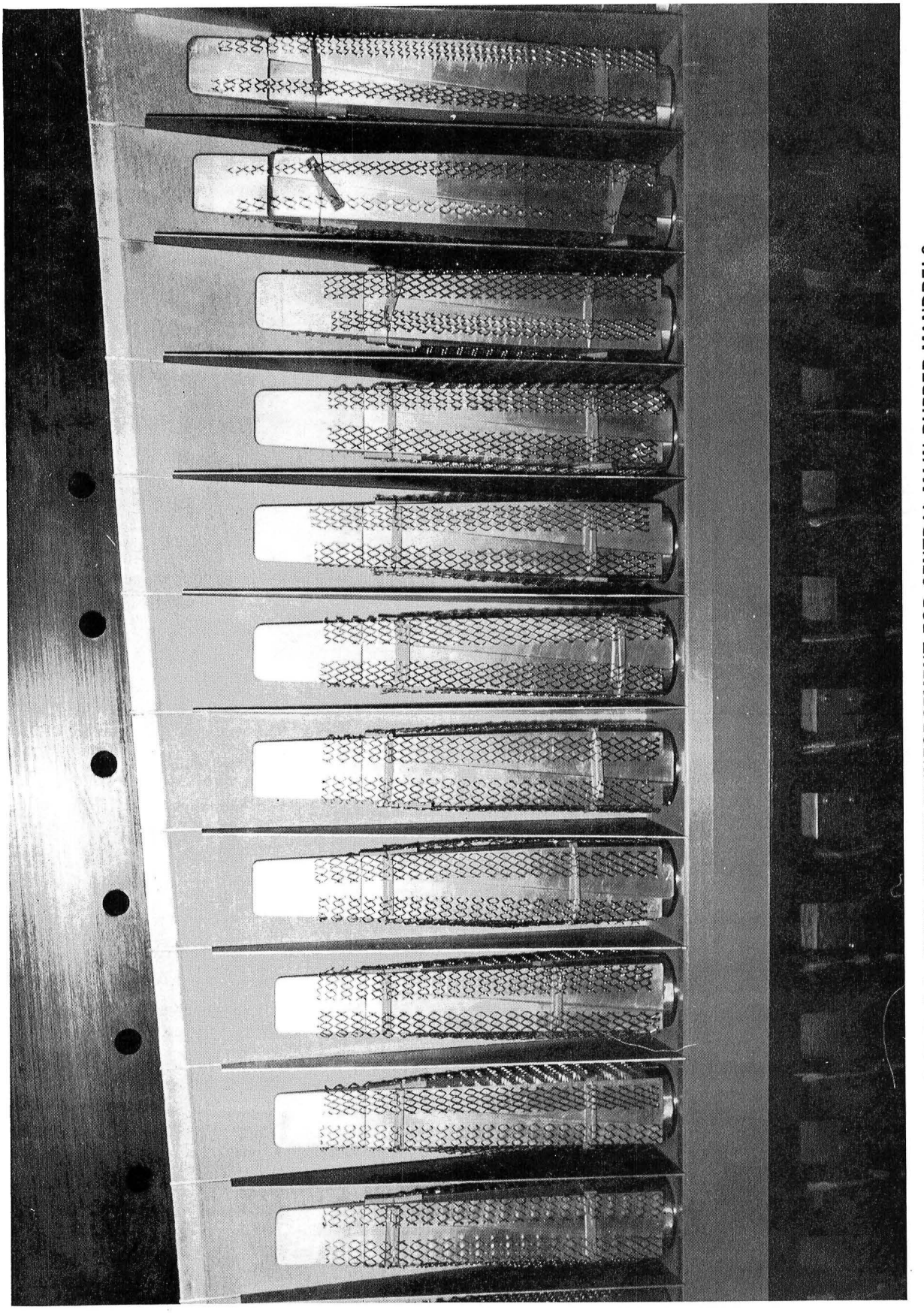

FIGURE P-3. METAL SCREEN REINFORCEMENT FOR CENTRAL MAIN RUBBER MANDRELS

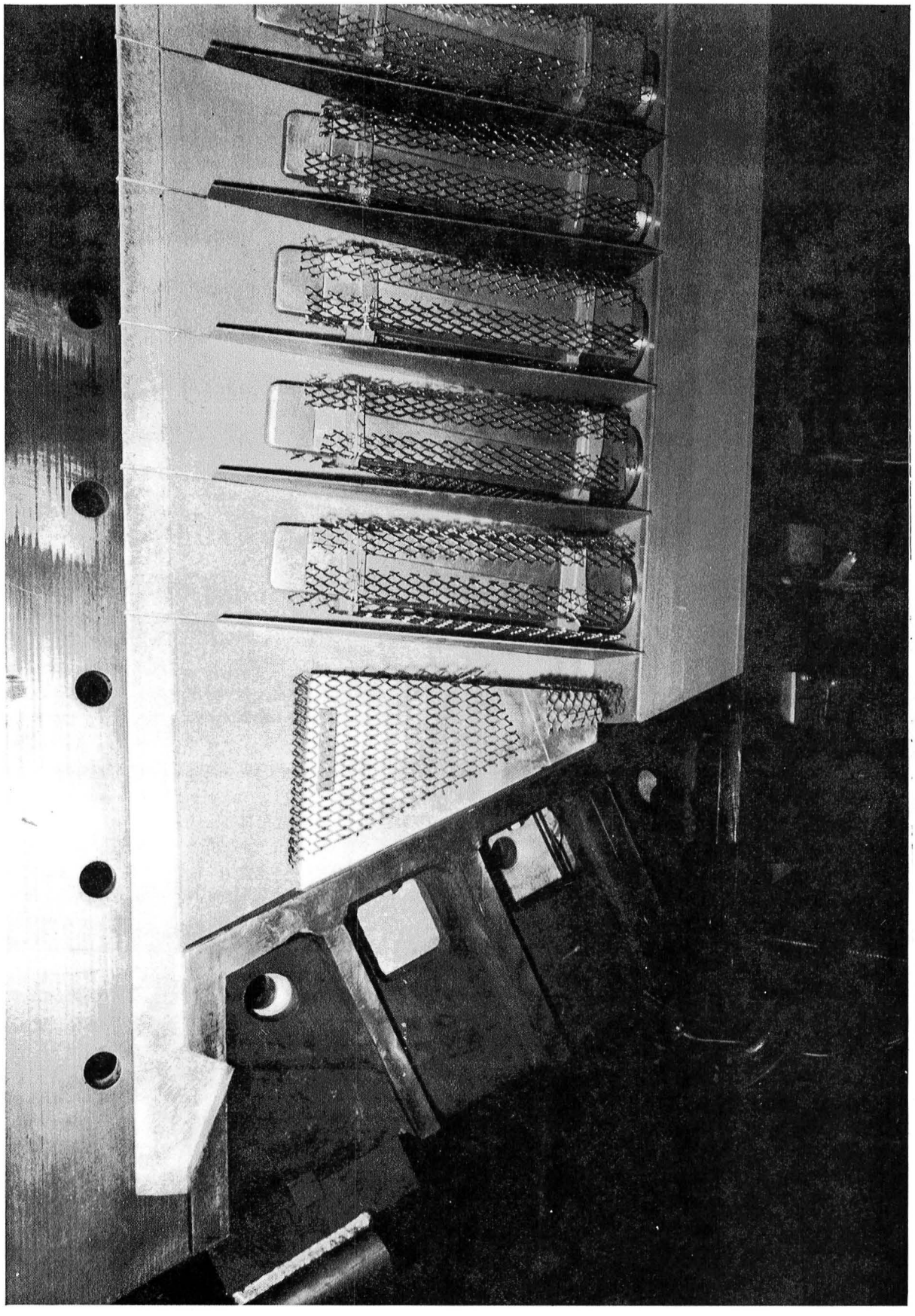

FIGURE P-4. METAL SCREEN REINFORCEMENT FOR UPPER MAIN RUBBER MANDRELS

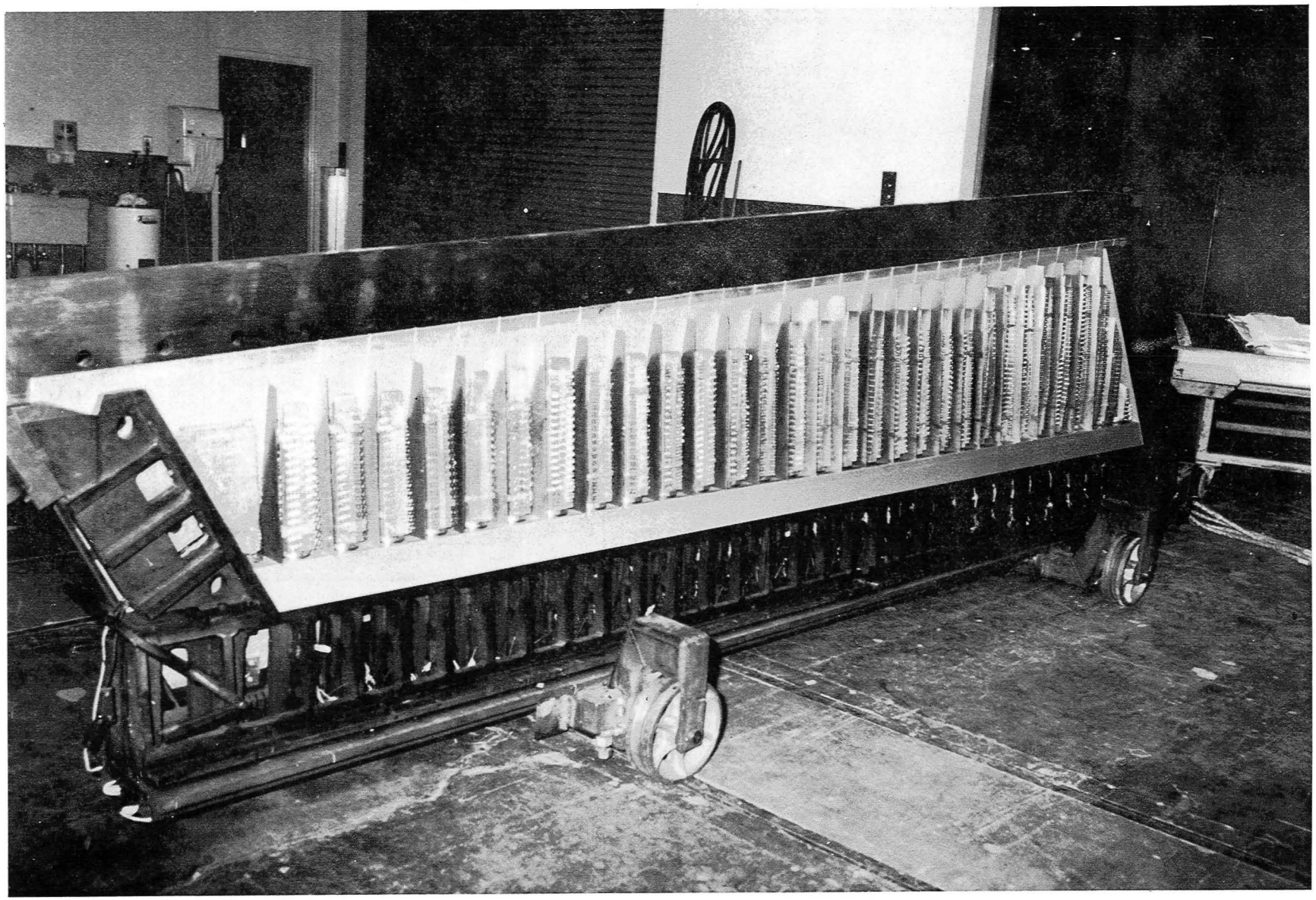

FIGURE P-5. VIEW OF R/H DUMMY SKIN, DUMMY RIBS, METAL MANDREL F/S FORWARD FLANGE RUBBER

TABLE P-1
DUMMY FRONT SPAR WEB THICKNESS

RUDDER STATION Z_{AR}	NUMBER OF LAYERS		REQUIRED[1] THICKNESS (cm)	ACTUAL THICKNESS (cm)
	BI-WOVEN	UNI-WOVEN		
400	4	16	0.381	
416.25				0.391
433.35				0.391
448.95				0.376
464.25				0.378
469.35	4	14	0.343	
479.55				0.340
494.85				0.338
505.05	4	12	0.320	
510.15				0.318
525.45				0.315
534.90	4	10	0.290	
539.50				0.287
553.30				0.284
555.47				

[1] NOMINAL BI-WOVEN LAYER t = 0.0343 cm
NOMINAL UNI-WOVEN LAYER t = 0.0152 cm

TABLE P-2
GAP MEASUREMENTS – FRONT SPAR FORWARD FLANGE RUBBER

SKIN	ZAR	SPIKE NO.	TOTAL MEASUREMENT (cm)	*ACTUAL GAP (cm)
–6	550.88	29	0.445	0.051
	539.50	27	0.447	0.053
	517.75	22	0.447	0.053
	505.05	20	0.452	0.058
	471.87	13	0.437	0.043
	459.15	11	0.439	0.046
	436.31	6	0.442	0.048
	421.95	4	0.414	0.020
	419.26	3	0.401	0.008
	407.70	1	0.419	0.025
–5	550.88	29	0.419	0.025
	539.50	27	0.455	0.061
	517.75	22	0.419	0.025
	505.05	20	0.445	0.051
	471.87	13	0.429	0.036
	459.15	11	0.457	0.064
	436.31	6	0.457	0.064
	430.61	5	0.419	0.025
	421.95	4	0.424	0.031
	419.26	3	0.457	0.064
	407.70	1	0.445	0.051

*ACTUAL GAP IS THE TOTAL MEASURED THICKNESS LESS 0.076 cm SHROUD THICKNESS AND 0.318 cm SKIN THICKNESS

TABLE P-3
RUBBER MANDREL VOLUMES – WATER OVERFLOW METHOD

BAY NO.	RUBBER VOLUME (cm)						
	SECTION A	SECTION B	SECTION C	SECTION D	SECTION E	SECTION F	TOTAL
4	904	935	1269	823	926	818	5675
11	797	828	478	890	938	369	4300
20	443	444	494	514	565	475	2935
27	309	294	336	354	360	390	2043

TABLE P-4
MEASUREMENT OF RUBBER GAP FOR RUDDER BAYS 4, 11, 20 AND 27

①	②	③	④	⑤	⑥	⑦	⑧	⑨	⑩	⑪	⑫
	INTERNAL MATERIAL VOLUME (cm^3)				TOOL BAY VOLUME(2)		GAP CAVITY			GAP (cm)(1)	
BAY NO.	RUBBER MANDREL	METAL MANDREL	COMPOSITE MATERIAL	TOTAL	(cm^3)	(cm^3)	(cm^3)	(cm^3)	BAY SURFACE AREA (cm^2)	MAX	MIN
4	5675	2642	361	8678	8897	8720	219	42.4	3295	0.066	0.013
11	4300	1493	288	6081	6235	6096	153	14.3	2589	0.058	0.005
20	2935	1205	231	4370	4582	4481	211	110	2057	0.102	0.053
27	2043	779	173	2995	3077	3001	88.5	6.1	1534	0.053	0.005
REF				② + ③ + ④			⑥ - ⑤	⑦ - ⑤		⑧ / ⑩	⑨ ⑩

(1) THESE RUBBER GAPS DO NOT INCLUDE AN ALLOWANCE OF ABOUT 0.010 cm FOR THE TEFLON TAPE PROTECTIVE LAYER

(2) THE LOCATION OF DUMMY RIBS INTO OVERSIZE SLOTS IN THE DUMMY SKINS (DUE TO THE TOLERANCE REQUIREMENTS OF PLACING 30 DUMMY RIBS IN 0.30 SLOTS IN LEFT-AND RIGHT-HAND DUMMY SKINS AT THE SAME TIME DURING THE RUBBER CASTING EFFORT) RESULTED IN THESE ESTIMATES OF MAXIMUM AND MINIMUM VALUES FOR TOOL BAY VOLUMES.

REFERENCES

1. Mass Property Data for the DC-10 Composite Upper Aft Rudder, Report MDC-J7452, Dated 2 February 1977.

2. Advanced Composite Rudders for DC-10 Aircraft — Design, Manufacturing and Ground Tests (Contract NAS1-12954), NASA Report CR-145068.

3. Walt Cremens and Harry Reinert, "A General Look at Thermal Expansion Molding," Volume 21 of the Twenty-First National SAMPE Symposium at Los Angeles, California, April 6-8, 1976.

4. Rudder Assembly Woven Graphite Composite, Upper Aft, DPS 1.621-2, Dated 12 January 1978.